DESIGN AND FABRICATION OF PLANAR ANTENNA WITH BAND-NOTCH CHARACTERISTICS FOR ULTRA-WIDEBAND APPLICATIONS

A Thesis

submitted in partial fulfillment of the requirements for the

award of the degree of

DOCTOR OF PHILOSOPHY

in

Electronics and Communication Engineering

by

Gurpreet Kumar

(41600324)

Supervised by

Dr. Daljeet Singh

Co-supervised by

Dr. Rajeev Kumar

LOVELY PROFESSIONAL UNIVERSITY

PUNJAB

2020

Declaration

I declare that the thesis entitled **"Design and Fabrication of Planar Antenna with Band-notch Characteristics for Ultra-wideband Applications"** has been prepared by me under the guidance of **Dr. Daljeet Singh,** Assistant Professor, School of **Electronics and Electrical Engineering** at **Lovely Professional University, Punjab, India,** and **Dr. Rajeev Kumar, Assistant Professor at Chitkara University Institute of Engineering and Technology, Punjab, India**. No part of this thesis has been included in or has formed the basis for the award of any Degree or Diploma or Fellowship of any institution or university anywhere previously.

I further declare that there is no falsification or manipulation in terms of research materials, equipment or processes, experiments, methods, models, modeling, data, data analysis, results, or theoretical work.

I have checked the thesis using Turnitin for ensuring that there is no plagiarized material in my thesis and wherever any copyrighted material has been included, the same has been duly acknowledged.

GURPREET KUMAR
School of Electronics and Electrical Engineering
Lovely Faculty of Technology and Sciences
Lovely Professional University
Phagwara, -144411 (Punjab)

We endorse the above declaration of Ph.D. student

Date: (Signature of the Ph.D. Supervisor)

(Signature of the Ph.D. Co-Supervisor)

Certificate

We certify that **GURPREET KUMAR** has prepared his thesis entitled "**Design and Fabrication of Planar Antenna with Band-notch Characteristics for Ultra-wideband Applications**", for the award of the Ph.D. degree of the Lovely Professional University, under our guidance. He has carried out the work at the **School of Electronics and Electrical Engineering**, Lovely Professional University.

Dr. DALJEET SINGH
Assistant Professor
School of Electronics and Electrical Engineering
Lovely Faculty of Technology and Sciences
Lovely Professional University,
Phagwara, Kapurthala-144411 (Punjab)

Dr. RAJEEV KUMAR
Assistant Professor
Chitkara University Institute of Engineering and Technology
Chitkara University,
Rajpura, Patiala-140401(Punjab)

Abstract

There are various technologies in the field of wireless communication that have emerged in the recent past for providing high data rates. However, it is very difficult to achieve these high data rates with very low power consumption. UWB systems provide a unique solution to this problem. This was made possible by the Federal Communication Commission (FCC) in 2002 when an unlicensed spectrum from 3.1-10.6 GHz was allocated to Ultra-wideband (UWB) systems. These systems utilize extremely low power signals for transmission and provide high data rates over a short-range. However, the major challenge in implementing these systems is the indoor and outdoor masks mentioned in FCC guidelines. These mask limits should be followed by UWB systems to avoid interference with other wireless systems lying in the UWB range. Otherwise, the overall signal transmission capacity of UWB systems as well as other wireless systems will be degraded. UWB antennas play an important role to tackle the aforementioned challenge of UWB systems. These antennas should possess band notch characteristics to achieve reliable signal transmission. Few other characteristics are also required in these antennas such as compact size, wide bandwidth, stable gain, and omnidirectional radiation pattern. Further, the time-domain performance of these systems should also be evaluated precisely since the signal transmission is done through narrow pulses.

Multiple techniques can be employed in antenna structures to achieve UWB operation as well as band notch characteristics. Therefore, this thesis focuses on designing and fabrication of the UWB antenna with band-notch characteristics. Initially, various techniques for achieving band notch characteristics in UWB antennas have been analyzed and the research gaps have been identified. Secondly, the design process for achieving UWB and band notch operation has been accomplished. Finally, on the basis of complete UWB system requirements and available research gaps in the design process of band-notched UWB antennas, novel designs have been presented and analyzed in this work. The results of the novel antenna designs presented in this work are compared with the state-of-the-art literature and validation of these designs has been accomplished through the fabrication and testing process.

Acknowledgements

High achievement always takes place in the framework of high expectation. The expectation was there and I begin with determined resolve and put in sustained hard work. It has been rightly said that every successful individual knows that his or her achievement depends on a community of persons working together but the satisfaction that accompanies the successful completion of any task would be incomplete without mentioning those people who made it possible.

This is to acknowledge with gratitude the guidance and suggestions from my supervisor, Dr. Daljeet Singh, and co-supervisor Dr. Rajeev Kumar for their support and motivation throughout the thesis work.

I am grateful to the members of the School of Research Degree Programme (RDP) for being in my entire research progress review panel, providing useful suggestions during the period. I am indeed thankful to all anonymous reviewers of my research papers submitted to various international journals and international conferences, due to which I was able to improve upon the work containing herein.

I am indebted to Honorable Chancellor, Worthy Pro-Chancellor, the Vice-Chancellor, and the successive Deans, LPU, for facilitating the administrative issues involved and encouraging me throughout.

I express my heartfelt gratefulness to Head of School, School of Electronics and Electrical Engineering, and the staff for their cooperation and support. I am also thankful to NITTTR, Chandigarh, Banasthali Vidyapith, Jaipur, and IIT Roorkee, Uttarakhand for their help in the simulation, fabrication, and testing process of the work.

No words of thanks are enough to express my deepest gratitude and sincerest love to my parents whose rock-solid faith in me kept me strong in all circumstances. I am also thankful to my wife Komal, and my brothers Kamal and Amani for their wholehearted, and endless support and patience. Last but not least, I bow my head before the Almighty God for showering His mercy on me for every moment.

Gurpreet Kumar

Table of Contents

	Title	Page No.
	Abstract	**iii**
	Table of Contents	**v**
	List of Abbreviations	**ix**
	List of Tables	**xi**
	List of Figures	**xiii**
Chapter 1	**Introduction**	1
	1.1 Overview	1
	1.2 UWB Systems	1
	1.3 Design Requirements of Antennas for UWB Systems	4
	1.4 Motivation	8
	1.5 Research Gaps	8
	1.6 Objectives	9
	1.7 Thesis Organization	9
Chapter 2	**Literature Survey**	**11**
	2.1 Introduction	11
	2.2 Slot, Stub and Parasitic Element Loaded Band Notched UWB Antennas	17
	2.3 Fractal Geometry Based Band-Notched UWB Antennas	23
	2.4 Metamaterials Based Band-Notched UWB Antennas	31
	2.5 EBG Structures Based Band-Notched UWB Antennas	41
	2.6 Reconfigurable Band-Notched UWB Antennas	47

2.7 Summary 54

Chapter 3 Design Process of Planar UWB Antennas with Band Notch Characteristics 56

3.1 Introduction 56

3.2 A CPW Fed planar UWB antenna 58

3.2.1 Antenna Structure 58

3.2.2 Parametric Study 59

3.2.3 Surface Current Distribution 63

3.3 Modified L-Slot UWB Antenna with Microstrip Coupled Feed 64

3.3.1 Antenna Design and Parameters 64

3.3.2 Parametric Analysis 65

3.3.3 Simulated Results 67

3.3.4 Measured Results 68

3.4 Circular Monopole UWB Antenna with a Band Notch 70

3.4.1 Design Outline 70

3.4.2 UWB Operation 71

3.4.3 Band-Notch Operation 74

3.4.4 Simulated Results 74

3.4.5 Measured Results 76

3.5 Summary 81

Chapter 4 Design and Efficient Analysis of a CPW Fed Beveled Patch UWB Antenna with Highly Optimized WLAN (5.15 – 5.825 GHz) Notch Band 82

4.1 Introduction 82

4.2 Design Configuration of the Proposed Antenna 86

4.3 Parametric Analysis 88

4.3.1 Selection of the Excitation Signal 88

4.3.2 Design Process 90

4.3.3 Notch Band Optimization 92
4.4 Time-domain Analysis and Phase Response of S_{21} 107
4.4.1 Dispersion Analysis 107
4.4.2 System Fidelity Factor 109
4.4.3 Group Delay 111
4.4.4 Phase Response of S_{21} 112
4.5 Measurement Results 113
4.6 Summary 119

Chapter 5 A Planar CPW fed UWB Antenna with Dual Rectangular Notch Band Characteristics Incorporating U-slot, SRRs, and EBGs 120
5.1 Introduction 120
5.2 Design Configuration of the Antenna 124
5.3 Design Process 125
5.3.1 Step 1: Design of the UWB antenna 125
5.3.2 Step 2: First Rectangular Notch Band Realization 126
5.4.3 Step 3: Second Rectangular Notch Band Realization 130
5.4 Parametric Study 131
5.4.1 Controlling the First Rectangular Notch 132
5.4.2 Controlling the Second Rectangular Notch 132
5.4.3 Surface Current Distribution 134
5.5 Time-Domain Analysis 136
5.6 Measured Results 138
5.7 Summary 141

Chapter 6 Conclusions and Future Scope 142
6.1 Conclusions 142
6.2 Future Works 143

List of Publications **144**

Bibliography **145**

List of Abbreviations

ABC	Artificial bee colony
BSF	Band stop filter
BPSO	Binary particle swarm optimization
CMOS	Complementary metal oxide semiconductor
CMT-EBG	Conventional mushroom-type electromagnetic bandgap structure
CPW	Co-planar waveguide
CRLH-TL	Composite right/left-handed transmission line
CSLA	Coupled sectorial loop antennas
CSSR	Complementary split-ring resonator
DC	Direct current
DE	Differential evolution
DMS	Defected microstrip structure
EBG	Electromagnetic bandgap
EIRP	Effective isotropic radiated power
EM	Electromagnetic
ERS	Elliptical ring slot
FCC	Federal Communications Commission
FET	Field effect transistor
FSS	Frequency selective surface
FTSE	Folded T-shaped element
GRIN	Gradient refractive index
GSRR	Split ring resonator in the ground plane
HIPERLAN	High performance local area network
HSIR	Hexagonal stepped impedance resonators
IEEE	Institute of Electrical and Electronics Engineering
IFS	Iterated function system
IFSLRR	Inverted F stub loaded rectangular resonator

ITU-R	International Telecommunication union – Radiocommunication Sector
MCSRR	Modified complementary split-ring resonator
MEMS	Micro-electro-mechanical systems
MIMO	Multiple input multiple output
MSR	M-shaped resonator
MSSF	Modified Sierpinski square fractal
MTM	Metamaterial
OET-S	Open-ended T-shaped stubs
PSD	Power spectral density
PSLR	Parallel stub loaded resonator
PSO	Particle swarm optimization
Q	Quality factor
ROC	Role of criterion
RSLR	Radial stub loaded resonators
RSRR	Rectangular Split Ring Resonator
SCRLH-TL	Simplified composite right-/left-handed transmission line
SDMS	Shaped defected microstrip structure
SFF	System fidelity factor
SIS	Stepped impedance stub
SOC	System on chip
SRR	Split ring resonator
T-SIR	T-shaped stepped impedance resonator
UWB	Ultra-wideband
VNA	Vector network analyzer
VSWR	Voltage standing wave ratio
WBAN	Wireless body area network
Wi-MAX	Wireless interoperability microwave access
WLAN	Wireless local area Network
WPAN	Wireless personal area Network
WUSB	Wireless universal serial Bus

List of Tables

Table No.	Title	Page No.
1.1	Design parameter requirements for UWB antennas	5
2.1	Notch frequency for different types of slot antennas	18
2.2	Different notched bands and their application using a slot, parasitic and stub loaded antennas	22
2.3	Different notched bands and their applications using distinct fractal geometry	31
2.4	Different notched bands and their applications using metamaterial structures	41
2.5	Different notched bands and their applications using EBG structures	46
2.6	Different notched bands and their applications using antenna reconfiguration techniques	53
3.1	Design parameters of the antenna in mm	58
3.2	Bandwidth of the antenna with variation in WF	60
3.3	Bandwidth of the antenna with variation in GW	62
3.4	Bandwidth of the antenna with variation in WP	62
3.5	Bandwidth of the antenna with variation in WP	62
3.6	Parameters with size in mm	65
3.7	Design parameters of the antenna in mm	71
4.1	Comparison of the proposed antenna and reference antenna designs with WLAN notch band characteristics	84
4.2	Dimensions of the proposed antenna in mm	87
4.3	Different values of notch band with variation in SW1	95
4.4	Different values of notch band with variation in the values of SW2	99

4.5 Different values of notch band with variation in SL 100

4.6 Different values of notch band with variation in SP 102

4.7 System fidelity factor values for different stages of the proposed antenna in the face to face and side by side directions 110

4.8 Cross polarization level in y-z and x-z plane 116

4.9 Comparison between gain and radiation efficiency for the proposed antenna 118

5.1 Comparison of the proposed antenna with existing work 122

5.2 Dimensions of the proposed antenna in mm 125

List of Figures

Fig. No.	Caption	Page No.
1.1	FCC spectrum mask	2
1.2	Spectrum for various wireless systems	3
1.3	PSD of the Gaussian pulse with higher-order derivatives	6
1.4	Pulse shaping factor vs peak frequency	7
2.1	Planar UWB antenna (a) Antenna prototype (b) Vector network analyzer setup for the measurement of the antenna (c) Simulated and measured S_{11} (d) Simulated and measured gain	12
2.2	Planar UWB antenna with three-notch bands (a) Antenna Prototype (b) Simulated and measured S_{11} (c) Simulated and measured gain	14
2.3	Equivalent circuits of UWB antennas (a) Foster canonical form for electrical antennas (b) Foster canonical form for magnetic antennas (c) Impedance model for radiating patch of UWB antenna (d) Equivalent circuit of macro model (e) Lumped equivalent circuit model of the antenna (f) Equivalent LC circuit model of the antenna (g) Equivalent circuit of band suppressed cone type monopole antenna	15
2.4	An equivalent circuit of the slot-loaded patches	18
2.5	Different types of slot, stub and parasitic element loaded antennas (a) Arched slot antenna (b) Hexagonal slot antenna (c) Spiral slot antenna (d) Ring slot antenna (e) U-slot antenna (f) H-slot Antenna (g) C shaped slot antenna (h) L-slot antenna (i) Elliptical ring slot (ERS) antenna (j) Parasitic element loaded antenna (k) Trapezoidal stub antenna *(l)* T shaped slot antenna (m) Hybrid slot antenna (n) W shaped slot antenna (o) Circular slot antenna	19

2.6 Different types of simulated and measured results in planar UWB band-notched antennas using slots (a) Simulated and measured and VSWR (b) Simulated and measured S_{11} (c) Gain versus frequency graph (d) Measurement of group delay (e) E-plane and H-plane radiation pattern 20

2.7 Common fractal geometries (a) Koch snowflakes/islands (b) Sierpinski gasket and carpets (c) Fractal trees 24

2.8 Construction stages of different fractal structures (a) Sierpinski gasket fractal (b) Koch snowflake fractal (c) Hilbert curve fractal 24

2.9 Four stages of construction of the Koch curve using IFS 24

2.10 Sierpinski Gasket final structure using IFS code 25

2.11 Different UWB band-notched designs with fractals (a) Koch curve (b) Fractal binary tree slot (c) 4 element Sierpinski knopp fractal (d) Gosper fractal-shaped (e) Cantor set fractal with T shaped stub (f) Fractal radiating patch in which a folded T-shaped element (FTSE) is embedded (g) Hybrid Fractal Slot (h) Modified crown-square shaped fractal slots in the ground plane with omega slot 25

2.12 Different types of simulated and measured results in the planar UWB band-notched antennas using fractal structure(a) Simulated and measured VSWR characteristics (b) Simulated and measured S_{11} (c) Simulated and measured peak gain (d) Measured group delay (e) E and H plane radiation pattern 27

2.13 Different types of commonly used ring resonators (a) Rectangular split ring resonator (RSRR) (b) Circular split ring resonator (c) Split ring resonator (SRR) and Complementary split-ring resonator (CSRR) with its equivalent circuits 32

2.14 Different UWB designs using metamaterial structures for achieving band notch characteristics (a) Circular split ring resonator (b) Rectangular split-ring resonator (c) Complementary split-ring resonator (d) Square spiral slot resonator (e) M shaped resonator (f) SRR in the slot of ground plane (GSRR) (g) Parasitic resonator 34

2.15 Different types of simulated and measured results of the planar UWB band-notched antennas with metamaterials (a) Simulated and measured VSWR (b) Simulated and measured S_{11} (c) Simulated and measured peak gain (d) Measured group delay (e) E and H plane radiation pattern 37

2.16 The Mushroom type EBG structure 42

2.17 UWB antennas with a different type of EBG structures for band notching (a) Band notched antennas with conventional mushroom-type electromagnetic bandgap structure (CMT-EBG) (b) Modified mushroom-type EBG structure (c) Periodic EBG structure 43

2.18 Different types of simulated and measured results in planar UWB band-notched antennas with EBG structures (a) Simulated and measured VSWR (b) Simulated (S_{11}) (c) Simulated and measured peak gain (d) Measured group delay (e) E and H Plane radiation pattern 44

2.19 The configuration of the reconfigurable antenna 48

2.20 Different reconfigurable UWB band-notched antenna designs (a) UWB antenna with ideal switches (b) UWB antenna with PIN diodes (c) UWB antenna with varactor (d) UWB antenna with optical switch (e) UWB antenna with magneto-dielectric material (f) UWB antenna with variable capacitors 49

2.21 Different types of simulated and measured results in the planar reconfigurable UWB band-notched antennas (a) Simulated and measured VSWR (b) Simulated S_{11} (c) Simulated and measured peak gain (d) Measured group delay (e) E and H plane radiation pattern 51

3.1 Design methodology for UWB antennas with band notch characteristics 57

3.2 Design structure of the antenna 59

3.3 (a) S_{11} with variation in WF (b) VSWR with variation in WF 60

3.4	(a) S_{11} with variation in GW (b) VSWR with variation in GW	61
3.5	Surface current distribution of the antenna at (a) 4 GHz (b) 6 GHz (c) 8 GHz (d) 10 GHz	63
3.6	Configuration of the antenna (a) Top view (b) Bottom view	65
3.7	Enhancement of antenna design (a) A1 (b) A2 (c) A3	66
3.8	S_{11} of A1, A2, and A3	66
3.9	Simulated S_{11} of the antenna design	67
3.10	Surface current distribution of the antenna at (a) 4 GHz (b) 6 GHz (c) 7 GHz (d) 9 GHz	68
3.11	Fabricated antenna (a) bottom view (b) top view	68
3.12	Measurement of the antenna with VNA	69
3.13	Simulated and measured S11 of the antenna	69
3.14	Design outline of the UWB band-notched antenna	71
3.15	Modified antenna structure for UWB operation	72
3.16	VSWR plot for the modified antenna structure	72
3.17	Surface Current concentration for the modified antenna at a different frequency (a) 3.7 GHz (b) 5.8 GHz (c) 7.5 GHz	73
3.18	VSWR plot of the band-notched antenna	75
3.19	Surface Current concentration for the final antenna design at different frequency (a) 3.70 GHz (b) 5.78 GHz (c) 7.50 GHz	75
3.20	Fabricated prototype antenna and its measurement setup	77
3.21	Measured vs Simulated VSWR	77
3.22	Measured vs Simulated radiation pattern at different frequency (a) 3.6 GHz (b) 5.07 GHz (c) 4.80 GHz (d) 6.54 GHz	78
3.23	Measured vs simulated gain	79
3.24	Radiation efficiency	80
3.25	Simulated group delay of the band-notched antenna	80
4.1	Geometry of the proposed design	87

4.2	PSD of the selected excitation signal	89
4.3	Evolution of the initial design with variation in ground aperture (a) Ground 1 (b) Ground 2 (c) Ground 3	90
4.4	VSWR plot of the initial design with variation in the ground plane	91
4.5	Current distribution of the initial design (a) Ground structure (b) Radiating patch	91
4.6	Design methodology used for achieving desired notch band	93
4.7	Initial design with different values of SW1 (a) 8 mm (b) 11 mm (c) 13 mm	94
4.8	Effect of SW1 on the center notch frequency	94
4.9	VSWR Plot with an optimum value of SW1 at 9.6 mm	95
4.10	S parameters with optimum values of SW1 at 9.6 mm	96
4.11	Current distribution at different frequency for SW1 value of 9.6 mm (a) 4.585 GHz (b) 5.486 GHz (c) 8.458 GHz	96
4.12	Effect of SW2 on the center notch frequency in VSWR plot	98
4.13	Effect of SW2 on the center notch frequency on S_{11} parameter	98
4.14	Effect of SL on the center notch frequency in VSWR plot	99
4.15	Effect of SL on the center notch frequency on S_{11} parameters	100
4.16	Effect of SP on the center notch frequency in VSWR plot	101
4.17	Effect of SL on the center notch frequency in S_{11} parameters	101
4.18	Stages of the beveled patch for bandwidth enhancement (a) Lower edge beveled (b) Lower and Upper edge beveled	103
4.19	VSWR plot with the beveled patch for bandwidth enhancement	103
4.20	S_{11} plot with the beveled patch for bandwidth enhancement	104

4.21 Equivalent circuit of the notch filter (a) Ideal WLAN notch filter (b) Designed notch filter 105

4.22 S_{11} response of the ideal and designed WLAN notch band filter 105

4.23 Equivalent circuit model of the proposed antenna 106

4.24 Normalized input and radiated signal of the different stages of the notched band antenna with face to face and side by side configuration (a) and (b) Initial UWB antenna, (c) and (d) WLAN notch band antenna without the beveled patch, (e) and (f) WLAN notch band antenna with beveled patch 108

4.25 The simulated and measured group delay of the proposed antenna 111

4.26 Magnitude and Phase response of S_{21} for the proposed antenna (a) Face to Face (b) Side by Side 112

4.27 Fabricated antenna and measurement setup (a) Photograph of the prototype of the designed antenna (b) Photograph of the measurement setup of the proposed antenna 114

4.28 Simulated and measurement results (a) VSWR (b) S_{11} parameters 115

4.29 Simulated and measured gain of the proposed antenna 116

4.30 Simulated and measured radiation pattern at different frequency (a) 4.63 GHz (b) 5.133 GHz (c) 6.5 GHz (d) 7.5 GHz 117

5.1 Design configuration of the proposed antenna 124

5.2 S_{11} of the Initial UWB antenna 126

5.3 S_{11} with U-slot 127

5.4 S_{11} with U-slot and SRRs pair 129

5.5 S_{11} with U-slot, SRRs pair, and EBG structures 131

5.6 Controllable rectangular notch by varying GS (mm) and GR (mm) 132

5.7 Controllable rectangular notch by varying EL1 133

5.8 Controllable rectangular notch by varying EL2 134

5.9 Surface current distribution at (a) 4 GHz (b) 6.46 GHz (c) 6.795 GHz (d) 9.24 GHz 135

5.10 Normalized input and radiated signal for the proposed antenna (a) Face to face (b) Side by side 137

5.11 PSD of the input and radiated signal of the proposed antenna (a) Face to Face (b) Side by side 137

5.12 Simulated and measured group delay of the proposed antenna 138

5.13 Antenna fabrication and measurement (a) Fabricated prototype of the antenna (b) Measurement setup of the proposed antenna 139

5.14 Simulated and measured gain of the antenna 139

5.15 Simulated and measured S_{11} of the antenna 140

5.16 Radiation pattern of the proposed antenna at (a) 3.48 GHz (b) 5.62 GHz (c) 7.68 GHz (d) 10.5 GHz 140

Chapter 1

Introduction

1.1 Overview

This chapter focuses on one of the vital technologies in the field of wireless communication i.e., Ultra-wideband (UWB) systems. These systems come under the unlicensed spectrum of the Federal Communications Commission (FCC) and provide a promising solution where very high data rates are required over a short-range. Therefore, the commercialization of products using this technology becomes very easy. Additionally, the signal power used for transmission in these systems is in microwatts, thus low power solutions with high data rates are possible [1-5]. These systems have numerous applications in the field of short-range wireless communication such as RADAR (e.g., Through wall RADAR, Ground-penetrating RADAR, Automotive RADAR), communication (e.g., wireless personal area networks (WPAN), Wireless body area networks (WBAN), Wireless universal serial bus (WUSB), Wireless high definition video), intelligent sensors (e.g., intelligent transport systems, position, and location tracking systems), and medical applications (medical imaging) [3-15].

This chapter is organized into seven sections. Section 1.1 describes the brief overview of the area under study. Section 1.2 and Section 1.3 give the introduction to UWB systems and the importance of antennas in UWB systems respectively. Further, Section 1.4 provides the motivation of the research, and Section 1.5 represents the various research gaps. Finally, Section 1.6 and Section 1.7 hold the objectives and thesis organization of the work respectively.

1.2 UWB Systems

UWB systems are based on transmitting narrow pulses in the time domain at a very small repetition rate. This provides a spectrum that is spread over a very large bandwidth. This technology came into existence officially on 14th Feb. 2002 when the FCC allocated few unlicensed bands for UWB systems in Part 15 rules such as 3.1-10.6

GHz, 22-29 GHz, and below 900 MHz. However, due to the commercialization point of view, the band providing 7.5 GHz bandwidth in the range of 3.1-10.6 GHz has become most popular. According to the definition provided by FCC for the UWB devices, they need to have a bandwidth of more than 500 MHz, and the signal power radiated by the devices should be having a very low effective isotropic radiated power (EIRP) i.e., -41.3 dBm/MHz [1-6]. Hence, the total power over the UWB range is the only portion of a milliwatt. Fig. 1.1 presents the spectrum mask of the UWB signal as per the FCC guidelines. The spectrum of UWB systems is very large as compared to narrowband system. These systems provide a fractional bandwidth of approximately 110% based on the center frequency (6.85 GHz) of the entire band [3-6]. Moreover, UWB systems have extremely low transmission power due to baseband transmission and very high sensitivity in comparison to the other radio communication systems. Therefore, this technology provides very high data rates for short-range indoor communication and the date rate significantly reduces for longer distances [2-8].

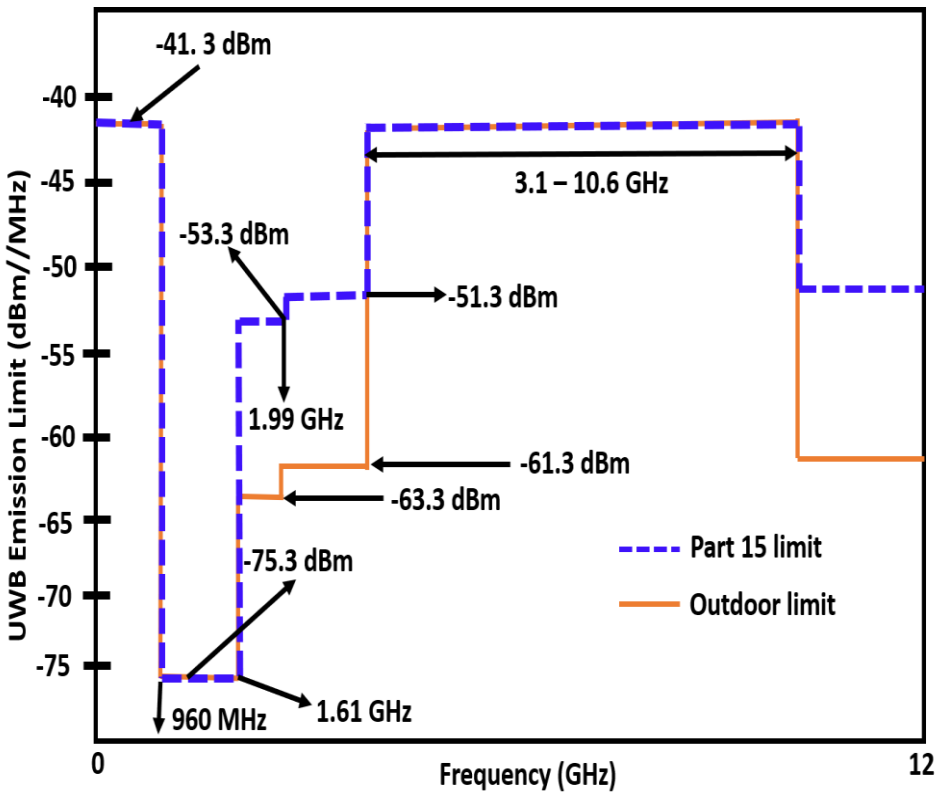

Fig. 1.1 FCC spectrum mask [3], [6]

There are many advantages of UWB systems as compared to other wireless technologies. Low power spectral density (PSD) limits the radiated UWB signal and it acts as noise to the other wireless systems. This results in higher security of transmission for UWB systems due to the low probability of detection. Besides, the UWB signal provides strong immunity to multipath fading because of wide bandwidth and baseband transmission. Furthermore, UWB technology provides a simplified architecture of transceivers [4]. Since the transmission and reception in UWB systems are done through limited power narrow pulses (Pico seconds to nanoseconds) of very low duty cycle (less than 0.5 %), this results in a considerable drop of power utilization by analog circuitry in a low-cost and low power complementary metal-oxide-semiconductor (CMOS) technology [5]. Fig. 1.2 represents the comparison of UWB systems to the other wireless systems.

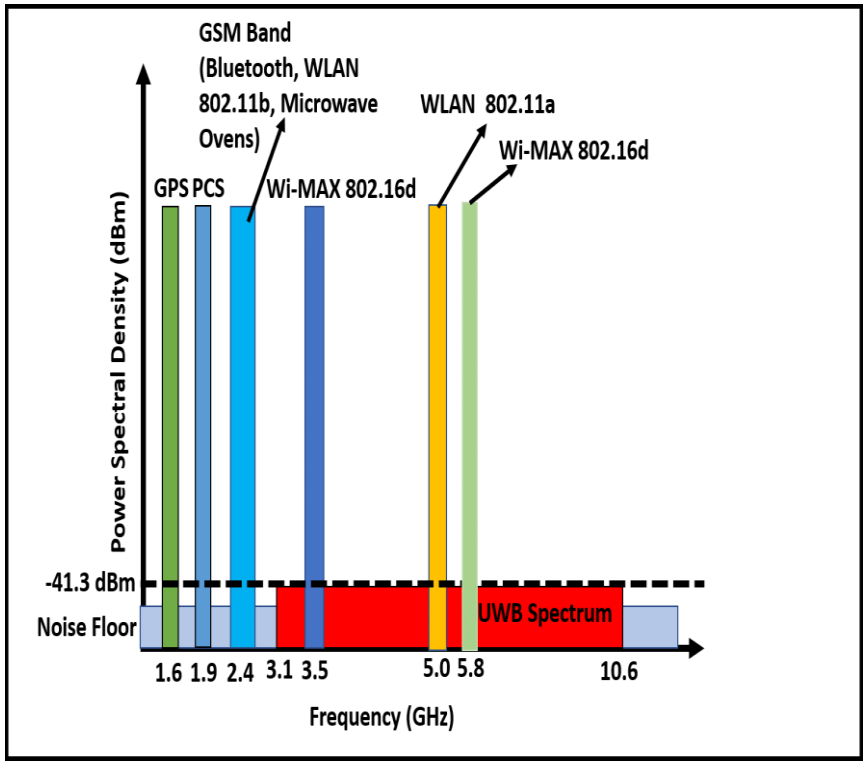

Fig. 1.2 Spectrum for various wireless systems [1-3], [14]

UWB systems utilize short pulse characteristics for transmitting and receiving. Thus, they provide fast data acquisition, which is very helpful in positioning and medical

applications. Therefore, it is essential to evaluate the time-domain performance of these systems, and parameters such as dispersion, group delay, and fidelity factor, etc. should be analyzed precisely.

1.3 Design Requirements of Antennas for UWB Systems

Antennas play a major role in the implementation of UWB systems as in these systems the baseband transmission and reception are impossible without the use of a suitable UWB antenna. These antennas differ from other narrowband antennas as antennas used for narrowband systems are tuned to a particular center frequency and generally have narrow bandwidths. However, UWB antennas deliver wider bandwidths (>500 MHz), and resonant operation is not mandatory. UWB antennas, on the other hand, should possess characteristics such as stable gain, omnidirectional radiation pattern, and linear phase with a fixed phase center. The design methodologies to achieve UWB operation are different for these antennas as compared to other narrowband antennas. While performing the UWB transmission, there is a ringing effect that occurs at the receiving antennas. This effect is due to the type of antenna designs used for transmission and reception and significantly decreases the overall speed of operation. To evade this ringing effect, these antennas are designed with low values of the quality factor (Q). These resistive antennas cause undesirable signals to perish very quickly which in turn provides the received pulse closer to the transmitted pulse. The value of the Q is calculated using [6]

$$Q = \frac{f_o}{f_H - f_L} \tag{1.1}$$

Where f_o represent center frequency and f_H , f_L are the higher and lower frequencies respectively. By reducing the value of Q, the antenna bandwidth can also be enhanced but this lessens the efficiency of the designed antenna. Therefore, it is important to maintain the tradeoff between all these parameters. Table 1.1 illustrates the different parameters vital for designing a UWB antenna [1-7].

Table 1.1 Design parameter requirements for UWB antennas

Parameter	Desired Value
Impedance bandwidth	>500 MHz (3.1 – 10.6 GHz)
Radiation efficiency	Higher (> 70 %)
Phase response	Almost linear
Radiation pattern	Omnidirectional
Gain	Low (1-5 dB)
Half power beamwidth (HPBW)	Wider (>60^0)
Physical size	Compact

There are different types of conformal and planar antenna designs that have been utilized by researchers to study and implement the UWB operation [1],[6]. Out of these designs, planar structures are more suitable for UWB applications because of their low profile and basic radiation properties [6],[14]. So, researchers have focused on planar antennas for various UWB applications.

The UWB systems should have a good time-domain performance to work efficiently for various UWB applications. Therefore, the time-domain parameters should be considered while designing a UWB antenna. The selection of an appropriate pulse is the foremost requirement while designing a UWB antenna. Typically, a Gaussian pulse can be used for this purpose and it is given by [8,9]

$$g(t) = \frac{A}{\sqrt{2\pi}\,\sigma}\; e^{-\frac{t^2}{2\sigma^2}} \qquad (1.2)$$

Where, A and σ give the peak amplitude and pulse shaping factor respectively. As the UWB antennas are not effective for direct current (DC), it is desirable to utilize higher derivatives of Gaussian pulses that have smaller DC components. These pulses should meet the FCC mask regulation. Hence n^{th} order derivative with an optimum value of σ for each derivative is calculated for the spectrum as wide as possible. The PSD for the individual derivative is normalized and scaled to the maximum value of acceptable PSD. It has been observed for lower-order derivatives ($n \leq 4$) for Gaussian pulse does not comply with the mentioned FCC mask as some part of the PSD for these pulses is

out of the range of desired value for UWB operation. The main cause of this constraint is that the peak frequency(f_p) or most of the energy lies in the lower frequency range. So, by the FCC guidelines, higher-order derivatives (n>4) should be chosen as their peak frequency increases with the increase in the order of derivative as illustrated in Fig. 1.3. Subsequently, the 5th order derivative is recommended for UWB antennas as the amount of complexity is lesser as compared to the higher-order derivatives [8]. However, the 7th order derivative can be used for outdoor UWB systems.

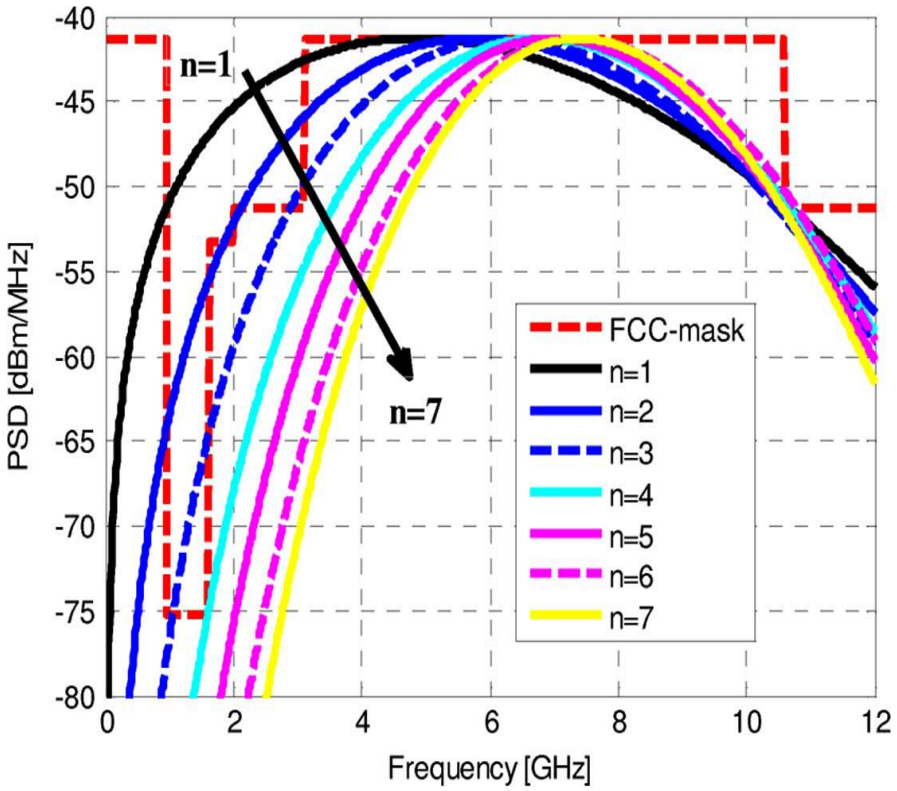

Fig. 1.3 PSD of the Gaussian pulse with higher-order derivatives [8]

The general relation between the (f_p), (σ), and the derivative order (d_o) by seeing the Fourier transform of the d_o^{th} derivative is presented by [8,10]

$$f_p = \sqrt{d_o}\ \frac{1}{\sigma\sqrt{\pi}} \qquad (1.3)$$

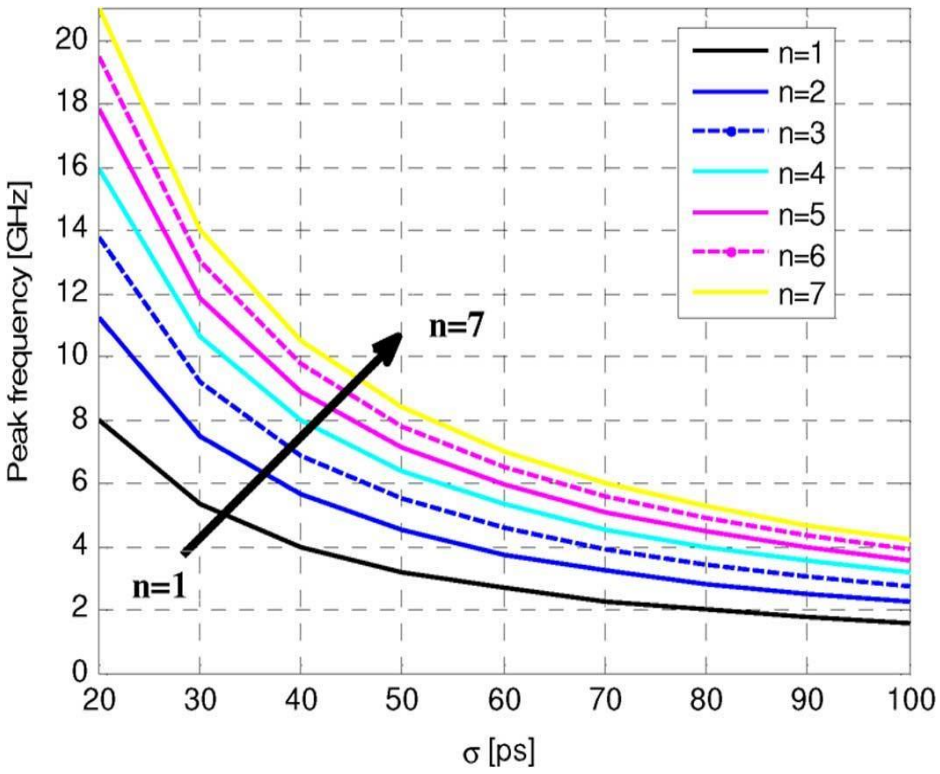

Fig. 1.4 Pulse shaping factor vs peak frequency [8]

Fig. 1.4 presents the variation of f_p with σ for n = 1,2……7. It is observed from Fig. 1.4 that the bandwidth of the signal upsurges as the value of σ decreases due to the inverse relation between bandwidth and time. The PSD of the signal is generally affected by the differentiation of the Gaussian pulse. Both, the bandwidth of the pulse and f_p changes by an order of differentiation and σ. Thus, with the increase in the derivative order, the pulse energy moves to higher frequency bands. Therefore, the spectrum is utilized efficiently [8].

System fidelity factor (SFF) is another time-domain parameter that needs to be addressed while designing the UWB antennas [11,12]. SFF is the cross-correlation between the input signal fed to the antenna and the signal measured at a certain distance transmitted by the antenna. It is used to measure the amount of distortion produced while transmitting the signal from the antenna. The cross-correlation between the transmitted signal at a distance and the input signal is calculated at every point and the maximum value the correlation gives the SFF. Its value varies from 0 to 1 where SFF $= 0$ means minimum correlation and SFF $= 1$ gives maximum correlation. UWB

antenna with SFF ≥ 0.8 is acceptable. This parameter is usually calculated in the face to face and side by side configuration of the antenna. However, in some designs, it has been computed in different directions by varying the value of the elevation angle (θ) [13]. Lastly, group delay response of the antenna has been also extensively analyzed in UWB antenna designs to evaluate the time-domain performance of the UWB antennas. It is the change in the total phase shift with respect to the angular frequency for a UWB antenna. Preferably, group delay should be constant for the UWB antenna, but it is only possible if the phase response for the antenna is strictly linear [12].

1.4 Motivation

Since the UWB spectrum is unlicensed, and its band lies in the range of other narrow-band systems, so practically the UWB antenna radiations should not interfere with existing narrowband systems, which lie in the same bandwidth such as Wireless Local Area Network (WLAN), Institute of Electrical and Electronics Engineering (IEEE) 802.11a standard working at 5.15-5.35 GHz, and 5.72-5.82 GHz, Worldwide interoperability for microwave access (Wi-MAX) working with a frequency band of 3.3-3.6 GHz, High-performance local area network (HIPERLAN) working at 5.15-5.82 GHz, C-Band applications in the range of 4-8 GHz, International Telecommunication Union Radiocommunication Sector (ITU-R) working in the range of 7.5-8.7 GHz, and X-band downlink satellite communication band working at 7.10-7.76 GHz. Therefore, UWB antennas need to notch the above-mentioned bands without affecting its desired characteristics. Accordingly, methods that provide enhanced solutions to accomplish band notching without affecting the overall performance of UWB antennas are required. Therefore, in the proposed work the design and investigation of the planar UWB antennas with band notch characteristics have been presented.

1.5 Research Gaps

Even though a lot of work has been done in designing of UWB antennas with band notch characteristics. There are still a few challenges that need to be addressed more precisely. The performance of UWB antennas should be analyzed in both the time and frequency domain. However, in numerous designs presented in the literature, the time-domain analysis has not been addressed meticulously. Besides, only frequency-domain

results, e.g., return loss (S_{11}), voltage standing wave ratio (VSWR), gain and radiation pattern has been presented. However, in UWB systems, the transmission is done through narrow pulses, which are severely affected by dispersion. Hence, parameters such as group delay, fidelity factor, transmitted pulse, etc., should be investigated appropriately. This analysis can also predict the distortion produced by the antenna. Furthermore, in the frequency-domain analysis, the magnitude and phase response of a transmission coefficient (S_{21}) should be examined for achieving reliable UWB antenna designs with the band notch characteristics.

In most of the UWB antenna designs, the band notches do not cover the complete bandwidth for the application. So, they do not provide effective rejection of the entire frequency band for a particular application. Hence, novel UWB antennas with rectangular notch can be designed as it will be useful for achieving wideband filtering for applications like 660 MHz for X-band downlink in satellite communication and 675 MHz for WLAN. Hybrid techniques, deliberating upon the design constraints such as antenna size, accurate filtering structure, optimal biasing networks, stable gain, and radiation properties should be employed for optimizing the antenna design to meet the requirements of future UWB systems.

1.6 Objectives

The objectives of the thesis are as follows:

1. To do a comparative analysis of planar antennas with band-notch characteristics for UWB applications.
2. To design a planar antenna with band-notch characteristics for UWB applications
3. To do fabrication of the proposed antenna.
4. To perform testing and do a performance evaluation of the proposed antenna for validation of results.

1.7 Thesis Organization

This thesis is organized into six chapters as follows:

Chapter 1 provides the introduction to the UWB systems and various regulations imposed by the FCC on these systems. Further, the importance of designing efficient

UWB antennas and their requirements have been presented. Based on this discussion, the motivation, research gaps, and objectives of the proposed work have been also given.

Chapter 2 delivers an exhaustive literature review for the proposed work. In this review, different techniques for achieving band notch characteristics in UWB antennas are presented. Moreover, the challenges, simulated and measured results, distinct notched bands, and their applications are also discussed in this chapter.

Chapter 3 gives the basic design process of planar UWB antennas and UWB antennas with band notch characteristics. Various popular techniques for achieving UWB and band notch operation (e.g., CPW feeding, monopole antenna structures, microstrip couple feeding, and slot-loading) are presented in Chapter 3.

Chapter 4 presents a planar antenna with highly optimized WLAN (5.15 – 5.825 GHz) notch for UWB applications. Its thorough investigation based on the overall UWB system requirements is given. The time-domain performance of the proposed antenna is assessed using dispersion, group delay, and system fidelity factor. In addition, the excitation signal is chosen carefully based on the indoor mask for UWB systems. The filter synthesis of the notched band, equivalent circuit model, phase response of the proposed antenna is also presented. Finally, experimental results as well as comparison with state-of-the-art literature has been also presented in Chapter 4 for validation of the proposed design.

Chapter 5 provides a novel planar UWB antenna with dual rectangular notch band characteristics (i.e., 5.94 – 7.50 GHz and 8.02 – 10.46 GHz). The parametric analysis for controlling both the notches has been also presented. Time-domain analysis, filter synthesis, and measured results have been demonstrated to show the suitability of this design for UWB systems.

Chapter 6 discusses the conclusions and future scope for the proposed work.

Chapter 2

Literature Survey

UWB systems provide a distinctive solution for short-range wireless communication due to large bandwidth and low power consumption in transmission and reception. However, for these systems, designing an antenna with optimal characteristics is a major challenge because it needs to avoid interference with existing narrowband systems (e.g., WLAN, Wi-MAX, HIPERLAN, ITU-R, etc.) in the UWB spectrum. To design a suitable antenna for UWB systems, multiple techniques (e.g., Slot, parasitic element and stub loading, using fractals, metamaterials (MTMs), and electromagnetic bandgap (EBG) structures have been reported in the literature. This chapter provides a comprehensive review of the mentioned techniques for achieving band notch characteristics in UWB antennas. Moreover, the challenges, simulated and measured results, different notched bands, and their applications are also discussed.

2.1 Introduction

With the expeditious development of wireless communication systems, the technologies that provide unique solutions or add-on to the existing wireless technologies are an area of extensive research for decades, and UWB systems provide a similar solution [14]. UWB systems have plenty of research potential in different fields such as RADARS, communication, and medical applications as discussed in [15-19]. However, in these systems, the designing of an efficient antenna is a major challenge, because it needs to possess stable gain, omnidirectional radiation pattern, and wide impedance bandwidth [16,17]. So, the preliminary work in the field of UWB antenna design with mentioned characteristics has been accomplished by employing different techniques [15-24].

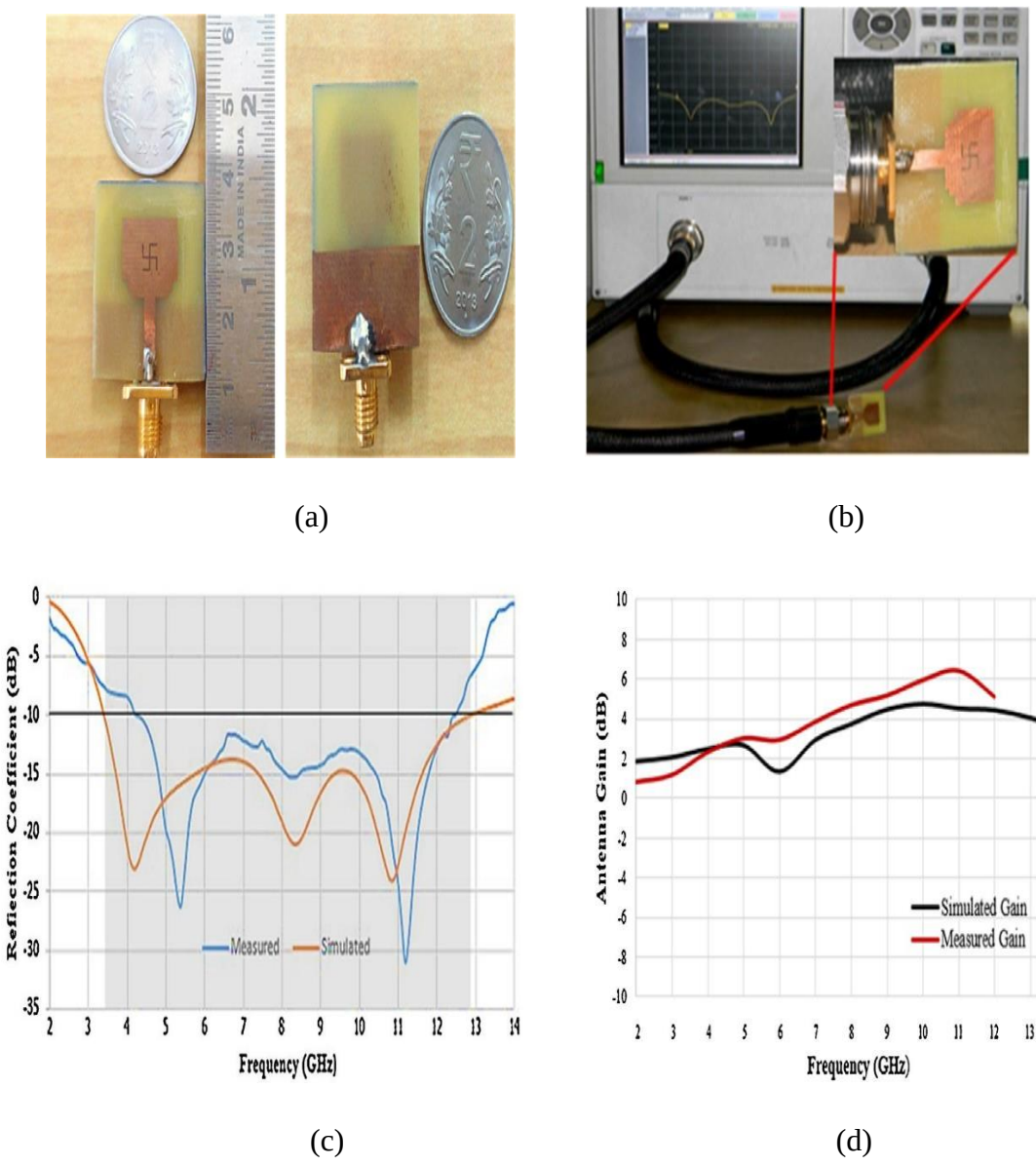

Fig. 2.1 Planar UWB antenna [19] (a) Antenna prototype (b) Vector network analyzer (VNA) setup for the measurement of the antenna (c) Simulated and measured S_{11} (d) Simulated and measured gain

The popular technique to design a planar UWB antenna is to incorporate different shapes and sizes of slots in the radiator and ground plane. This basic technique enhances S_{11}, gain, and an input impedance of the antenna. Furthermore, for achieving omnidirectional radiation pattern and wide impedance bandwidth, planar monopole structures, and co-planar waveguide (CPW) feeding technique has been extensively utilized in designing of UWB antennas [17-22]. Further, for attaining the optimal

characteristics, the combinations of these techniques have been utilized [19,24]. The design of a monopole planar UWB antenna with its measurement setup has been presented in Fig. 2.1 (a) and Fig. 2.1 (b) [19]. This antenna structure utilizes partial ground plane, feed gap, and slots. This reduces the size of the antenna without affecting its overall performance in terms of wide impedance bandwidth and stable gain, etc. This is visualized in Fig. 2.1 (c) and Fig. 2.1 (d).

Other techniques like magnetic coupling, inserting slits and modifying ground plane, n-shaped feeding structure, optimized and broadband differential feed, etc. have been used in the antenna structures for achieving the required UWB operation [20-24]. For example, in [20], the magnetic coupling between the two symmetrically organized sectorial loops have been used for the designing of the UWB antenna. In this design, many Coupled Sectorial Loop Antennas (CSLA) with dissimilar geometrical configurations are used to achieve enhanced magnetic coupling to attain the desired UWB characteristics.

The UWB spectrum is an unlicensed spectrum and its band lies in the range of other narrow-band systems. Therefore, UWB antenna radiations should not interfere with existing narrowband systems, which lie in the same bandwidth such as WLAN, IEEE 802.11a standard, and Wi-MAX, HIPERLAN, ITU-R, C-Band applications, and X-band downlink satellite communication band [25-33]. Thus, UWB antennas need to notch the above-mentioned bands without affecting its desired characteristics. Fig. 2.2 (a) presents a planar UWB antenna with triple-band notch characteristics, i.e., Wi-MAX, WLAN, and X-Band satellite communication. In this design, UWB operation has been accomplished by using two round slots in the beveled radiating patch. Furthermore, for achieving the band notch characteristics, three-round shape slots and two C shape slots have been etched in the radiating patch and the beveled ground plane respectively. Additionally, it has been observed that the overall performance of the UWB antenna has not been affected while achieving band notch characteristics in the UWB range as represented in Fig. 2.2 (b) and Fig. 2.2 (c) [25].

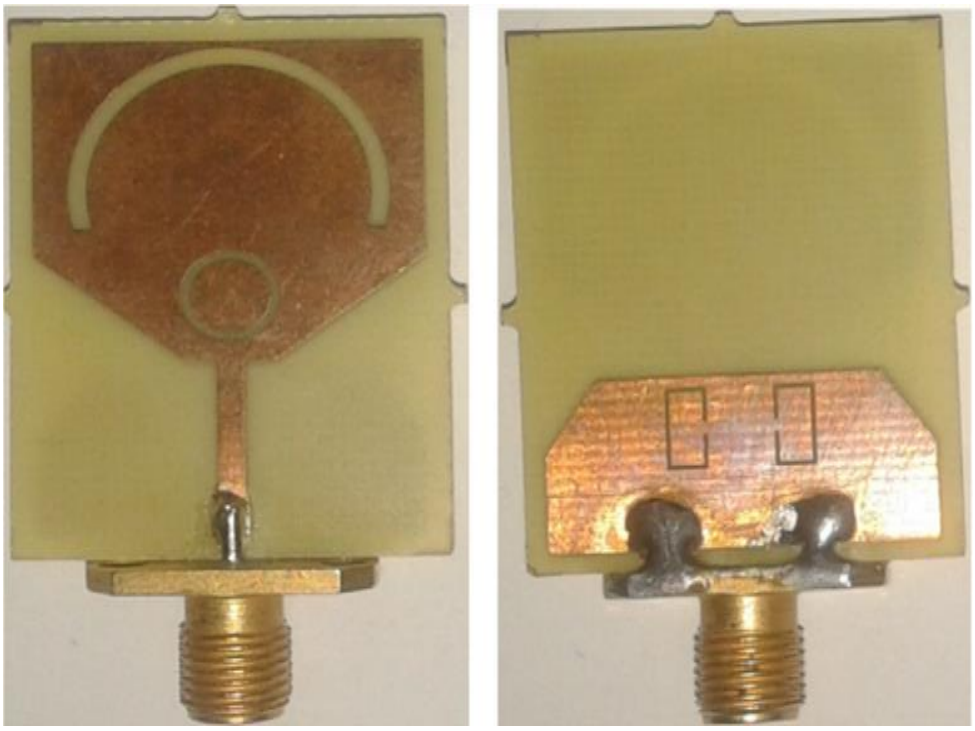

(a)

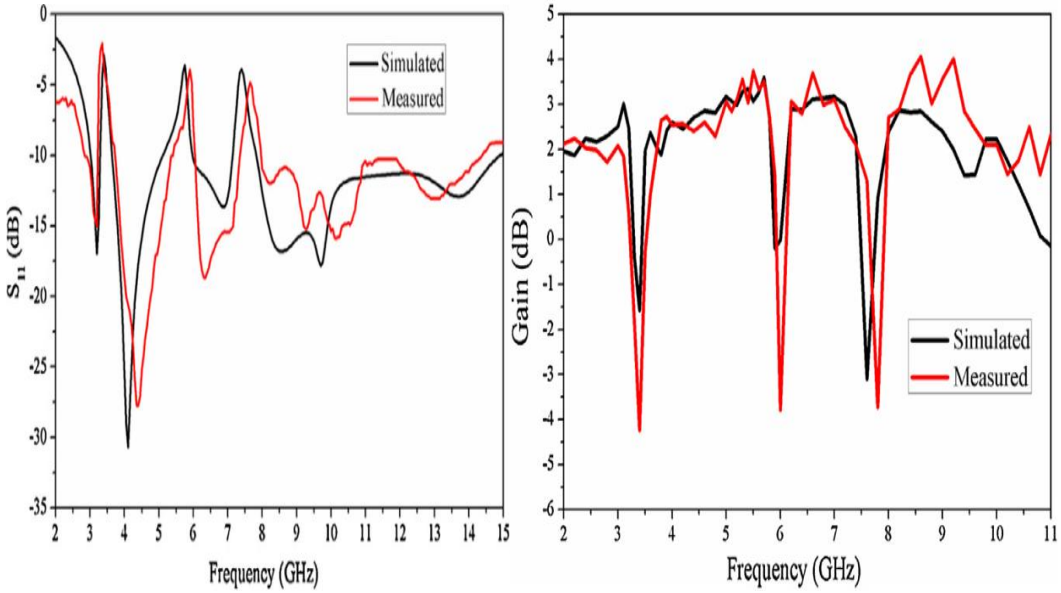

(b) (c)

Fig.2.2 Planar UWB antenna with three-notch bands (a) Antenna prototype (b) Simulated and measured S_{11} (c) Simulated and measured gain [25]

Band notch characteristics in UWB antennas are comparable to the designing of filters at the very high frequency. To describe the band notch characteristics of UWB antennas, different equivalent circuits have been investigated in the literature [26-32]. Some of the popular equivalent circuits are Foster canonical forms [27], impedance model [28], macro model [29], and lumped equivalent circuit model or an equivalent LC model [30, 31] and are given in Fig. 2.3.

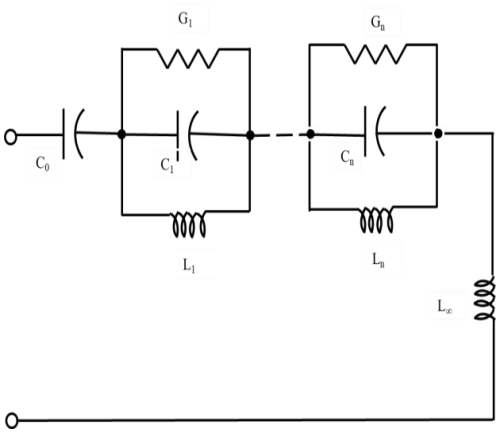

(a)

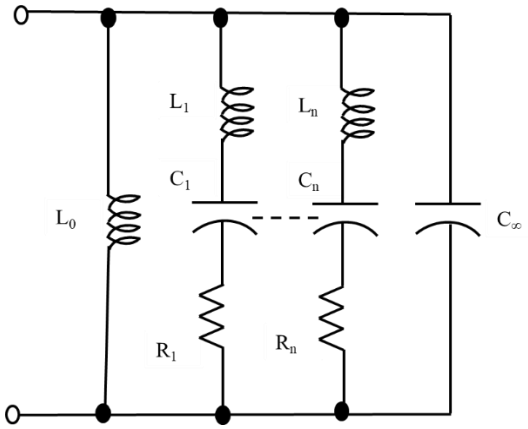

(b)

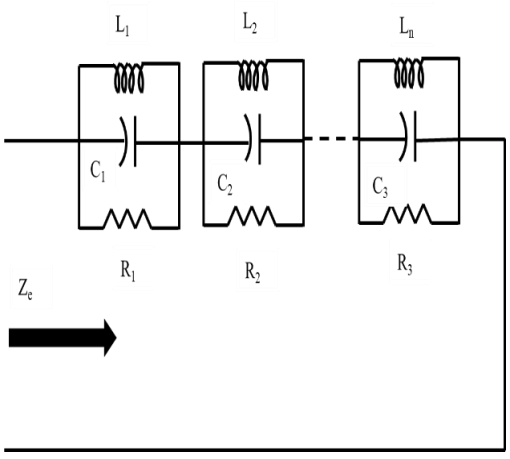

(c)

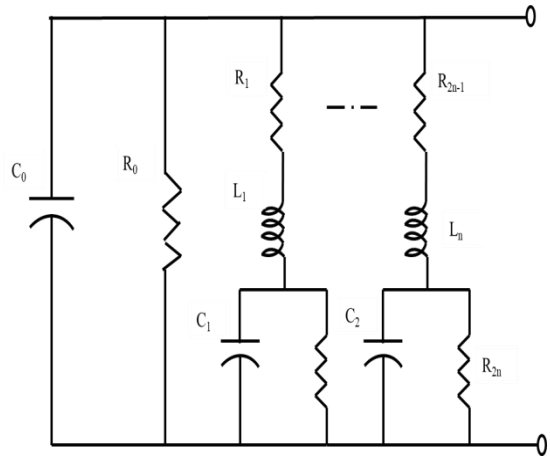

(d)

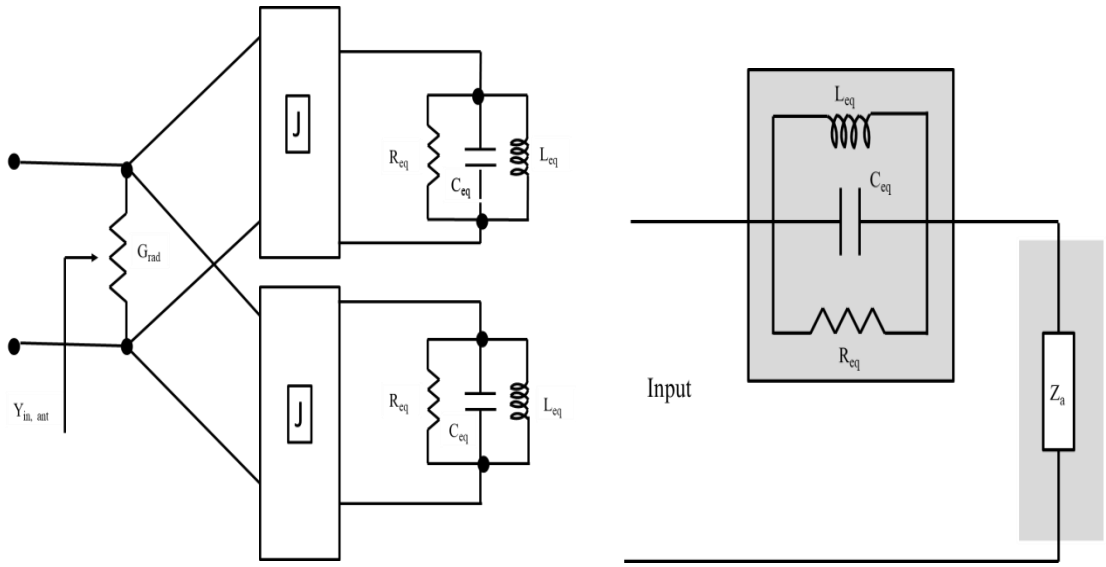

(e) (f)

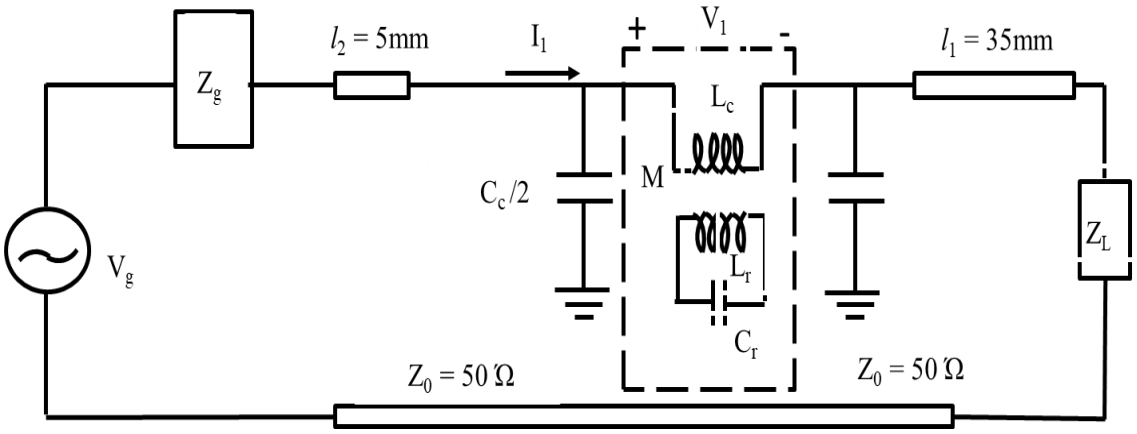

(g)

Fig. 2.3 Equivalent circuits of UWB antennas (a) Foster canonical form for electrical antennas [27] (b) Foster canonical form for magnetic antennas [27] (c) Impedance model for radiating patch of UWB antenna [28] (d) Equivalent circuit of macro model [16] (e) Lumped equivalent circuit model of the antenna [30] (f) Equivalent LC circuit model of the antenna [31] (g) Equivalent circuit of band suppressed cone type monopole antenna [32].

These models do not provide the complete solution of the operational characteristics of the UWB antenna due to the approximations of the electromagnetic properties of the antenna. Out of these techniques, even the best technique gives at least a 30% variation

in the simulated results when matched with the numerical results of the equivalent circuit model for the rejection band [32]. So other methods, which provide enhanced solutions to accomplish band notching without affecting the overall performance of UWB antennas are also available in the literature.

The chapter is organized into seven sections, and each section gives a comprehensive review of the different techniques used for achieving band notch characteristics in UWB antennas. Section 2.1 provides the introduction of the band-notched UWB antennas. Section 2.2 describes the role of slots, stubs, and parasitic elements. Section 2.3 represents the different types of fractal techniques and Section 2.4 describes the use of MTMs. Section 2.5 gives the detail of EBG structures and Section 2.6 describes the different types of switching techniques. Furthermore, Section 2.7 holds the summary. Additionally, a table of referenced antennas providing details about different techniques, the frequency range of the notch band and their application are given. The simulated and measured results are also provided for different techniques of antenna designs under study.

2.2 Slot, Stub and Parasitic Element Loaded Band-Notched UWB Antennas

UWB antennas require wide impedance bandwidth with band notch characteristics. The easiest way to accomplish this is by loading slots, stubs, and parasitic elements in the radiating patch and ground plane. Loading the slots in the radiating patch causes a reduction in patch size that changes the resonating frequency which leads to multi-band operation [33]. Similarly, it can also be utilized for calculating the notch frequency function in the UWB antennas.

For filtering out the narrow frequency bands, various types of slots are used such as U-slot, L-slot and ring slot, etc. Moreover; the loading of slots in the conducting patch element can cause meandering of the surface current distribution paths of the exciting patch and results in lowering the resonating frequency [34-36]. These antennas are extensively used because of their simple configuration and affordable planar technology.

Table 2.1 Notch frequency for different types of slot loaded antennas [30-38]

Slot Type	**Notch frequency**	**Parameters in notch frequency**
C slot	$F_n = \frac{C}{2L\sqrt{\varepsilon_{eff}}}$	F_n = Notch frequency L = Length of the slot L = $\frac{\lambda_g}{2}$ λ_g = Guided wavelength C = Speed of light ε_{eff} = Effective dielectric constant $\varepsilon_{eff} = \frac{\varepsilon_r + 1}{2}$
U-slot	$F_n = \frac{C}{2(L_s + W_s)\sqrt{\varepsilon_{eff}}}$	L_s = Length of U-slot W_s = Width of U-slot
L-slot	$F_n = \frac{C}{(L_1 + L_2 + h_b)\sqrt{\varepsilon_{eff}}}$	L_1 = Horizontal length L_2 = Vertical length h_b = Substrate height
Small strip	$F_n = \frac{C}{(4L_s\sqrt{e_{eff}})}$	L_s= Length of the strip

Table 2.1 provides the expressions for calculating the notch frequency for different types of slot antennas [30-38]. The expressions of notch frequency in Table 2.1 are dependent on the length and width of the slot as well as the effective dielectric constant of the antenna substrate. Besides, the slot on the patch can be analyzed with the help duality principle of the dipole and slot antenna. The equivalent circuit of the slot-loaded patch is given in Fig. 2.4 [39] in which the values of R_1, L_1, and C_1 depend upon the effective dielectric constant, Q, and the thickness of the substrate.

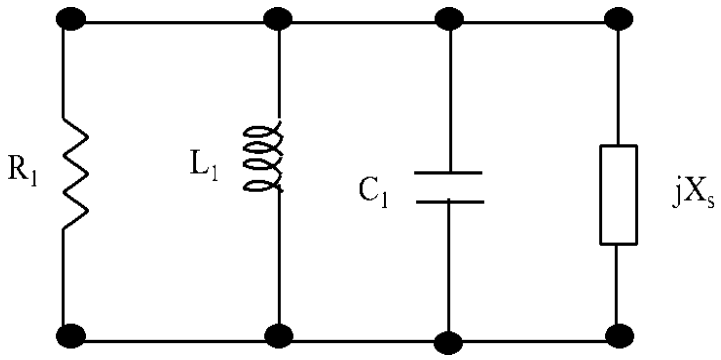

Fig. 2.4 An equivalent circuit of the slot-loaded patches [39]

From the equivalent circuit of Fig. 2.4, the input impedance of the slot is given by:

$$Z_s = R_s + j X_s \qquad (2.1)$$

Where R_s and X_s are the real part and the imaginary part of the input impedance (Z_s). The total input impedance (Z_{in}) of the slot-loaded patch is given by:

$$\mathrm{Z_{in}} = [\mathrm{R_1} - 1 + \mathrm{j}\,\omega\,\mathrm{C_1} + (\mathrm{j}\,\omega\,\mathrm{L_1}) - 1 + (\mathrm{j}\,\mathrm{X_s}) - 1] - 1 \qquad (2.2)$$

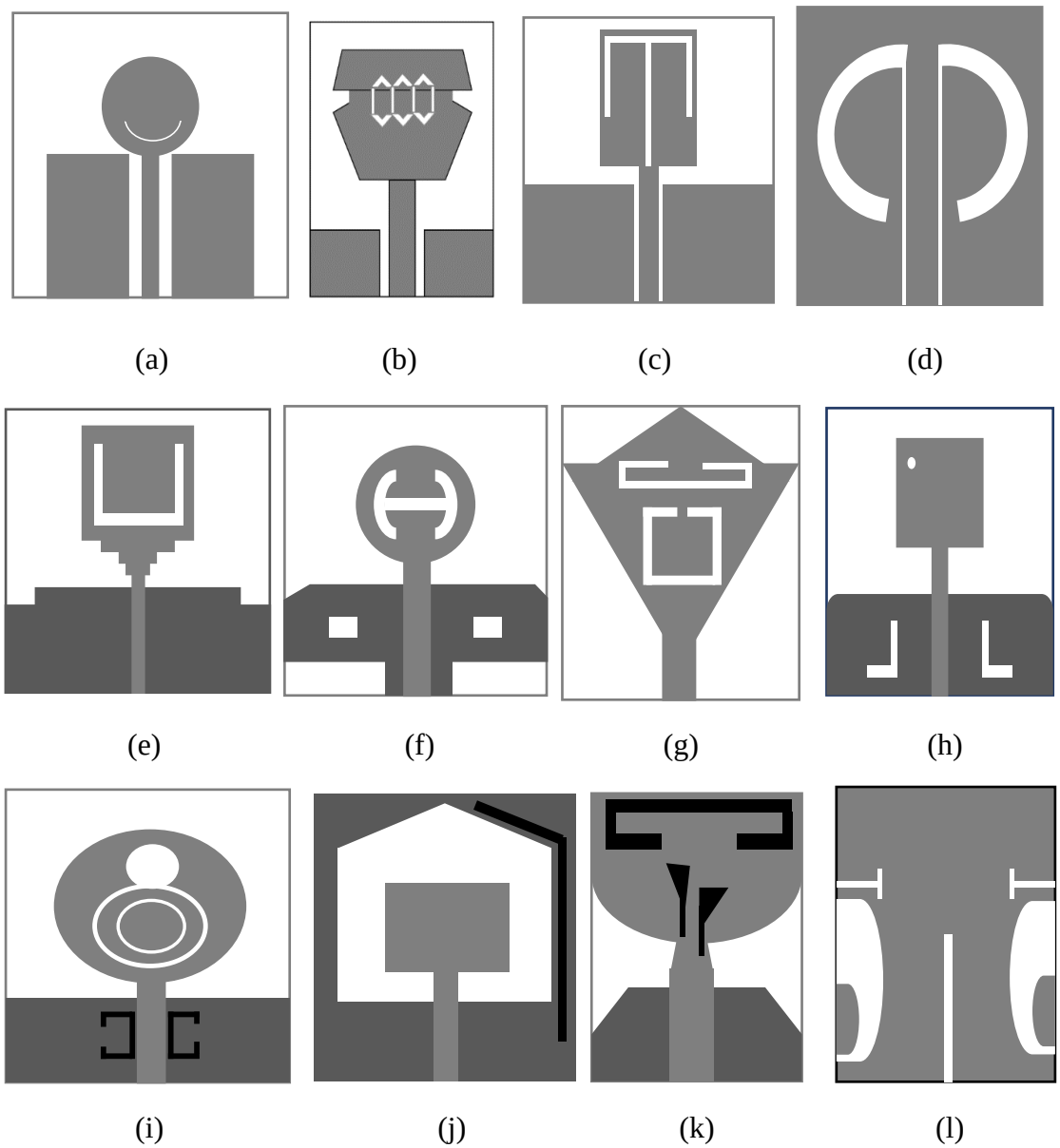

(a) (b) (c) (d)

(e) (f) (g) (h)

(i) (j) (k) (l)

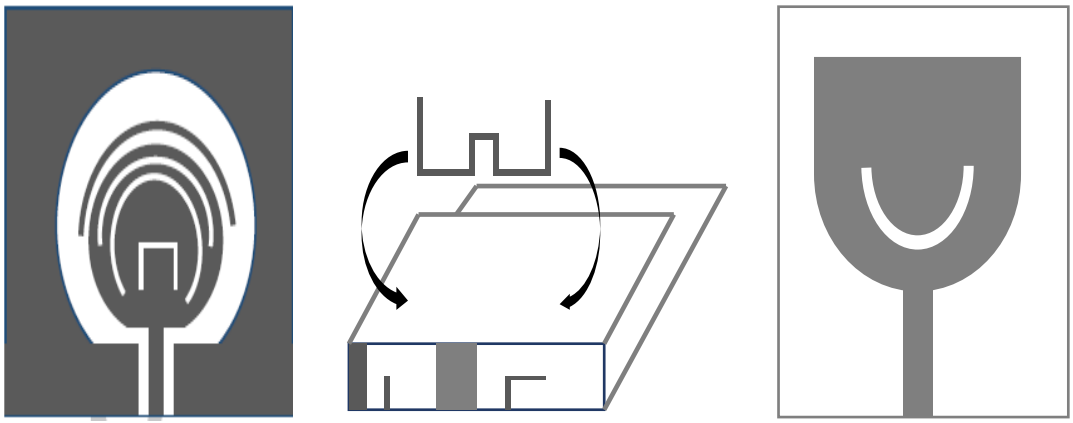

(m) (n) (o)

Fig. 2.5 Different types of slot, stub and parasitic element loaded antennas (a) Arched slot antenna [34] (b) Hexagonal slot antenna [42] (c) Spiral slot antenna [43] (d) Ring slot antenna [40] (e) U-slot antenna [36] (f) H-slot Antenna [45] (g) C shaped slot antenna [38] (h) L-slot antenna [26] (i) Elliptical ring slot (ERS) antenna [47] (j) Parasitic element loaded antenna [53] (k) Trapezoidal stub antenna [54] *(l)* T shaped slot antenna [51] (m) Hybrid slot antenna [55] (n) W shaped slot antenna [44] (o) Circular slot antenna [50]

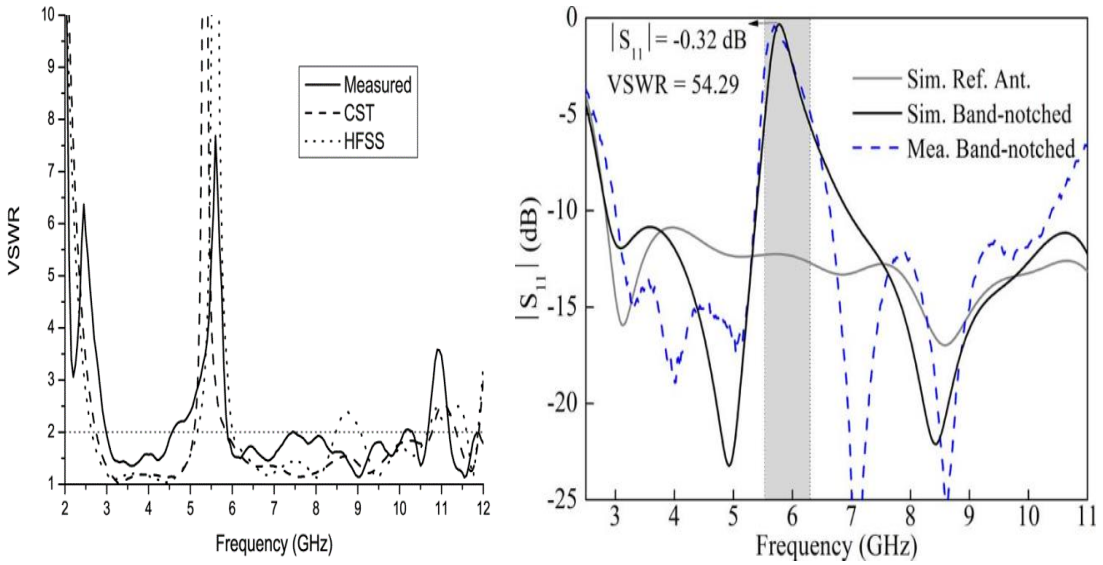

(a) (b)

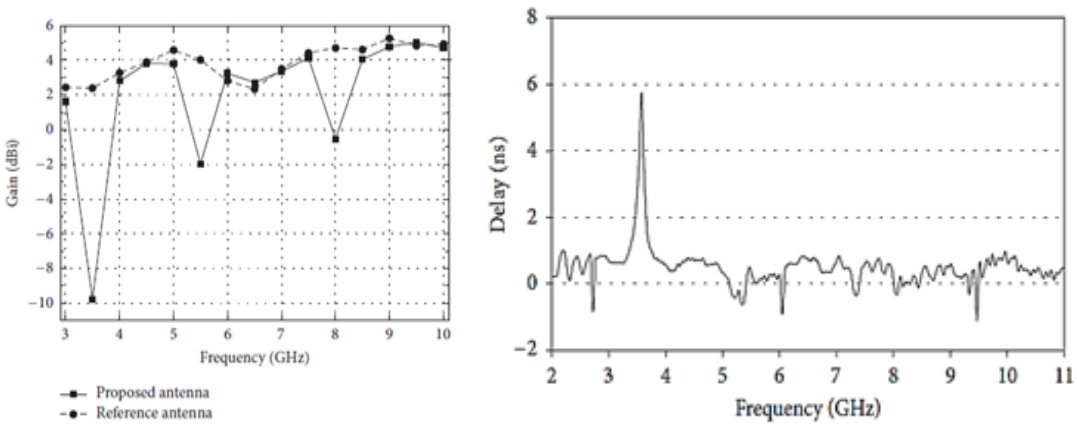

(c) (d)

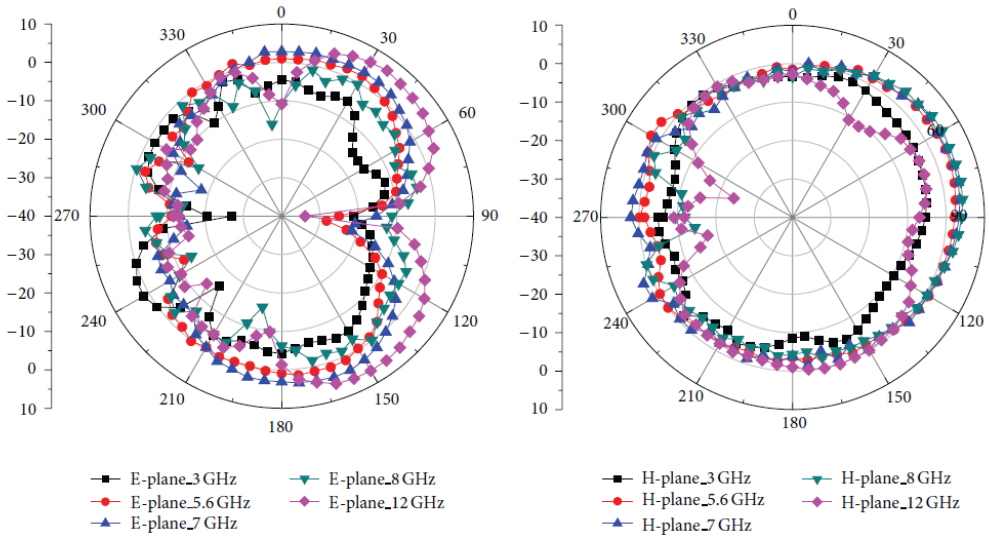

(e)

Fig. 2.6 Different types of simulated and measured results in planar UWB band-notched antennas using slots (a) Simulated and measured and VSWR [34] (b) Simulated and measured S_{11} [31] (c) Gain versus frequency graph [49] (d) Measurement of group delay [53] (e) E-plane and H-plane radiation pattern [55]

Using these basic design equations, different UWB antennas have been designed with slots, parasitic elements, and stubs, as presented in Fig. 2.5, to provide the band notching characteristics with minimum interference [33-57]. Likewise, in Fig. 2.5 (a) the UWB antenna with an arched slot is presented. This design provides band notch for the WLAN band as depicted in Fig. 2.6 (a). In this design, the band notch function is controlled by the position of the slot. Furthermore, the notch frequency band can be

altered by changing the width and length of the slot [34]. Also, Fig. 2.5(d) represents the UWB antenna where

Table 2.2 Different notched bands and their application using a slot, parasitic and stub loaded antennas

Reference	Type of slot	Notch Band frequency (GHz)	Notch band Application
[26]	L-Slot	3.5	Wi-MAX
[34]	Arched Slot	5.15-5.825	WLAN
[36]	U-slot	5.15-5.35 and 5.725-	WLAN
[38]	C shaped slots	3.38-3.82 and 5.3-5.8	Wi-MAX and WLAN
[42]	Hexagonal	5-5.7	WLAN
[43]	Spiral	3.57, 5.12, and 8.21	Wi-MAX, WLAN, and Satellite downlink X-Band
[44]	W shaped Slot	5.08-6	WLAN
[45]	H Slot	3.3-3.6 and 5.1-5.9	Wi-MAX and WLAN
[46]	L shaped slits	5	WLAN
[47]	Elliptical ring slot (ERS)	3.3-3.8, 5-6 and 7.1-7.9	Wi-MAX, WLAN, and Satellite downlink X band
[48]	Open-end slot	5.15-5.825	WLAN
[49]	Nonuniform width slot	3.5, 5.5 and 8.1	Wi-MAX, WLAN, and Satellite downlink X-Band
[50]	Circular Slot	5.5	WLAN
[51]	T shaped slot	5.2	WLAN
[52]	C shaped annular ring	5.1–5.9	IEEE 802.11a and HIPERLAN/2
[53]	Parasitic Element	3.31–3.84	Wi-MAX
[54]	Trapezoid s and a C-shaped slot	3.5 and 5.2-5.8	Wi-MAX and WLAN
[55]	Hybrid Slots	8.01-8.55, 5.15-5.35, 5.75-5.85, and 7.25-7.75	ITU band, WLAN, and X-Band satellite signals

better impedance matching can be achieved between the free space and the transmission line over the wider bandwidth by gradually altering the width of the radiating slot [40]. The radiating antenna with a slotted plate providing the enhanced stopband characteristics with improved control using electromagnetic coupling is presented in [41]. The parasitic element and stub in this antenna design provide enhanced band notch

function in the desired band. Similarly, different types of slots (e.g., L-slot [26], arced slot [34, 35], U-slot [36], Ring slot [40], Hexagonal slot [42], spiral slot [43], W shape slot [44], H-slot [45], Elliptical ring slot (ERS) [47] and T shape slot [51]) have been presented in the literature. In addition to these designs, Fig. 2.5 (m) shows an antenna design using hybrid slots to achieve dual, triple, and quad-band notching in the UWB range. These slots enhance the notch frequency band and radiation characteristics of the antennas as compared to antenna structures possessing a similar type of hybrid slots as reported in [55-57]. Fig. 2.6 (e) represents the E and H plane radiation pattern of an antenna with hybrid slots, and it can be visualized that the antenna provides an omnidirectional radiation pattern in both planes. Table 2.2 represents the different types of notch bands using slot loaded, parasitic elements, and stub loaded antennas.

2.3 Fractal Geometry-Based Band-Notched UWB Antennas

The initial usage of the fractal geometry-based antenna was in the design of frequency selective surfaces (FSS) to provide multi-band operation and miniaturization in the antenna structure. Apart from it, they are also used to improve the bandwidth and impedance of the antenna [58]. These characteristics of fractal geometry prove to be useful in designing of UWB antenna with band notch characteristics. Even though a lot of fractal geometries have been reported in the literature, but Sierpinski gasket and carpet, Koch snowflakes/islands, Hilbert Curve, and fractal trees are the most popular fractal geometries. Fig. 2.7 represents some common fractal geometries of antennas, and the formation stages of different fractal structures are shown in and Fig.2.8. Mathematically, these structures can be created using the iterated function system (IFS) which is a flexible system for generating fractal structures, and Fig.2.9 represents the different stages of the fractal structure using IFS code. Furthermore, Fig.2.10 shows the final fractal structure using the IFS code of the Sierpinski gasket.

Based on the literature, different planar antennas using fractal techniques have been discussed in this section, for example; Fig 2.11 (a) represents a Koch fractal slot, which is used to achieve frequency notch function in UWB antenna [59]. In this design, the band notching and wideband impedance matching have been accomplished by employing a half-

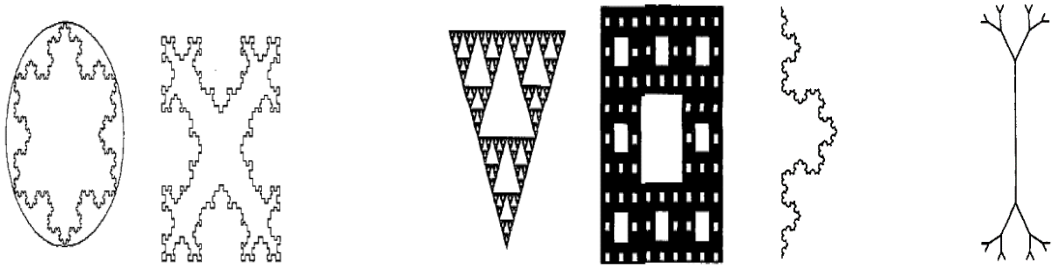

(a) (b) (c)

Fig. 2.7 Common fractal geometries [58] (a) Koch snowflakes/islands (b) Sierpinski gasket and carpets (c) Fractal trees

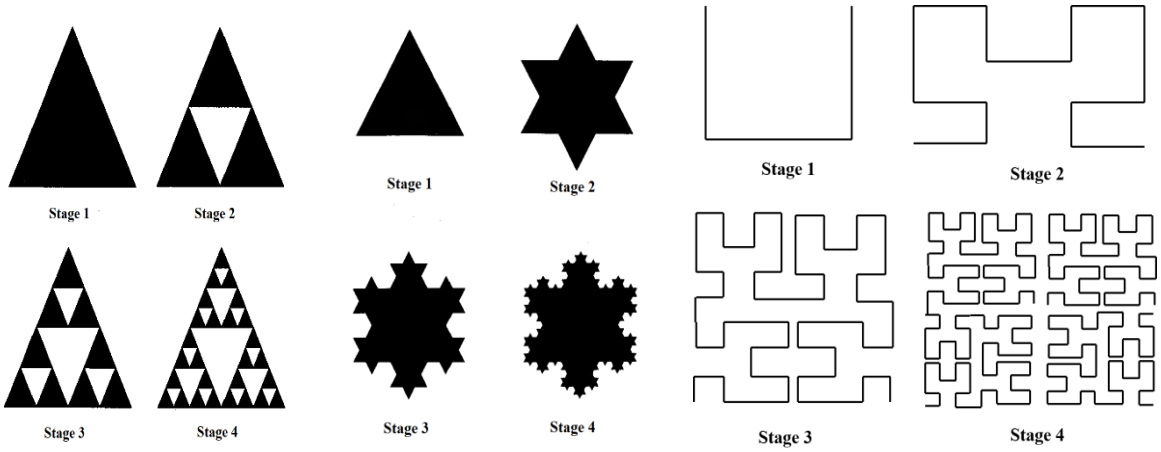

(a) (b) (c)

Fig. 2.8 Construction stages of different fractal structures [58] (a) Sierpinski gasket fractal (b) Koch snowflake fractal (c) Hilbert curve fractal

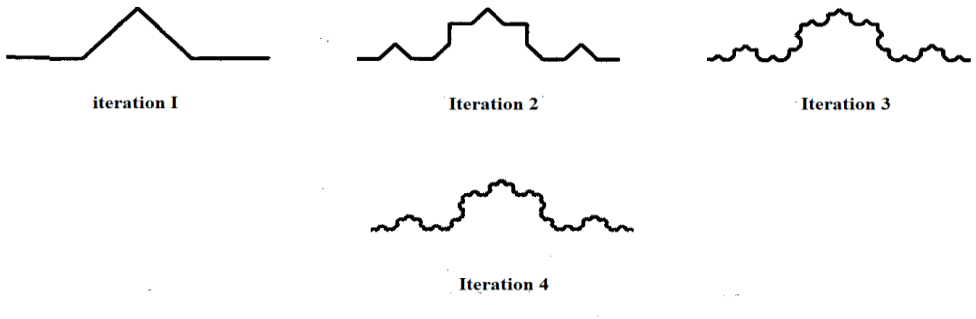

Fig. 2.9 Four stages of construction of the Koch curve using IFS [58]

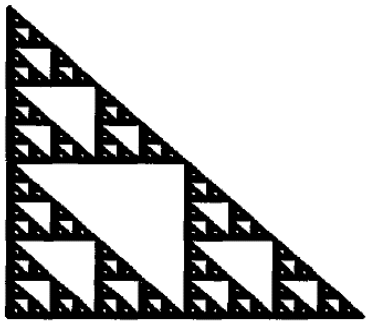

Fig. 2.10 Sierpinski gasket final structure using IFS code [58]

wave resonant structure. This structure is designed by embedding the Koch curve fractal in the conventional wide slot of this design. Additionally, the length of the structure can be changed to tune the central notch frequency. Whereas in [60], the Koch fractal geometry with C shape slots is used to achieve the band notching characteristics, desired miniaturization, and wideband operation. Moreover, the design achieves better isolation between the antenna monopoles using ground stubs. Similarly, the combination of the Koch curve fractal and T shaped stub has been used in [61] to achieve the dual-band notching characteristics in the UWB range. Also, the design in [61] achieves the additional notch bands due to the interaction between the Koch curve fractal and T stub.

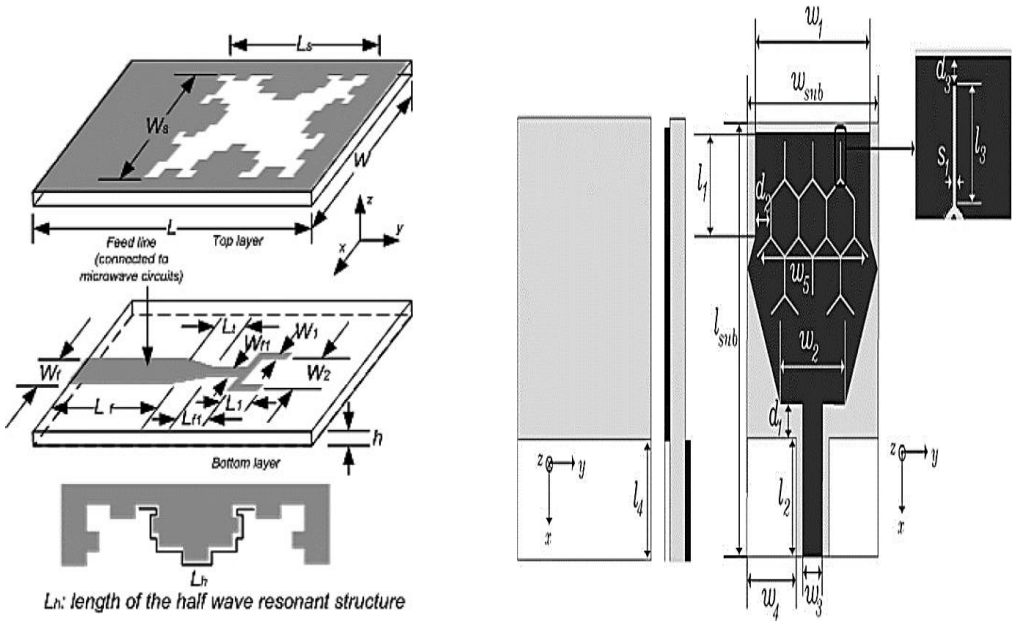

(a) (b)

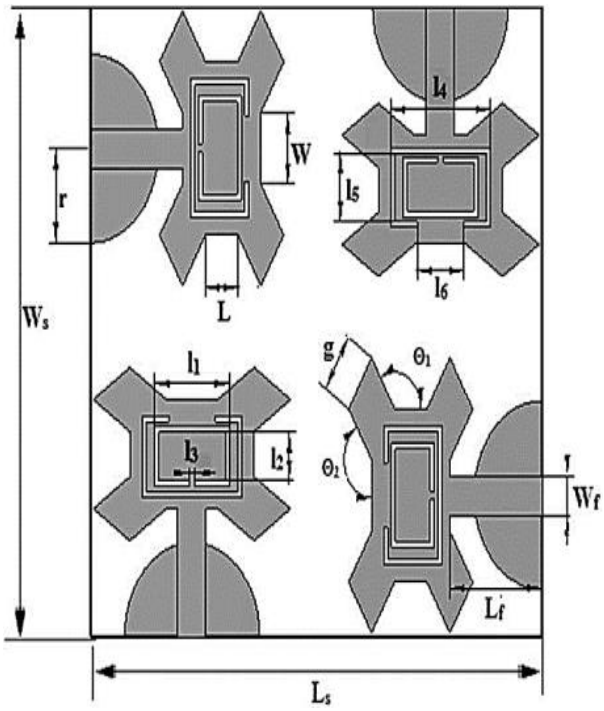
Ws
r
W
L
l4
l5
l6
l1
l3
l2
g
Θ1
Θ2
Wf
Lf
Ls

(c)

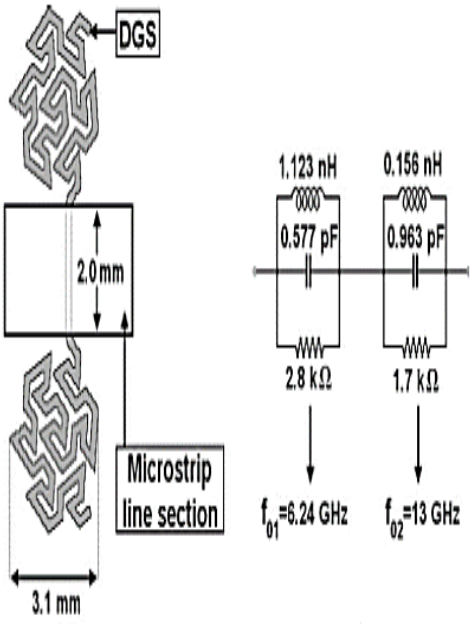
DGS
2.0 mm
Microstrip line section
3.1 mm
1.123 nH
0.577 pF
2.8 kΩ
0.156 nH
0.963 pF
1.7 kΩ
f01=6.24 GHz
f02=13 GHz

(d)

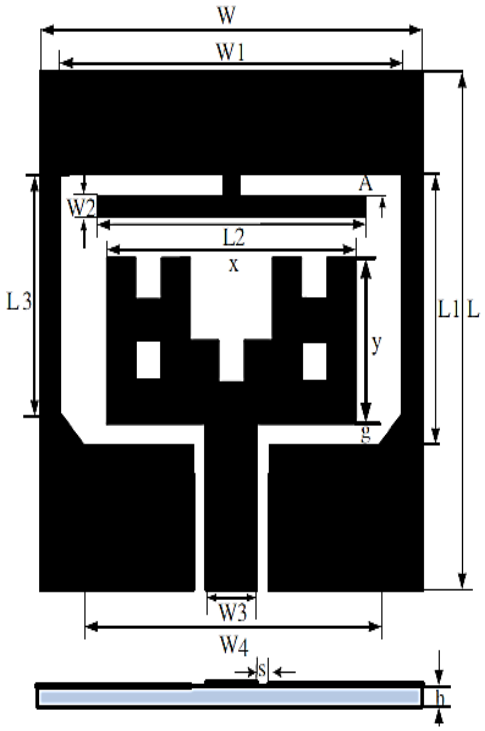
W
W1
W2
A
L2
x
L3
y
L1
L
g
W3
W4
s
h

(e)

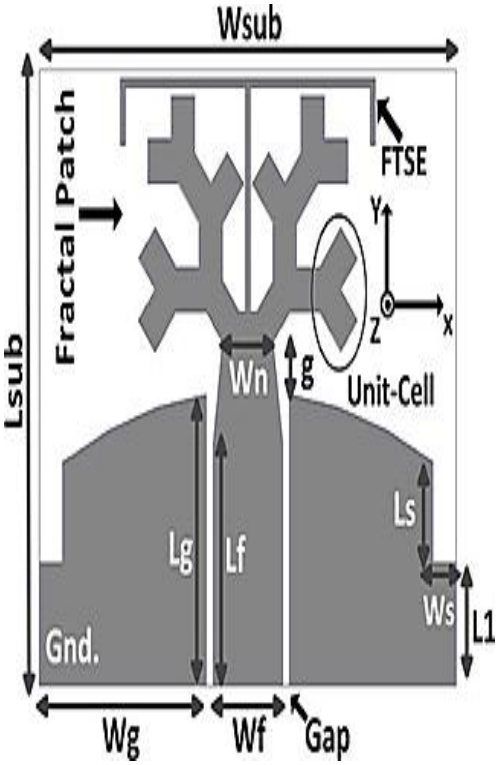
Wsub
Lsub
Fractal Patch
FTSE
Y
Z
X
Wn
g
Unit-Cell
Ls
Lg
Lf
Ws
L1
Gnd.
Wg
Wf
Gap

(f)

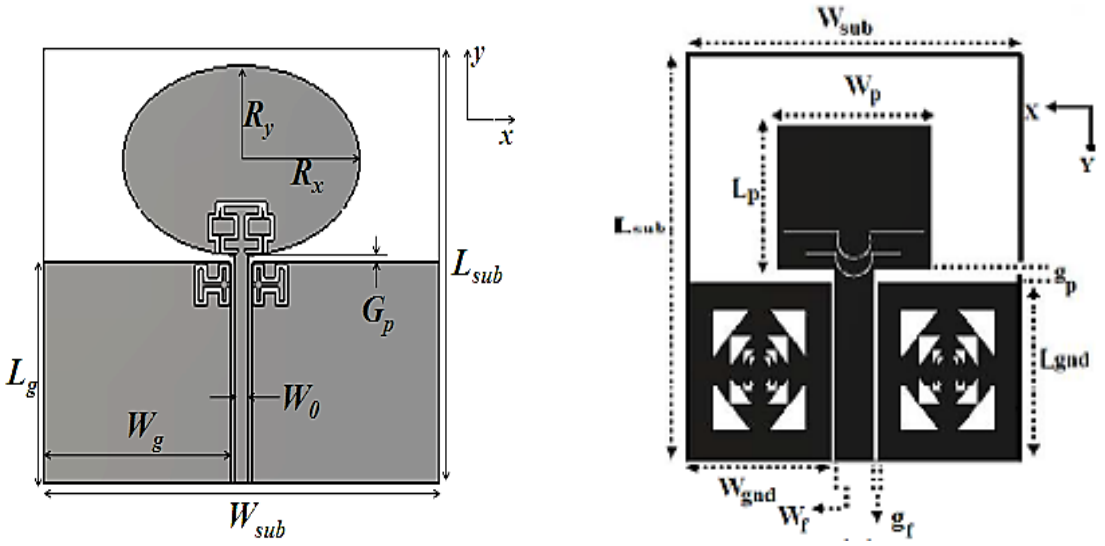

(g) (h)

Fig. 2.11 Different UWB band-notched designs with fractals (a) Koch curve [59] (b) Fractal binary tree slot [69] (c) 4 element Sierpinski knopp fractal [66] (d) Gosper fractal-shaped [70] (e) Cantor set fractal with T shaped stub [71] (f) Fractal radiating patch in which a folded T-shaped element (FTSE) is embedded [74] (g) Hybrid fractal Slot [76] (h) Modified crown-square shaped fractal slots in the ground plane with omega slot [75]

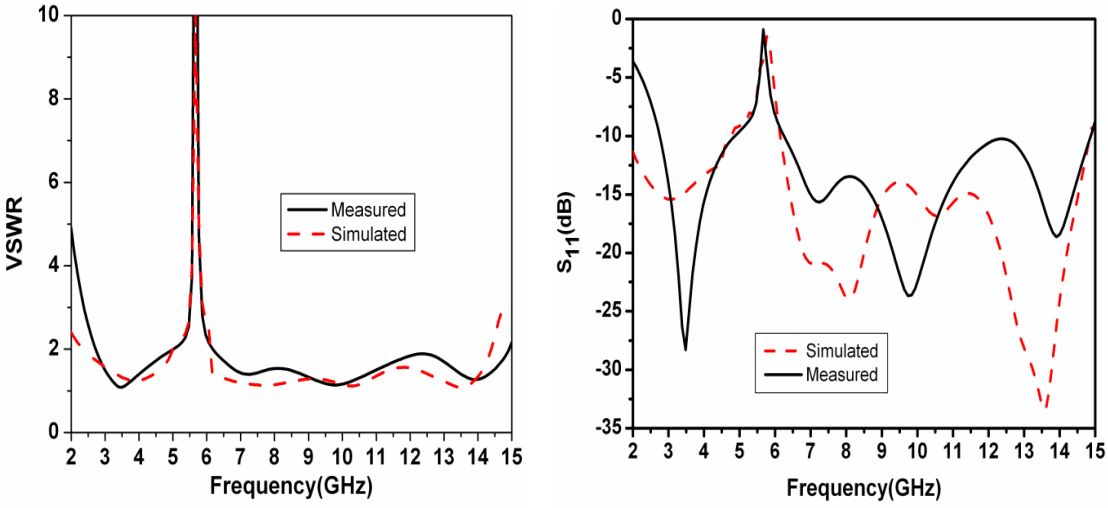

(a) (b)

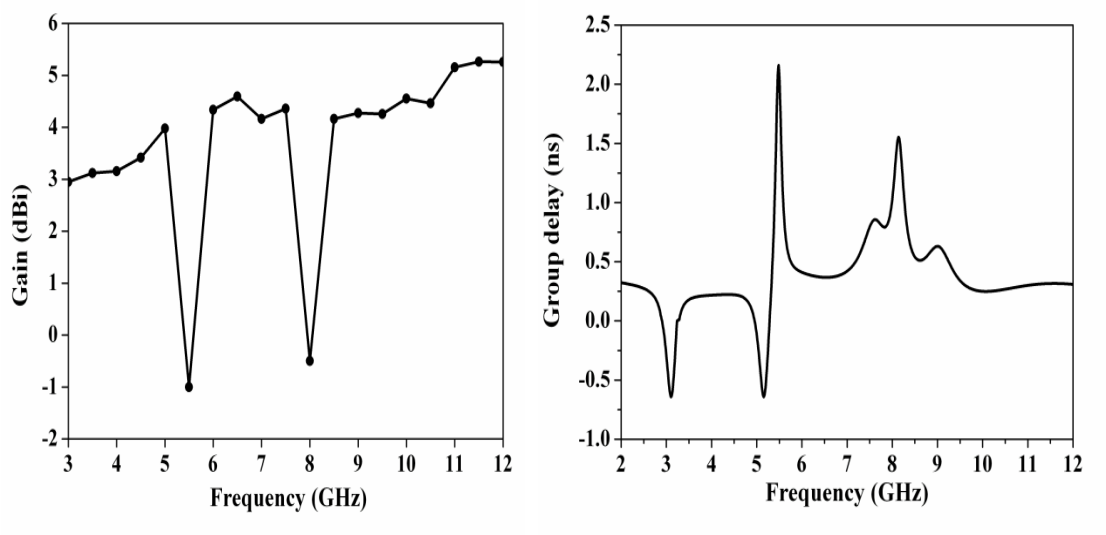

(c) (d)

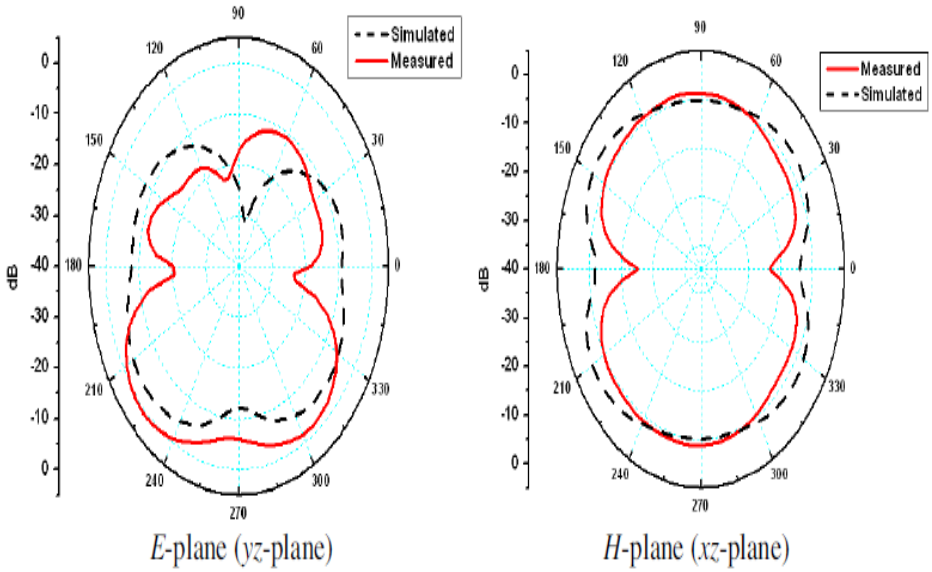

(e)

Fig. 2.12 Different types of simulated and measured results in the planar UWB band-notched antennas using fractal structure (a) Simulated and measured VSWR characteristics [62] (b) Simulated and measured S_{11} [62] (c) Simulated and measured peak gain [67] (d) Measured group delay [67] (e) E and H plane radiation pattern [62]

The Sierpinski gasket and carpet fractal slots are used to achieve the band notches in the UWB range with the miniaturization of the radiating patch as well as the ground

plane of the antenna [62-66]. Additionally, these fractal geometries can be used with or without slots for achieving the notch band operation. For example, a meandered slot [62] and Y shaped slots [63] have been used with the Sierpinski carpet fractal radiating element. From a meandered shape slot, the single band-notch characteristic in the frequency range of 5.15-5.825 GHz is achieved, and also the VSWR, $S_{11,}$ and radiation pattern results are acceptable, which are shown in Fig. 2.12 (a), Fig. 2.12 (b) and Fig.2.12 (e) respectively. Similarly, in [64] a reverse U-slot has been used with a modified Sierpinski square fractal (MSSF) in the antenna structure for realizing the band notching characteristics. In this antenna, a very simple configuration and a slot are used in the feed line to improve the radiation and band notching of the antenna. Whereas in [65], the Sierpinski gasket fractal loaded antenna using two different slots, i.e., U-slot and elliptical slot are used to achieve the dual-band notching in the UWB spectrum and also, fractal geometry has been used to provide the better impedance at lower frequencies. Likewise, Fig.2.11 (c) represents a novel dual notched multiple input and output (MIMO) antenna using Sierpinski Knopp fractal geometry [66], and this antenna possesses a very low mutual coupling in the entire UWB band. Moreover, it uses the complementary split-ring resonator (CSRR) to get the band notches.

Hilbert curve slot is another fractal technique, which is used extensively for miniaturization of the antenna structures. Equally, it can be used to achieve band notch characteristics in the UWB antenna as reported in [67, 68]. In [67] Hilbert curve geometry with space-filling characteristics has been used in the radiating patch and ground plane of the design for miniaturization of UWB antenna structures without affecting characteristics such as gain and group delay, which are shown in Fig.2.12 (c) and Fig. 2.12 (d) respectively. These results show that gain reduces to a minimum value at the notch bands, i.e., 5.15-5.85 GHz and 7.9-8.4 GHz, as well as the group delay, is more than 1ns for mentioned bands as required for UWB systems. Similarly, in [68], Hilbert fractal geometry has been used with a parasitic resonator for achieving single band notch characteristics. In both designs, fractal geometry provides excellent miniaturization in antenna structure without any effect on the overall performance of the antenna.

The literature reveals that fractal binary tree slot is also very popular fractal geometry in UWB antennas [69-76]. So, this geometry of fractal binary tree slot has been used in the UWB antenna to attain the dual-band notching as displayed in Fig. 2.11 (c) which is given in [69]. In this design, the fractal slot having four iterations in a binary tree with branch splitting angles at 120^{o} and the slot is subtracting from the radiating element which provides the dual-band notching in the UWB range. This band notching is achieved due to the change in the current distribution of the overall structure. Further, there are so many other fractal geometries used in radiating element and ground plane to achieve the band notching in UWB antennas such as Gosper fractal-shaped [70], Cantor Set fractal with T-shaped stub [71, 72], Circular Apollonian fractal shaped [73], a fractal radiating patch with a folded T-shaped element (FTSE) [74], Modified crown-square shaped fractal slots with the omega slot [75], Hybrid fractal slots [76] and Modified fractal slot [77].

All these modified fractal slots provide certain advantages over the traditional fractal geometries. For example, Fig.2.11 (d) shows a Gosper fractal geometry that provides better sharpness factor and selectivity for the designed band-reject filter without affecting the size of the antenna [70], Fig. 2.11 (e) shows the use of the Cantor set fractal with a T shaped tuning stub [71], and Fig. 2.11 (f) shows the use of FTSE for providing the band notch function [74].

Similarly, Fig. 2.11 (h) shows that a crown square-shaped fractal has been embedded in the ground plane of the antenna to provide enhanced impedance bandwidth [75]. In the same design, dual omega slots have been used in the radiating element to provide dual-band notching in the UWB range. Besides, this antenna possesses an omnidirectional radiation pattern and a stable gain. The hybrid fractal has also been utilized for achieving dual band notches in the UWB range [76] as shown in Fig. 2.11 (g). This antenna uses the combination of the Euclidean curve and Moore curve to generate a hybrid fractal and this fractal geometry is etched from the radiating element as well as CPW feeding is used in the antenna to provide notch band at the frequencies of 5.5 GHz and 8.1 GHz. Table 2.3 represents the different fractal techniques, notch band frequencies, and their applications.

Table 2.3 Different notched bands and their applications using distinct fractal geometry

Reference	Type of fractal	Notch Band frequency (GHz)	Notch band Application
[59]	Koch fractal slot	4.65 to 6.40	WLAN and C Band
[60]	Koch Fractal with C shaped	5.5	WLAN
[61]	Fractal Koch with T shaped stub	3.5 and 5.8	Wi-MAX and WLAN
[62]	SIERPINSKI CARPET Fractal	5.15-5.825	IEEE802.11a and HIPERLAN/2
[63]	Sierpinski carpet fractal	5.15-5.825	IEEE802.11a and HIPERLAN/2
[64]	Modified Sierpinski square fractal antenna	5 – 6	WLAN
[65]	Sierpinski fractal with an elliptical slot	5.2 and 7	WLAN and RFID Band
[66]	4 Element Sierpinski Knopp fractal	3.5 and 5.4	Wi-MAX and WLAN
[67]	Hilbert curve slots	5.15-5.85 and 7.9-8.4	HIPERLAN/2 and X-Band uplink satellite communication systems
[68]	Modified Hilbert Fractal Parasitic Resonator	7.89-8.83	X-band satellite communication
[69]	Fractal binary tree slot	5.65 and 9.9	WLAN and X Band
[71]	Cantor set fractal with T shaped stub	5.0-6.3 and 5.1 -5.9	HIPERLAN/2 and IEEE 802.11a
[73]	Circular Apollonian fractal shaped	5.125-5.825	IEEE802.11a and HIPERLAN/2
[74]	Fractal radiating patch in which a folded T-shaped element (FTSE) is embedded	3.3-4.2	Wi-MAX (IEEE 802.16) and C-band systems
[75]	Modified crown-square shaped fractal slots in the ground-plane with omega slot	5.5 and 7.5	IEEE802.11a and HIPERLAN/2 and X-band for satellite communication
[76]	Hybrid Fractal Slots Moore and Euclidean boundary curve)	5.5, 6.8, and 8.1	WLAN and X-Band satellite communication
[77]	Modified fractal slot	5.59 - 6.09	WLAN

2.4 Metamaterials Based Band-Notched UWB Antennas

From the last decade, a lot of work was done on MTMs for the enhancement of antenna parameters (i.e., radiation efficiency, impedance bandwidth, and gain, etc.) [78,79]. Similarly, MTMs can be utilized to achieve and enhance band notch characteristics in UWB antennas. The MTMs are the artificial periodic structures which are made up of

sub-wavelengths elements which bring the structures at negative permittivity and permeability of a certain resonant frequency, e.g. Split ring resonators (SRR) and complementary split-ring resonators (CSRR) are the most common MTM structures that have been described by the researchers for achieving band notches in UWB antennas [80-88]. Ring resonators are the structure in which coupling between the two resonators with different resonating frequency is done to achieve a new resonating frequency which depends upon the coupling values of the two rings [89]. The SRRs and CSRRs can have a square and circular shape as depicted in Fig. 2.13. Suppose if the resonating frequencies of the two loops in the split ring are f_1 and f_2 and a change in resonance values due to mutual coupling is represented by f_m. Then the resonant frequency of each loop is given by:

$$F_1 = \frac{c}{2L_1\sqrt{\varepsilon_e}} \qquad (2.3)$$

$$F_2 = \frac{c}{2L_2\sqrt{\varepsilon_e}} \qquad (2.4)$$

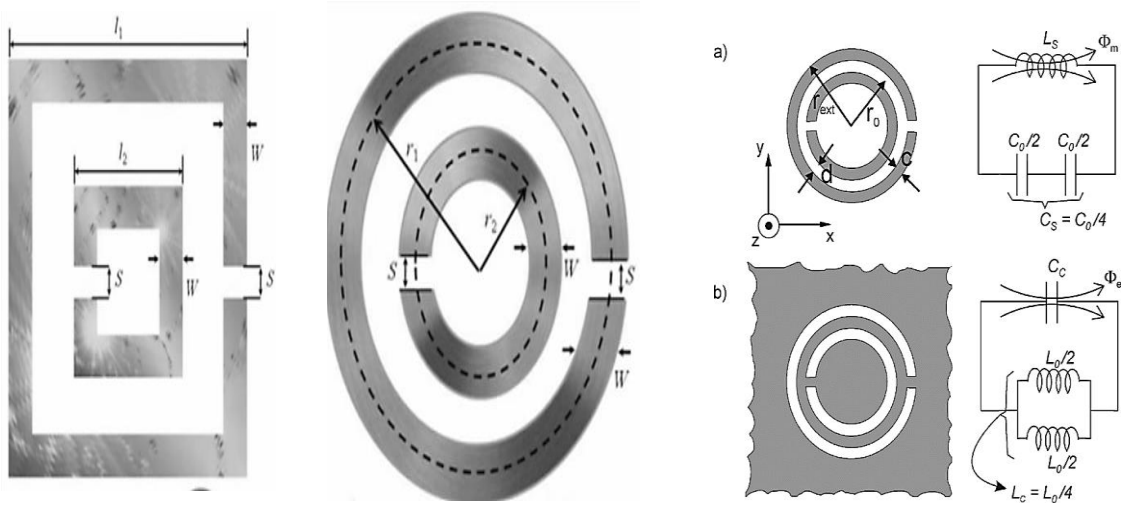

(a) (b) (c)

Fig. 2.13 Different types of commonly used ring resonators [79] (a) Rectangular split ring resonator (RSRR) (b) Circular split ring resonator (c) Split ring resonator (SRR) and Complementary split-ring resonator (CSRR) with its equivalent circuits

Here L_1, L_2 is the average loop lengths and similarly for SRR, $r_1$and r_2 represent the radius of the inner and the outer circular ring respectively. The resonance of each loop occurs at the half-wavelength (λ/2) and can be calculated as:

For the square ring:

$$L_1 = 4 \times l_1 - s - 4 \times w$$

$$\mathrm{L}_2 = 4 \times l_2 - s - 4 \times w$$

For the circular ring:

$$L_1 = 2\pi \times r_1 - s$$

$$L_2 = 2\pi \times r_1 - s$$

These basic equations of SRRs and CSRRs are only used for the loops with single resonant frequency or resonant mode. It can be analyzed that SRRs behave like an LC circuit resonator that could be excited by the external magnetic field which exhibits a powerful diamagnetism beyond the first resonance and also, they have cross-polarization effects so that the excitation with the polarized signal is possible [79]. Thus, SRRs can be considered as resonating magnetic dipole excited by an axial magnetic field. The CSRR's intrinsic model circuit is derived from SRR, as shown in Fig. 2.13(c), and it is also called the dual complement of SRR. In the dual complement of SRR, the inductance is replaced by capacitance and a series combination of capacitances is replaced by the parallel combination of inductances. So, the duality principle is followed exactly in the absence of any dielectric substrate. Based on this analysis, various planar antennas with band notch characteristics have been presented in the literature [80-102].

In [80], the triple band notching is achieved with the combination of multiple slots and SRRs coupled with the feeding structure. This CPW fed antenna is analyzed with three novel structures of the antenna in three steps. The final structure also provides stable gain and good radiation characteristics in the UWB range. Besides this, the time-domain performance of the antenna structure is also provided in [80]. Different designs using various metamaterial structures for achieving the band notching in the UWB

range and are shown in Fig. 2.14. Fig. 2.14 (a) presents a CPW fed circular patch dual band-notched antenna with the T-shaped strips and SRR [81]. In this design, the SRR exists at the bottom edge of the radiating patch which introduces a second notch frequency. For achieving band notch function at two frequencies, SRRs are embedded in the co-planar ground plane of the antenna, and the third band notch has been achieved by the U-slot in the feed structure. Furthermore, the proposed antenna achieves an omnidirectional radiation pattern throughout in the UWB range. Fig. 2.15 (c) displays the simulated peak gain of this antenna, which lies in the range of 2 to 4.8 dB. Likewise, the sharp triple-band notching in [82] has been achieved with the combination of SRR and U-slots in the antenna designing. Moreover, the antenna provided a flat group delay response, minimal variation in gain, and radiation efficiency in the passband.

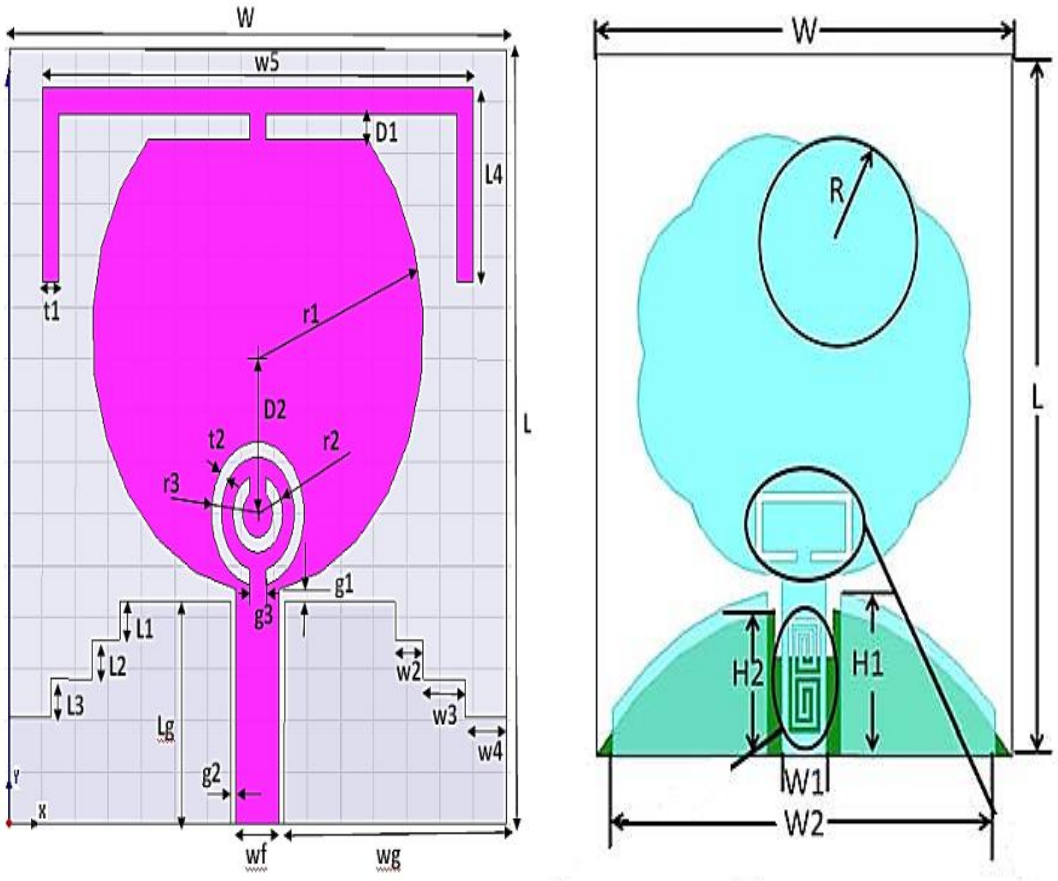

(a) (b)

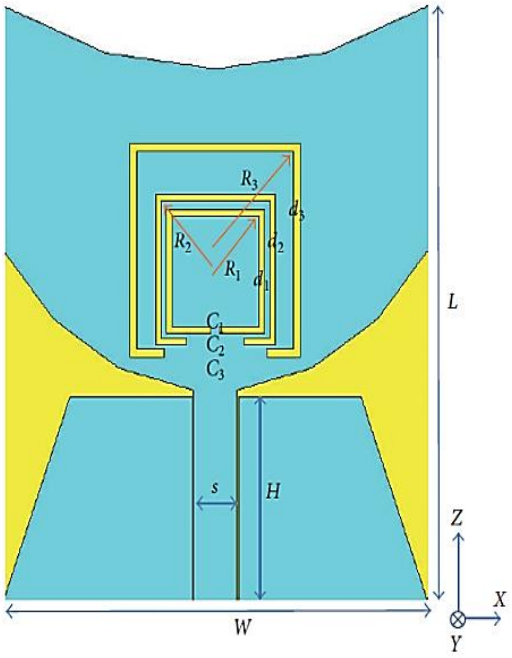
R3
d3
R2
d2
R1
d1
C1
C2
C3
L
s
H
Z
X
Y
W

(c)

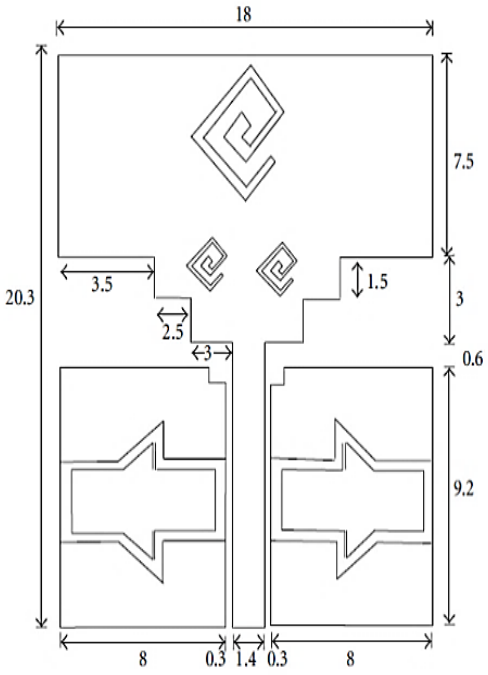
18
7.5
20.3
3.5
1.5
3
2.5
3
0.6
9.2
8
0.3
1.4
0.3
8

(d)

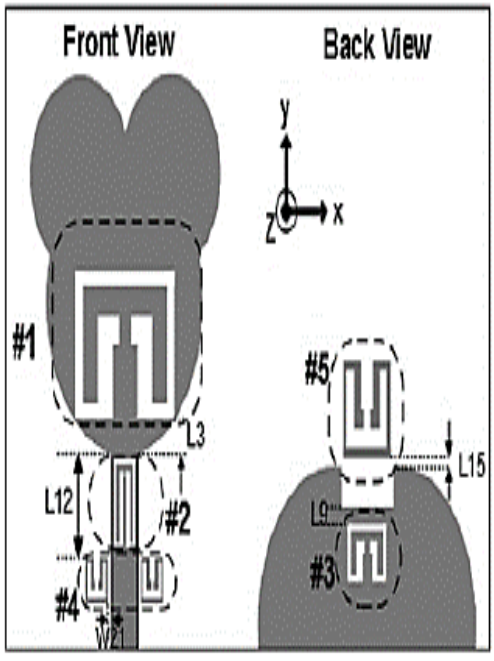
Front View
Back View
y
x
z
#1
L3
L12
#2
#4
W21
#5
L15
L9
#3

(e)

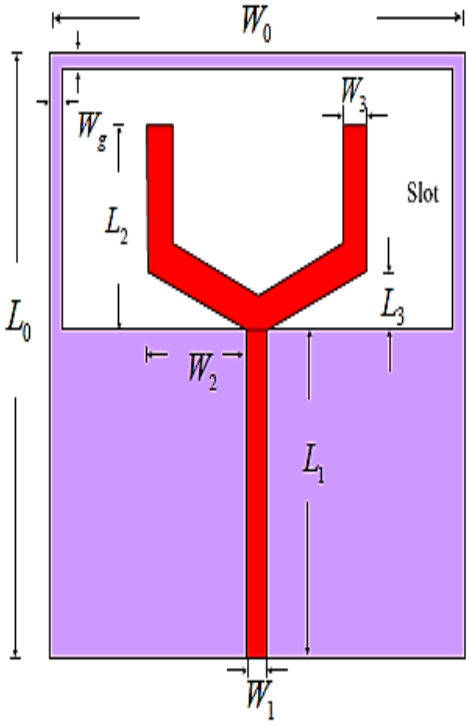
W0
Wg
W3
Slot
L2
L3
L0
W2
L1
W1

(f)

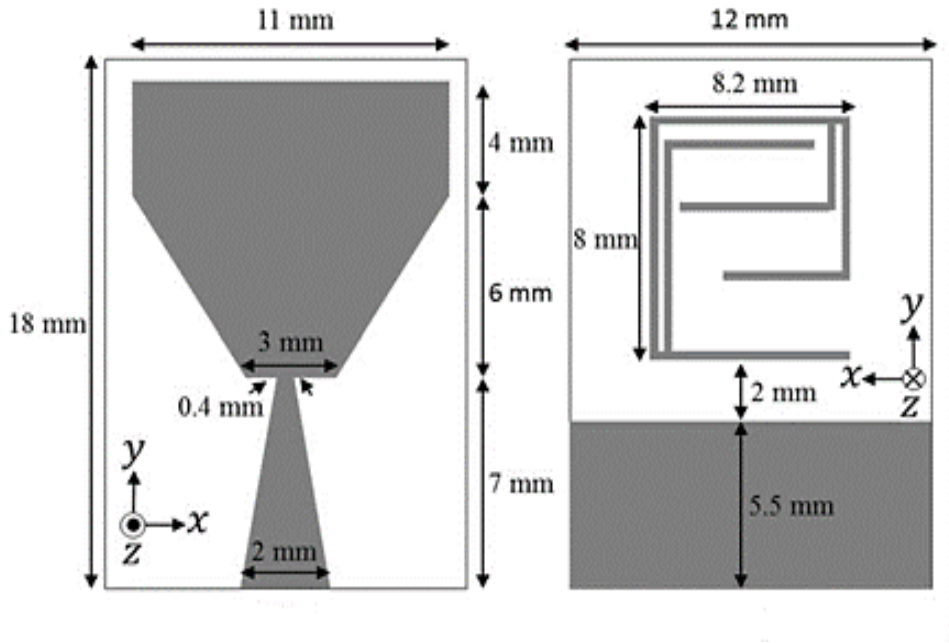

(g)

Fig. 2.14 Different UWB designs using metamaterial structures for achieving band notch characteristics (a) Circular split ring resonator [81] (b) Rectangular split-ring resonator [84] (c) Complementary split ring resonator [86] (d) Square spiral slot resonator [90] (e) M shaped resonator [93] (f) SRR in the slot of ground plane(GSRR) [94] (g) Parasitic resonator [96]

As discussed above, the antenna designs are having circular split-ring resonators. Similar to circular SRRs the rectangular split-ring resonators (RSRR) have been reported for achieving band- notch characteristics in UWB antennas [83], Fig. 2.14 (d) shows an RSRR etched at the radiating element for achieving the single band notching and also a spiral-shaped defected microstrip structure (SDMS) is introduced in the feed structure for achieving the second band notch [84]. Furthermore, the group delay of the proposed antenna delay lies in the limit of 1ns, except for the two notch bands as shown in Fig. 2.15 (d). Similarly, another UWB antenna with dual-band notching is proposed in [85]. In this design, two RSRRs are used in the radiating patch for achieving the dual-band notching. Additionally, fractal geometry is used in this design, which provides the miniaturization and very large impedance bandwidth.

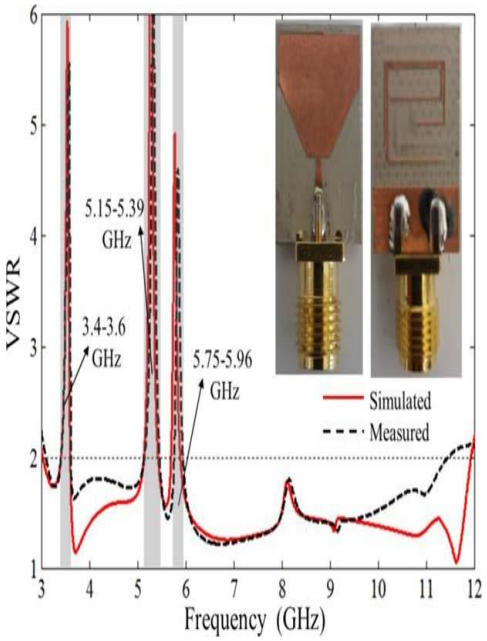
VSWR
Frequency (GHz)
5.15-5.39 GHz
3.4-3.6 GHz
5.75-5.96 GHz
Simulated
Measured

(a)

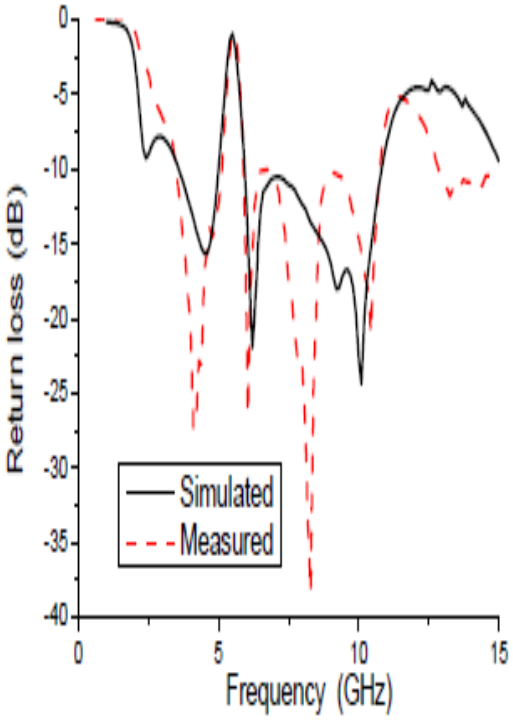
Return loss (dB)
Frequency (GHz)
Simulated
Measured

(b)

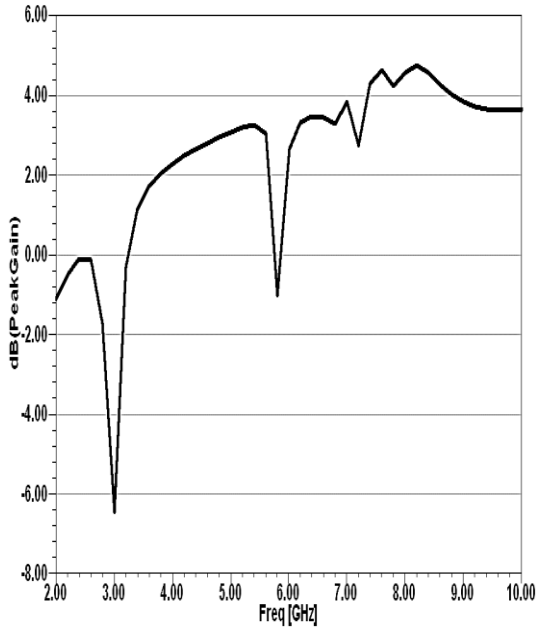
dB(PeakGain)
Freq [GHz]

(c)

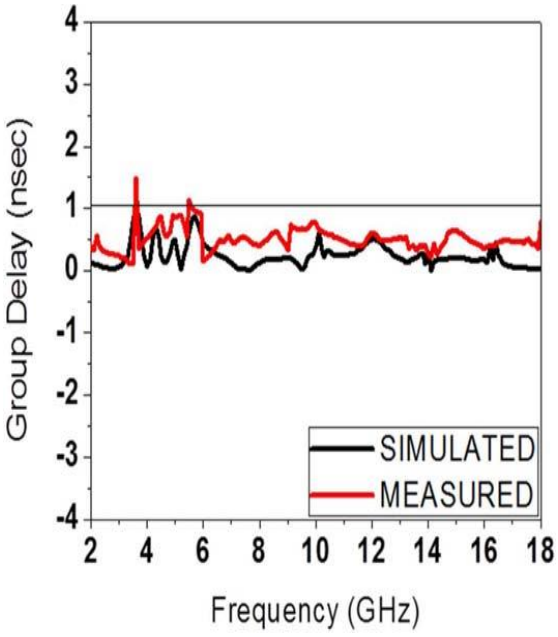
Group Delay (nsec)
Frequency (GHz)
SIMULATED
MEASURED

(d)

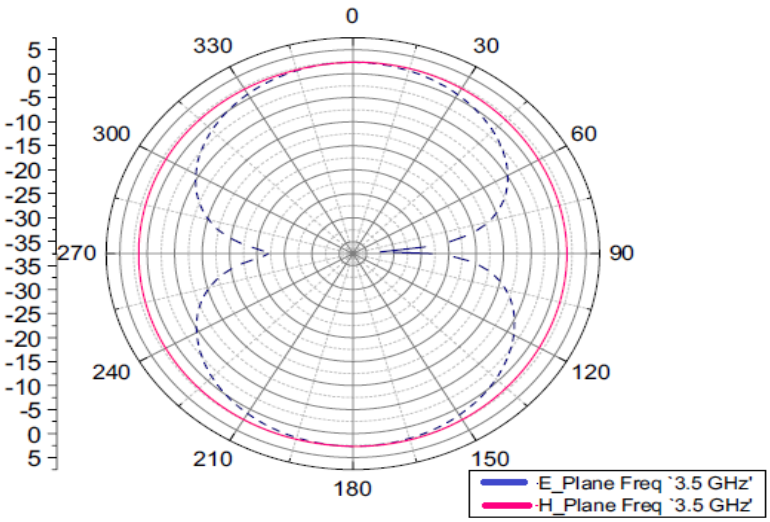

(e)

Fig. 2.15 Different types of simulated and measured results of the planar UWB band-notched antennas with MTMs (a) Simulated and measured VSWR [96] (b) Simulated and measured S_{11} [94] (c) Simulated and measured peak gain [81] (d) Measured group delay [84] (e) E and H plane radiation pattern [88]

As discussed at the starting of the section, CSRRs have been also utilized by researchers in the UWB antennas for achieving the band notching. Similarly, in [86], a CPW fed UWB antenna with three notches, as depicted in Fig 2.14 (c), with CSRRs embedded on the radiating element is proposed and it provides very sharp band rejection capabilities with an omnidirectional radiation pattern for the entire UWB range. Likewise, UWB antenna with similar characteristics having the slotted CSRR and a circular radiating patch for single-band notch has been presented in [87]. In this design, thickness and the gap between the edges of the split creates band notching characteristics in the UWB range. Moreover, in [88], a monopole UWB antenna with the CSRR etched on the circular radiating patch, and a slot structure has been used within the feed line for achieving triple-band notching, and Fig.2.15 (e) is used to represent the omnidirectional radiation pattern of E and H plane for the passband.

Furthermore, a novel CPW fed modified complementary split-ring resonator (MCSRR) UWB antenna with multiple notches is proposed in [89]. In this antenna, six slotted

MCSRR in the radiating patch and the ground plane have been incorporated for achieving five-band notch frequencies and miniaturization.

Eventually, so many other types of metamaterial structures have been reported by researchers for achieving band notch characteristics in the UWB range [90-102]. Metamaterial structures embedded in all these antennas are derived from the above-mentioned structures. For example, Fig. 2.14 (d) shows a square spiral-shaped resonator, which is etched on the radiating element and ground plane of the antenna [90]. Both resonators in the proposed design have different sizes and achieve five different notch bands in the UWB spectrum. In [91], the CPW fed planar antenna incorporating nested split ring resonator [NSRR], stepped impedance resonator [SIR], and two T- shaped stubs for achieving the dual-band notch characteristics with omnidirectional radiation pattern has been reported. In this antenna structure, the notched bands can be changed by varying the dimensions of SIR and NSRR. Likewise, in [92] another compact CPW fed UWB antenna with dual-band notching, having an omnidirectional radiation pattern is achieved using an arc-shaped stepped impedance resonator, which is inserted in the circular ring type radiating patch, and a spiral SIR etched in the feedline. Similarly, Fig. 2.14 (e) displays the five M-shaped resonators (MSRs) of one/half wavelengths are integrated on the radiating patch, feedline, and ground plane to achieve quintuple band rejection capabilities in the antenna structure which is presented in [93]. Another novel planar UWB antenna has been proposed in [94] with single-band notch function and the Fig. 2.14 (f) shows the antenna structure of a conventional fork-shaped radiating patch and an SRR in the slot of the ground plane (GSRR), where notch frequency is controlled by the coupling between GSRR and coupling line. For this antenna, the S_{11} plot has been represented in Fig.2.15 (b) which displays the single band notch characteristics in the range of 5-6 GHz. Moreover, Table 2.4 is used to represent the notch band frequency and its application for these designs.

In [95], the different type of UWB antenna with wide bandwidth has been presented, and also the performance evaluation has been discussed for portable devices. It is concluded from the paper that the size reduction in wideband and UWB antennas is an essential parameter. So, Fig. 2.14 (g) represents an antenna design employing a new technique using parasitic resonators on the radiating surface and ground plane for

achieving dual and triple-band notching in the UWB range [96], [97]. Fig. 2.15 (a) represents the simulated and measured results for VSWR of a triple band-notched antenna using parasitic resonators. By properly placing the parasitic resonator on the radiating surface the sharp cut-offs can be attained in the notched bands and also, it can decrease the total size of the antenna structure. In [98-100] researchers have achieved miniaturization in the planar antennas having a wide bandwidth. In [98], two miniaturized UWB antennas filled with composite right-/left-handed transmission line (CRLH-TL) metamaterial structures have been proposed with good radiation properties over a wide bandwidth. In [99] a novel miniaturized UWB antenna based on a similar metamaterial structure has been presented. In this antenna structure, the inductive and capacitive components with metal through-holes have been implemented and achieved good radiation properties. Moreover, L and T-shaped slits have been etched for the reduction of size and bandwidth improvement. In [100], another compact UWB antenna with a simplified composite right-/left-handed transmission line (SCRLH-TL) MTM structure has been proposed, and E shaped slits are used in the radiating patches for the enhancement of the antenna parameters.

In [91] MIMO UWB planar antenna has been presented. This structure possesses two microstrip-fed antennas with triple band-notched characteristics and uses the radial stub loaded resonators (RSLR) and T shaped stubs for providing better isolation. The triple band notching in this antenna structure has been achieved by incorporating a defected microstrip structure (DMS) based band stop filter (BSF) and an inverted π shaped slot and also coupling between the two-antenna structure can be adjusted by changing the parameters of RSLR loaded T-shaped stub. Similarly, in [102] a compact UWB MIMO antenna with dual-band notching has been presented. This antenna utilizes CSRR to achieve enhanced band notching and also a novel SRR based isolator has been used to improve the isolation in the overall antenna structure. Finally, other types of MTMs and metasurfaces (e.g., gradient refractive index (GRIN) meta-surfaces, focusing metasurfaces, anisotropic metasurfaces, etc.) can be also utilized for achieving miniaturization and gain enhancement in UWB antennas [103-108].

Table 2.4 Different notched bands and their applications using metamaterial structures

Reference	Type of Metamaterial resonator	Notch Band frequency (GHz)	Notch band Application
[81]	Circular Split Ring Resonator	3.3 - 3.8 and 5.15 - 5.825	WLAN and Wi-MAX
[82]	The rectangular split-ring resonator	3.3-3.8, 5.15-5.825 and 7.25-8.395	Wi-MAX, WLAN, and Satellite X-band
[83]	Circular and rectangular Split Ring Resonator	3.3-3.8, 5.15-5.35, 5.725 -5.825 and 5.85-5.925	Wi-MAX, WLAN and DSRC
[84]	The rectangular split-ring resonator	3.3-3.7, 5.15-5.85	Wi-MAX and WLAN
[85]	Square spiral slot resonator	2.4-2.8, 3.2-3.7, 5.5-6 and 6.5-7	Wi-MAX, WLAN, and Satellite downlink X –Band
[86]	Complementary split-ring resonators	3.9, 5.2, and 5.9	C Band, WLAN, and HIPERLAN/2 WLAN
[87]	The complementary split-ring resonator	5.5	WLAN
[88]	The slotted Complementary split ring resonator	5.5	WLAN
[89]	Modified complementary split ring resonator	3.0, 4.0, 5.0, 6.0 and 7.0	Chipless RFID
[93]	M-shaped resonator	2.35 - 2.61, 3.16 - 3.69, 5.0 - 6.1, 7.2 - 7.7 and 8.1 - 8.74	WLAN, Wi-MAX, Satellite downlink X-Band and ITU 8 GHz band
[94]	Split ring resonator in the slot of the modified ground plane (GSRR)	5-6	WLAN
[96]	Parasitic microstrip resonator	3.4-3.6, 5.15-5.39, and 5.75-5.96	Wi-MAX and WLAN
[97]	Dual Parasitic microstrip resonators	5 - 5.4 and 7.8 - 8.4	WLAN and ITU Band

2.5 EBG Structures Based Band-Notched UWB Antennas

In recent years, EBG structures have become very appealing in the field of antenna engineering due to its numerous advantages such as compactness [109], effective bandwidth control, and the minimum effect on antenna's radiation pattern [110]. EBG structures are 3-D periodic entities that halt the propagation of electromagnetic (EM) waves in a particular band of frequency for all polarization states and angles. This terminology is taken from the photonic bandgap phenomena in optics realized by periodic structures. These structures have also been employed in UWB antennas to

achieve band notching characteristics and miniaturization. Practically, it is very difficult to realize EBG structures so the restricted band-gap structures are preferred [110]. The most common EBG structure utilized in antennas is a mushroom type because of its miniaturization properties, which are essential for antenna structures [100].

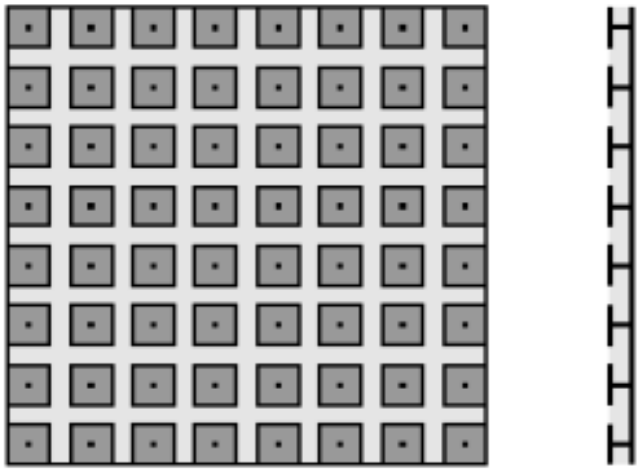

Fig. 2.16 The mushroom type EBG structure [109]

Fig. 2.16 demonstrates the mushroom type EBG structure. The mushroom type band-gap structure has four parts, which are a dielectric substrate, a ground plane, radiating patches (metallic), and connecting vias. Furthermore, this structure also has different stop bands for surface wave propagation. The operation of this type of EBG can be explained by an LC filter array, where L and C are inductance and capacitance respectively, and these values are calculated from the current flow through the vias and gap between the patches which are adjacent to each other. The values of L and C can be calculated as [109]

$$L = \mu_0 \, h \tag{2.5}$$

$$C = \frac{W\varepsilon_0(1+\varepsilon_r)}{\pi}\cosh^{-1}\left(\frac{2W+g}{g}\right) \tag{2.6}$$

where w and g represent the patch width and gap width, μ_0, ε_r, and ε_0 represent permeability of free space, dielectric constant, and permittivity of free space respectively. The prediction of the bandgap can be done with the help of the following equation:

$$w = \frac{1}{\sqrt{LC}} \tag{2.7}$$

$$BW = \frac{\Delta w}{w} = \frac{1}{\eta}\sqrt{\frac{L}{C}} \tag{2.8}$$

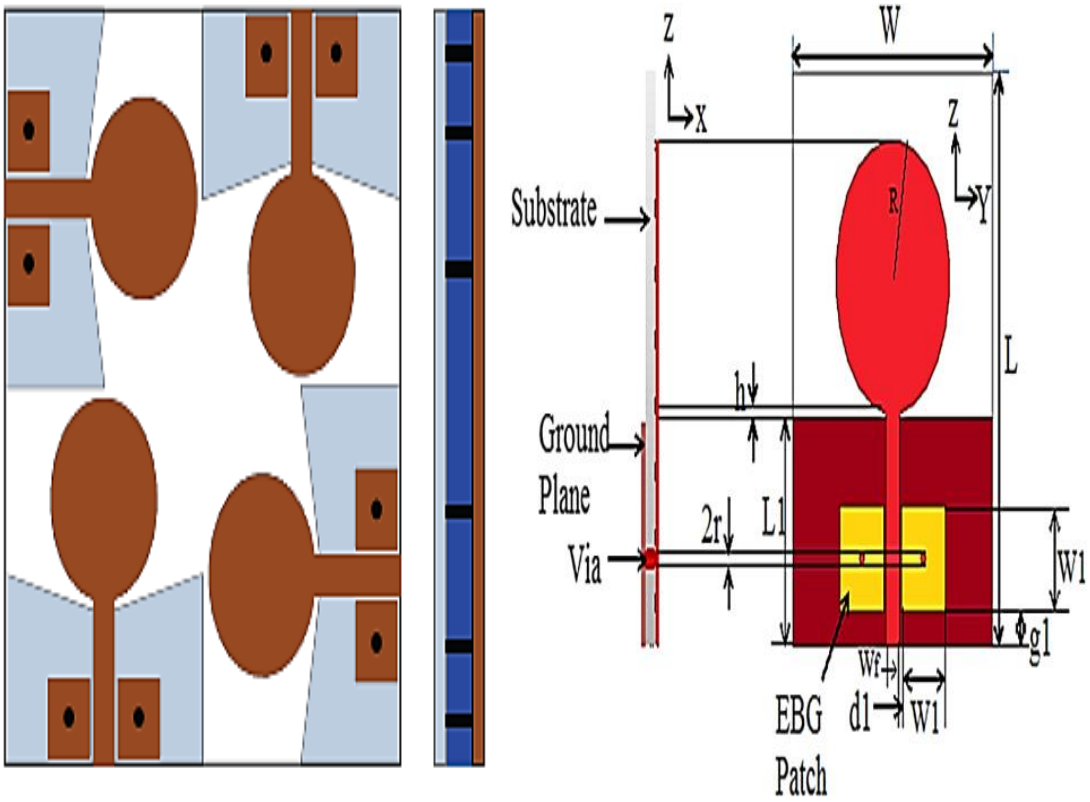

(a) (b)

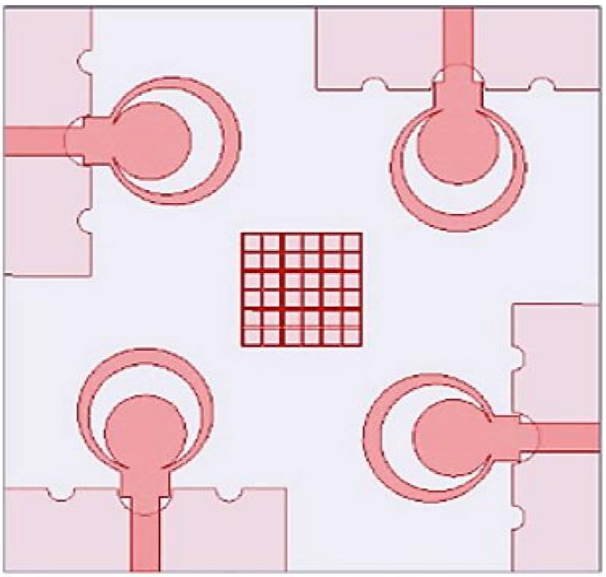

(c)

Fig. 2.17 UWB antennas with a different type of EBG structures for band notching (a) Band notched antennas with conventional mushroom-type electromagnetic bandgap structure (CMT-EBG) [113] (b) Modified mushroom-type EBG structure [116] (c) Periodic EBG structure [119]

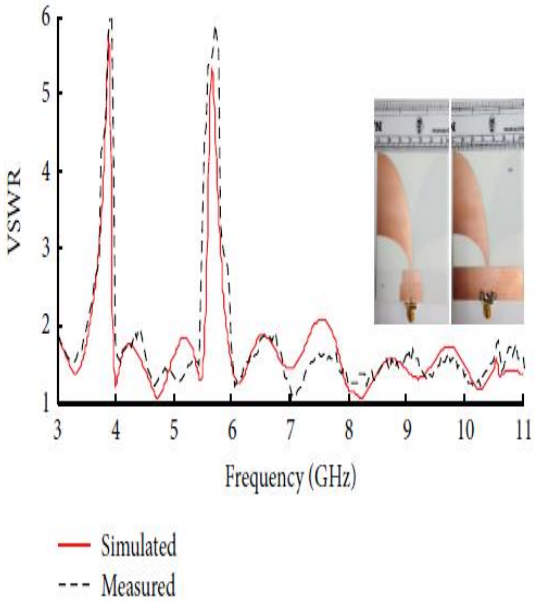

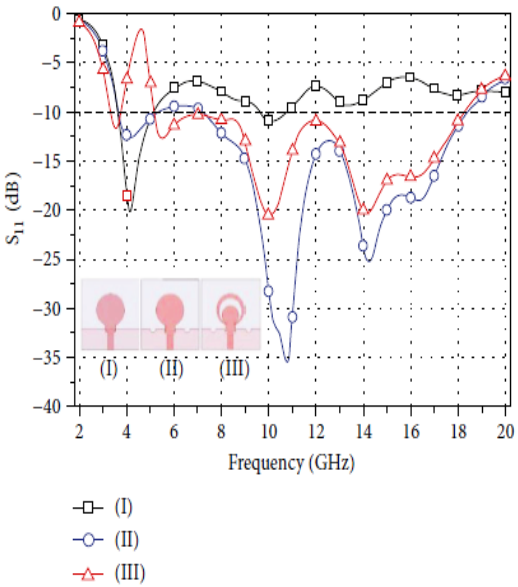

(a) (b)

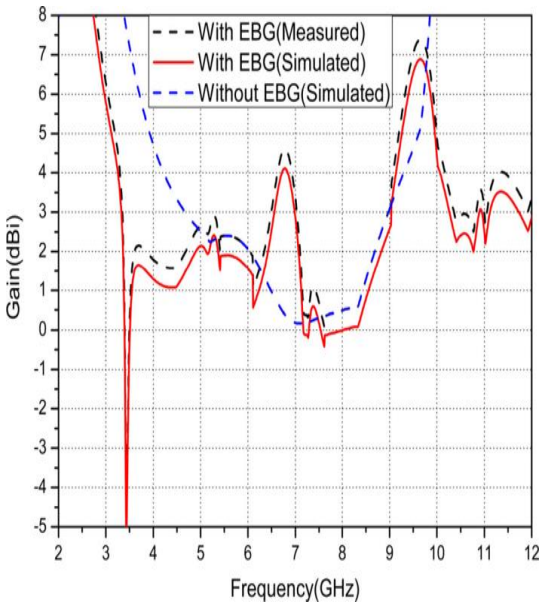

(c)

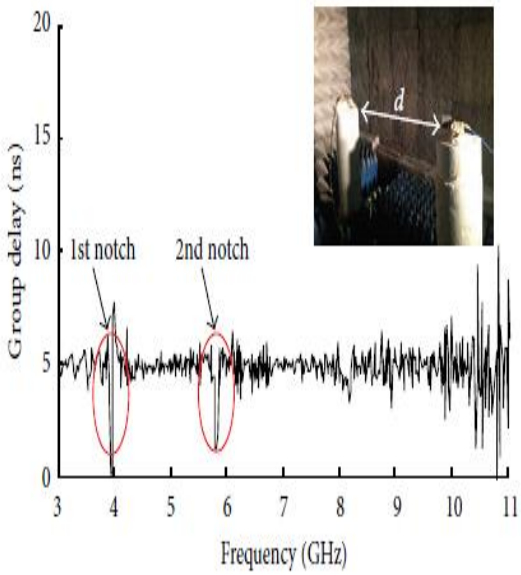

(d)

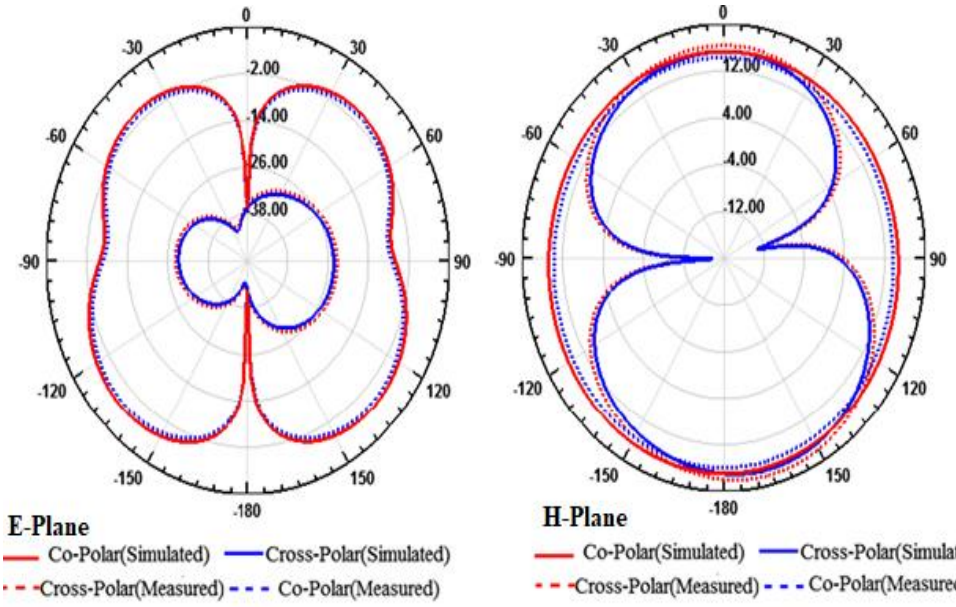

(e)

Fig. 2.18 Different types of simulated and measured results in planar UWB band-notched antennas with EBG structures (a) Simulated and measured VSWR [114] (b) Simulated S_{11} [119] (c) Simulated and measured peak gain [116] (d) Measured group delay [114] (e) E and H Plane radiation pattern [116]

Many UWB planar antennas with band notch characteristics have been investigated using these equations and models [101-120]. In [111], a novel technique has been presented for multiple bands notching within the pass-band of the UWB monopole antenna. The antenna structure utilizes a mushroom-type EBG structure coupled with a microstrip line that has various advantages such as reject frequency tenability, efficient dual reject band design, reject bandwidth controllable capacity, and stable radiation patterns. Likewise, in [112], the mushroom-type EBG structure is implemented in the vicinity of the transmission line to achieve the band notching. Also, it does not affect the behavior of the radiating patch and the radiation characteristics of the antenna. Moreover, by adjusting the physical parameters of the EBG structure, the desired reject band characteristics can be achieved.

Table 2.5 Different notched bands and their applications using EBG structures

Reference	Type of EBG structure	Notch Band frequency (GHz)	Notch band Application
[111]	Mushroom-type	5.2- 5.8	WLAN
[112]	Mushroom-like	5.5	WLAN
[113]	Mushroom-like	5.36-6.34	WLAN
[114]	Mushroom-like EBG cells	3.6-3.9 and 5.6-5.8	Wi-MAX and WLAN
[115]	Dual mushroom-type	5.150-5.825 and 7.10-7.76	WLAN and Satellite downlink *X*-band
[116]	Modified Inductance enhanced mushroom-type EBG structure	3.3-3.8 and 5-6	Wi-MAX and WLAN
[117]	Modified electromagnetic-band gap (M-EBG) structure	3.5 and 5.5	Wi-MAX and WLAN
[118]	Two spirals EBG structures	5.2 and 5.8	WLAN
[119]	Periodic EBG structures	4.6	INSAT
[120]	Two mushroom-type	3.5 and 5.8	Wi-MAX and WLAN

Fig. 2.17 (a) presents the UWB MIMO antenna with single-band rejection capabilities by employing a mushroom-like EBG structure. In this design, mutual coupling between the antenna elements has been decreased using a stub structure which acts as a band-

reject filter to reduce the effect of the surface current between antenna elements [113]. In [114], the dual-band rejection capability with High-Q stopband characteristics is achieved using the two mushroom-like EBG cells along with the feed structure. In [114], the simulated and measured results of VSWR show the two notches, i.e., 3.6-3.9 GHz and 5.6-5.8 GHz in the UWB range and shown in Fig. 2.18 (a). Similarly, group delay results for [114] are shown in Fig. 2.18 (d) which depicts the simulated and the measured value of group delay. One more design with the mushroom-like EBG structure is presented in [115], which possesses the single band-reject capabilities similar to the design presented in [113], but in this design, wide rectangular band notch characteristics are achieved by the tuning of resonant frequencies of two EBG structures and integrating them. Besides, this structure can tune the frequency and width of the rectangular notched band by changing the parameters of the EBG structure.

2.6 Reconfigurable Band-Notched UWB Antennas

The reconfigurable antennas have emerged as a distinctive solution to fulfill the demand of a single wireless platform. To fulfill this demand, different characteristics of the antenna such as frequency, radiation pattern, and polarization should be made reconfigurable. To achieve this, mechanical movable parts, phase shifters, attenuators, diodes, switches, active materials are used [121]. This mechanism has also been utilized in UWB antennas to achieve tunable band notch characteristics. There are a lot of parameters that need to be taken into consideration to achieve reconfigurability in an antenna, especially in RF switches. These parameters are bandwidth, characteristic impedance, isolation, insertion loss, switching speed, expected lifetime, and power handling. Additionally, under microwave frequencies, low-pass switches act like resistors (R_{on}) when they are in on state, and act as capacitors (C_{off}) when they are in the off state, but bandpass switches act as one capacitor when they are in on state, and behave like a different capacitor when they are in the off state. Moreover, at higher frequencies, factors like bond-wire inductance, ground inductance, and transmission line parameters make the circuit modeling complicated. Similarly, parasitic resistances limit the higher-frequency hop and the Figure-of-merit of the switch.

The cutoff frequency can be calculated as [122]:

$$f_c = \frac{1}{2\pi\, C_{off}\, R_{on}} \tag{2.9}$$

The highest operating speed of the switch is approximately $\frac{f_c}{10}$, whereas the switching speeds of semiconductor switches and mechanical switches are in nanoseconds and milliseconds respectively. Due to this reason, in most of the designs, the semiconductor switches (PIN diodes, Field effect transistors (FETs), Varactor diodes, Micro-Electro - Mechanical-Systems (MEMS) switches, etc.) are preferred rather than the mechanical switches. Fig. 2.19 presents a simple configuration of the reconfigurable antenna with switches and shorted slots, to switch between polarizations [121].

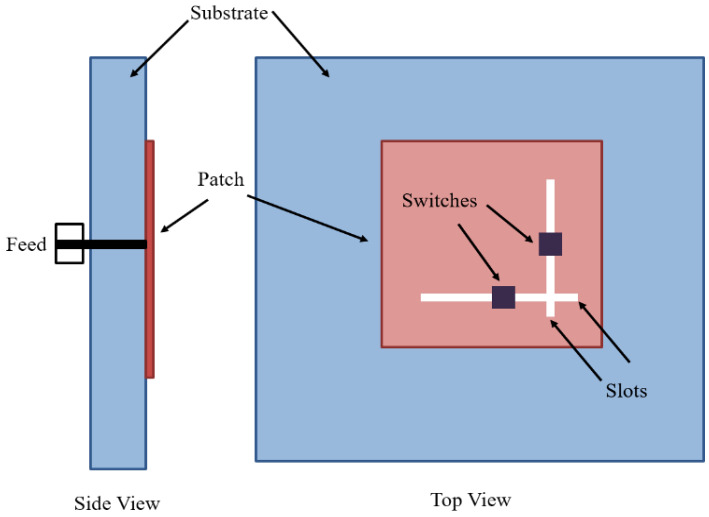

Fig. 2.19 The configuration of the reconfigurable antenna [121]

The ideal switches have been used for the reconfigurability of the single, dual, and triple notched band in UWB antennas [123-130]. In all these antenna structures, different techniques have been utilized by the researchers for achieving band-notched operation in the UWB antenna. In [123-124], the dual-band notching is attained by using stepped impedance stub (SIS), stepped impedance resonators (SIR), and hexagonal stepped impedance resonators (HSIR). Similarly, in [125, 130] the dual-band notching is achieved in a CPW fed planar UWB antenna by inserting a T-shaped stepped impedance resonator (T-SIR) on a circular patch and by engraving a parallel stub loaded

resonator (PSLR) in the feedline. Likewise, a combination of open-ended T-shaped stubs (OET-S) and inverted F stub loaded rectangular resonator (IFSLRR) has been used in [127] for achieving dual band notching. Furthermore, Fig. 2.20 (a) shows the design of the triple band-notched antenna by employing defected microstrip structure (DMS), BSF, and an inverted π shaped slot [126]. Its S_{11} results are represented in Fig. 21 (b) in which the three-band notches of this antenna at 4.2-6.2 GHz, 6.6- 7 GHz, and 12.2- 14 GHz can be observed. Moreover, Fig. 2.21 (a), Fig. 2.21 (c) and Fig. 2.21 (e) represents the different simulation and measurement results of a dual band-notched antenna (i.e., simulated and measured VSWR, gain plot, and radiation pattern) [130].

In the above-mentioned antenna designs, the analysis of the reconfigurable behavior of the notched band in the UWB antenna has been done only at the simulation level. This is because the addition of switches in the antenna prototype requires an additional biasing network during SMT of switches on the prototype. It makes the antenna structure more complex due to which the simulated results do not match the measured results [127].

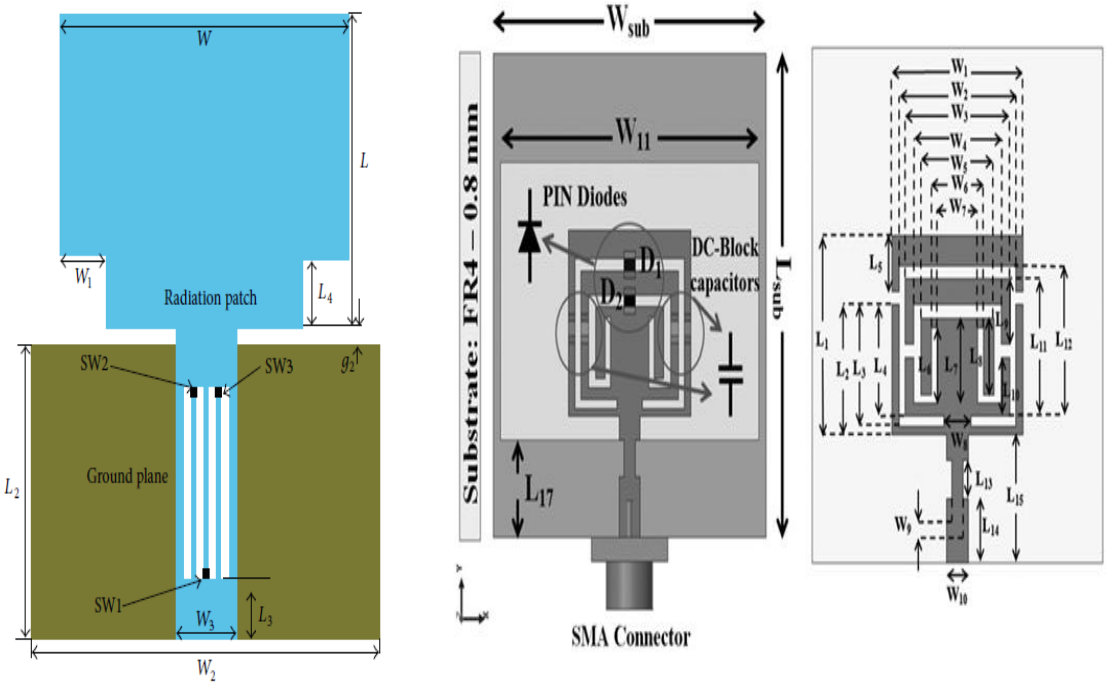

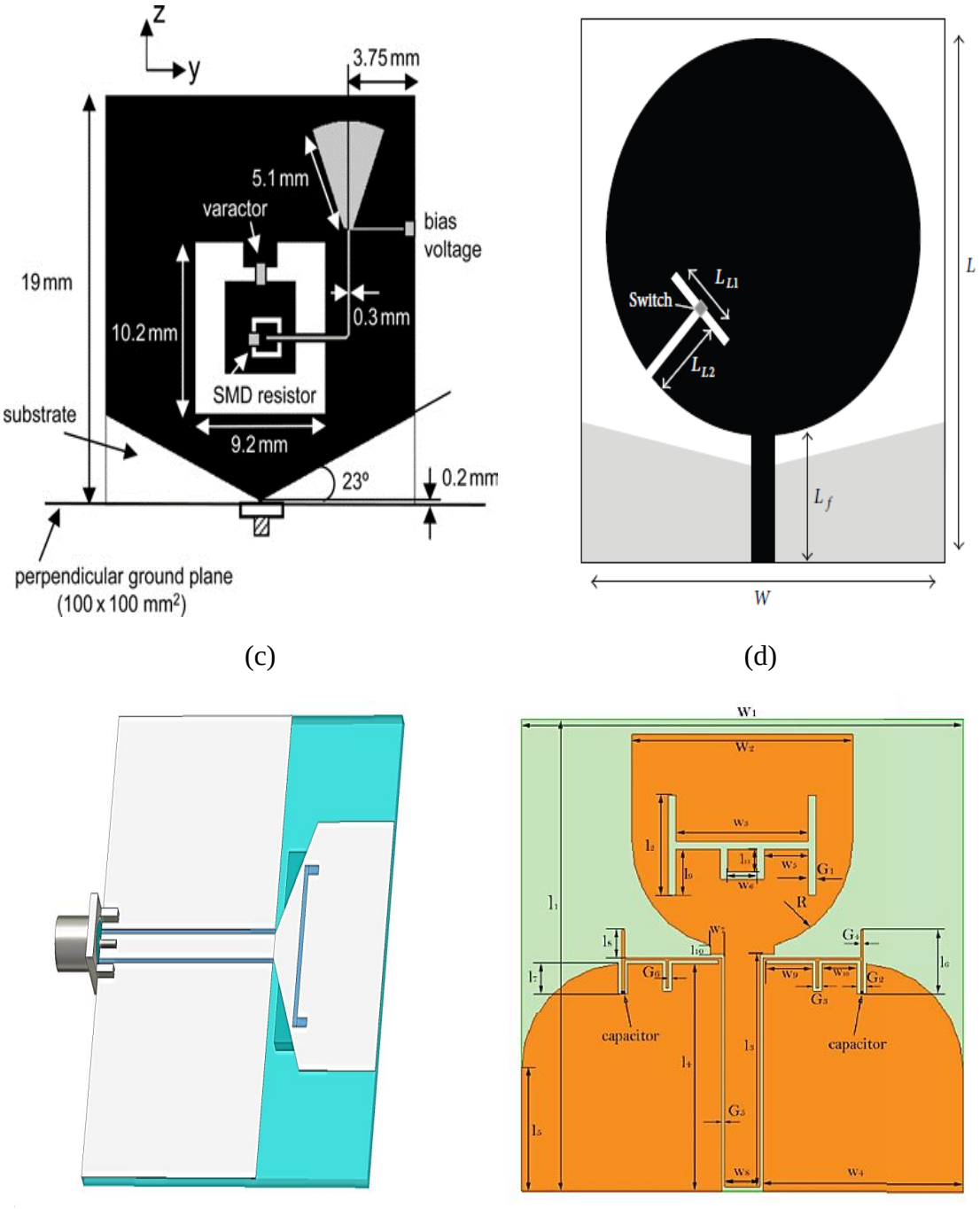

(c) (d)

(e) (f)

Fig. 2.20 Different reconfigurable UWB band-notched antenna designs (a) UWB antenna with ideal switches [126] (b) UWB antenna with PIN diodes [131] (c) UWB antenna with varactor diodes [134] (d) UWB antenna with optical switch [137] (e) UWB antenna with magneto-dielectric material [138] (f) UWB antenna with variable capacitors [140]

As per the discussions above, designing an efficient biasing circuit is very important for tunable band-notched UWB antennas. Nevertheless, various designs using PIN diodes and varactor diodes have been presented by the researchers to attain the reconfigurable behavior in the UWB band-notched antenna [131-136]. Fig. 2.20 (c) represents a UWB slot antenna with single and dual notched functions having switchable behavior, and the switching operation has been accomplished by introducing two PIN diodes in the slot of the radiating patch to achieve band-notched characteristics in UWB antenna [118]. Similarly, a single and dual notched antenna using PIN diodes is proposed in [119]. Another design using four PIN diodes for UWB bandwidth coverage with single and dual-band notches has been presented in [13]. This antenna utilizes parasitic elements to improve the frequency response in the simulation.

Similar to PIN diodes, the varactor diodes are also used in the UWB band-notched antennas and are described in [134-135]. Varactor diodes are embedded on the resonating slot and provide tunable resonating behavior as presented in [134] as shown in Fig. 2.20 (c), Besides, it provides independent controlling of the notch band by effective electronic tuning by varying the bias voltage of the varactor diode [135]. Furthermore, in [136], both the PIN diodes and varactors are used in the antenna structure. In this design, PIN diodes can provide a switching action, whereas the varactor diode can be used for tuning

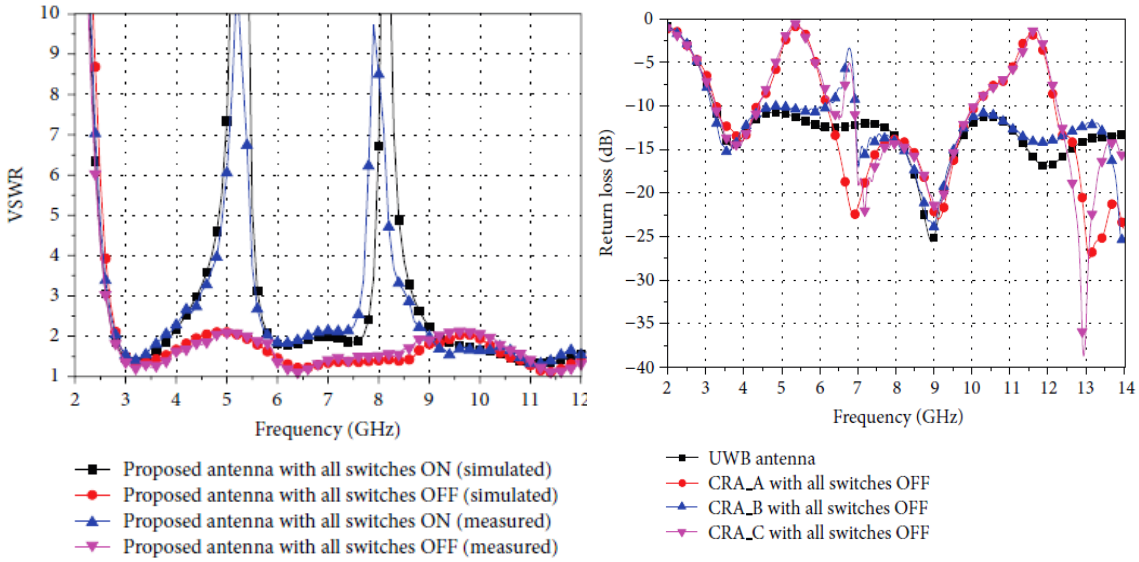

(a) (b)

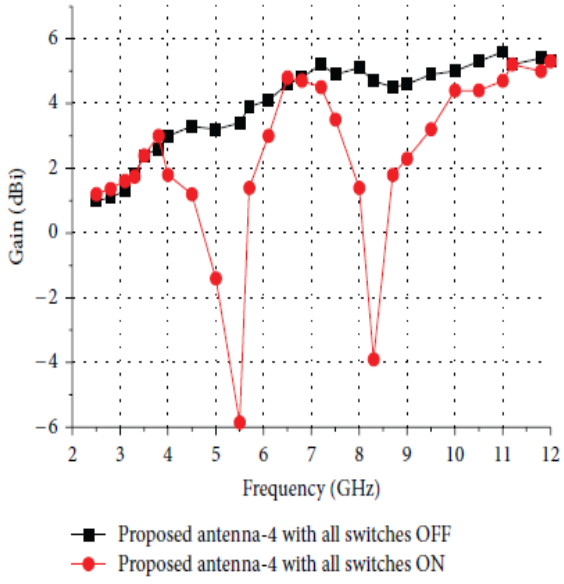

(c)

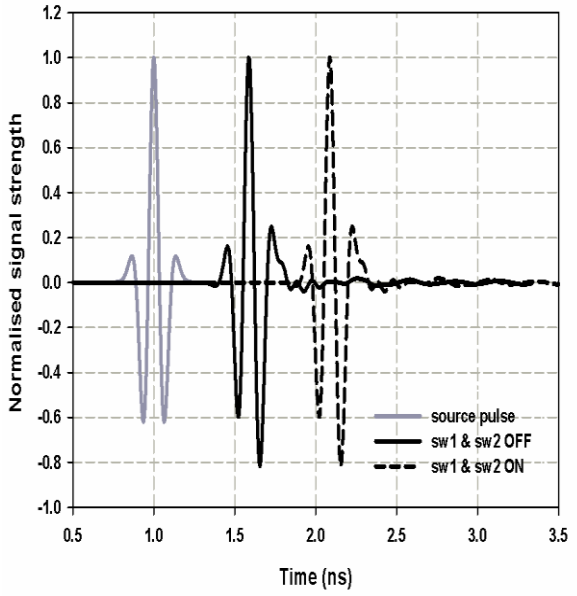

(d)

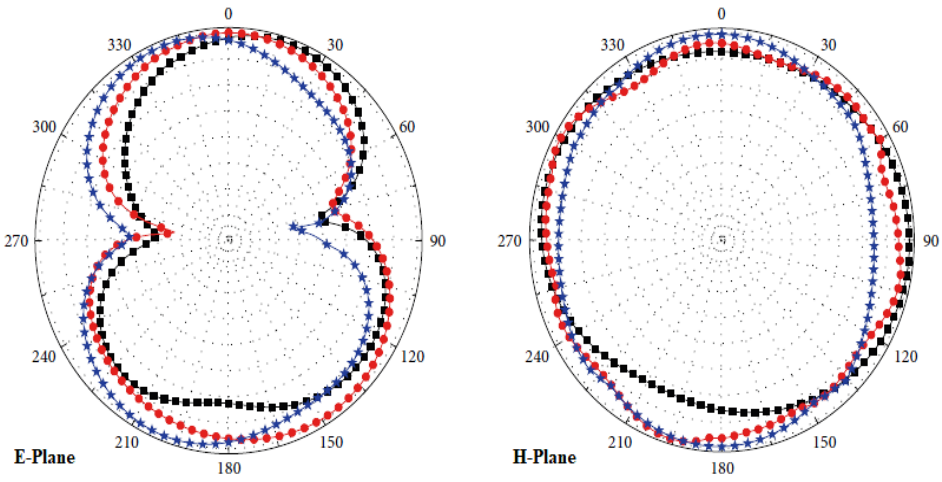

(e)

Fig. 2.21 Different types of simulated and measured results in the planar reconfigurable UWB band-notched antennas (a) Simulated and measured VSWR [119] (b) Simulated S_{11} [115] (c) Simulated and measured peak gain [119] (d) Measured group delay [118] (e) E and H plane radiation pattern [119]

Similarly, so many other techniques have been proposed in literature like using an optical switch (Fig. 2.20 (d)), magneto-dielectric (Fig. 2.20 (e)), and variable capacitors (Fig. 2.20 (f)) [137-140]. Moreover, other techniques incorporating different types of metasurfaces with the combination of PIN diodes and varactor diodes can be used for achieving tunable characteristics in UWB antennas [131-144] and Table 2.6 represents the notched band frequencies and their applications for different reconfigurable UWB antennas with band notch characteristics.

Table 2.6 Different notched bands and their applications using antenna reconfiguration techniques

Reference	**Type of switch for reconfiguration**	**Notch Band frequency (GHz)**	**Notch band Application**
[125]	Ideal switches	3.8-5.9 and 7.7-9.2	C-band, WLAN, and X-band
[126]	Ideal switches	4.2 - 6.2, 6.6 to 7.0 and 12.2	C-band and WLAN
[127]	Ideal switches	3.5 and 8.2	Wi-MAX and X-band
[128]	Ideal switch	3.3-3.6 and 5.15-5.35	Wi-MAX and WLAN
[129]	Ideal switches	3.3 - 3.6	Wi-MAX
[131]	PIN diodes	3.15-3.85 and 5.43-6.1	Wi-MAX, C-band and WLAN
[132]	PIN diodes	3.3-3.6, 5.15-5.35 and 8.2	Wi-MAX, WLAN, and 8.2GHz
[13]	PIN diodes	5.1-5.7 and 7.2-7.8	WLAN and downlink X-band
[134]	Varactor diodes	4.1 - 6.8	WLAN and C-band
[135]	Varactor diodes	5 - 6	WLAN
[136]	PIN Diodes-varactor diodes	4.2-4.8 and 5.8-6.5	C-band and WLAN
[137]	Optical switch	3.5-5	Wi-MAX and WLAN
[138]	magneto-dielectric materials	1.7-8	WLAN, Wi-MAX, and C-band
[139]	Variable capacitors	3-4	Wi-MAX
[140]	Variable capacitors	3.5 and 7	Wi-MAX and C-Band

2.7 Summary

Due to the growing demand for devices with high data rates and low power consumption, researchers are looking for solutions, which provide optimum results for each application. UWB systems provide this solution for short-range wireless communication with very little power consumption.

This chapter had addressed the challenges involved in designing of UWB antennas for notch band characteristics. Designing an optimal planar UWB antenna with band notch characteristics to provide minimum interference with other existing wireless technologies is the major challenge in the implementation of UWB systems. Therefore, different techniques for achieving the band notch characteristics in the UWB range with their advantages and disadvantages have been discussed in this study. The band notch characteristics in UWB antennas are a very strong function of the electrical size of the antenna. So, to achieve this, various parameters and techniques have been taken into consideration, such as loading slots and parasitic elements, inserting slits and fractal techniques, etc.

The main advantage of using these techniques is to provide band notch characteristics with a simple structure of the antenna. Besides, these techniques have been used in combination with fractal, metamaterial, and EBG structures to achieve the sharp cutoff in-band notching with good radiation properties. Another, major challenge of the UWB band-notched antennas is the designing of an accurate filtering structure to reject the undesired bands from the UWB range. So, the researchers have used SRRs and CSRRs in the antenna structures to achieve sharp filtering of the undesired band, and also these planar metamaterial structures have been employed in combination with other techniques such as slot-loading, using stubs and fractals to achieve optimum performance. The EBG structures have been used to achieve miniaturization in UWB antennas with band notch characteristics. These structures also provide stable radiation characteristics as compared to the other techniques. Moreover, these structures are utilized in combination with other techniques to achieve band notching. The reconfigurable band-notched antennas with switches and tunable materials have also been proposed, but it requires an additional biasing network, which increases the

complexity and power requirements of the antenna structure. To conclude, all the mentioned techniques have a significant role in designing a band-notched UWB antenna and as stated above, each technique has certain design constraints, which should be addressed in future antenna designs.

Chapter 3

Design Process of Planar UWB Antennas with Band-Notch Characteristics

3.1 Introduction

The main objective of this chapter is to study and describe the design procedure to design a UWB antenna with band notch characteristics. As discussed in Chapter 2, multiple techniques have been employed by the researchers to achieve the band notch characteristics in planar UWB antennas. However, first step in all these designs is to achieve the UWB operation.

A UWB antenna needs to possess certain characteristics such as stable gain, omnidirectional radiation pattern, and decent time-domain performance. Therefore, in this chapter, the design procedure of UWB antenna designs possessing all these characteristics as well as band notches is presented. The design process of the UWB antenna design with band notch characteristics contains few steps in all the designs and those are given below:

- Analyze the UWB antenna design requirements
- Designing the preliminary UWB antenna based on the state of the art
- Parametric study of the antenna for optimal results
- Selection of notch band-structure
- Parametric study of notch band-structure
- Notch band realization without affecting the essential parameters for UWB operation
- Fabricate the designed antenna and perform testing
- Validate the operation of designed UWB antenna by comparing the simulation results with measured results

Based on these steps Fig. 3.1 demonstrates the basic design methodology used to design the UWB antenna with notch band characteristics. This chapter lays the

groundwork in order to understand the simulation and fabrication process of UWB antennas with band-notched characteristics. For this task, three different antenna designs, similar to antenna designs available in the literature have been analyzed. The first two designs represent the UWB antennas while the third design represents a UWB antenna with band notch characteristics.

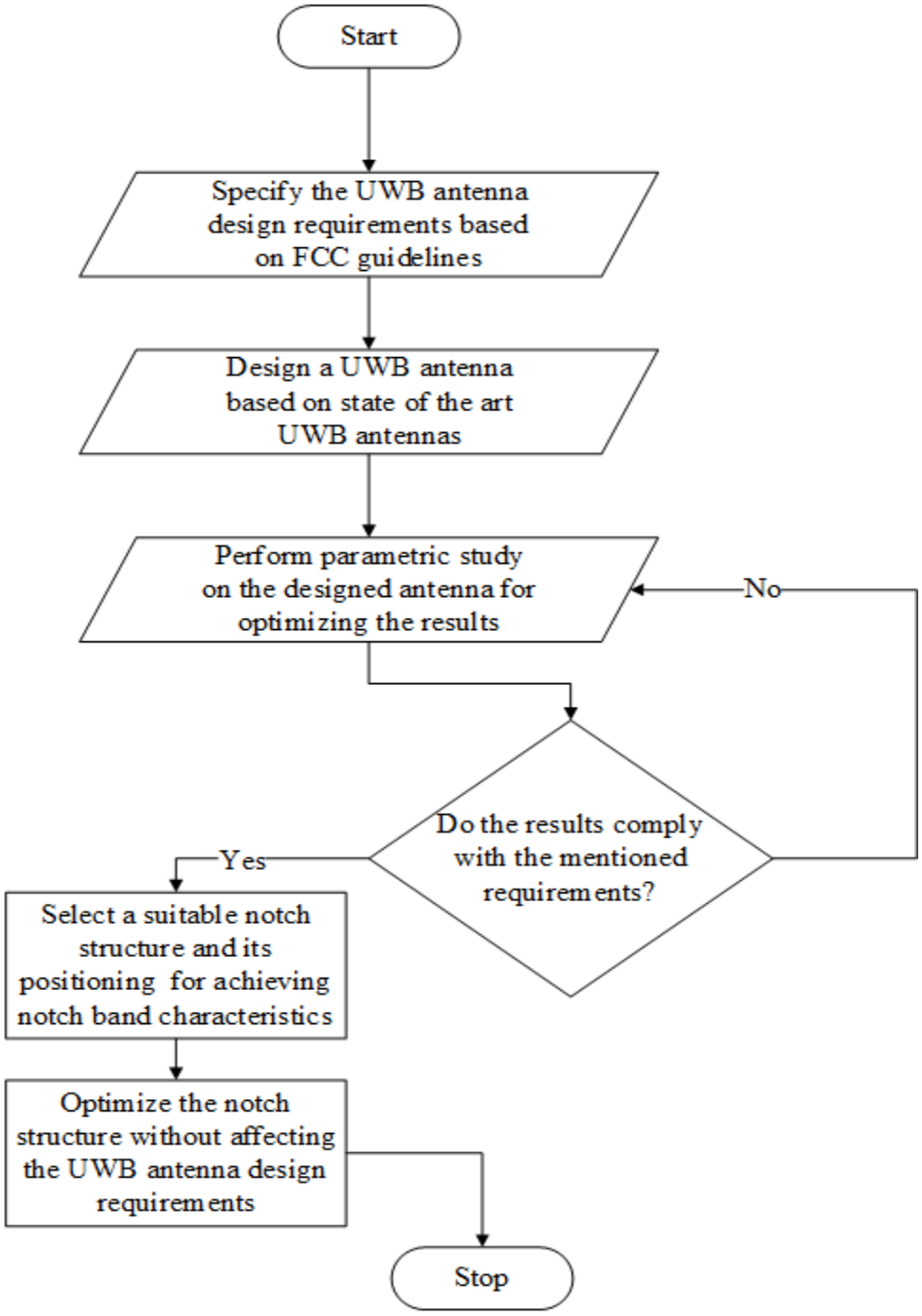

Fig. 3.1 Design methodology for UWB antennas with band notch characteristics

This chapter is organized into five sections. Section 3.1 represents the introduction whereas Section 3.2 and Section 3.3 demonstrate the design process of planar UWB antenna. Further, Section 3.4 represents the design process of the UWB antenna with band notch characteristics. Finally, Section 3.5 holds a summary of the chapter.

3.2 A CPW Fed Planar UWB Antenna

The UWB antenna design needs to satisfy some of the key characteristics like $Return\ loss < -10dB\ and\ VSWR < 2$ throughout the UWB range. Further, the bandwidth achieved from the UWB antenna should be greater than 500 MHz. In addition, the FCC guidelines for the UWB systems should be strictly followed. CPW feeding technique has been extensively used in UWB antennas for achieving higher bandwidth as compared to other conventional feeding techniques. In this technique, the ground plane and radiating patch are in same plane and due to lesser coupling between the elements wider bandwidth is possible. The design also comprises of a U-shaped stub and rectangular slots in the radiating patch. The final analyzed design provides an impedance bandwidth of 8.12 GHz from 2.71 – 10.83 GHz.

3.2.1 Antenna Structure

The antenna is having a compact size of 27×21×1.6 mm^3. Fig. 3.2 represents the top view and dimensions for the final design. The CPW feeding with a characteristic impedance of 50Ω, an FR4 substrate with a dielectric constant of 4.3, and a tangent loss of 0.025 has been utilized in the design. The ground plane structure has been modified to achieve the desired gain and radiation properties. Table 3.1 presents the final dimensions of the proposed antenna.

Table 3.1 Design parameters of the antenna in mm

WS	21	WF	3.2	GW	1
LS	27	LF	6.27	GW1	5.5
GL1	1.31	GL3	2.1	GL5	5.3
GW2	1.31	GW4	7.5	GL2	2.1
GW3	2.6	GW5	4.4	GL4	12.9
LP	8.4	HS	1.6	WP	12

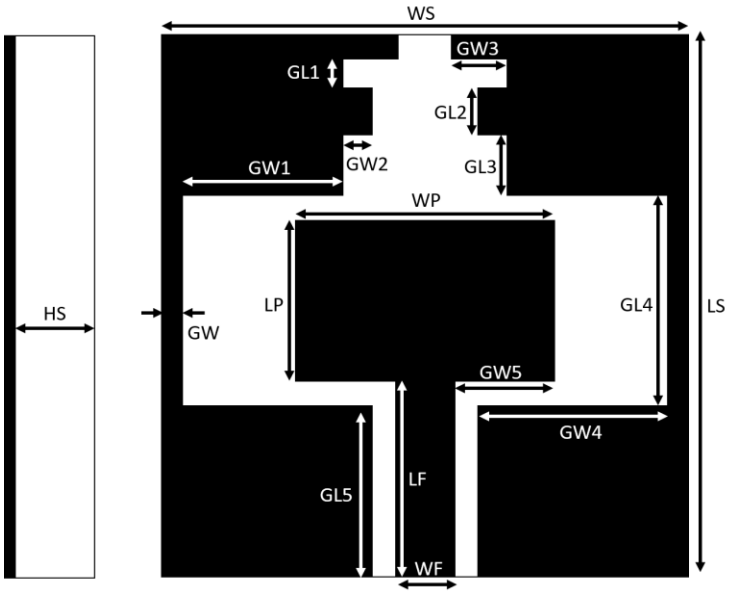

Fig. 3.2 Design structure of the antenna

3.2.2 Parametric Study

In this section, the parametric study of the designed antenna is presented. The main focus of this study is to achieve the desired bandwidth for UWB operation i.e., 3.1-10.6 GHz. Also, the stable gain and radiation properties of the antenna are evaluated while achieving this operation. All the parameters mentioned in Table 3.1 have been analyzed in the simulation.

- *Effect of WF*

The parameter WF changes the bandwidth of the designed antenna as the value of f_h varies from 10 GHz to 11.07 GHz with a variation of WF from 2.6 mm to 3.4 mm. However, this parameter has a negligible impact on the f_l as it varies in the range of 2.69-2.78 GHz. The maximum bandwidth is attained with WF = 3.4 mm and it provides a bandwidth of 8.38 GHz i.e., 2.69-11.07 GHz. However, WF = 3.2 mm has been selected as the final value of WF as it also gives good performance related to other essential parameters for UWB operation. Fig. 3.3 and Table 3.2 demonstrates the bandwidth as well as the various values of f_h and f_l with a variation of WF.

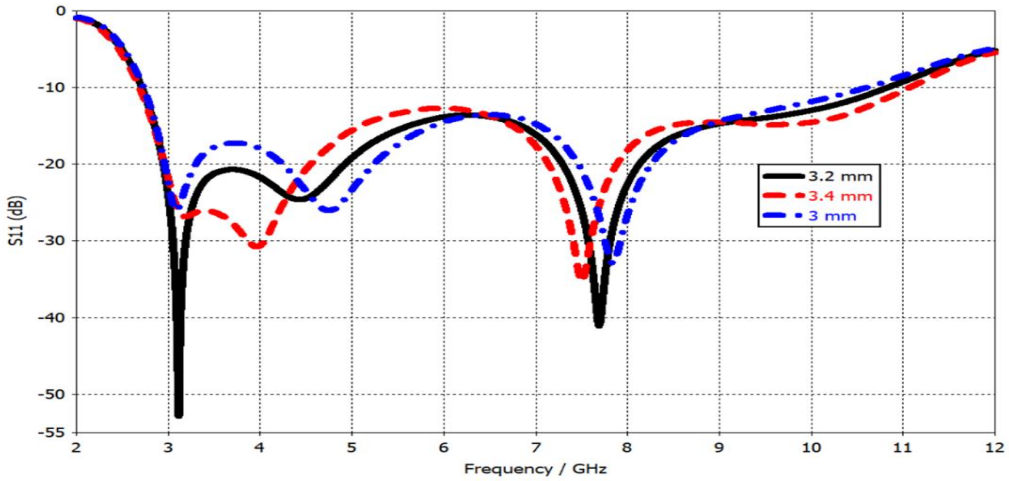

(a)

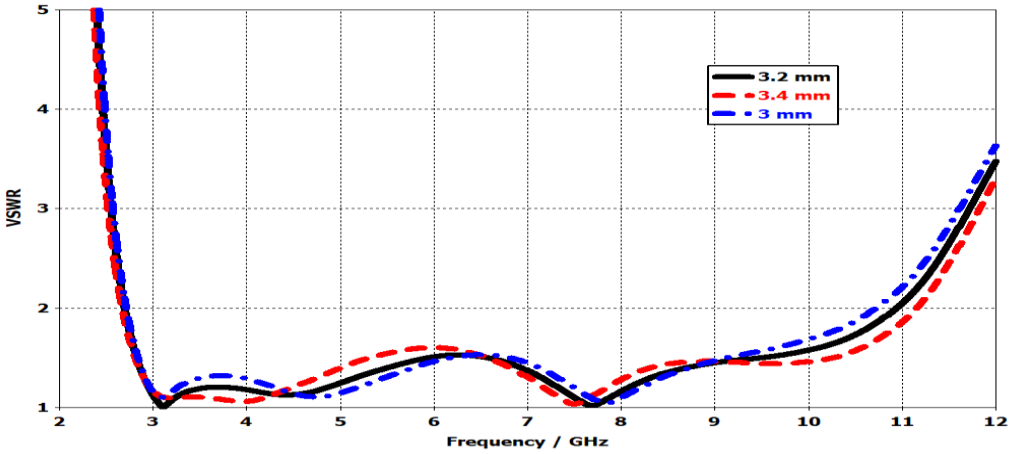

(b)

Fig. 3.3 (a) S_{11} with variation in WF (b) VSWR with variation in WF

Table 3.2 Bandwidth of the antenna with variation in WF

Value of WF (mm)	**Lower Frequency (GHz) (f_l)**	**Higher Frequency (GHz) (f_h)**	**Bandwidth (GHz) ($f_h - f_l$)**
2.6	2.76	10.2	7.44
2.8	2.73	10.47	7.74
3	2.7	10.73	8.03
3.2	2.71	10.83	8.12
3.4	2.69	11.07	8.38

- *Effect of GW*

Similar to WF, the parameter GW also varies the bandwidth of the antenna. However, GW affects the lower frequency f_l unlike WF which mainly has an impact on the higher frequency f_h.The values of GW are varied from 0.5 mm to 2 mm and bandwidth fluctuates between 7.4 GHz – 8.83 GHz in the UWB range. Fig. 3.4 reveals the impact of GW on S_{11} (dB) and VSWR of the antenna. Table 3.2 presents different values of f_h and f_l along with bandwidths. Finally, GW = 1mm is selected as it provides good agreement with other antenna parameters.

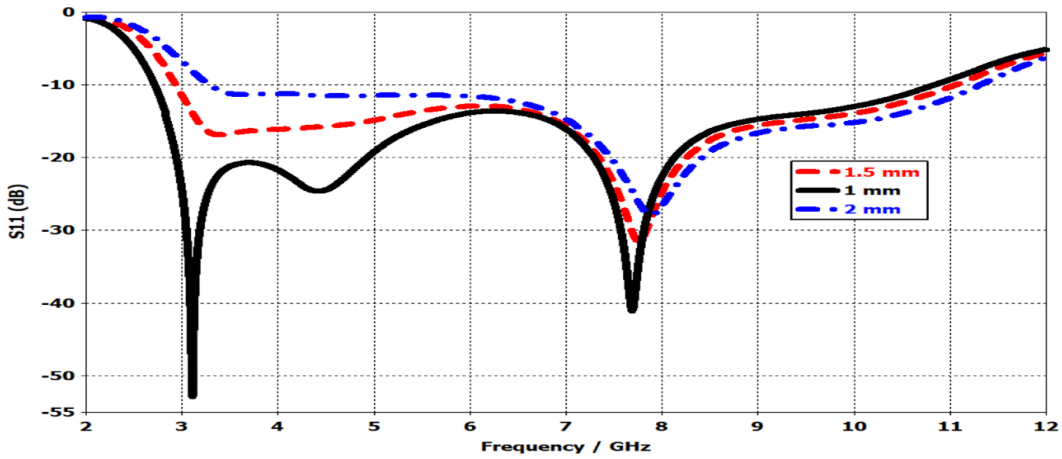

(a)

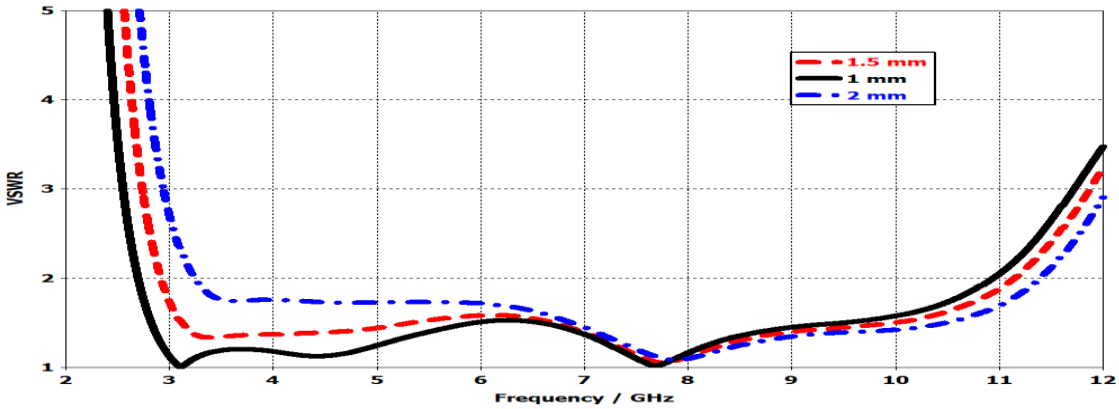

(b)

Fig. 3.4 (a) S_{11} with variation in GW (b) VSWR with variation in GW

Table 3.3 Bandwidth of the antenna with variation in GW

Value of GW (mm)	**Lower Frequency (GHz) (f_l)**	**Higher Frequency (GHz) (f_h)**	**Bandwidth (GHz) ($f_h - f_l$)**
0.5	2.46	10.8	8.34
1	2.71	10.83	8.12
1.5	2.91	11.15	8.24
2	3.29	11.31	8.02

Table 3.4 Bandwidth of the antenna with variation in WP

Value of WP (mm)	**Lower Frequency (GHz) (f_l)**	**Higher Frequency (GHz) (f_h)**	**Bandwidth (GHz) ($f_h - f_l$)**
10	2.67	10.86	8.19
11	2.69	10.92	8.23
12	2.71	10.83	8.12
13	2.73	10.70	7.97
14	2.77	10.53	7.8

Table 3.5 Bandwidth of the antenna with variation in GL3

Value of GL3 (mm)	**Lower Frequency (GHz) (f_l)**	**Higher Frequency (GHz) (f_h)**	**Bandwidth (GHz) ($f_h - f_l$)**
0.6	2.69	8.24	5.55
1.1	2.7	10.40	7.7
1.6	2.71	10.68	7.97
2.1	2.71	10.83	8.12
2.6	2.72	10.94	8.22
3.1	2.73	11.03	8.3

Similarly, the effect of WP and GL3 on antenna bandwidth can be observed in Table 3.4 and Table 3.5 respectively which represent the variation in the bandwidth of the antenna with WP and GL3.

3.2.3 Surface Current Distribution

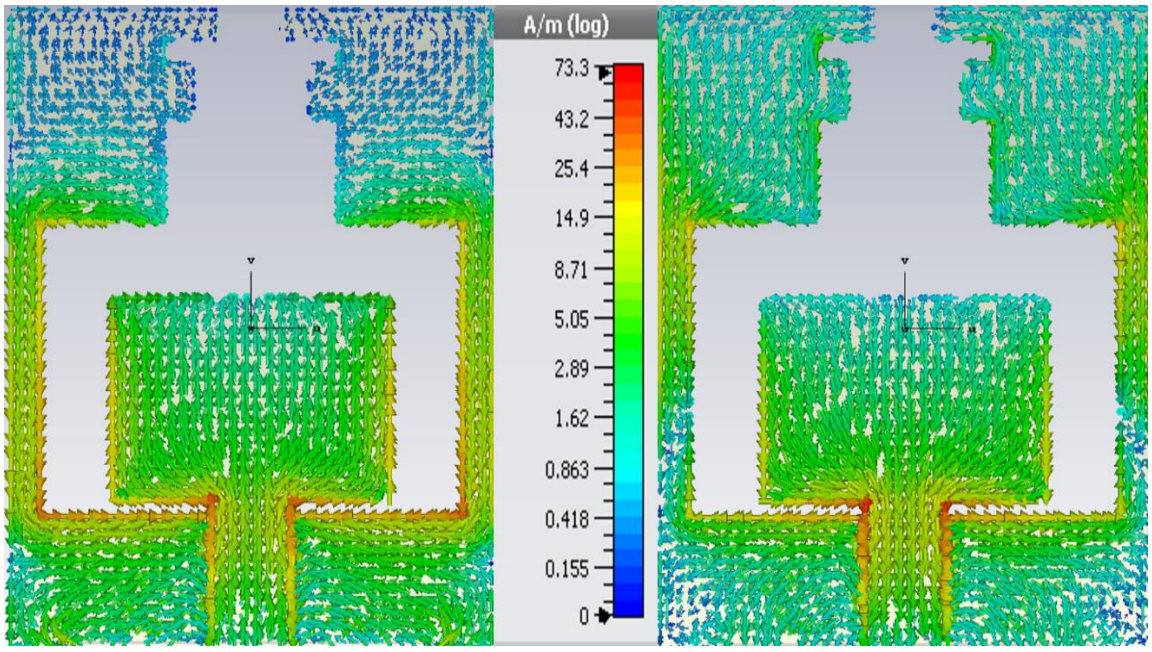

(a) (b)

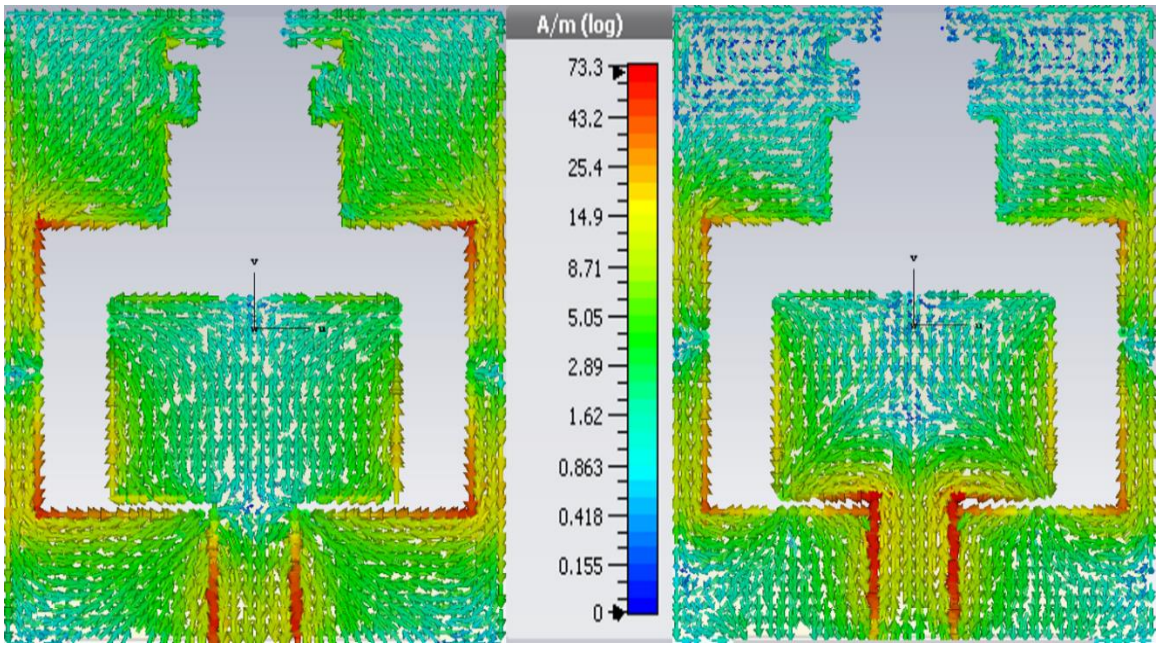

(c) (d)

Fig. 3.5 Surface current distribution of the antenna at (a) 4 GHz (b) 6 GHz (c) 8 GHz (d) 10 GHz

Fig. 3.5 represents the surface current distribution of the antenna for different frequencies in the UWB range. It can be observed that most of the current concentration is near the feedline and the side arms of the ground plane. This distribution is almost uniform throughout the UWB range except at a few higher frequencies where the volume of the current increases slightly. Due to this, the radiation characteristics of antenna get effected at these frequencies. However, the overall UWB performance remains unaffected at these frequencies.

3.3 Modified L-Slot UWB Antenna with Microstrip Coupled Feed

In this section, A UWB antenna with an L-shaped slot and a coupled microstrip feedline is analysed. To realize the L-shaped slot antenna for the UWB operation, a stub is added to a rectangular shaped slot of the ground plane. Further, the position of the feed-line is optimized to attain the desired bandwidth. The size of the proposed antenna is very small i.e., 25×25×1.6 $mm^{3,}$ and is designed and fabricated on the FR4 substrate. This antenna provides the impedance bandwidth (S_{11} < -10 dB) of 8.19 GHz (2.8-10.99 GHz). Moreover, the antenna offers a stable radiation pattern and a gain of more than 2.8 dB over the UWB range.

3.3.1 Antenna Design and Parameters

The antenna design is given in Fig. 3.6 and parameter dimensions of the design are given in Table 3.6. The antenna is designed on a commercially cheap FR4 substrate having a thickness of 1.6 mm, dielectric constant (ε_r) of 4.4, and a loss tangent of 0.025. Initially, a rectangular slot of 16×21.7 mm^2 is made on the ground plane of the antenna. Then, in order to achieve the enhanced impedance bandwidth, a stub of size 10.75 mm is added from the right side of the ground plane toward its center. This forms the L-shape slot in the ground plane of the antenna. Furthermore, to overcome the coupling between the ground plane and feedline, a small slot of width W2 is made at the bottom of the ground plane as shown in Fig. 3.6. The position of the microstrip line is optimized to realize efficient UWB operation.

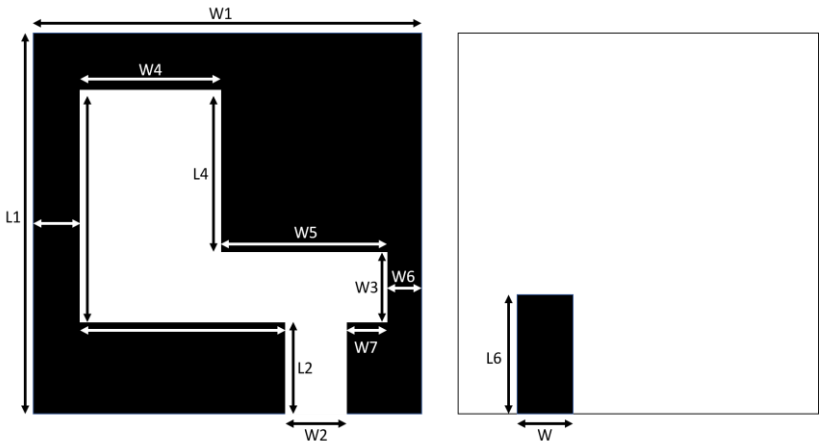

(a) (b)

Fig. 3.6 Configuration of the antenna. (a)Top view (b) Bottom view

Table 3.6 Parameters with size in mm

W1	25	W8	13.5
W2	3	L1	25
W3	4.3	L2	4.8
W4	10	L3	5.25
W	3	h	1.6
W7	3	L6	9.75
W6	1	L5	15
W5	9.5	L4	10.75

3.3.2 Parametric Analysis

Fig. 3.7 shows the modifications in the antenna design which resulted in the improved bandwidth of the design. The first design in Fig. 3.7 (a) is antenna A1 with a rectangular slot and a centered positioned microstrip feedline on either side of the substrate. In order to, then to enhance the impedance BW, a stub is added from the right side of the ground plane toward its center which results in antenna design A2 of Fig. 3.7 (b). The enhanced BW can be visualized in Fig. 3.8. Furthermore, to optimize the UWB operation, the feedline is shifted towards the right edge from the center of Antenna 2 which resulted in antenna design A3 shown in Fig. 3.7 (c).

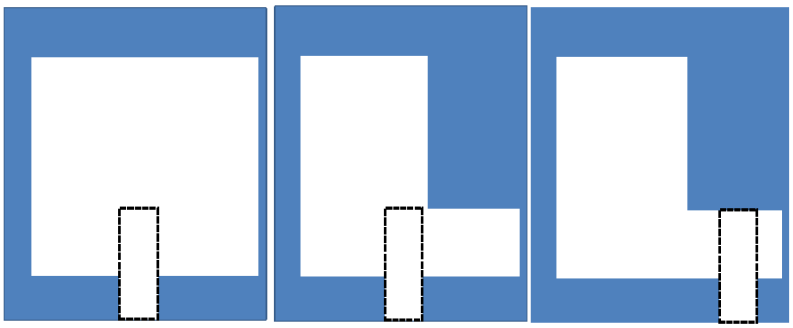

(a) (b) (c)

Fig. 3.7 Enhancement of antenna design (a) A1 (b) A2 (c) A3

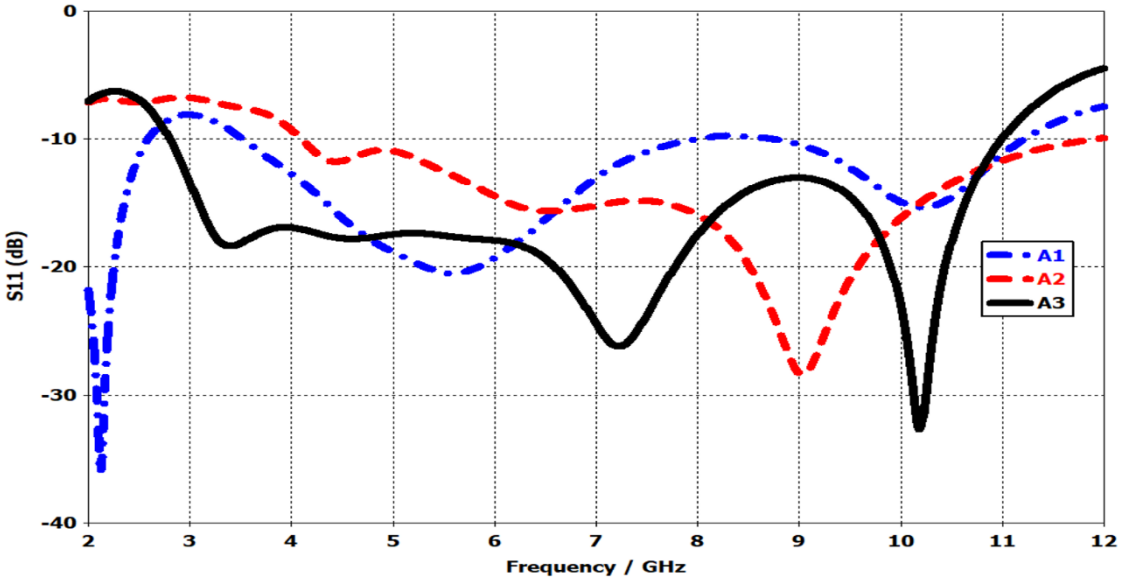

Fig. 3.8 Reflection coefficient (S_{11}) of A1, A2, and A3

For the mathematical analysis of the antenna design, the perimeter of the overall slot (S_p) is calculated from Fig. 3.6 and represented as

$$S_p = L5 + W4 + L4 + W5 + L3 + W7 + 2L2 + W2 + W8 \qquad (3.1)$$

Now, the resonance frequency can be calculated using S_p as [31], [33]

$$f_r = \frac{c}{S_p \sqrt{\in_{eff}}} \qquad (3.2)$$

where, f_r is the resonance frequency, c represents the velocity of light and ε_{eff} is the effective dielectric constant. The ε_{eff} is calculated using [31], [33]

$$\varepsilon_{eff} = \frac{\epsilon_r+1}{2} + \frac{\epsilon_r-1}{2}\left[1 + \frac{12h}{w}\right]^{-1/2} \quad (3.3)$$

where the second part of Eq. (3.3) is very small and is neglected. therefore, Eq. (3) can be approximately written as $\varepsilon_r + 1/2$.

3.3.3 Simulated Results

The simulated result of S_{11} parameter is shown in Fig. 3.9. It can be visualized from Fig. 3.9 that the lower frequency (f_L) and higher frequency (f_H) of operation for the final design are 2.8 GHz and 10.99 GHz respectively. Thus, the antenna design provides an overall bandwidth of 8.1 GHz. The surface current distribution of the final design is illustrated in Fig. 3.10. It can be observed from Fig. 3.10 that the overall current distribution does not change much throughout the UWB range i.e., across the feedline and L-slot.

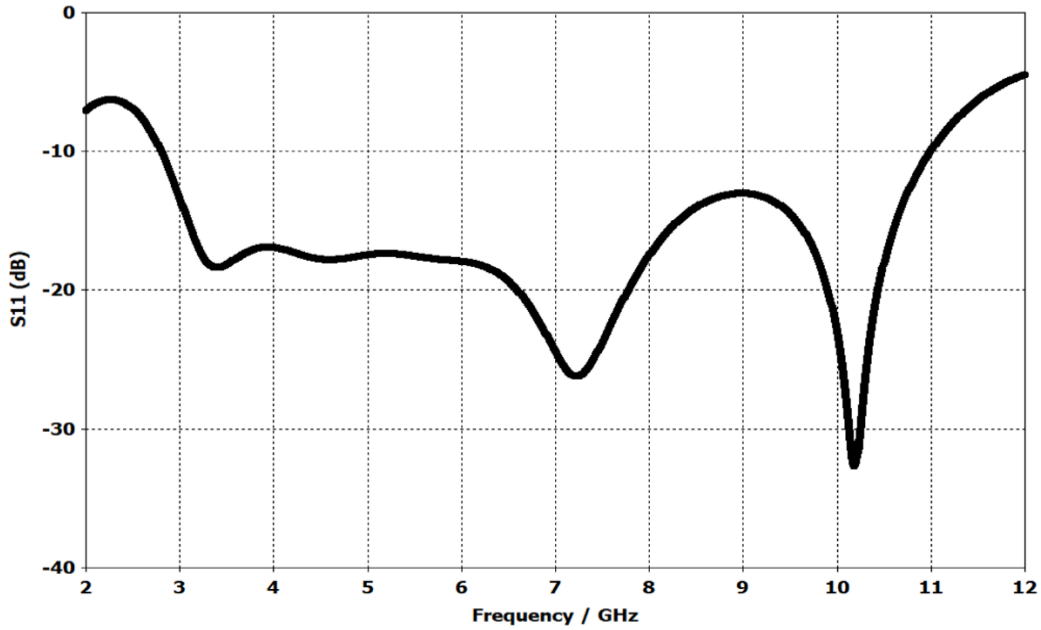

Fig. 3.9 Simulated S_{11} of the antenna design

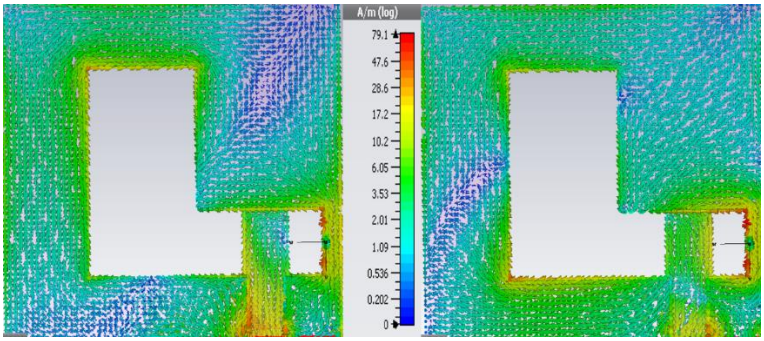

(a) (b)

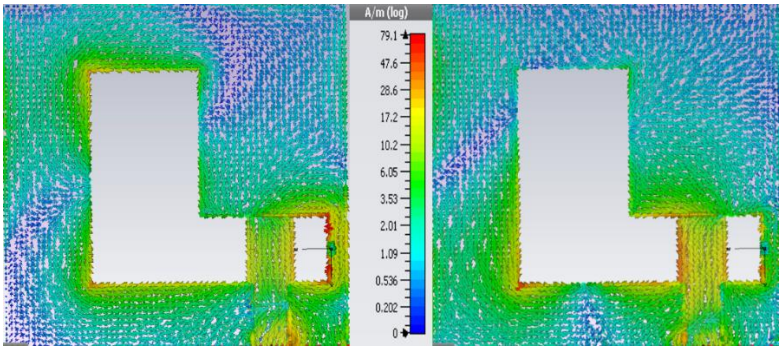

(c) (d)

Fig. 3.10 Surface current distribution of the antenna at (a) 4 GHz (b) 6 GHz (c) 7 GHz (d) 9 GHz

3.3.4 Measured results

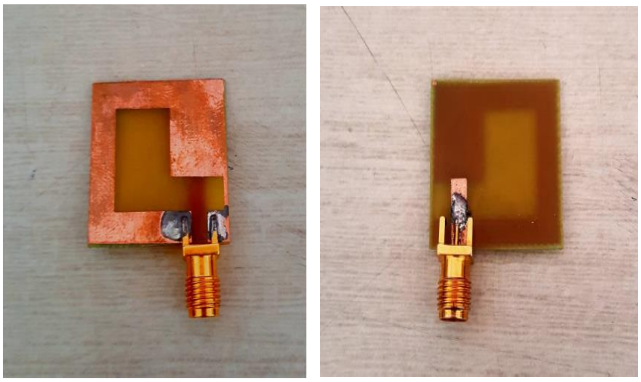

(a) (b)

Fig. 3.11 Fabricated antenna (a) Top view (b) Bottom view

Fig. 3.12 Measurement of the antenna with MS46322A VNA

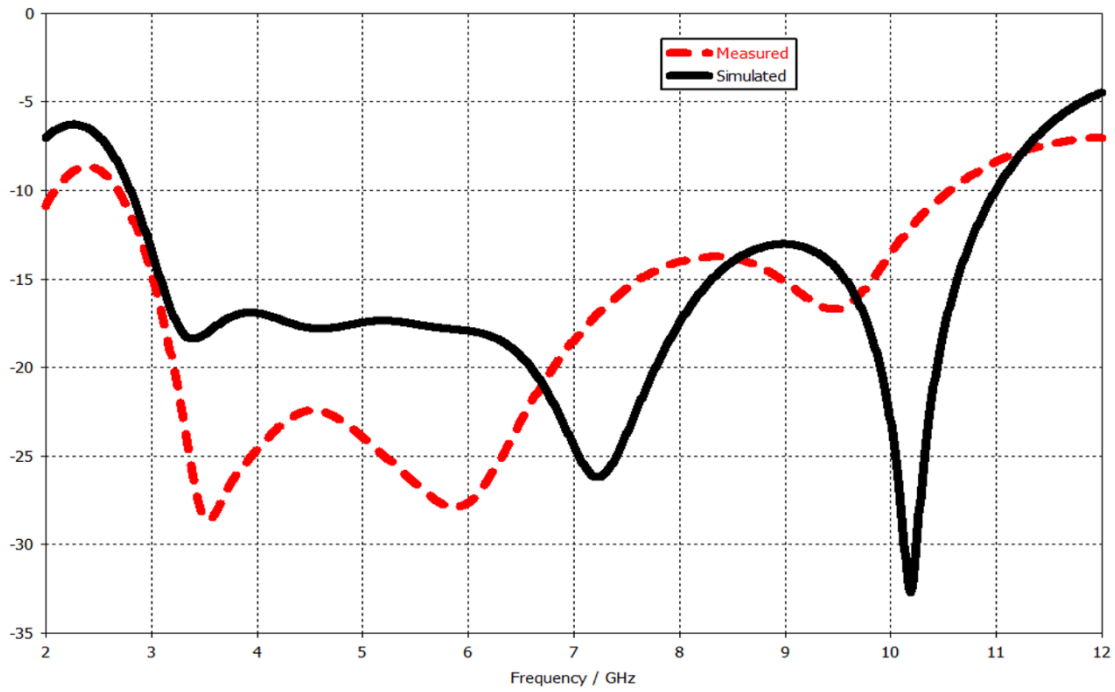

Fig.3.13 Simulated and measured S_{11} of the antenna

Fig. 3.11 and Fig. 3.12 presents the fabricated prototype and measurement setup. For the experimental verification of the design, the prototype of A3 has been fabricated and measured results are obtained with VNA (MS46322A). The simulated and measured results show good agreement with each other as illustrated in Fig. 3.13. However, the

values of f_H and f_L are slightly different in the measured results. This discrepancy in the measured results is possibly due to the fabrication and connector losses. In measured results the values of f_H and f_L are 10.55 GHz and 2.69 GHz respectively providing a bandwidth of 7.86 GHz as compared to the 8.1 GHz bandwidth obtained by simulated results. To summarize, the overall performance of the designed antenna is as per the requirements of UWB systems.

3.4 Circular Monopole UWB Antenna with a Band Notch

In this section, a circular monopole UWB antenna with notch band characteristics at 5.8 GHz is presented. The antenna is having a compact size of 30×30×1.6 mm^3 and is etched on a low-cost FR4 substrate with a loss tangent of 0.025. The monopole structure is used to achieve a large bandwidth and an omnidirectional radiation pattern. The band notch characteristics in the design have been achieved by engraving a modified U-slot in the circular patch. The designed antenna provides stable gain except for notch band and good time-domain characteristics which are essential for the UWB antenna. The measured, as well as simulated results, show good agreement with each other.

3.4.1 Design Outline

As mentioned in the literature [19], [26], [38], the monopole antenna structures provide higher bandwidth as compared to the traditional antenna structures. Hence, a compact planar monopole antenna has been designed as represented in Fig. 3.14. The radiation properties of the structure have been further enhanced by using a circular radiator and modifying the ground. The radius of the circular patch has been adjusted to attain the desired bandwidth and also the ground has been modified to achieve enhanced radiation properties. The antenna is engraved on the FR4 substrate with a loss tangent of 0.025 and the overall volume of the structure is 30×30×1.6 mm^3. Further, the thickness of the substrate is chosen as 1.6 mm which is easily available commercially. For achieving the required notch band, a modified U-shape slot is engraved on the radiator. The positioning, as well as the dimensions of the slot, have been altered for achieving the desired notched band. Table 3.7 presents the various design parameters for the proposed design.

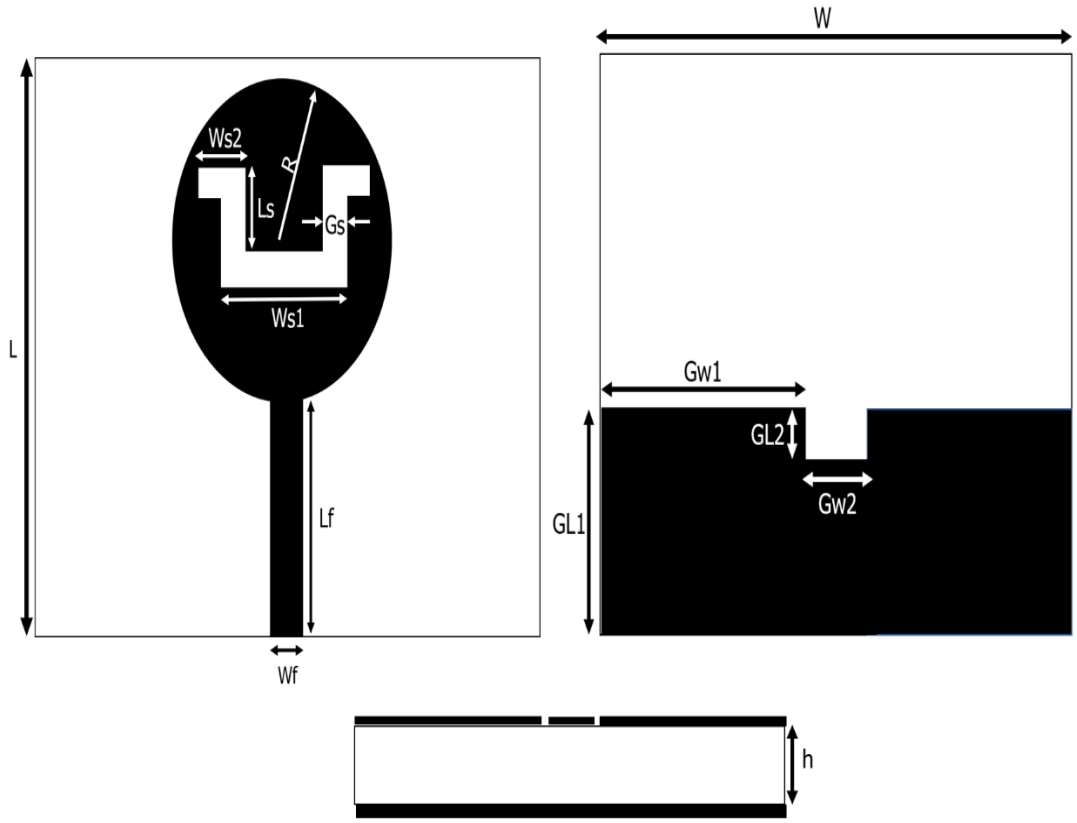

Fig. 3.14 Design outline of the UWB band-notched antenna

Table 3.7 Design parameters of the antenna in mm

R	9	Wf	1.6	Gw1	12.5	W	30	Ls	6	L	30	GL2	2
Gs	2	Ws1	11	GL1	9	Ws2	3.5	Lf	9	Gw2	5	h	1.6

3.4.2 UWB Operation

Initially, a circular shaped radiating patch with parameter R = 10 mm and a simple ground plane for monopole operation is selected. This simple structure provides a bandwidth of 4.50 GHz from 3.60 GHz to 8.10 GHz. However, the radiation properties were not as per the UWB antenna requirement. Hence, parameter R value of the radiator is altered as well as a rectangular stub is engraved on the ground plane for achieving the optimal operation. Finally, as shown in Fig. 3.15 the final selected value of R= 9 mm and the modified ground structure has a rectangular stub with optimized dimensions of GL2 = 2 mm and Gw2 = 5 mm.

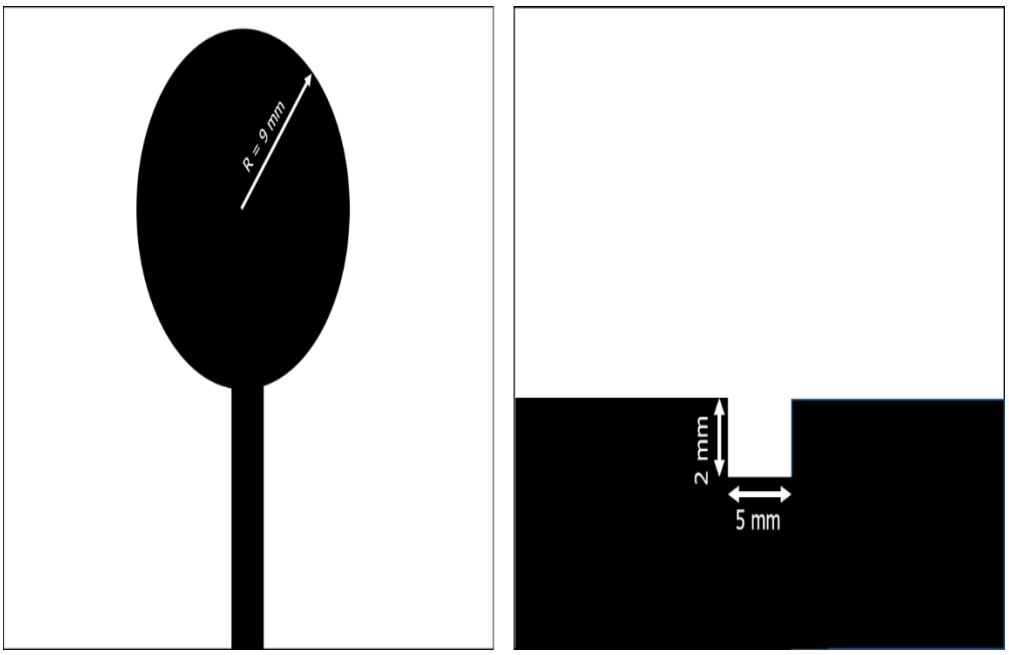

Fig. 3.15 Modified antenna structure for UWB operation

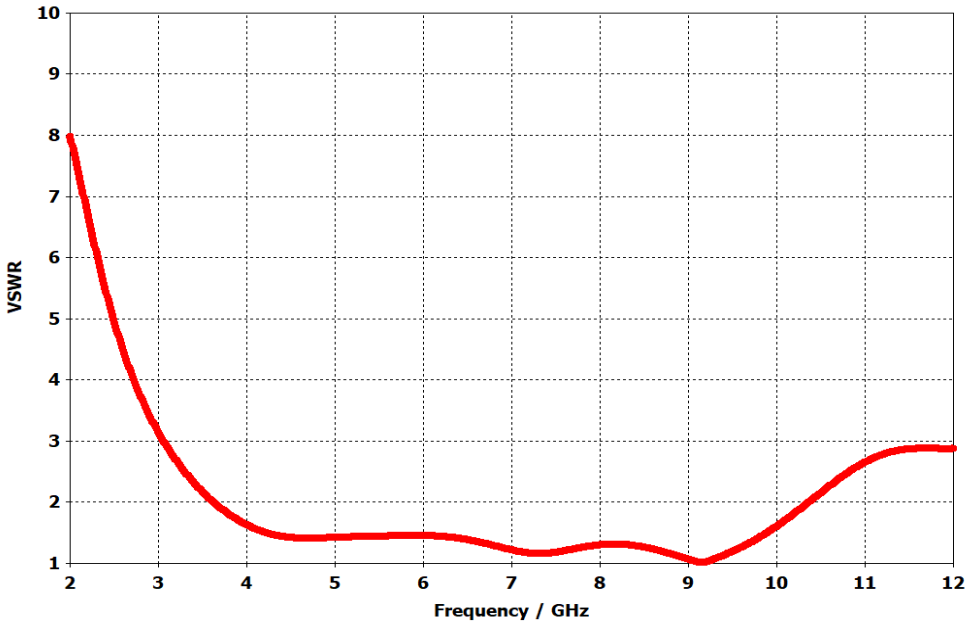

Fig. 3.16 VSWR plot for the modified antenna structure

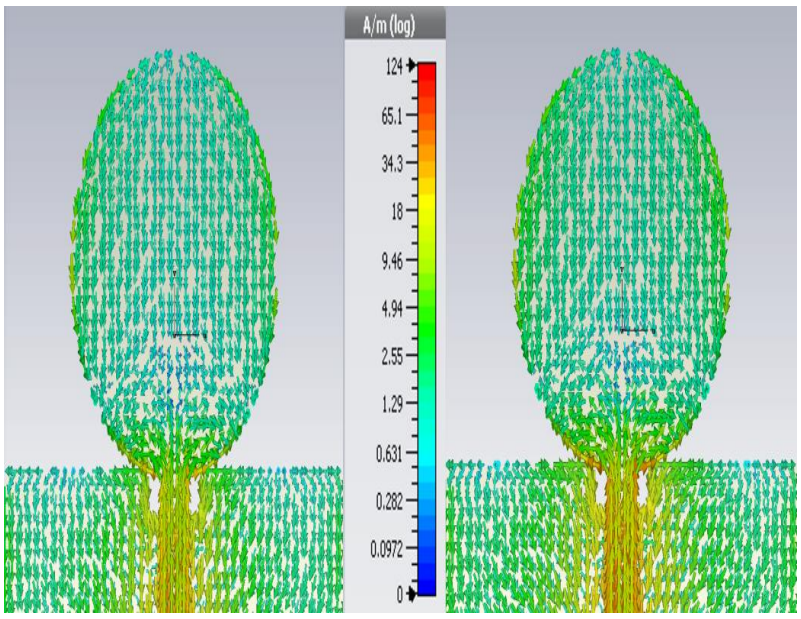

(a) (b)

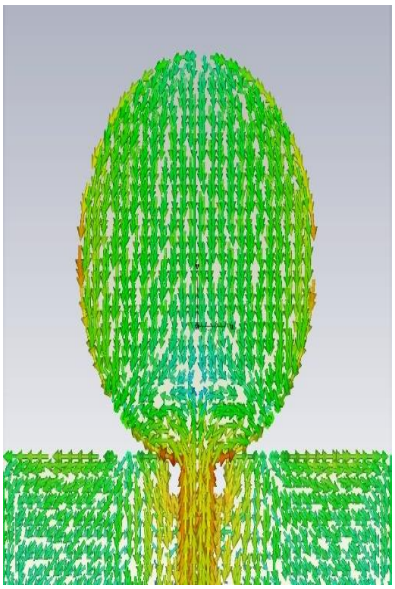

(c)

Fig. 3.17 Surface current concentration for the modified antenna at a different frequency (a) 3.7 GHz (b) 5.8 GHz (c) 7.5 GHz

After the parametric analysis, the modified antenna structure provides the bandwidth of 6.74 GHz i.e., 3.62 GHz to 10.36 GHz. A bandwidth improvement of 2.24 GHz is achieved from the initial antenna structure. Further, this structure provides good

radiation properties and stable gain which is essential for UWB antennas. Fig. 3.16 presents the VSWR plot for the modified antenna structure for the UWB operation. The surface current for the antenna also remains same throughout the bandwidth for UWB operation which is portrayed in Fig. 3.17.

3.4.3 Band-Notch Operation

As discussed in Section 3.4.2, the band notch operation in the proposed design is implemented using a modified U-slot. Firstly, a traditional U-shaped slot is chosen and the dimensions are chosen based on the design equation for U-slot which is given by [36,37]

$$F_n = \frac{C}{2(L_n + W_n)\sqrt{\varepsilon_{eff}}} \tag{3.4}$$

where, L_n is the slot length, W_n is the slot width, F_n is the center notch frequency which is at 5.8 GHz, ε_{eff} is the effective dielectric constant of the substrate and C is the velocity of light = $3X10^{8} m/sec$. By using Eq. (3.4), the slot dimensions are calculated. However, the notch frequency in the simulated results is observed at 5.21 GHz that is different from the desired notch band center frequency. Therefore, the dimensions, as well as the structure of the U-slot are modified to achieve the precise center notch frequency. Further, the positioning of the U-slot is also done precisely to achieve the desired results.

3.4.4 Simulated Results

The presented UWB antenna achieves a bandwidth of 7.19 GHz from 3.43 GHz to 10.62 GHz as visualized in Fig. 3.18. The notch band from 5.07 GHz to 6.54 GHz with a center notch frequency of 5.78 GHz and a small variation of 0.02 GHz is observed in the simulated results. The radius of the circular radiator, along with the dimensions of ground structure, are accustomed to achieve the mentioned results. While modifying the antenna structure for notch operation, to get the best results, the other required parameters for UWB operation are also observed precisely.

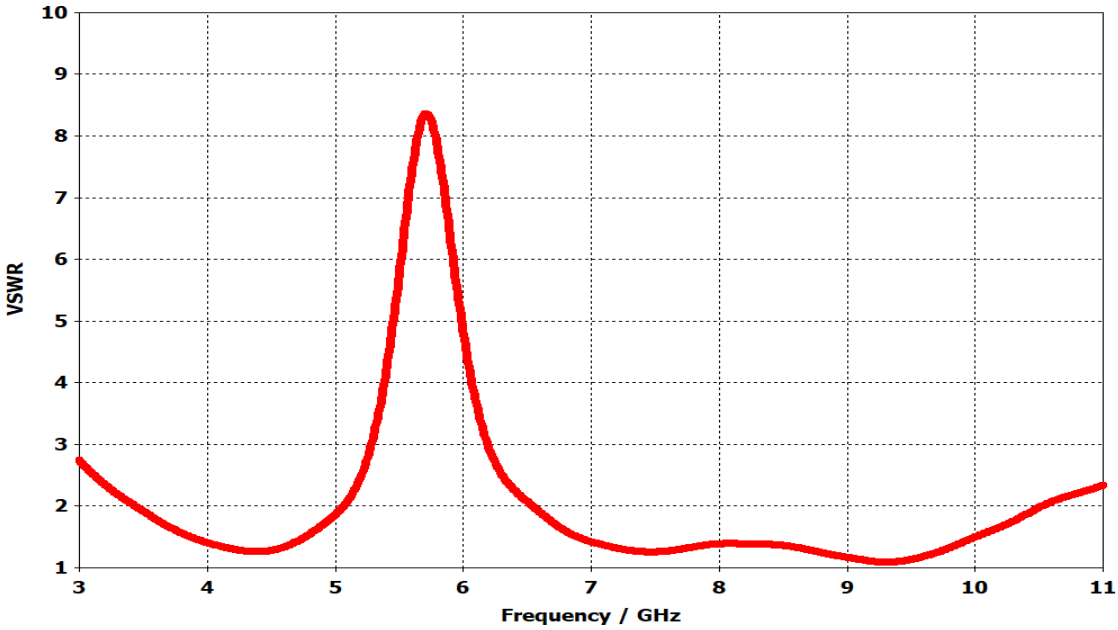

Fig. 3.18 VSWR plot of the band-notched antenna

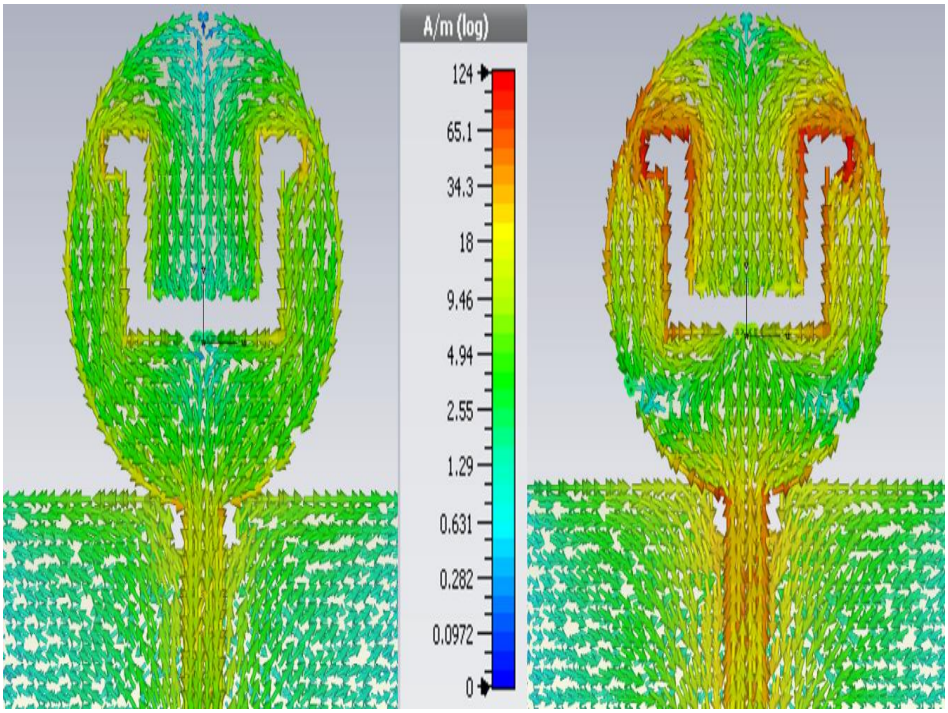

(a) (b)

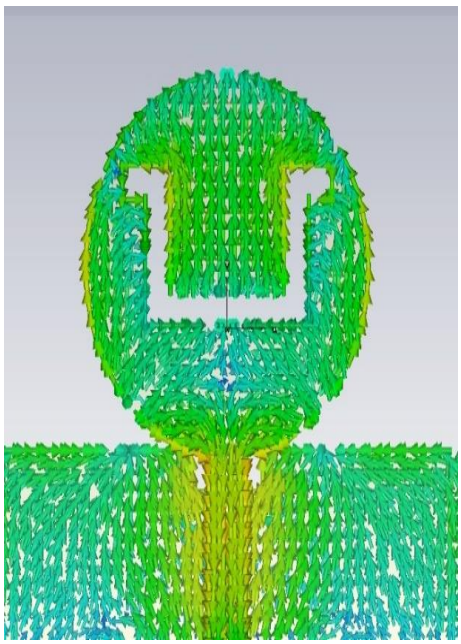

(c)

Fig. 3.19 Surface current concentration for the final antenna design at different frequency (a) 3.70 GHz (b) 5.78 GHz (c) 7.50 GHz

The surface current of the given antenna at different frequencies is presented in Fig. 3.19. This can be visualized from Fig. 3.19 that the current concentration is maximum at the modified U-shape slot intended for the center notch frequency i.e., 5.78 GHz. Due to this, the mentioned notch frequency is completely suppressed by the engraved notch band structure. However, for other two frequencies, the U-shaped slot is not resonating and thus antenna provides the UWB operation.

3.4.5 Measured Results

The prototype of the antenna, as well as its measurement setup, is presented in Fig. 3.20. MS46322A (Anritsu) VNA having a range of 1 MHz to 20 GHz is used for the measurement of group delay and VSWR. For measurement of the gain as well as radiation pattern, the antenna was positioned in the anechoic chamber with a distance which is more than the minimum far-field distance from the reference antenna. For the measurement of the group delay, two similar antennas were placed in face to face configuration with a distance greater than the aforementioned far-field distance.

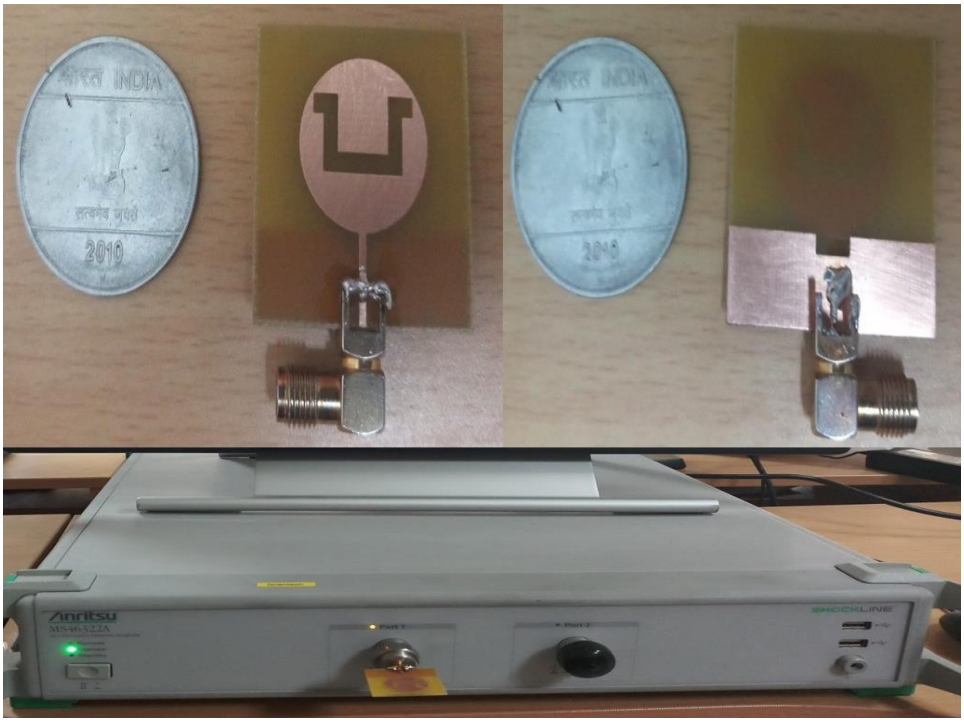

Fig. 3.20 Fabricated prototype antenna and its measurement setup

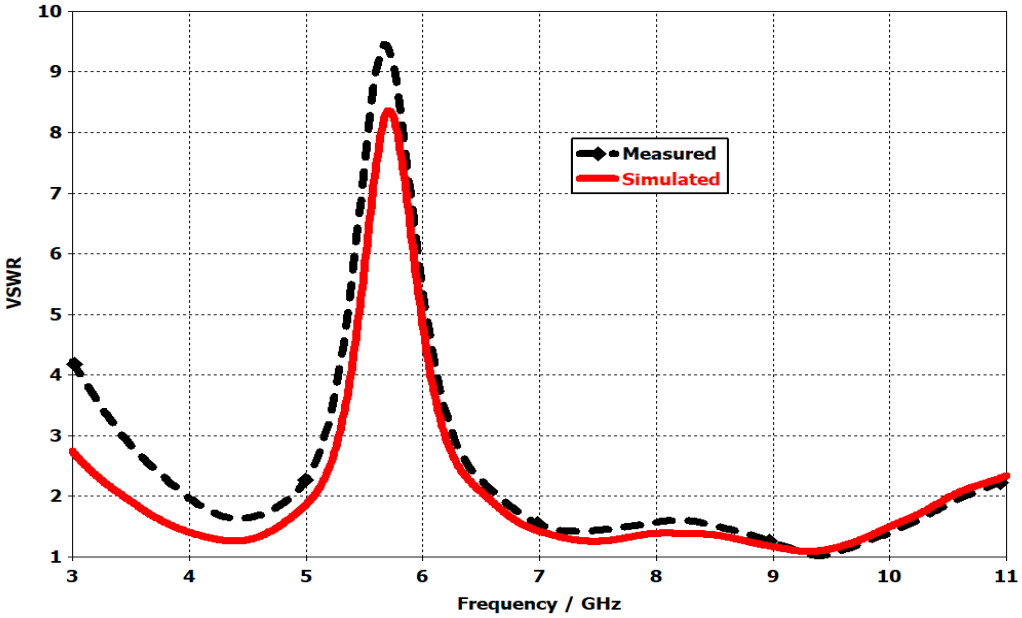

Fig. 3.21 Measured vs Simulated VSWR

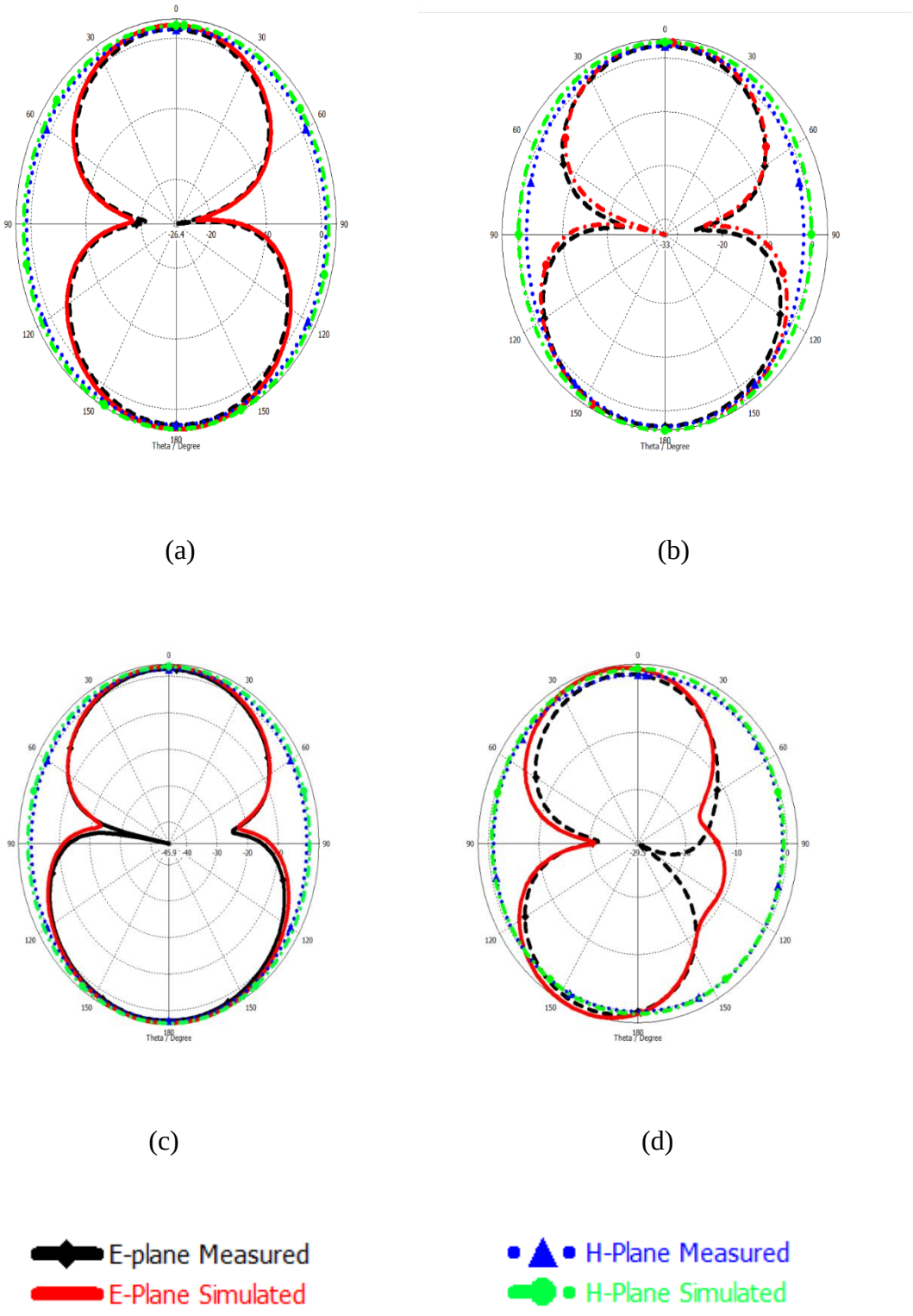

Fig. 3.22 Measured vs simulated radiation pattern at different frequency (a) 3.6 GHz (b) 5.07 GHz (c) 4.80 GHz (d) 6.54 GHz

The measured and simulated VSWR show suitable agreement with each other as depicted in Fig. 3.21. The lower and higher frequency for UWB operation is slightly shifted to 3.96 GHz and 10.7 GHz respectively. For notch band operation the center frequency is 5.72 GHz and a small difference of 0.06 GHz is calculated between the simulated and measured results. The measured bandwidth for the notch is a tad higher than the simulated notch bandwidth i.e., 1.76 GHz ranging from 4.88 GHz to 6.64 GHz. The E-Plane and H-plane normalized radiation patterns at a different frequency in the UWB band are presented in Fig. 3.22. The radiation pattern at all mentioned frequencies is omnidirectional in H-plane which is as per the requirement of UWB systems. Further, the E-plane radiation pattern is following the desired radiation pattern except for slight variation at frequencies greater than 6 GHz in the UWB band as portrayed in Fig. 3.22 (d). The gain and radiation efficiency are presented in Fig. 3.23 and Fig. 3.24 respectively. it can be visualized from Fig. 3.23 that the gain is almost stable for the UWB range with a variation of 4 dB and 3 dB except for the notched band where the gain reduces to -3.13 dB and 0.82 dB for measured and simulated results respectively. Similarly, the simulated radiation efficiency is in the range of 73% to 88% except for the notch band where it is reduced to 32% approximately.

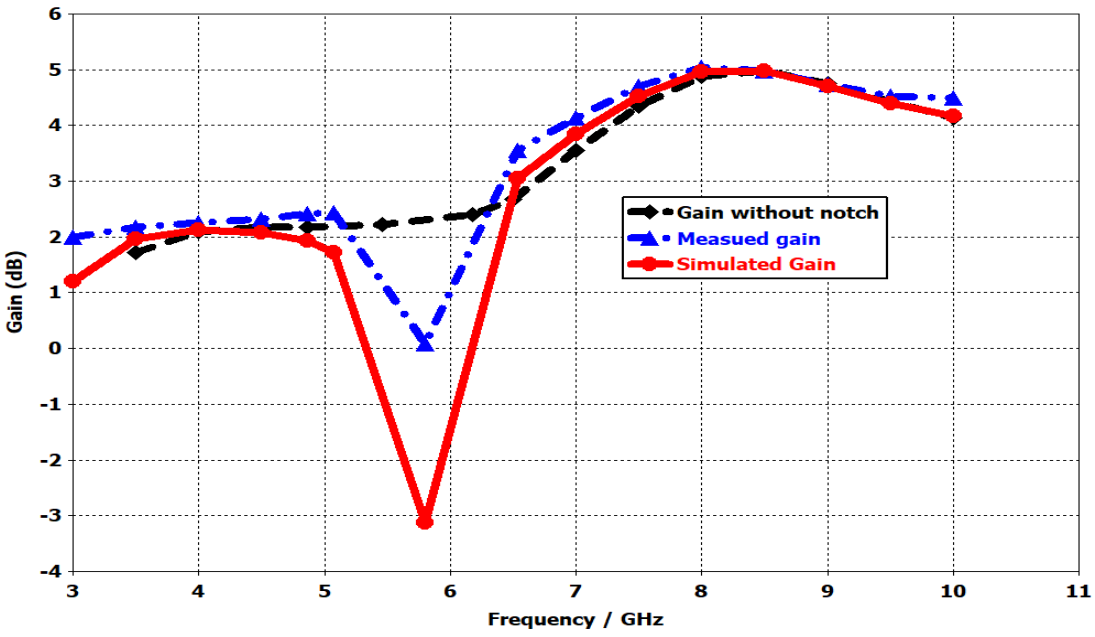

Fig. 3.23 Measured vs simulated gain

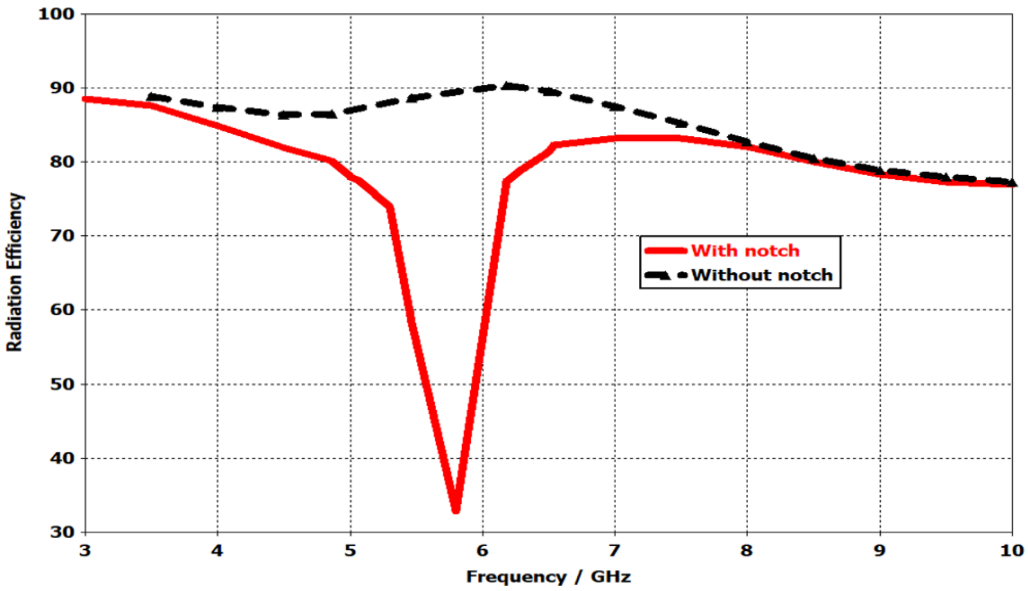

Fig. 3.24 Radiation efficiency

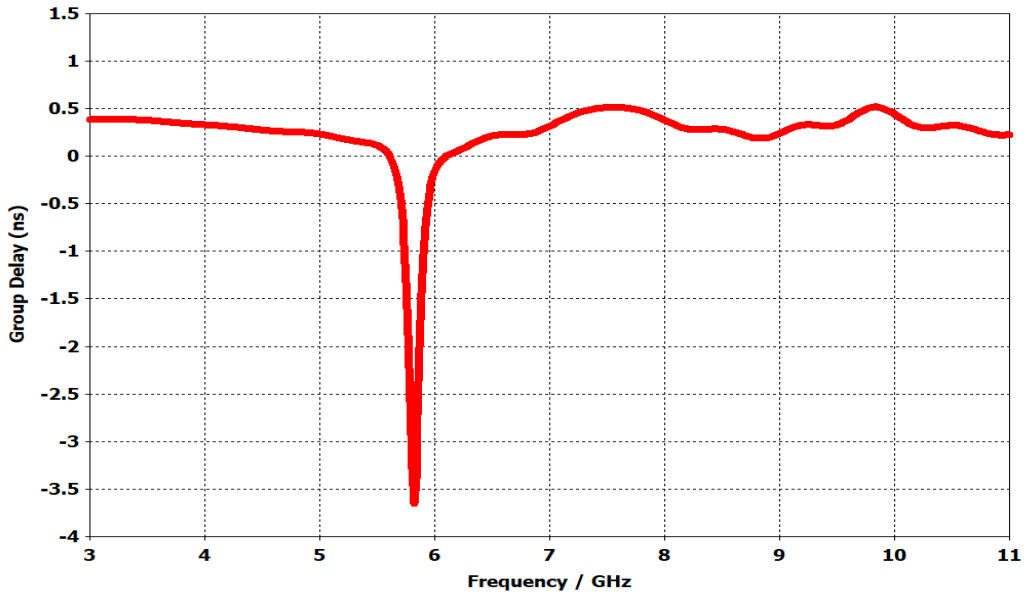

Fig. 3.25 Simulated group delay of the band-notched antenna

Finally, to estimate the time-domain performance of the designed antenna, the group delay of the antenna is presented in Fig. 3.25. It gives the information about the amount of distortion available in the radiated signal via the UWB antenna at a distance.

Flat group delay in the UWB range depicts minimum distortion in the radiated signal and as depicted by Fig. 3.17 linear group delay is observed i.e., in the range of 0 ns to 1 ns except for the notch band where the value is -3.64 ns.

3.5 Summary

In this chapter, three UWB antenna designs have been presented to demonstrate the basic design process for achieving UWB and band notch operation in the planar antenna structures. These designs have been analyzed during the simulation process and different techniques to achieve UWB operation have been employed such as CPW feeding, monopole antenna structure, coupled microstrip feeding, and slot-loading. The most common technique to achieve band notch characteristics i.e., slot-loading has been also demonstrated. To validate the results, antenna designs 2 and 3 have been fabricated and tested. However, while analyzing the design process some other important aspects mentioned in Chapter 1 and Chapter 2 related to UWB antenna design with band notch characteristics have not been discussed thoroughly such as time-domain performance (fidelity factor, dispersion analysis), selection of excitation signal and filter synthesis for band notch operation. These parameters have been discussed thoroughly in the final proposed antenna designs of the thesis in Chapter 4 and Chapter 5.

Chapter 4

Design and Efficient Analysis of a CPW Fed Beveled Patch UWB Antenna with Highly Optimized WLAN (5.15 – 5.825 GHz) Notch Band

In this chapter, a planar antenna with highly optimized WLAN (5.15 – 5.825 GHz) notch for UWB applications is thoroughly investigated based on the overall UWB system requirements. The time-domain performance of the proposed antenna is assessed using dispersion, group delay, and system fidelity factor. Also, the excitation signal is chosen carefully based on the indoor mask for UWB systems. Finally, the filter synthesis of the notched band, equivalent circuit model, phase response, and experimental results have been also presented to validate the results.

4.1 Introduction

In the past decade, the world has seen the proliferation of UWB antenna designs and out of these, the planar antennas have gained popularity amongst researchers due to their small size, cost-effectiveness, near omnidirectional radiation pattern and wideband operation. Therefore, extensive work has been done to elevate the performance of planar UWB antennas by optimizing their shape. For this purpose, various techniques and methods have been developed like to control impedance bandwidth, the use of beveled shape is preferred instead of conventional circular or rectangular shapes or augmenting the shape and size of the ground plane [9], [25], [145-152].

The major challenge in designing a UWB antenna to optimize its radiating and notching characteristics simultaneously. A straightforward and effective way of achieving UWB operation with band notch characteristics is the usage of the additional band-stop filter. On the other hand, similar filtering characteristics can be achieved by introducing a slot in the antenna. This results in the reduction of interference among the UWB system and other existing wireless systems without the need for any extra hardware. Various

techniques such as loading slots and parasitic elements, embedding Split ring resonator structures, EBG structures, and switches have been employed for this task [148].

In [152], a compact resonant cell engraved on the CPW feed is employed as a BSF. In [153], band notching is acquired by inserting L-shaped and ring resonators into the ground plane. To further enhance the notch band performance, two stubs and slits of half-wavelength are designed in the circular patches and tapered slot, respectively in [154]. Also, to illustrate the performance of the notch band, a measure in terms of roll-off criterion (ROC) has presented by evaluating the ratio of the -3 dB bandwidth to the -10 dB bandwidth of the rejected band in [155].

It is a challenge to etch the UWB radiating patch directly without using any parasitic structures or additional filters [156-158]. So, one should find a more suitable form of the fragment and its location of engraving on the patch or ground plane to attain the desired band notch characteristics. Recently, due to the flexibility provided by these structures, they have found applications in several UWB antenna designs [111],[159],[160]. Another important parameter is to select an appropriate impulse signal to excite the UWB antenna that satisfies the FCC indoor mask with good power efficiency. But very few antenna designs have addressed the use of pulse design techniques for UWB systems [9],[11], [169-171].

In UWB systems, as the transmission is done through narrow pulses in the time domain, therefore it is also essential to investigate the UWB antenna performance in the time domain. So, parameters such as dispersion, group delay, fidelity factors should be analyzed meticulously [12], [46], [149], [157], [165], [167].

Various designs for achieving single, dual, triple, and quad-band notch characteristics have been proposed in [25], [146], and [148]. However, only a few designs have used optimization techniques for achieving desired notch band characteristics i.e., Artificial Bee Colony (ABC) and differential evolution (DE) [149], Binary particle swarm optimization (BPSO) [154], Particle swarm optimization (PSO) [160], genetic algorithms [172]. But, while realizing optimum notch band characteristics using mentioned algorithms, the key point to note is that the analysis of other desired UWB

antenna parameters such as gain, radiation pattern, and group delay is not included in the optimization process.

Table 4.1: Comparison of the proposed antenna and reference antenna designs with WLAN notch band characteristics

Ref.	**Antenna size (mm^2)**	**Max. gain over passband (dB)**	**Peak gain at rejected center freq. (dB)**	**Notched band**	**Structure used for notch band**	**Notch band optimization**	**Time-domain analysis**
[34]	45 × 36	7	-2	5 - 6	Arched Slot	----	----
[46]	30 × 30	9	-2	5 – 6	Two symmetrical L-shaped slits	----	Yes
[51]	33 × 26	6	-0.7	4.7 – 5.5	T-shaped open slot	----	----
[52]	18.17 × 17.16	6.7	- 6	5.1 - 5.9	C- shaped annular ring	----	----
[111]	38 × 40	6	-2.5	5.2 - 5.8	EBG Structure	----	----
[149]	29 × 29	3.3	-4	5.1 - 5.9	Inverted U slit and C strips	Yes	----
[150]	30 × 24	----	----	5.15 - 5.85	Inserting slits	Yes	----
[151]	----	----	-3.3 and 4	5.05 - 5.35 and 5.66 - 5.83	Open loop resonator	Yes	----
[152]	30.72 × 26.82	----	----	5.2 - 5.8	L shaped parasitic stubs	----	----
[153]	32 × 28	6	-1	5 - 5.6	Dual Y shaped slot	----	----
[154]	10 × 16	----	----	4.88 - 5.36 and 5.64 - 6.04	------	Yes	----
[155]	35 × 35	6	-1.5	4.8 - 5.7	C-shaped slots	----	----
[156]	40 × 31	6.2	-7	5.24	Open loop resonator	----	----

Ref.	Antenna size (mm^2)	Max. gain over passband (dB)	Peak gain at rejected center freq. (dB)	Notched band	Structure used for notch band	Notch band optimization	Time-domain analysis
[157]	29 × 30	3.5	-20	5.2 – 5.95	Square Ring resonator	----	Yes
[158]	34 × 34	3.97	-21	5.35 - 5.75	Folded Strips	----	----
[160]	32 × 28	----	----	5.138 - 5.945	Trapezoidal slot and rectangular slot	Yes	----
[161]	35 × 30	5	-35	5.24 - 6.46	Open Loop resonator	----	----
[162]	22 × 8.5	----	-4	5.15 - 5.85	Open ended slot and short end ring ended slot	Yes	----
[163]	35 × 24	5	-34	5 – 6	Elliptical Slot and pair of T-shaped stubs	Yes	----
[164]	20.1 × 61	6	-17	4.844 – 6.190	Inverted L slots	Yes	----
[165]	----	7	- 10	5.17 - 6.14	Quarter wavelength slot resonator	----	Yes
[166]	30 × 28	7	-4	5.2 - 6	half-wavelength stubs and slits	----	----
[167]	32 × 26	5.2	-5.3	5- 6	EBG Structure	----	Yes
[168]	25 × 25	2	-10	5 – 6	U-shaped Slot	----	----
Proposed work	25 × 25	5.83	-4.65	5.133 – 5.833	C Shaped slot	Yes	Yes

Since, by including these parameters, the design complexity of the algorithms increases drastically and the steady-state condition is difficult to obtain. Therefore, in the proposed design the above-mentioned research gap has been addressed. A compact

planar CPW fed beveled patch UWB antenna with highly optimized WLAN notch band characteristic is presented in this work.

The notch optimization in the design has been accomplished by analyzing a C-shape slot and its dimensions have been divided into multiple fragments. Each fragment has been analyzed and optimized based on the desired notch band (5.15-5.825 GHz) and its center frequency i.e., 5.487 GHz. Also, other UWB antenna parameters such as stable gain, omnidirectional radiation pattern, flat group delay response, and fidelity factor have been thoroughly studied. Moreover, the selection of excitation signal based on the FCC indoor mask, filter synthesis, phase response, and measured results are also presented. The comparison of the proposed antenna with other antenna designs with WLAN notch band characteristics is presented in Table 4.1.

This chapter is organized into six sections. Section 4.1 provides the introduction of the chapter. Section 4.2 and Section 4.3 give the design configuration and parametric analysis of the proposed antenna respectively. Further, Section 4.4 presents the time domain analysis and phase response of S_{21} for the designed antenna. Finally, Section 4.5 and 4.6 hold the measurement results of the proposed antenna and summary of the chapter respectively.

4.2. Design Configuration of the Proposed Antenna

As discussed in Section 4.1, the common procedure for designing the UWB antenna is to incorporate the CPW feeding and to use monopole antenna structures. This improves the impedance bandwidth and supports in achieving an omnidirectional radiation pattern which is essential for UWB operation. Hence, CPW feeding is used in the proposed design. Along with the aforesaid procedure, the band notch characteristics in the design are achieved by etching an enhanced C-shaped slot from the radiating patch. The dimensions of the slot are carefully chosen for attaining improved WLAN notch (5.15 GHz-5.825 GHz). This structure is engraved on the FR4 substrate having a dielectric constant of 4.3 and loss tangent of 0.025. The height of the substrate is kept constant i.e., 1.6 mm which is one of the standards for PCB thickness. The geometry of the proposed antenna structure is given in Fig. 4.1 and t can be visualized from Fig. 4.1

that the antenna comprises of the beveled patch, CPW feed, and an enhanced C shaped slot. The final dimensions of the proposed antenna design are listed in Table 4.2.

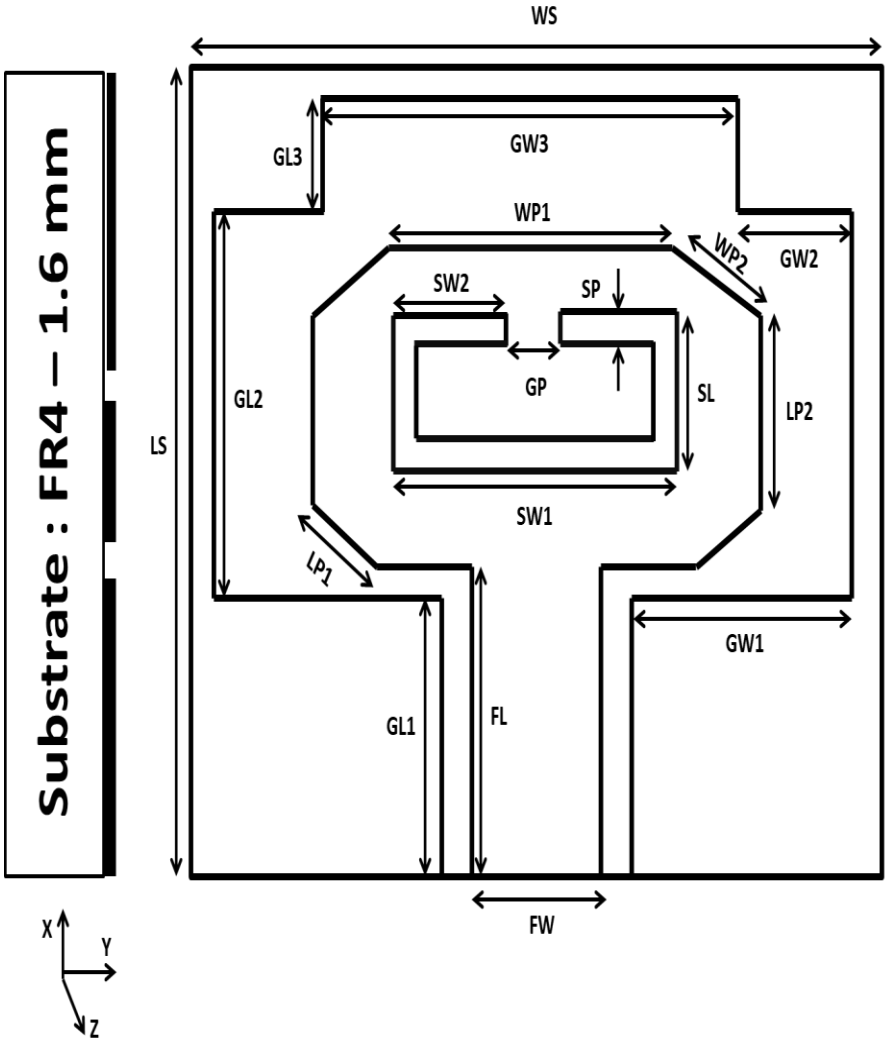

Fig. 4.1 Geometry of the proposed design

Table 4.2 Dimensions of the proposed antenna in mm

LS	25	LP1	1.83	WS	25	LP2	5.5	GL1	8
WP1	10.35	GL2	11	WP2	2.62	GL3	5	FL	9
GW1	9.6	FW	3.8	GW2	6	SW1	9.6	SP	1
GW3	11	SW2	3.8	SL	3	GP	2	h	1.6

4.3 Parametric Analysis

In this section, the parametric analysis of the proposed antenna has been presented. These parameters include the selection of the excitation signal, design process, notch band optimization, bandwidth enhancement, filter synthesis, and equivalent circuit model.

4.3.1 Selection of the Excitation Signal

UWB systems need to operate within the indoor mask provided by the FCC, (EIRP< 41.3 dBm/MHz), for the entire band of operation (3.1-10.6 GHz). Therefore, the excitation signal for the UWB antenna should be chosen such that its spectrum lies within the FCC mask in the frequency domain. Ignoring this fact, most of the antenna designs available in the literature have used first-order Gaussian pulse as an excitation signal in the UWB design [34], [51], [147], 148], [151-154]. Hence one of the essential requirements of the UWB systems has been compromised and the practical performance of the antenna is affected. However, keeping this fact into consideration, a 5th order Gaussian pulse is used for the excitation of the antenna in the proposed design and its spectrum lies in the FCC indoor mask [9],[11], [169-172]. The Gaussian pulse in the time domain is represented as [170]

$$g(t) = \frac{A}{\sqrt{2\pi}\sigma}\ e^{-\frac{t^2}{2\sigma^2}} \tag{4.1}$$

where A denotes the peak amplitude of Gaussian pulse and σ represents the pulse shaping factor or time constant. The first and fifth-order derivative for the Gaussian pulse is given as:

$$g^{(1)}(t) - \frac{A\ t}{\sqrt{2\pi}\,\sigma^3}\ \ e^{-\frac{t^2}{2\sigma^2}} \tag{4.2}$$

$$g^{(5)}(\mathrm{t}) = \mathrm{A}\cdot\left(-\frac{\mathrm{t}^5}{\sqrt{2\pi}\cdot\sigma^{11}} + \frac{10\mathrm{t}^3}{\sqrt{2\pi}\cdot\sigma^9} - \frac{15\mathrm{t}}{\sqrt{2\pi}\cdot\sigma^7}\right)\cdot\ \mathrm{e}^{-\frac{\mathrm{t}^2}{2\sigma^2}} \tag{4.3}$$

where n represents the nth derivative. The Fourier transform of the nth order derivative can be calculated as

$$X(f) = A(j2\pi f)^{2n}\, e^{-\frac{(2\pi f\sigma)^2}{2}} \tag{4.4}$$

Finally, the PSD can be calculated from (4) as:

$$P(F) = A^2(2\pi f)^{2n}\, e^{-(2\pi f\sigma)^2} \qquad (4.5)$$

The Power Spectral Density (PSD) of the excitation signal for the proposed design is shown in Fig. 4.2. The peak frequency and bandwidth of the excitation signal have been optimized by varying the values of σ so as to meet the FCC indoor mask.

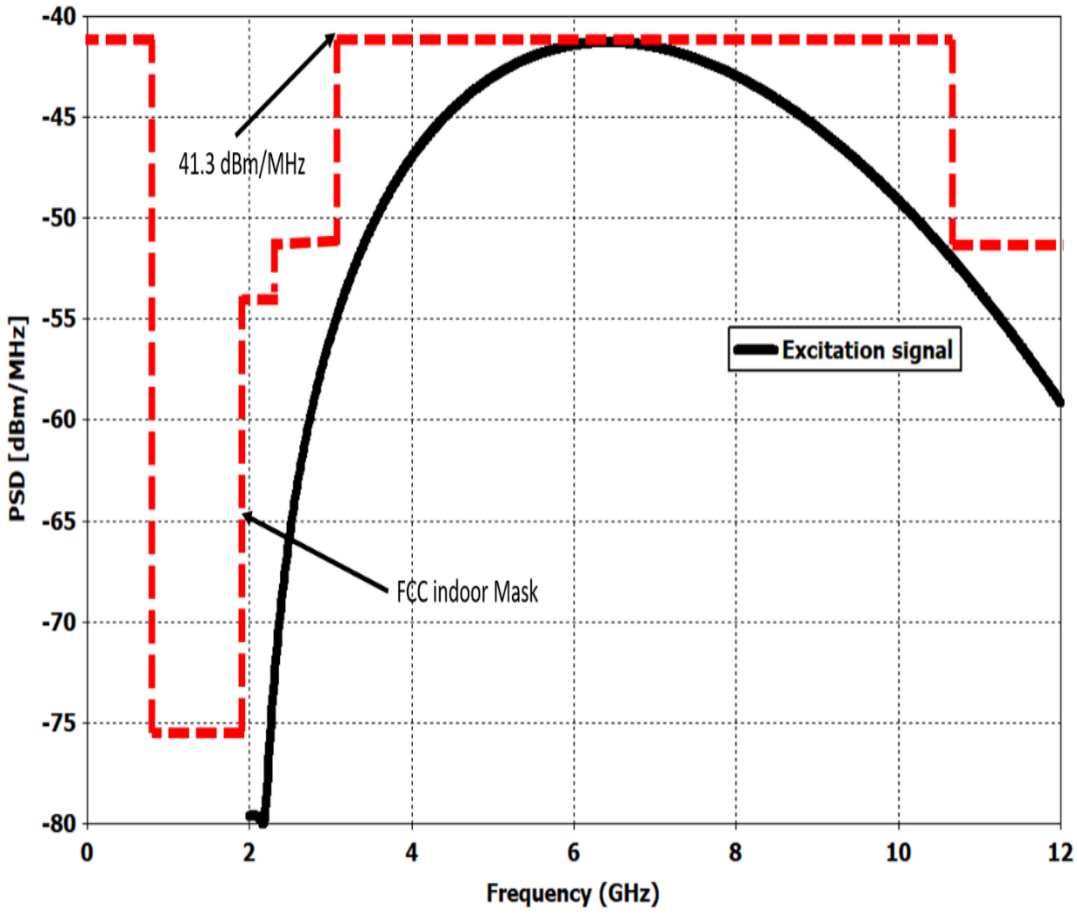

Fig. 4.2 PSD of the selected excitation signal

The calculated impedance bandwidth for the Gaussian Pulse and 5th order Gaussian pulse is 59.18 % and 92.37 % respectively. An important point to note here is that even though higher bandwidth is achieved using a Gaussian pulse but 5th order Gaussian pulse has been used for excitation of the proposed antenna to comply with FCC indoor mask.

4.3.2 Design Process

An antenna configuration with CPW feeding is used for achieving the UWB operation. The initial dimensions for the radiating patch and shape of the ground plane are taken from similar designs available in the literature [25], [145-147]. Fig. 4.3 presents the evolution of the initial design with variation in the ground aperture for achieving UWB operation.

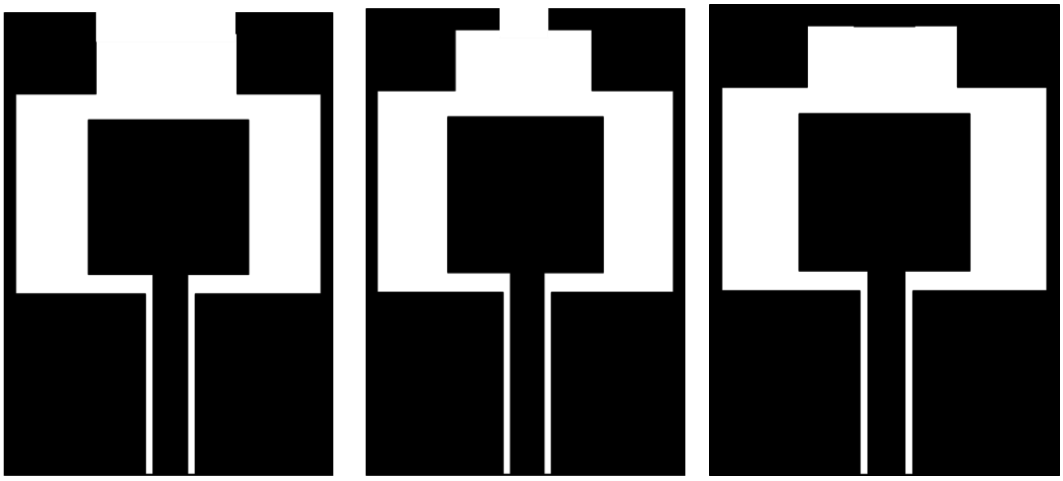

(a) (b) (c)

Fig. 4.3 Evolution of the initial design with variation in ground aperture (a) Ground 1 (b) Ground 2 (c) Ground 3

After taking the initial dimensions, in the first step, the ground aperture is modified by taking the length and width of the radiating element as $\lambda_f/4$, where λ_f is the guided wavelength of the microstrip feed line. The length and width of the ground aperture affect the bandwidth of the proposed antenna. Thus, factors associated with it are altered and studied to not only enhance the bandwidth but also for other antenna parameters i.e., gain, radiation pattern, group delay, etc. Fig. 4.4 shows the VSWR plot of the initial design with variations in the ground aperture. In the process of selecting the ground plane, the length and width of the radiating element are also modified i.e., 8 mm and 15 mm respectively. The bandwidth of the initial design is calculated to be 3.496 GHz. Apart from this, other parameters like gain, radiation pattern, and group delay, etc. of the design are befitting for UWB operation.

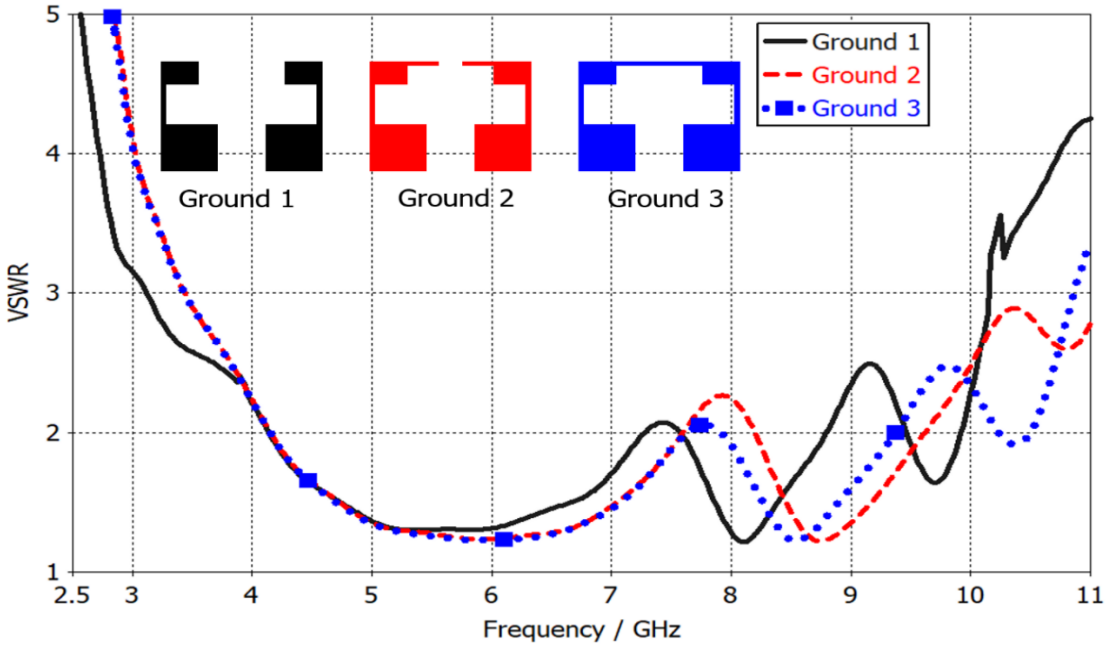

Fig. 4.4 VSWR plot of the initial design with variation in the ground plane

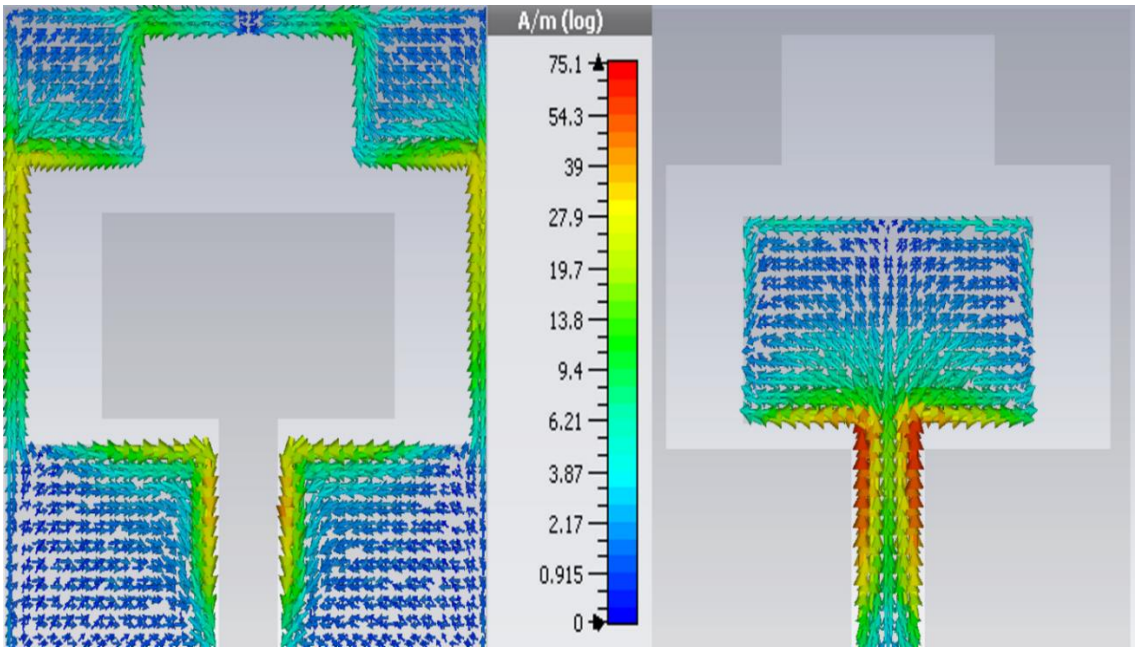

(a) (b)

Fig. 4.5 Current distribution of the initial design (a) Ground structure (b) Radiating patch

The current distribution at center frequency is shown in Fig. 4.5. It can be observed from Fig. 4.5 that the current concentration is maximum at the lower and side edges of the ground plane. Further, the current concentration is maximum at the lower center and lower edges of the radiating patch, which in turn provides UWB operation.

4.3.3 Notch Band Optimization

For effective implementation of optimized WLAN (5.15-5.825 GHz) notch band characteristics in the UWB antenna, a C-shaped slot is used in the radiating element. This slot acts as a BSF in the antenna structure. The dimensions of the slot are optimized in such a way that the other parameters of the UWB antenna are not affected. Hence, a parametric study for the positioning and dimensions of the antenna is done comprehensively. The initial dimensions of the C shape slot are chosen from the expression [146]:

$$f_{notch} = \frac{c}{2\, L_{slot}\, \sqrt{\in_{eff}}} \tag{4.6}$$

Where C indicates the speed of light, L_{slot} represents the total length of the C-shaped slot, $\in_{eff}$ is the effective dielectric constant i.e., $\in_r + 1/2$. Here $\in_r$ is the dielectric constant of the substrate.

The overall length of the slot is given by $L_{slot} = SW1 + 2SL + 2SW2$ .The center rejection frequency for the WLAN band is 5.487 GHz. Hence, the calculated length for the slot is 16.4 mm. However, in simulation results, the center notch frequency is observed at 5.843 GHz which is having a percentage error of 6.48 % from the desired notch band center frequency. Ideally, for the UWB antenna, notch band (WLAN) of 675 MHz from 5.15 GHz to 5.825 GHz is desired. Therefore, in this work, the optimization of the different slot parameters is done without affecting the other essential parameters for achieving the ideal UWB operation. The methodology used to optimize the notch for WLAN is presented using a flow chart given in Fig. 4.6.

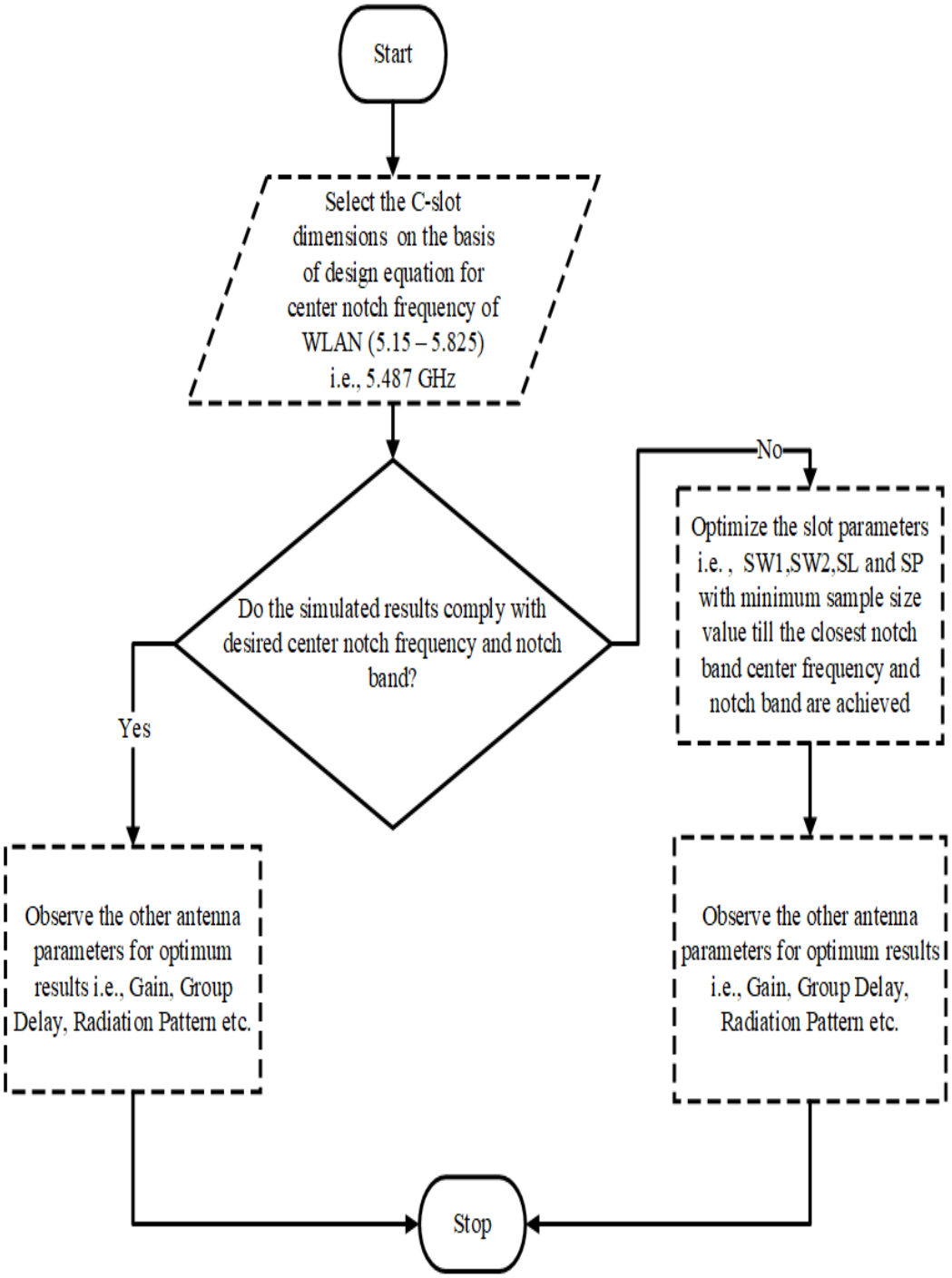

Fig. 4.6 Design methodology used for achieving desired notch band

- *Effect of SW1 and SW2*

Fig. 4.7 and Fig.4.8 show the designs with different SW1 values and different values of center notch frequency in the VSWR plot respectively. For clarity, only three values have been used to show the variation in the notch band frequency. However, the actual

values are changed from 7 mm to 13 mm and the notch band center frequency varies from 4.099 GHz to 7.338 GHz approximately. Table 4.3 is used to represent the complete variation in notch band center frequency with the change of SW1 values.

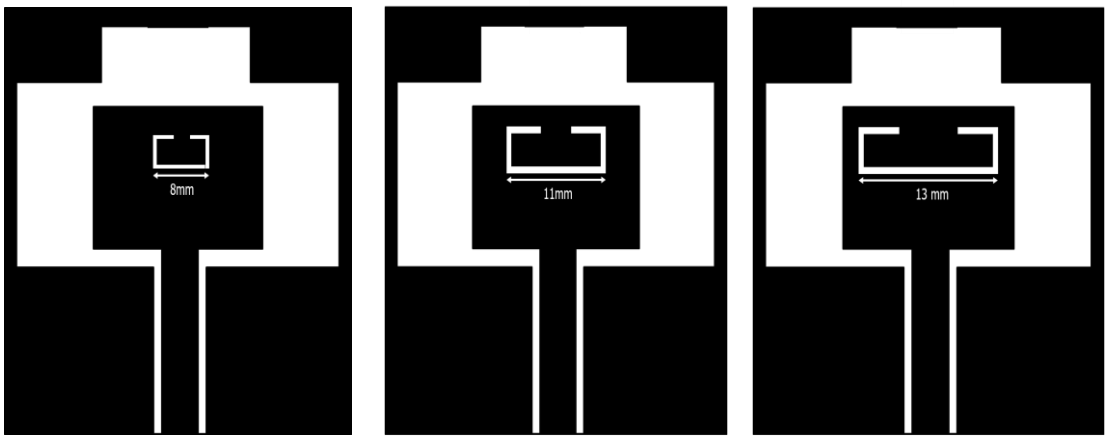

(a) (b) (c)

Fig. 4.7 Initial design with different values of SW1 (a) 8 mm (b) 11 mm (c) 13 mm

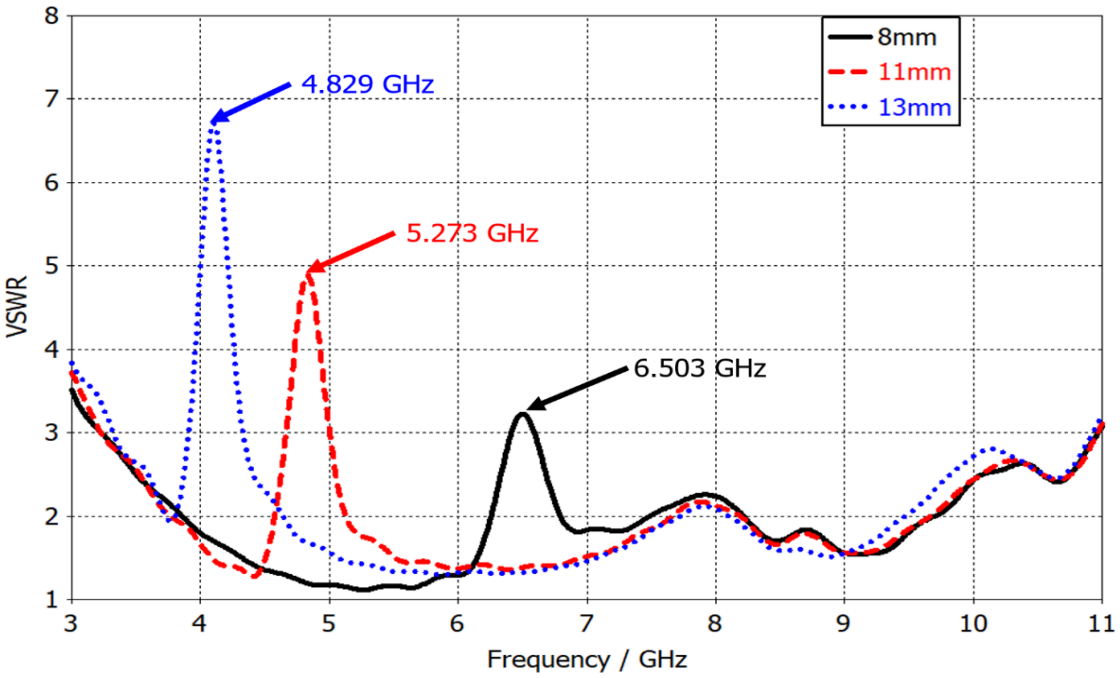

Fig. 4.8 Effect of SW1 on the center notch frequency

Table 4.3 Different values of notch band with variation in SW1

Value of SW1 (mm)	Center Frequency (GHz)	Notch Band (GHz)	Bandwidth (GHz)
7	7.338	7.039 – 8.047	1.008
8	6.503	6.258 - 6.775	0.517
9	5.809	5.564 - 6.095	0.531
10	5.273	5.031 - 5.554	0.523
11	4.829	4.571 – 5.129	0.558
12	4.445	4.191 – 4.840	0.649
13	4.099	3.801 - 4.651	0.850

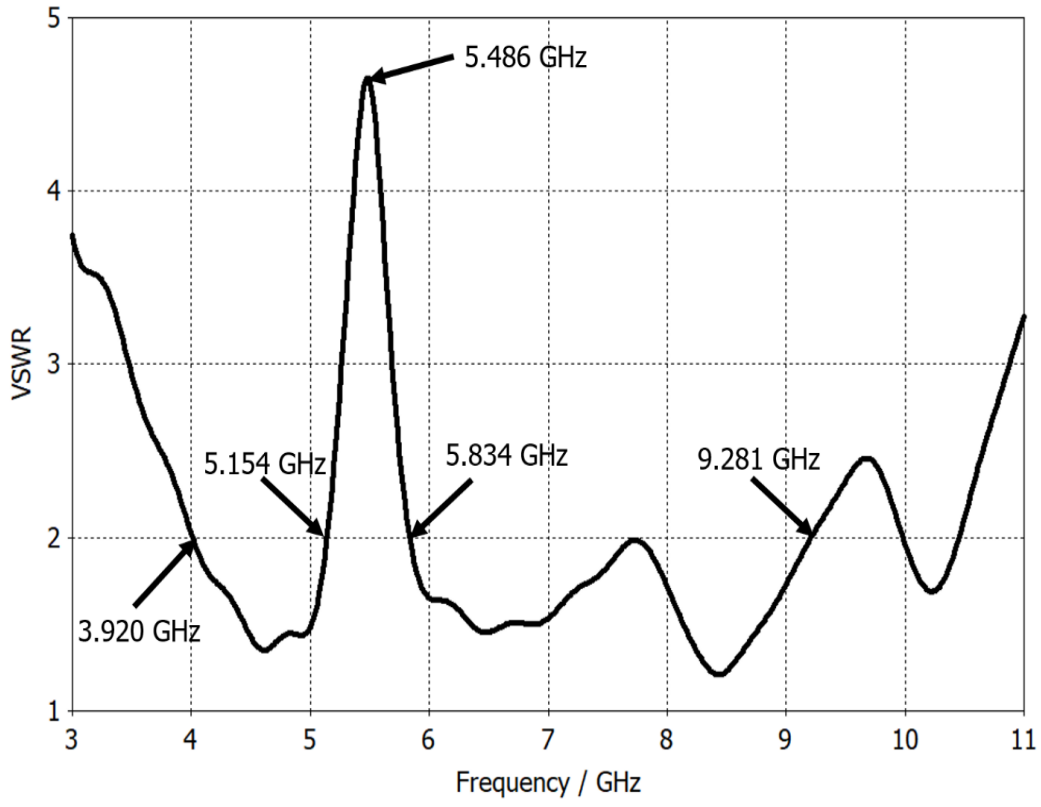

Fig. 4.9 VSWR plot with an optimum value of SW1 at 9.6 mm

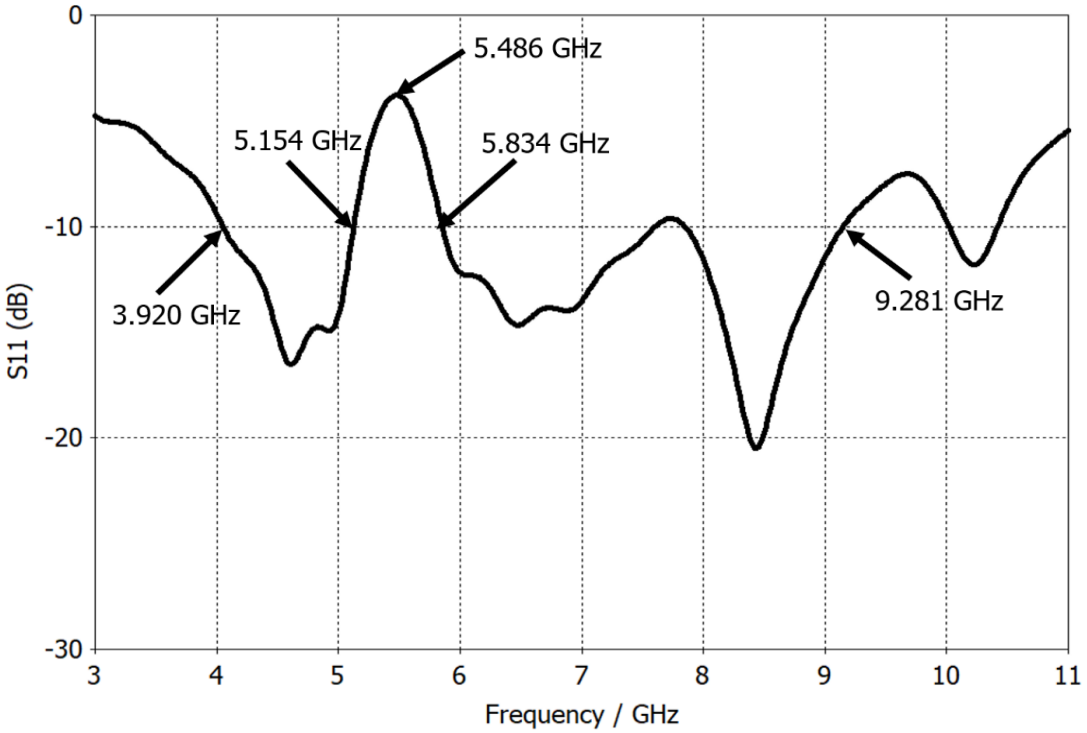

Fig. 4.10 S parameters with optimum values of SW1 at 9.6 mm

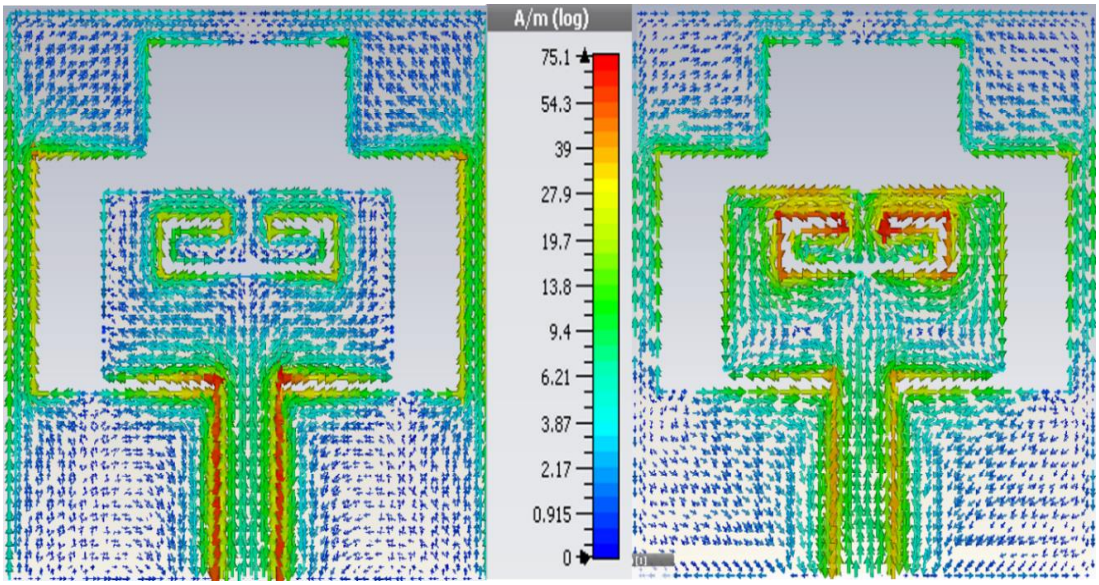

(a) (b)

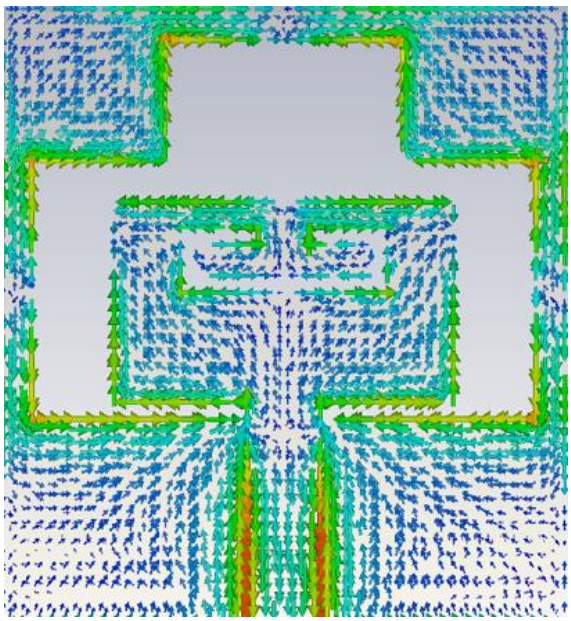

(c)

Fig. 4.11 Current distribution at a different frequency for SW1 value of 9.6 mm (a) 4.585 GHz (b) 5.486 GHz (c) 8.458 GHz

From Table 4.3, it has been observed that the SW1 values, i.e., 9 mm and 10 mm, are providing the best result till now corresponding to the ideal desired notch band (5.15 - 5.825 GHz) with the center frequency of 5.487 GHz and bandwidth of 675 MHz. Hence, the value between 9 mm to 10 mm is selected for the optimum result.

The values of the SW1 are changed from the range of 9 mm to 10 mm with a sample size of 0.1 mm and it has been found that 9.6 mm is the optimum value for the desired results which can be visualized in Fig. 4.9 and Fig. 4.10. Furthermore, the current distribution at the notch band center frequency and two passband frequencies are presented in Fig. 4.11. It can be visibly observed from Fig. 4.11(b) that the current distribution of the antenna is more concentrated near the edges of the slot at center notch frequency, which in turn induces notch band and also, the current distribution is having less concentration at the slot for passband frequencies which is depicted by Fig.4.11(a) and Fig.4.11 (c).

Similarly, the effect of SW2 is portrayed by the VSWR and S_{11} plot in Fig. 4.12 and Fig. 4.13 respectively. The value of SW2 is varied from 2.8 mm to 4.6 mm with a

sample size of 0.2 mm. Five different notch bands are achieved with five different values of SW2. The center notch frequency varies from 4.949 GHz to 5.871 GHz. The lower frequency of the notch band changes from 4.717 GHz to 5.459 GHz whereas the upper frequency of the notch band changes from 5.181 GHz to 6.301 GHz. Table 4.4 is used to demonstrate the complete variation in notch band and center frequency.

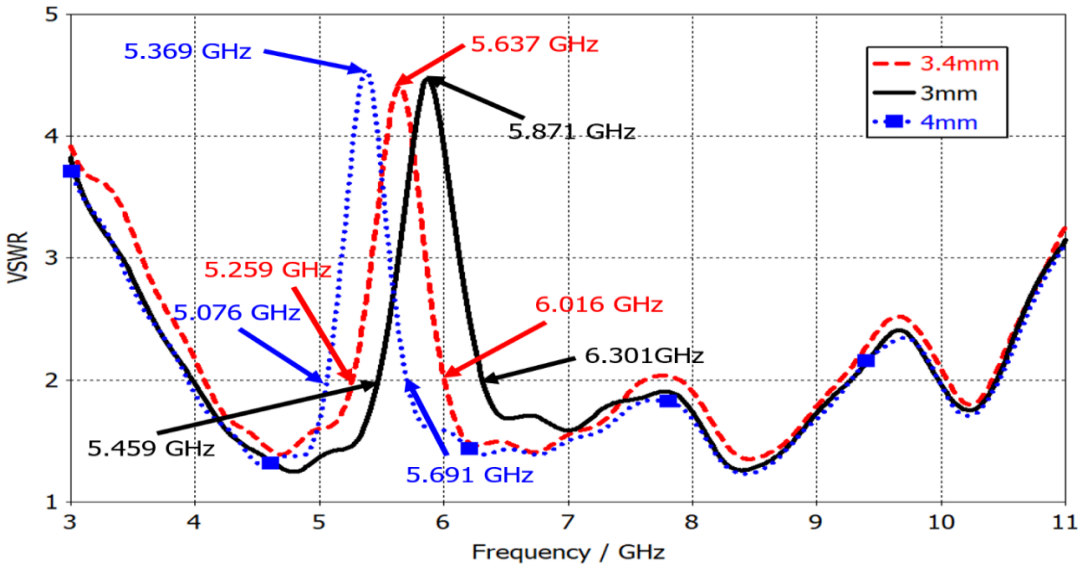

Fig. 4.12 Effect of SW2 on the center notch frequency in VSWR plot

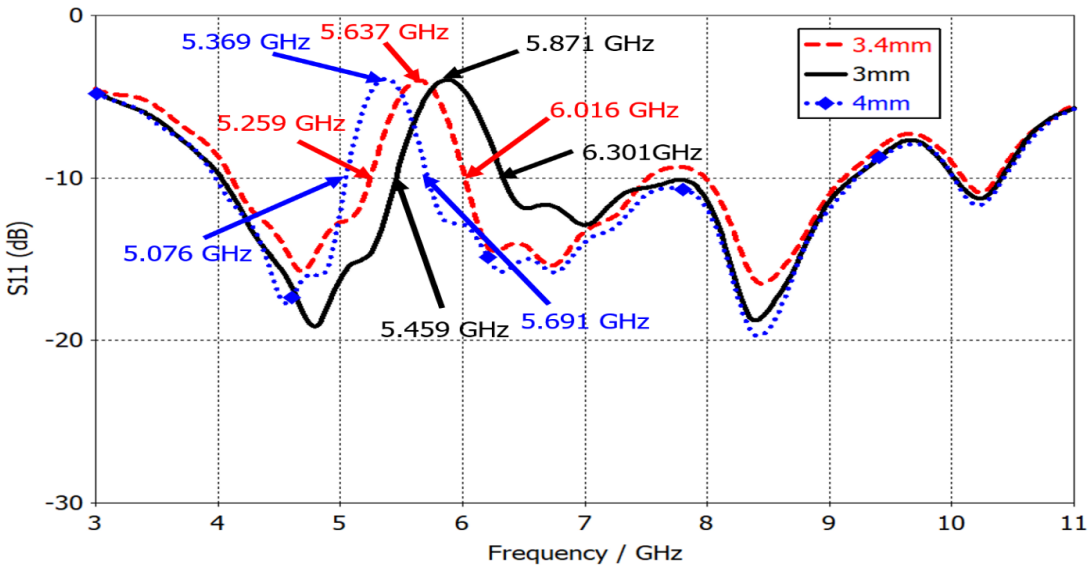

Fig. 4.13 Effect of SW2 on the center notch frequency on S_{11} parameter

Table 4.4 Different values of notch band with variation in the values of SW2

Value of SW2 (mm)	Center Frequency (GHz)	Notch Band (GHz)	Bandwidth (GHz)
2.8	5.573	5.242 - 5.952	0.710
3	5.871	5.459 – 6.301	0.842
3.2	5.770	5.407 – 6.181	0.774
3.4	5.637	5.275 - 6.106	0.831
3.6	5.573	5.242 - 5.952	0.710
3.8	5.486	5.154 – 5.834	0.680
4	5.369	5.076 – 5.691	0.615
4.2	5.237	4.943- 5.530	0.587
4.4	5.111	4.854 – 5.382	0.528
4.6	4.949	4.717- 5.207	0.490

- *Effect of SL and SP*

SL is also part of the length which contributes to the total length of the L_{slot}.Therefore, analysis of the deviations in SL also plays a vital role similar to SW1 and SW2. Here the range of SL is altered from 2.5 mm to 3.5 mm with a sample size of 0.1 mm

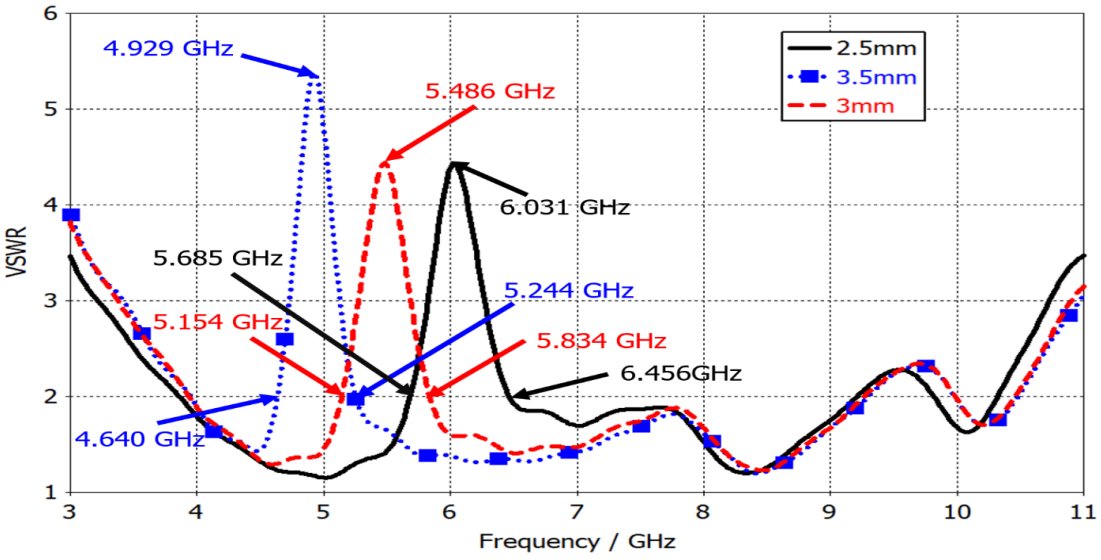

Fig. 4.14 Effect of SL on the center notch frequency in VSWR plot

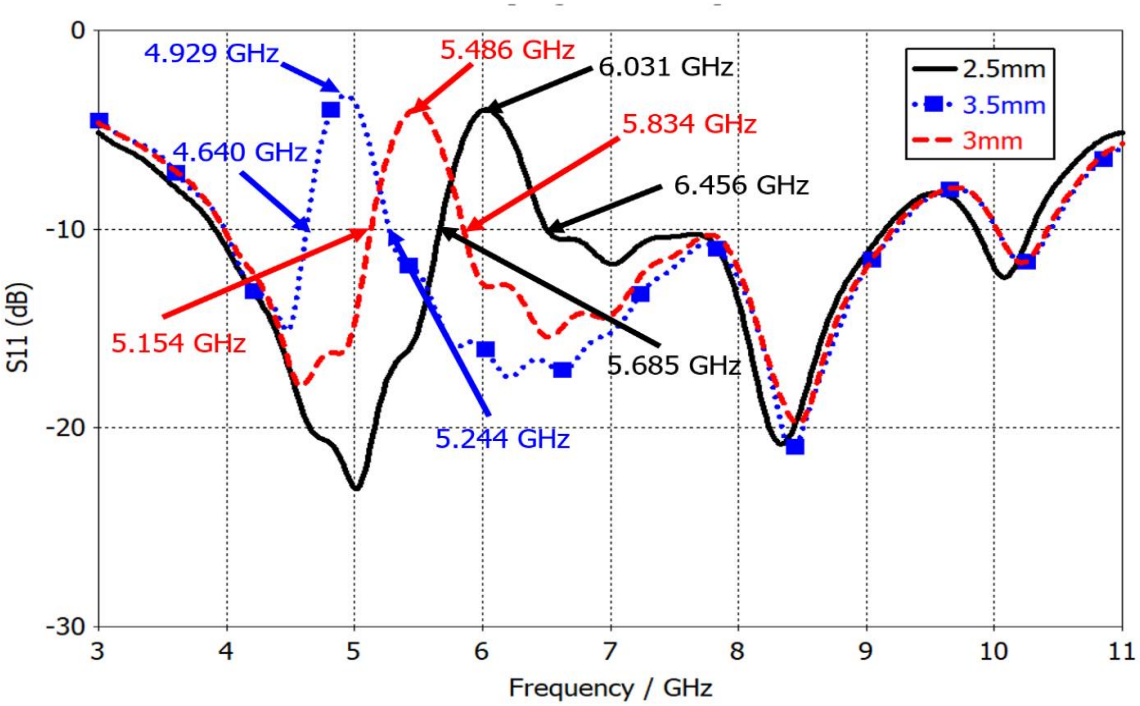

Fig. 4.15 Effect of SL on the center notch frequency on S_{11} parameters

Table 4.5 Different values of notch band with variation in SL

Value of SL (mm)	Notch Band Center Frequency (GHz)	Notch Band (GHz)	Bandwidth (GHz)
2.5	6.031	5.685 – 6.456	0.771
2.6	5.883	5.562 – 6.306	0.744
2.7	5.794	5.461 - 6.190	0.729
2.8	5.685	5.377 – 6.051	0.674
2.9	5.579	5.247 – 5.944	0.697
3	5.486	5.154 – 5.834	0.680
3.1	5.370	5.063 – 5.707	0.644
3.2	5.264	4.948 – 5.596	0.648
3.3	5.159	4.852 -5.481	0.629
3.4	5.042	4.750 – 5.364	0.614
3.5	4.929	4.640 – 5.244	0.604

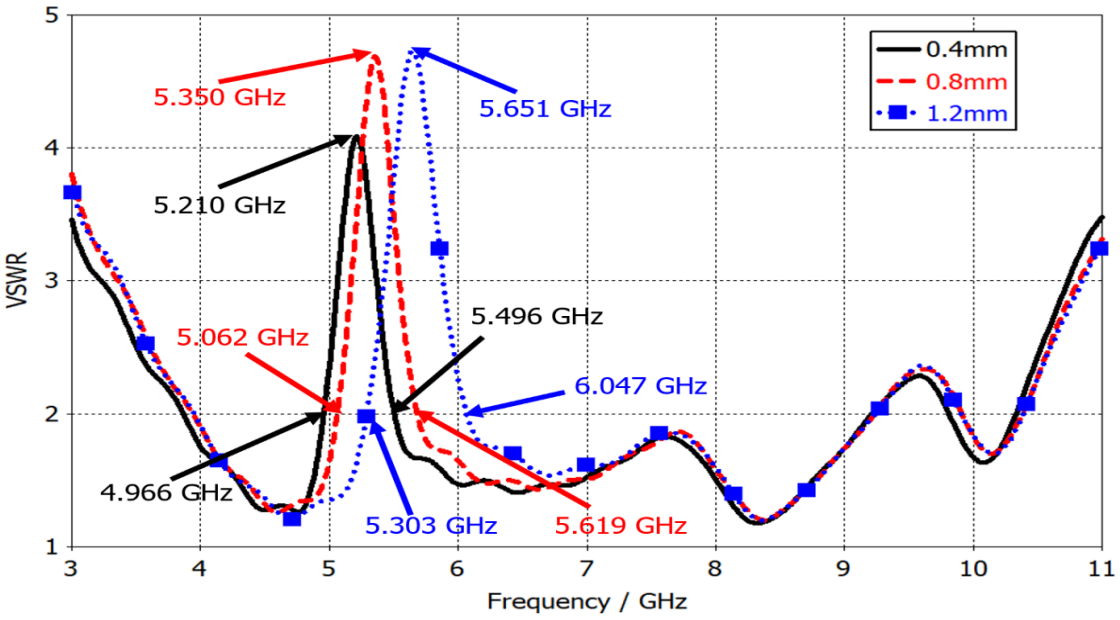

Fig. 4.16 Effect of SP on the center notch frequency in VSWR plot

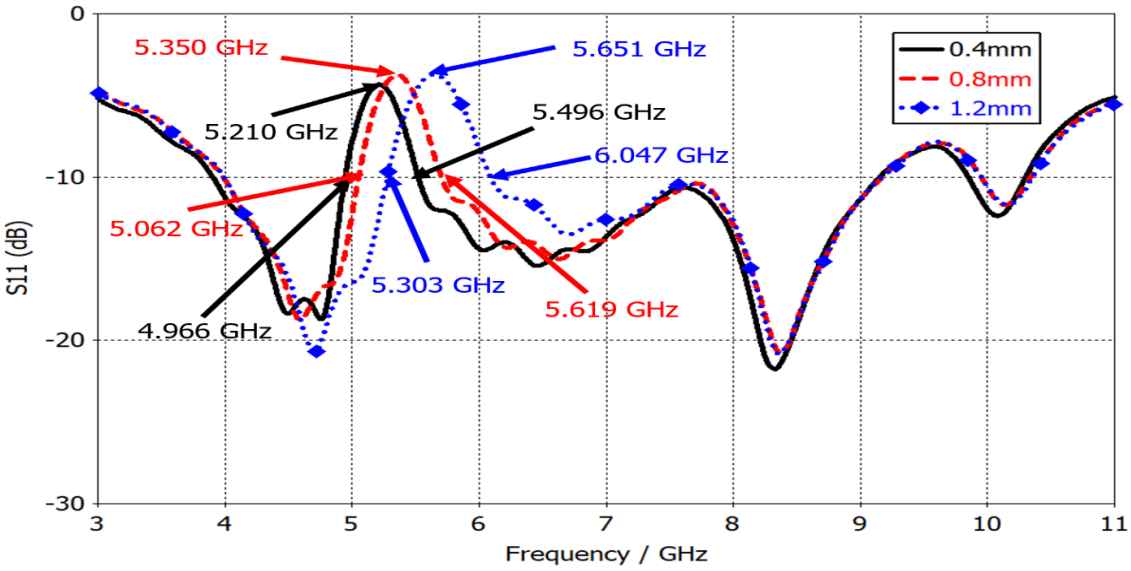

Fig. 4.17 Effect of SL on the center notch frequency in S_{11} parameters

During this variation, the value of the SW1 and SW2 remains constant. Fig. 4.14 and Fig. 4.15 are used to present the effect of SL on the notch band. Table 4.5 is used to present the complete variation in center notch frequency and well as the lower and upper frequency of the notched band. The center frequency varies from 4.929 GHz to

6.031 GHz and the lower and upper frequency of the notched band changes from 4.640 GHz to 5.685 GHz and 5.244 GHz to 6.456 GHz respectively. Hence, it has been observed from Table 4.5 that the optimum value of SL is taken as 3 mm.

The effect of SP can be observed in Fig. 4.16 and Fig. 4.17. This parameter doesn't have much effect on the notch band as compared to other dimensions of L_{slot}. Here the parametric variation is done from 0.2 mm to 1.6 mm with a sample size of 0.2 mm. When the thickness of the slot is changed, the current distribution does not change drastically. However, as given in Table 4.6, a small difference in the center notch frequency and notch band is observed. Finally, after the complete optimization process of the slot dimensions, (i.e. SW1= 9.6 mm, SW2 = 3.8 mm, SL= 3 mm and SP= 1 mm), the percentage error of the center notch frequency has been reduced from 6.48% to 0.02%. Hence, a notched band (WLAN) of 5.154 GHz to 5.834 GHz with a center frequency of 5.486 GHz and bandwidth of 680 MHz is achieved with the percentage error of only 0.02 %. from the center frequency.

Table 4.6 Different values of notch band with variation in SP

Value of SP (mm)	Notch Band Center Frequency (GHz)	Notch Band (GHz)	Bandwidth (GHz)
0.2	5.234	5.015 – 5.480	0.771
0.4	5.210	4.966 – 5.496	0.744
0.6	5.240	4.963 – 5.562	0.729
0.8	5.350	5.062 – 5.678	0.674
1.0	5.486	5.154 – 5.834	0.697
1.2	5.651	5.303 – 6.047	0.744
1.4	5.811	5.488 – 6.315	0.827
1.6	6.068	5.641- 6.649	1.008

- *Bandwidth enhancement*

The presented UWB antenna structure is having an impedance bandwidth of 5.360 GHz i.e., from 3.920 GHz to 9.280 GHz. As depicted in Fig. 4.18, the beveling technique is used on the radiating element for achieving higher bandwidth [25]. Both the upper and

lower edges of the patch have been beveled with different beveling angle and the optimized values of beveling angle, LP1, and WP2 have been chosen.

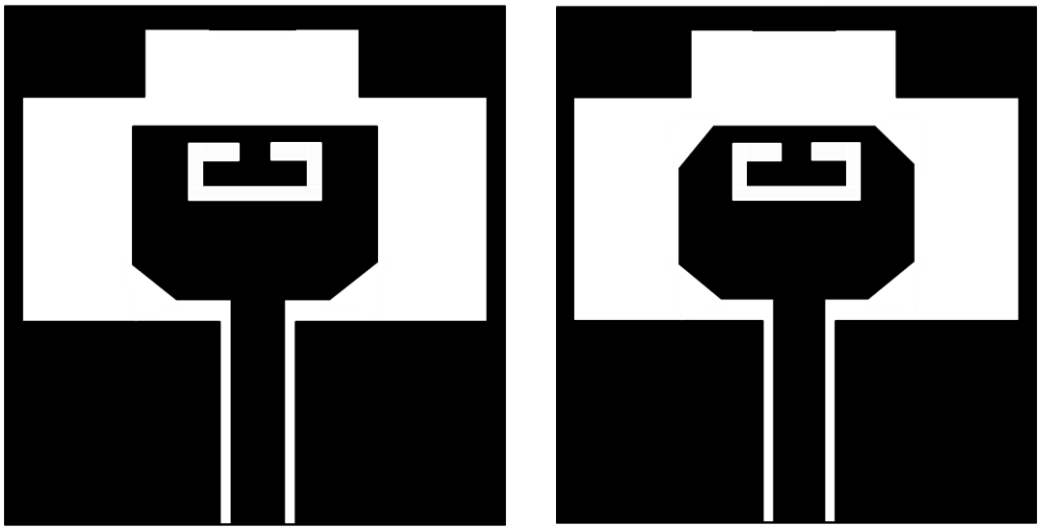

Fig. 4.18 Stages of the beveled patch for bandwidth enhancement (a) Lower edge beveled (b) Lower and Upper edge beveled

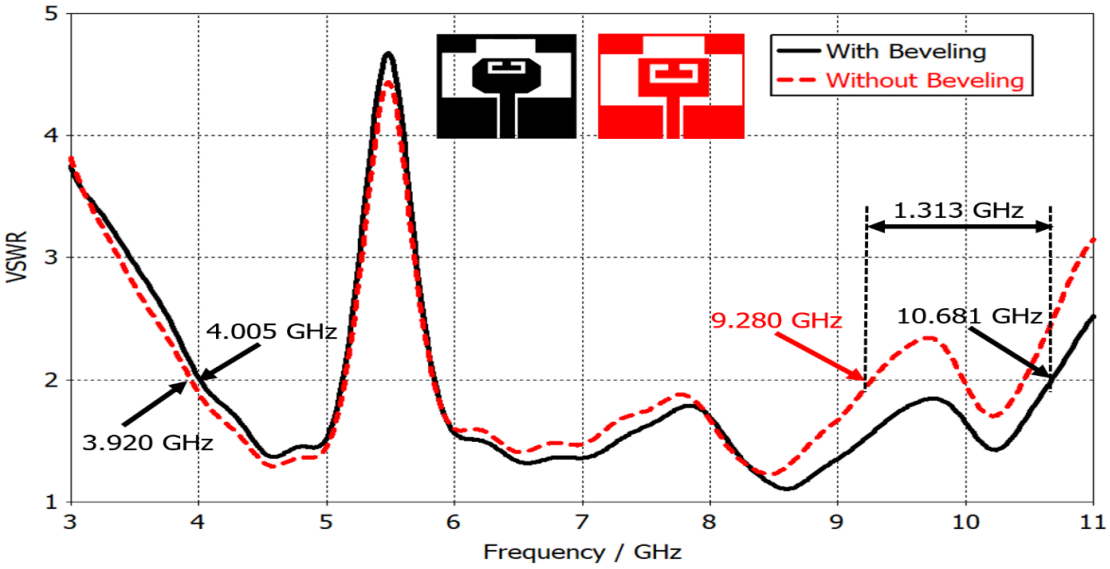

Fig. 4.19 VSWR plot with the beveled patch for bandwidth enhancement

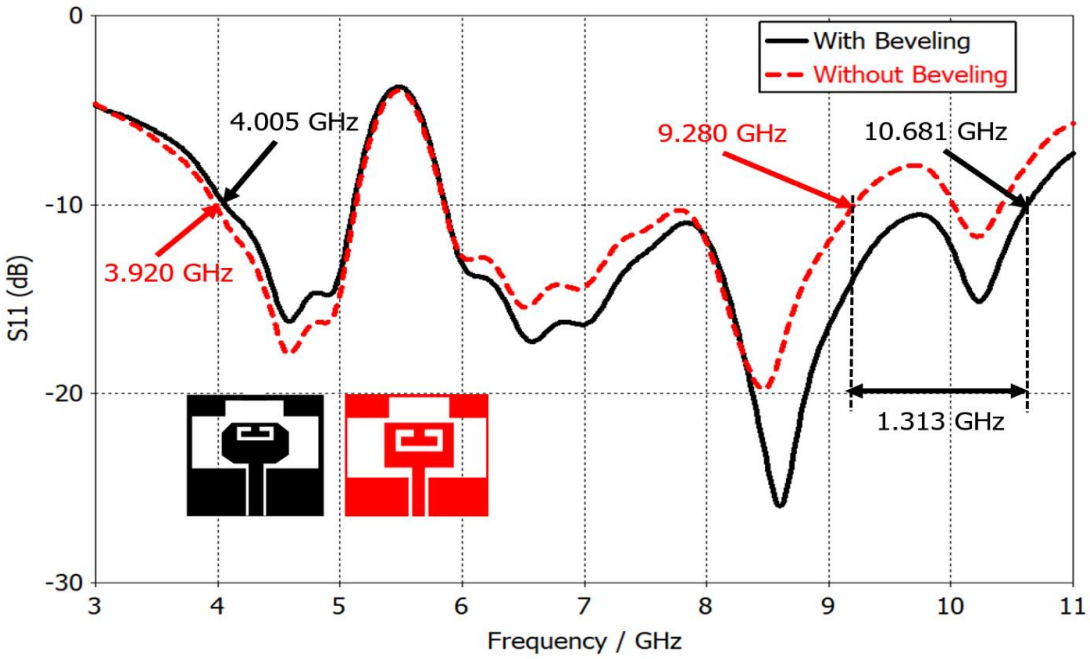

Fig. 4.20 S_{11} plot with the beveled patch for bandwidth enhancement

As presented in Fig. 4.19 and Fig. 4.20, the lower frequency of the UWB range is slightly shifted towards the higher end of the range i.e., from 3.920 GHz to 4.003 GHz. Similarly, notch band frequency has been changed to 5.133 GHz to 5.833 GHz with a center frequency of 5.483 GHz, but a higher Impedance bandwidth of 6.673 GHz is achieved. Also, the upper frequency is lying near to the upper cut off frequency of UWB systems i.e., 10.681 GHz. Finally, the overall bandwidth enhancement of 1.313 GHz is achieved without affecting the other parameters related to the UWB operation.

- *Filter synthesis and equivalent circuit model*

The C-Shaped slot is working as a BSF in this design. Therefore, the Ideal WLAN notch filter is synthesized to find the optimum values of the circuit elements for the equivalent circuit design of the proposed antenna. For the ideal WLAN notch filter, the notch frequency range should vary from 5.150 GHz to 5.825 GHz (675 MHz) with a center notch frequency of 5.487 GHz. However, the designed notch band filter of the proposed

design is having a small variation in the notch band and center notch frequency i.e., 5.133 GHz to 5.833 GHz (700 MHz) and 5.483 GHz respectively.

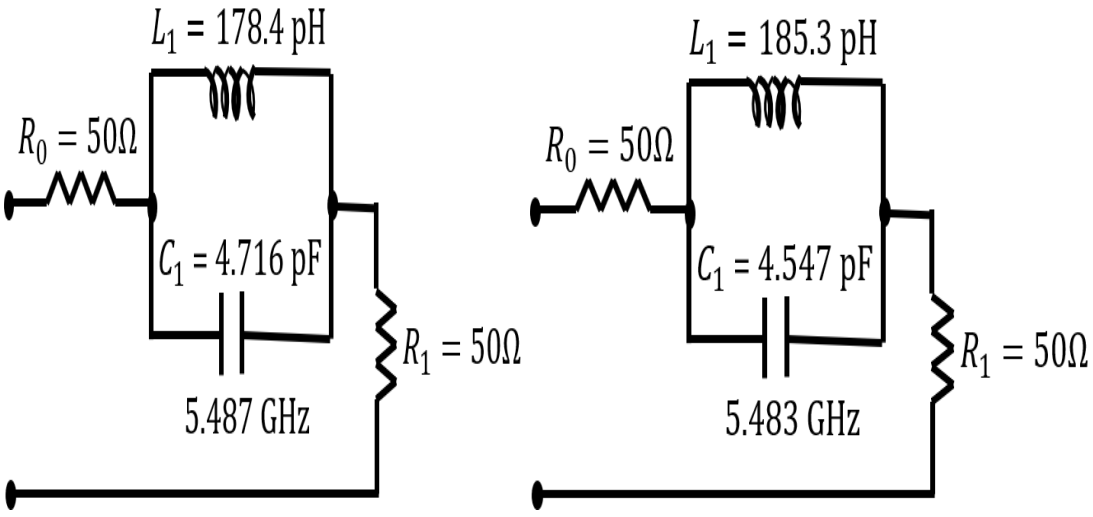

(a) (b)

Fig. 4.21 Equivalent circuit of the notch filter (a) Ideal WLAN notch filter (b) Designed notch filter.

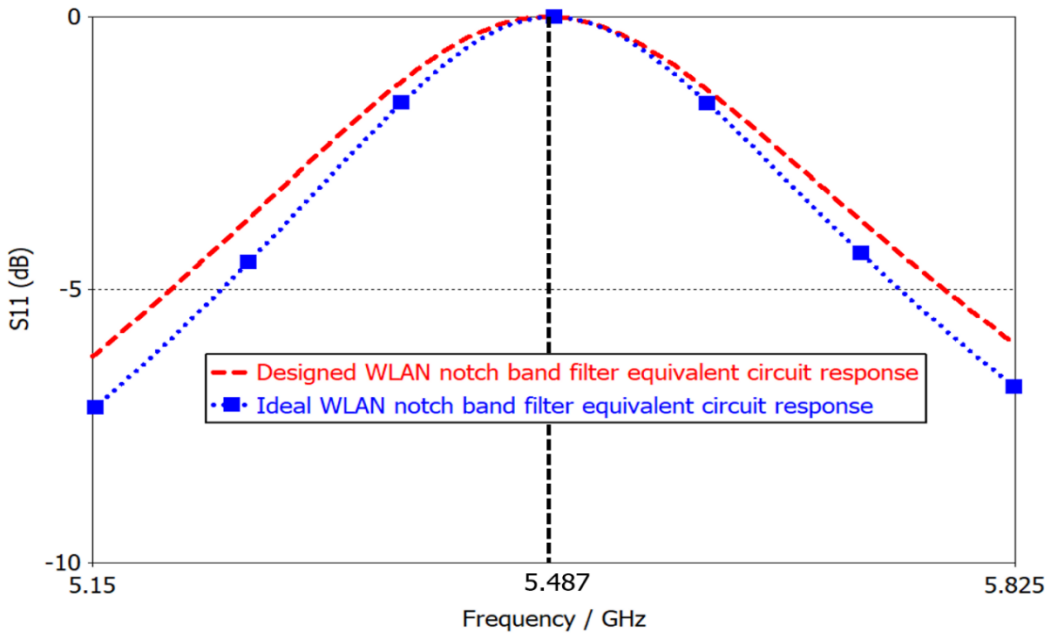

Fig. 4.22 S_{11} response of the ideal and designed WLAN notch band filter

Fig. 4.21(a) and 4.21(b) represent the equivalent circuit of the ideal WLAN notch filter and designed a notch filter for the proposed antenna respectively. Here the values of $L_1$and C_1 are calculated using the center notch frequency and bandwidth of the notched band using filter synthesis tool available in CST Microwave Studio. Also, the simulated S_{11} response for equivalent circuits is presented in Fig. 4.22.

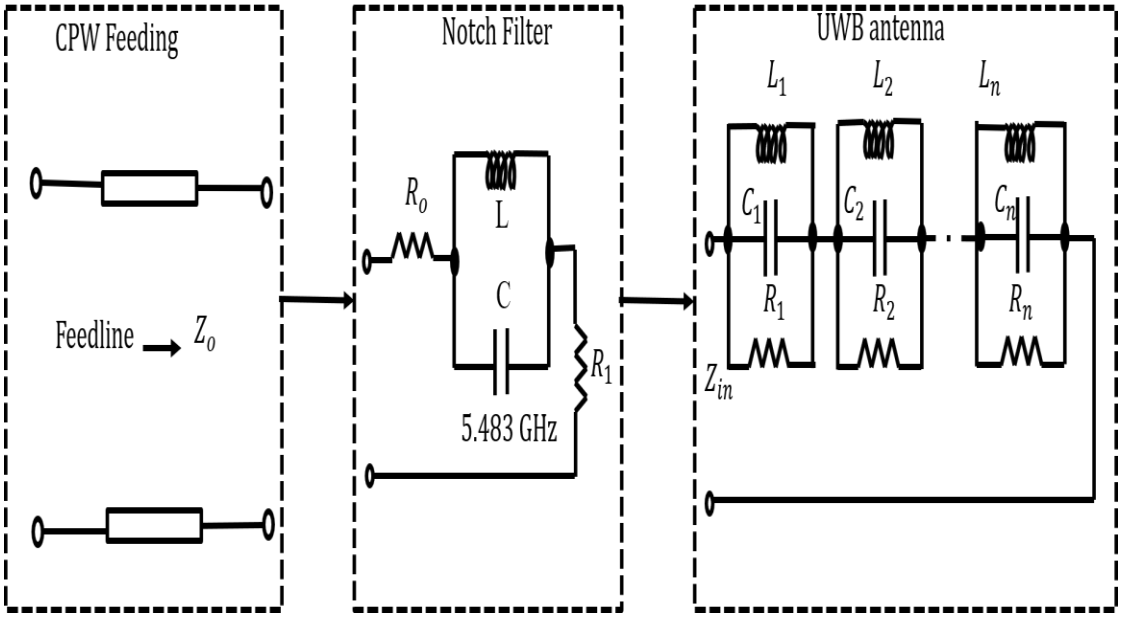

Fig. 4.23 Equivalent circuit model of the proposed antenna

The equivalent circuit model of the proposed antenna can be divided into three parts i.e., CPW Feeding, notch filter, and UWB antenna. Theoretically, the CPW feed in the antenna is considered as a transmission line with a characteristic impedance of Z_0 and impedance model of the UWB antenna can be approximately represented by several RLC parallel circuits in series as it is a combination of multiple resonances to achieve matching bandwidth for UWB operation [146]. Hence, the equivalent circuit model of the proposed antenna is given in Fig. 4.23.

In this model, the input impedance of the UWB antenna can be expressed as [146]

$$Z_{in} = \sum_{i=1}^{n} \frac{jw \cdot R_i \cdot L_i}{R_i \cdot (1-\omega^2 \cdot L_i \cdot C_i)+jw \cdot L_i} \qquad (4.7)$$

Equ. (4.7) can be utilized to compute the values of R, L, and C components. Moreover, the real part can also be considered to find the value of the lumped component using the following equation [146]

$$R_{in} = \sum_{i=1}^{n} \frac{R_i}{1+R_i \cdot \left(\frac{1}{L_i \cdot 2\pi f} - C_i \cdot 2\pi f\right)^2} \quad (4.8)$$

Multiple impedance data about frequencies from the real part of the radiator's input impedance can be obtained by simulation. By putting this data into equation curve fitting and an iterative method, the values of R_i , L_i and C_i can be calculated [146].

4.4. Time-Domain Analysis and Phase Response of S_{21}

The time-domain analysis is an important parameter in the UWB antenna design. Hence, this section provides the parameter wise time-domain analysis of the proposed UWB antenna. Also, the phase response to evaluate the phase linearity has been presented.

4.4.1 Dispersion Analysis

In UWB systems, the time domain analysis is vital in predicting the amount of distortion produced by the UWB antenna. Hence, the dispersion analysis of the transmitted and received pulse of the proposed antenna has been carried out. As discussed in Section 4.3, the fifth-order Gaussian pulse is used to excite the antenna. The radiated signal from the antenna is observed at a distance of 600 mm with face to face and side by side direction [13].

It can be viewed from Fig. 4.24 that the normalized transmitted and received signal at the mentioned distance with the face to face and side by side direction is almost identical. Though, some ringing phenomenon is detected in the received signal in both of the designs with C shaped Slot i.e., with and without the beveled patch. This phenomenon is due to the energy storage effect of the used substrate and filtering structure of the proposed antenna. However, this phenomenon is negligible in the initial design without the C-shape slot.

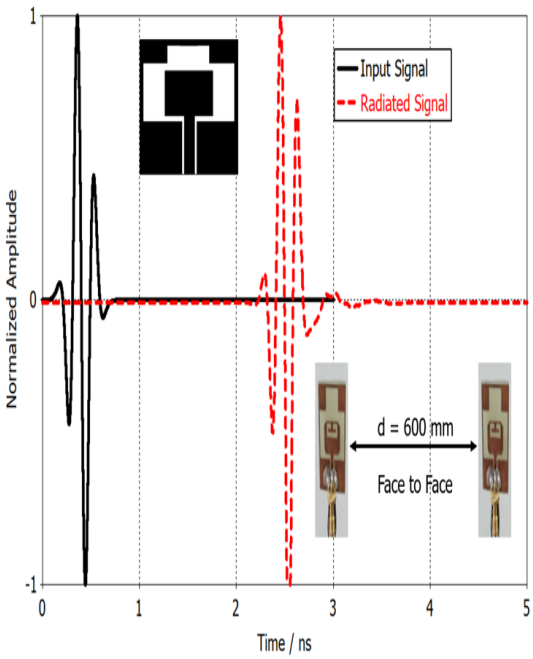
Input Signal
Radiated Signal
d = 600 mm
Face to Face
Normalized Amplitude
Time / ns

(a)

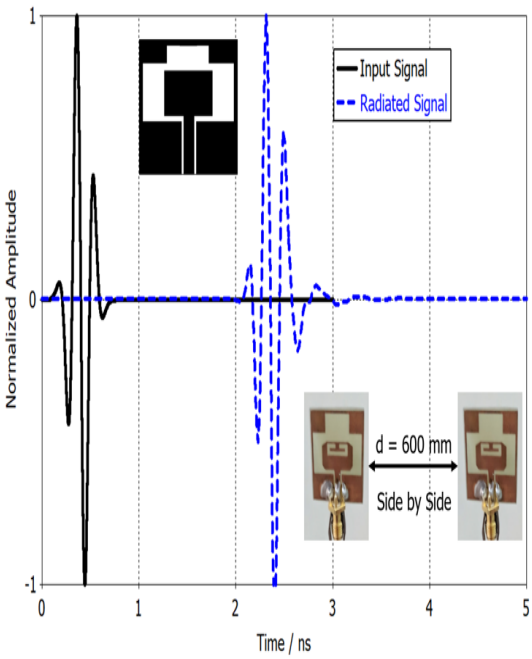
Input Signal
Radiated Signal
d = 600 mm
Side by Side
Normalized Amplitude
Time / ns

(b)

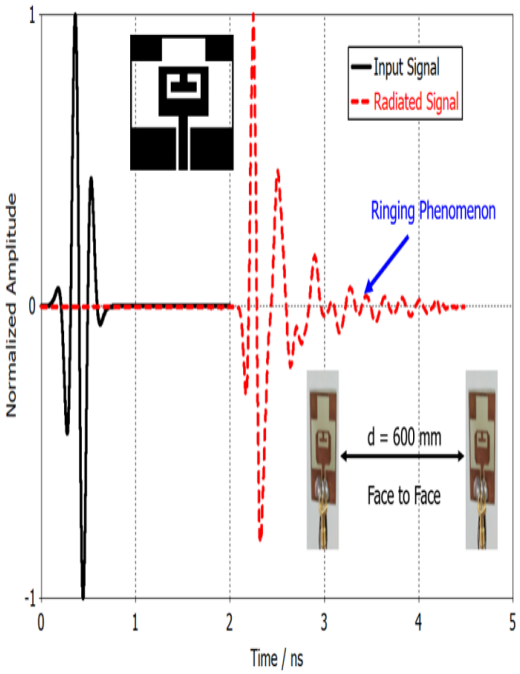
Input Signal
Radiated Signal
Ringing Phenomenon
d = 600 mm
Face to Face
Normalized Amplitude
Time / ns

’’

(c)

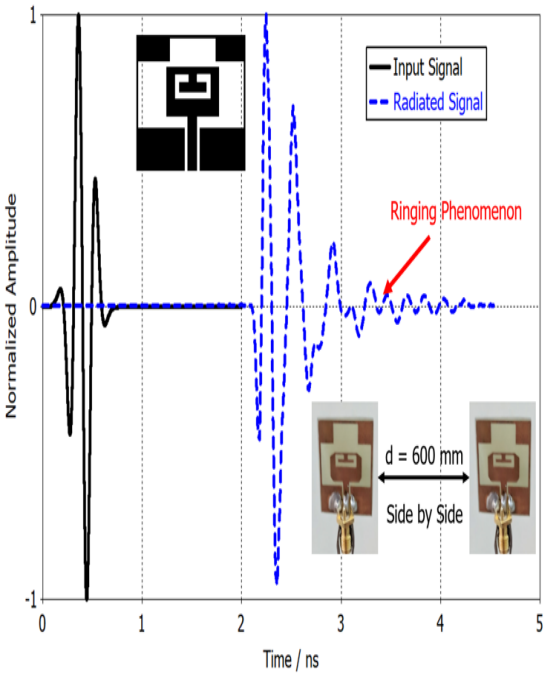
Input Signal
Radiated Signal
Ringing Phenomenon
d = 600 mm
Side by Side
Normalized Amplitude
Time / ns

(d)

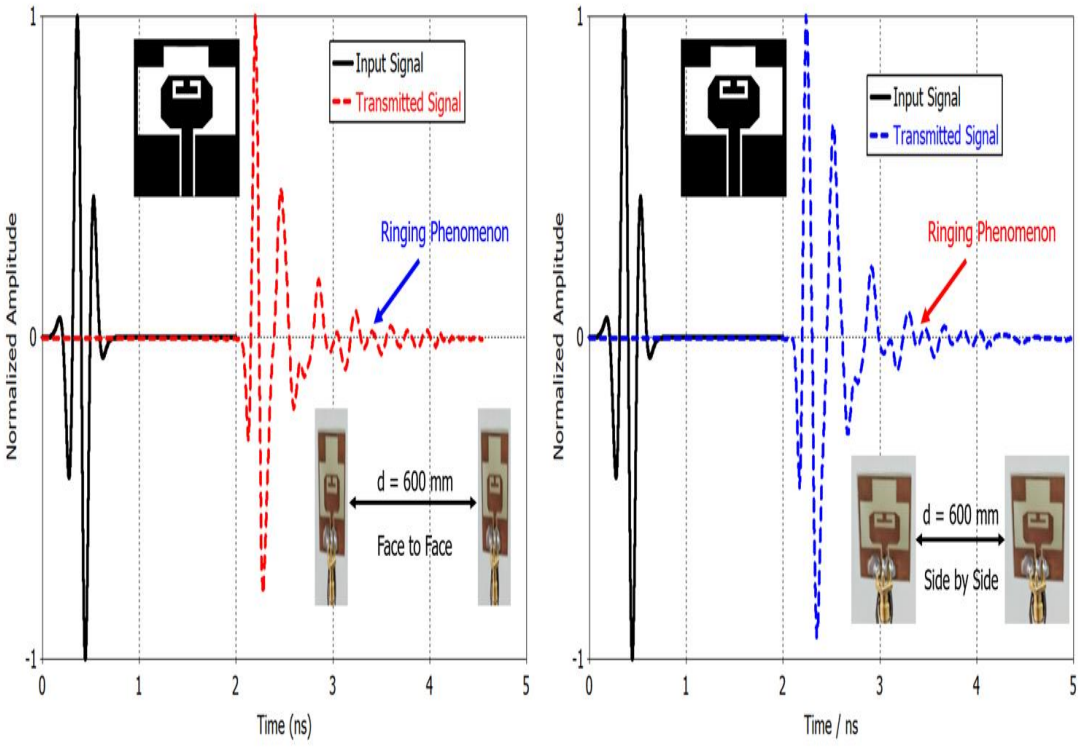

(e) (f)

Fig. 4.24 Normalized input and radiated signal of the different stages of the notched band antenna with face to face and side by side configuration (a) and (b) Initial UWB antenna, (c) and (d) WLAN notch band antenna without the beveled patch, (e) and (f) WLAN notch band antenna with beveled patch

4.4.2 System Fidelity Factor

One another important factor for the time-domain analysis of the UWB antenna is the system fidelity factor. It is based on the cross-correlation between input excitation signal $i(t)$ fed to the antenna and corresponding signal $r(t)$ radiated by the antenna which is measured at a distance. For this task, the input excitation signal and radiated signal are usually normalized as [13]

$$\hat{\imath}(t) = \frac{i(t)}{\left[\int_{-\infty}^{+\infty} |i(t)|^2 \, dt\right]^{1/2}} \qquad (4.9)$$

and

$$\hat{r}(t) = \frac{r(t)}{\left[\int_{-\infty}^{+\infty} |r(t)|^2 \, dt\right]^{1/2}} \qquad (4.10)$$

Then the cross-correlation between the two signals is calculated at each point in time and the peak value of correlation is taken as system fidelity factor which is computed using

$$\text{SFF} = max_{\tau} \int_{-\infty}^{+\infty} \hat{\imath}(t)\, \hat{r}(t+\tau)\, dt \qquad (4.11)$$

The minimum and maximum values of correlation correspond to system fidelity factor values are 0 and 1 respectively. In UWB antennas, the minimum acceptable value for the system fidelity factor is greater than 0.80. For the proposed antenna, the values of the system fidelity factor have been calculated for different configurations as given in Table 4.7. It can be observed from Table 4.7 that all the measured values of the final designs are above 0.80 value which confirms that a very low distortion is observed in the radiated signal at a distance of 600 mm. Moreover, for the final design, the maximum value of fidelity factors is 0.9495 (face to face) and 0.9338 (side to side), which is very near to one.

Table 4.7 SFF values for different stages of the proposed antenna in the face to face and side by side directions

Design configuration	Face to Face	Side by Side
Initial UWB antenna with no notch	0.9843	0.9761
WLAN notched UWB antenna without beveled patch	0.8993	0.8721
WLAN notched UWB antenna with beveled patch	0.9495	0.9338

4.4.3 Group Delay

Group delay is used to assess the degree of distortion produced by the radiated signal of the UWB antenna. Usually, the flat group delay indicates minimal distortion. Fig. 4.25 shows the simulated and measured group delay of the proposed antenna. CST Microwave Studio has been used for simulation of group delay by placing two antennas face to face at more than far-field distance. Similarly, two identical proposed WLAN band-notched antennas were placed in the aforementioned configuration and MS46322A (Anritsu) VNA has been used for measurement which has a range of 1 MHz to 20 GHz.

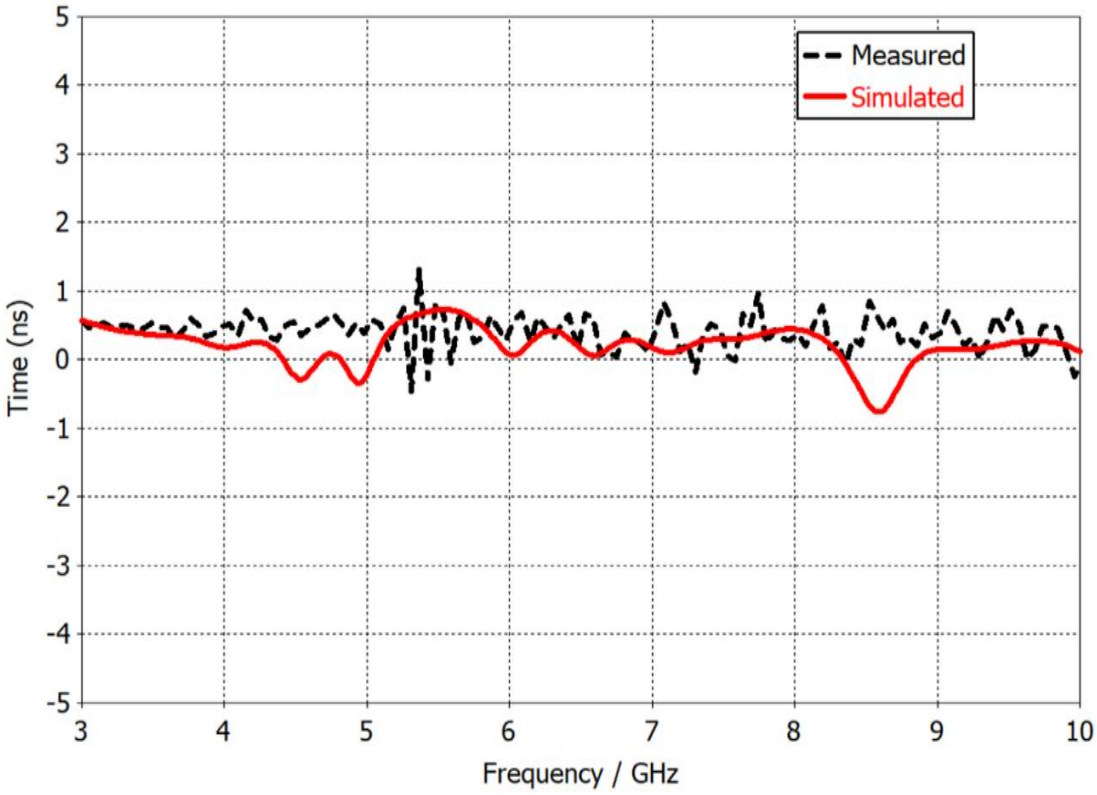

Fig. 4.25 The simulated and measured group delay of the proposed antenna

The simulated and measured results show constant group delay between 0 ns to 1 ns in the UWB range which depicts minimum pulse distortion. Further, the maximum group delay value of 0.738 ns at 5.534 GHz and 1.316 ns at 5.367 GHz are observed in

simulated and measured results respectively, which lies in the desired range of notch band.

4.4.4 Phase Response of S_{21}

Fig. 4.26 shows the simulated transmission coefficient (S_{21}) for face to face and side by side configurations. As observed from Fig 4.26, the magnitude of S_{21} is almost constant, (except for the notched band), with the variation of -14 dB for face to face and -13 dB for side by side-configuration. As expected, the phase response is linear throughout the UWB range except for the notch band. The reason for more variation in S_{21} or non-linearity in phase response at the notched band is due to a sudden change in resonance of the proposed antenna.

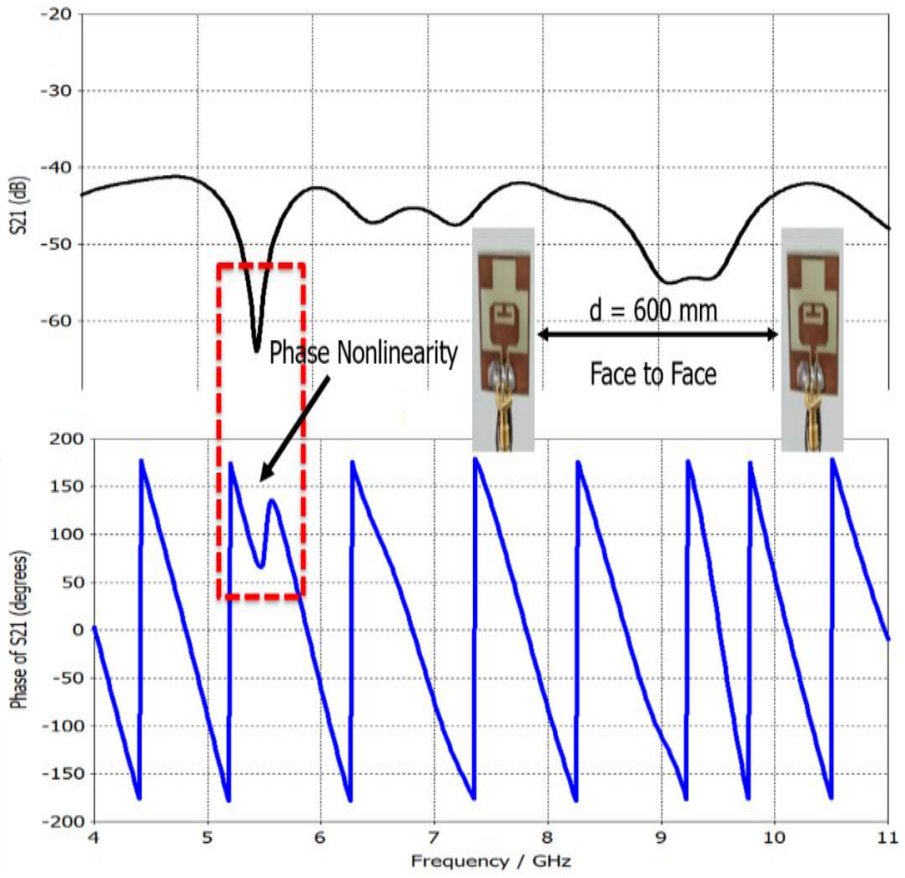

(a)

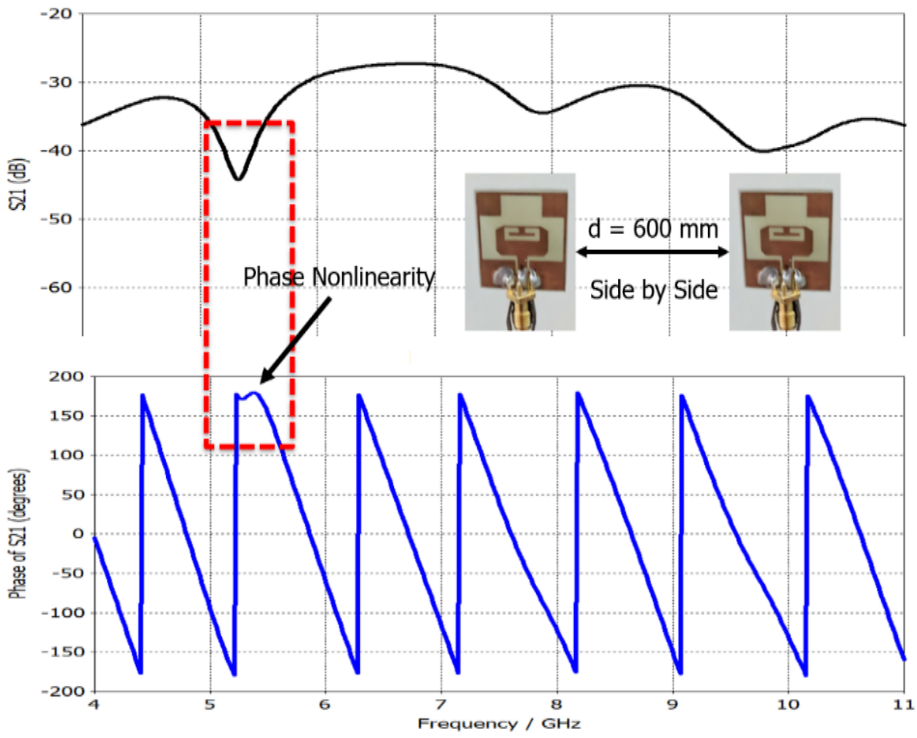

(b)

Fig 4.26 Magnitude and phase response of S_{21} for the proposed antenna (a) Face to face (b) Side by side

4.5 Measurement Results

Fig. 4.27 (a) and (b) shows the prototype and the measurement setup of the proposed antenna respectively. MS46322A (Anritsu) VNA with a range of 1 MHz to 20 GHz is used for the measurement of 1D results i.e., VSWR, group delay, S_{11}, etc. Similarly, for measurement of the gain and radiation pattern, the proposed antenna was placed in an anechoic chamber with more than Far-field distance from the reference antenna. However, for group delay measurement the two identical antennas were placed in face to face orientation with a distance of 600 mm. The simulated and measured results show good agreement with each other as depicted in Fig. 4.28 (VSWR and S_{11}). The center notch frequency is shifted from 5.5483 GHz to 5.628 GHz and the notch band is changed from 5.088 GHz to 6.012 GHz in the measured result. This change could be

due to the practical limitation of generating 5th order Gaussian signal and fabrication, connector, and cable losses.

(a)

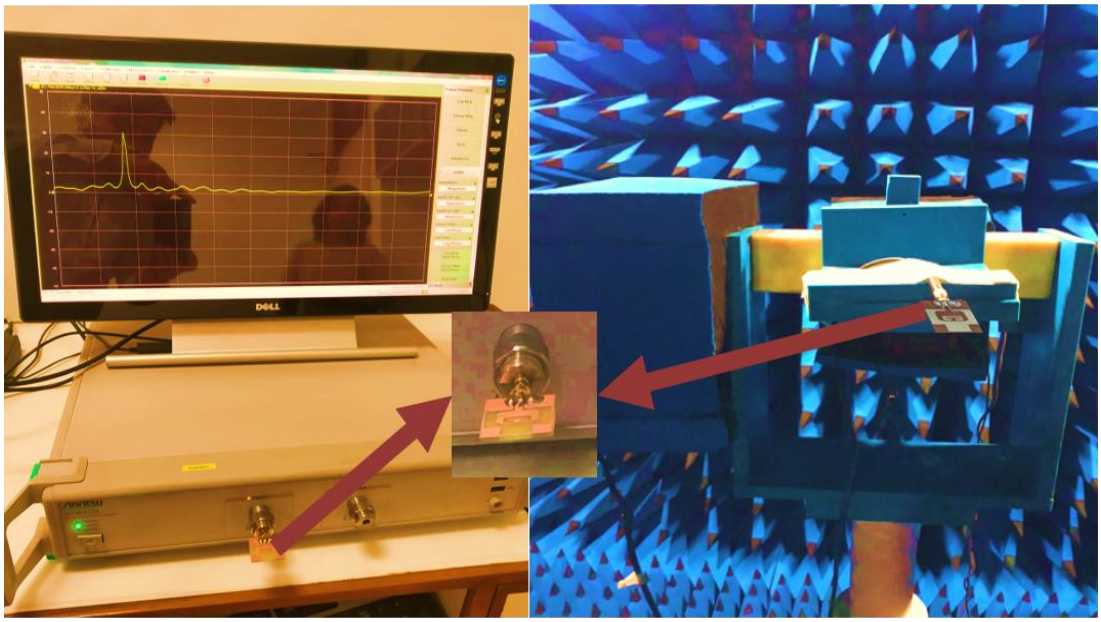

(b)

Fig. 4.27. Fabricated antenna and measurement setup (a) Photograph of the prototype of the designed antenna (b) Photograph of the measurement setup of the proposed antenna

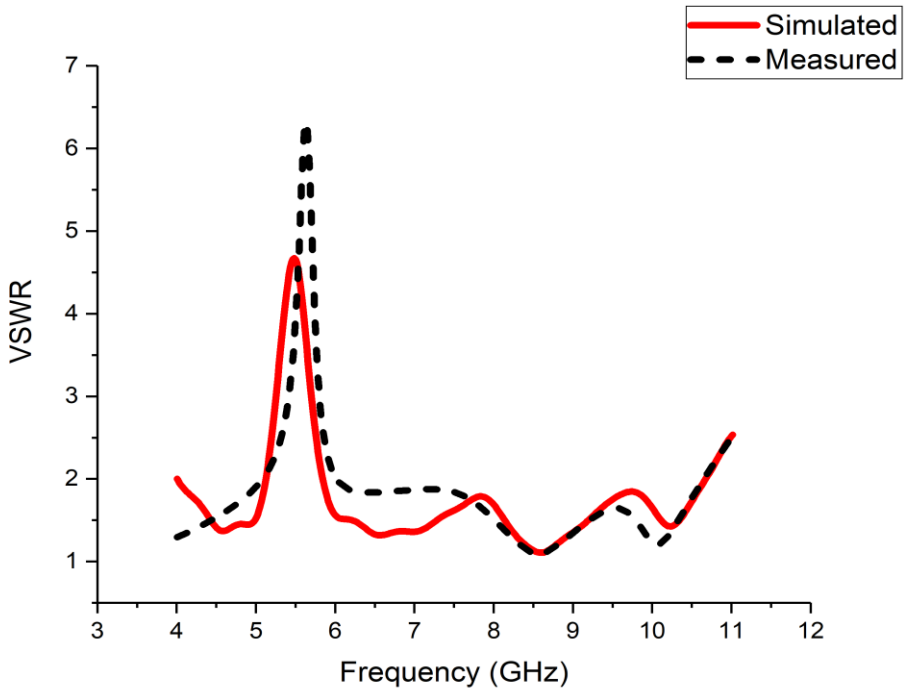

(a)

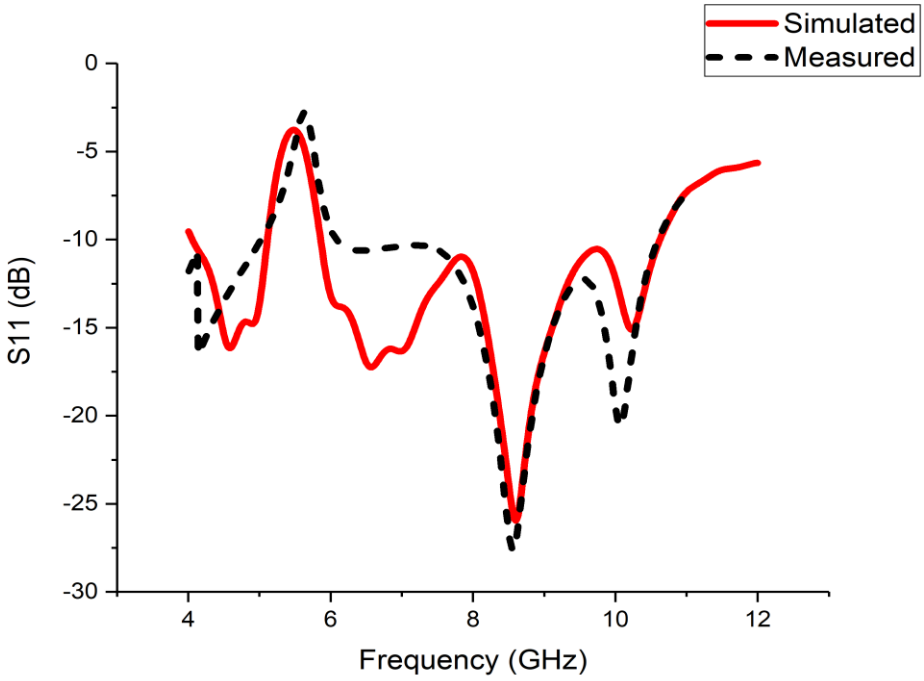

(b)

Fig. 4.28 Simulated and measurement Results (a) VSWR (b) S_{11} parameters

Table 4.8 Cross polarization level in y-z and x-z plane

Frequency (GHz)	Simulated cross-polarization level E-Plane (y-z Plane) (dB	Measured cross-polarization level E-Plane (y-z Plane) (dB)	Simulated cross-polarization level H-Plane (x-z Plane) (dB)	Measured cross-polarization level H-Plane (x-z Plane) (dB)
4	-41.86	-47.57	-13.46	-8.32
4.63	-44.84	-50.31	-18.48	-7.11
5.13	-42.01	-43.35	-18	-6.3
5.83	-38.91	-31.31	-13.6	-6.22
6.5	36.90	-38.28	13.25	-5.09
7	35.45	-39.74	-15.66	-6.39
7.5	33.17	-33.44	-10.69	-13.23
8.3	30.46	-33.48	-6.47	-8.72
9.3	-24.1	33.36	-5.52	8.18
10.6	33.37	29.79	6.50	7.17

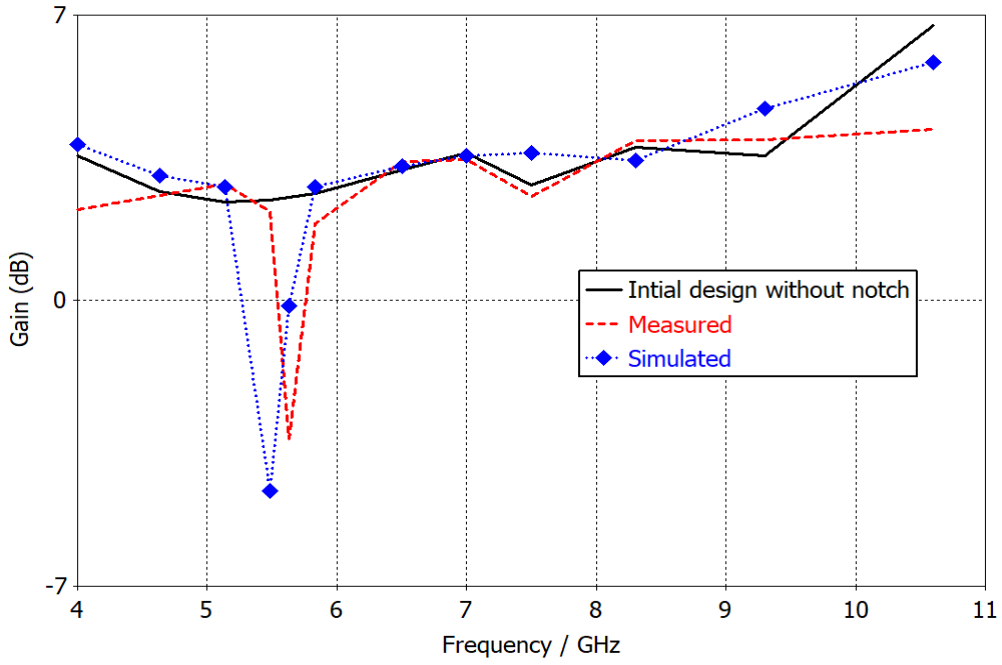

Fig. 4.29 Simulated and measured gain of the proposed antenna

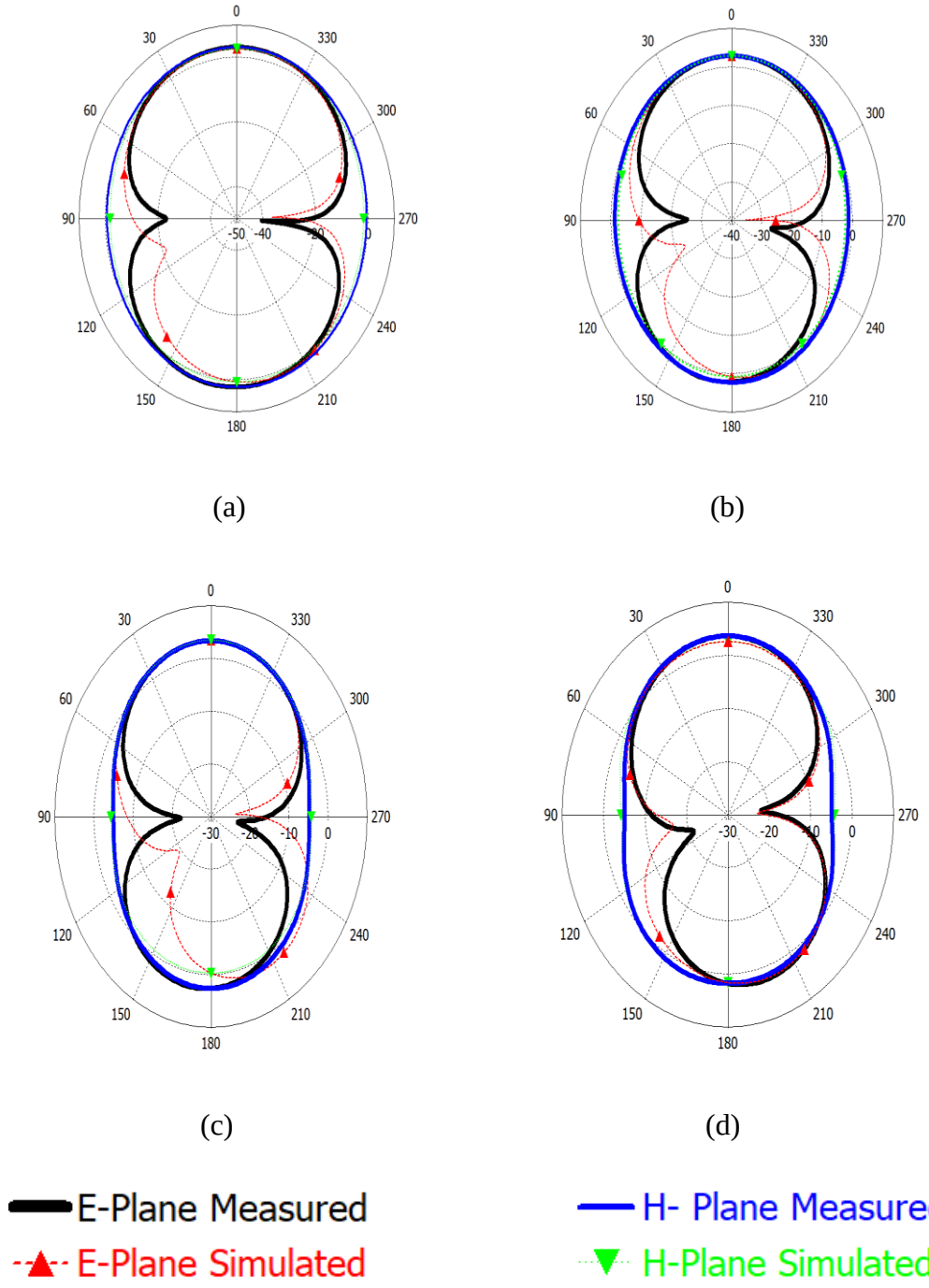

Fig. 4.30. Simulated and measured radiation pattern at different frequency (a) 4.63 GHz (b) 5.133 GHz (c) 6.5 GHz (d) 7.5 GHz

Similarly, the normalized E-Plane (y-z plane) and H-plane (x-z plane) radiation patterns at 4.63 GHz, 5.133 GHz, 6.5 GHz, and 7.5 GHz are given in Fig. 4.30. As observed in Fig. 4.29 of the x-z plane, the radiation pattern is relatively omnidirectional, which is useful for the UWB operation. Further, the simulated and measured results depict that

the antenna is the linearly polarized in the y-z direction as the cross-polarization level is observed below -20 dB in theta direction and the x-z plane, the level of cross-polarization is observed more than -10 dB (apart from the perpendicular direction to the antenna). Table 4.8 has been used to show the cross-polarization level at a different frequency. Similarly, the normalized E-Plane (y-z plane) and H-plane (x-z plane) radiation patterns at 4.63 GHz, 5.133 GHz, 6.5 GHz, and 7.5 GHz are given in Fig. 4.30. As observed in Fig. 4.29 of the x-z plane, the radiation pattern is relatively omnidirectional, which is useful for the UWB operation. Further, the simulated and measured results depict that the antenna is the linearly polarized in the y-z direction as the cross-polarization level is observed below -20 dB in theta direction and the x-z plane, the level of cross-polarization is observed more than -10 dB (apart from the perpendicular direction to the antenna). Table 4.8 shows the cross-polarization level at a different frequency

Table 4.9 Comparison between gain and radiation efficiency for the proposed antenna

Frequency (GHz)	**Simulated Efficiency (%)**	**Measured Efficiency (%)**	**Simulated Gain (dB)**	**Measured Gain (dB)**
4	87.53	80.7	3.84	2.23
4.63	90.66	82.37	3.06	2.59
5.13	84.59	81.78	2.79	2.85
5.48	16.53	77.47	-4.65	2.19
5.62	43.09	16.91	-0.14	-3.38
5.83	87.82	76.81	2.79	1.9
6.5	85.69	81.78	3.3	3.2
7	86.08	82.65	3.55	3.46
7.5	90.26	85.95	3.63	2.56
8.3	88.31	83.19	3.44	3.92
9.3	91.28	88.47	4.7	3.94
10.6	91.04	84.58	5.83	4.21

As depicted in Fig. 4.29, the simulated and measured gain varies from 2.79 dB to 5.83 dB and 1.89 dB to 4.21 dB respectively in the UWB range except for the band notch. However, at notch frequency, the simulated and measured gain is -4.65 dB and -3.38 dB respectively. Furthermore, the simulated gain of the initial aforementioned design is also presented in Fig.4.29. The radiation efficiency also radically falls to a minimal value at the center notch frequency. Table 4.9 is used to represent the comparison between the gain and radiation efficiency at different frequencies in the UWB range for simulated and measured results.

4.6. Summary

A comprehensive analysis of a WLAN notch band antenna for UWB applications has been presented in this chapter. The proposed antenna has a notch band characteristic from 5.133 – 5.833 GHz with a center frequency of 5.483 GHz. The traditional optimization technique has been utilized on the C-shaped notch structure for achieving the desired notch band characteristics. Also, the essential parameters required for UWB operation have been precisely monitored while achieving notch band optimization. The percentage error of only 0.07%. has been observed as compared to the ideal center frequency for the WLAN notch band. Furthermore, the time-domain analysis for the proposed antenna has been done meticulously and it meets the requirements for the practical UWB systems. In the future, this process approach can be used to design and analyze the higher-order notch band filters by embedding MTMs and EBG structures.

Chapter 5

A Planar CPW Fed UWB Antenna with Dual Rectangular Notch Band Characteristics Incorporating U-slot, SRRs, and EBGs

In this chapter, a planar UWB antenna with dual rectangular notch band characteristics (i.e., 5.94 – 7.50 GHz and 8.02 – 10.46 GHz) is presented. The size of the antenna is very compact ($25\times25\times1.6$ mm^3) and is designed on a low-cost FR4 substrate. Co-planar waveguide (CPW) feed and beveling techniques have been utilized for achieving the UWB operation. In order to yield the first rectangular notch, a U-slot and a pair of split-ring resonators (SRRs) have been embedded into the radiating patch and the backside of the design respectively. The coupling between these two structures has been adjusted so as to achieve rectangular band notch operation. Further, the second rectangular notch has been achieved by introducing the two mushroom type electromagnetic band-gap (EBG) structures on the opposite side of the CPW feed. Also, the parametric analysis for controlling both the notches has been presented. Finally, time-domain analysis, filter synthesis, and measured results have been demonstrated to show the suitability of this design for UWB systems.

5.1. Introduction

Ultra-wideband (UWB) technology provides a unique solution in the field of high speed short-range indoor communication [145-148], [173-174]. However, it is still a major challenge to avoid interference with already existing bands in the aforementioned spectrum such as WLAN, Wi-MAX, X-Band downlink, and uplink for satellite communication, C- Band uplink and downlink for satellite communication, and ITU-R [148], [174], etc. One effective way to resolve this issue is to reject these bands at the front end of UWB systems. Hence, UWB antennas should possess band notch characteristics [145],[147], [175],[177].

Multiple design techniques have been provided in the literature for achieving band-notch characteristics in the UWB antennas i.e., slot and parasitic element loading, using fractals, embedding split-ring resonators (SRRs) and electromagnetic bandgap (EBG) structures [146], [148], [178-180]. Further, Varactor diodes, PIN diodes, and Micro-Electro-Mechanical Systems (MEMS) have been also used to achieve reconfigurable operation in UWB antennas with band-notch characteristics [148] [181].

The aforementioned designs have a common drawback that has not been assessed meticulously i.e., all these designs have a spiculate curve for notch band characteristics [46], [115]. These characteristics can be compared with the stopband characteristics of a first-order band stop filter where maximum rejection is provided to only a small range of frequencies [46], [115], [182]. However, the various notch bands have a higher range of frequencies that needs to be suppressed. Therefore, the notch band characteristics in the UWB antenna designs should have a flat notch band response. This is similar to increasing the order of the band-stop filter for improving the band-reject characteristics [46],[115], [182-186]. This problem has been addressed only in a few designs [115]. These designs have used the concept of merging the resonance of two notch structures and inducing higher-order or rectangular notch band characteristics.

In [185], the pair of SRRs has been utilized on the backside of the CPW feedline of the monopole design. The inductive coupling between the pairs of SRRs and radiator yields higher-order notch band characteristics. Likewise, in [186], a UWB antenna with the differential stepped slot is presented with two rectangular notches. In this letter, a common mode and differential mode suppression technique have been employed to achieve the desired UWB operation and quarter-wavelength slits are engraved in the ground plane of the antenna for achieving dual rectangular notches. Further, half-wavelength stubs have been used alongside the microstrip line for sharp selectivity. However, the structure utilized in [186] was very complex, which leads to lower efficiency in achieving other UWB antenna characteristics [115]. Hence in [115], a rectangular notch band was realized by employing two mushroom type EBG structures on the backside of the CPW feed line of a circular monopole antenna design.

Table 5.1 Comparison of the proposed antenna with existing work

Ref Ant.	**Antenna size (mm^2)**	**Notch band controllability**	**Structure or Technique used**	**Notched band**	**Time-domain analysis**	**No. of rectangular notches**
[46]	25 × 16	Yes	Dual EBG structures	5.1 – 5.9 GHz	No	1
[115]	48 × 50	Yes	Dual EBG structures	5.15- 5.825 GHz and 7.1 -7.76 GHz	No	1
[162]	22 × 8.5	No	Open and short ended half-wavelength split-ring slot	5.15 – 5.85 GHz	No	1
[183]	44 × 44.4	No	Dual open-circuited stubs	5.25 -5.775 GHz	Limited	1
[184]	38 × 42	No	Inductive coupling and folded strips	5.075 – 5.375 GHz	No	1
[185]	50 × 50	No	Pairs of SRR	6.2 -7.02 GHz	No	1
[186]	28 × 18	Yes	Common mode and differential mode operation	5.1 – 6 GHz, 7.83 – 8.47	No	2
This work	25 × 25	Yes	U- slot, SRRs pair, and dual EBG structures	5.94-7.5 GHz and 8.02 – 10.46 GHz	Yes	2

In this design, the CPW feed works as the ground plane for both of the EBG structures. The rectangular notches can be tuned by changing the length and width of EBG structures and merging their resonances. A similar process has been followed in [46] to produce rectangular notch band characteristics. Also, few other techniques have been employed in other designs to provide higher-order notch bands such as double open-

circuited stubs [183], folded strips, and inductive coupling [184], and half wavelength short ended split-ring slot [162].

One important observation is that in all the designs [46],[115], [182-186] the only focus was on achieving higher-order notch band characteristics with sharp selectivity. However, the performance of these designs has been not been evaluated based on UWB system requirements i.e., selection of excitation signal based on indoor FCC mask, time-domain analysis (dispersion, group delay, fidelity factor), filter synthesis of notch notched bands, etc. Further, the dual rectangular notches (i.e., 5.1 – 6 GHz and 7.83 – 8.47 GHz) have been only achieved in a single design [186] with limited performance evaluation based on the desired UWB system requirements. Therefore, in the proposed UWB antenna the dual rectangular notches (i.e., 5.94 – 7.50 GHz and 8.02 – 10.46 GHz) are achieved with the desired UWB system requirements. Table 5.1 is used to compare the proposed work with the designs available in the literature.

The initial design approach used in the proposed antenna is based on CPW feeding and beveling techniques to achieve the UWB operation. For achieving the first rectangular notch band characteristics, a U-slot and a pair of SRRs have been used in the radiating patch and the backside of the design respectively. Here the U-slot provides the initial spiculate notch and then the resonance of the pair of SRRs is merged to achieve the higher-order notch. Further, for achieving the second rectangular notch, two mushroom type EBG structures have been utilized in the backside of the CPW feed line. The dimensions of these two EBG structures have been chosen carefully to achieve the optimized rectangular notch. Also, the equivalent circuit model, time-domain analysis, and measured results of the proposed design have been presented to validate the results.

This chapter is divided into seven sections. Section 5.1 represents the introduction and Section 5.2 presents the design configuration of the antenna. Further, the design process and a parametric study are presented in Section 5.3 and Section 5.4 respectively. Section 5.5 and Section 5.6 provides the time domain analysis and measured results. Finally, Section 5.7 holds a summary of the proposed work.

5.2. Design Configuration of the Antenna

The design configuration of the proposed antenna is shown in Fig. 5.1. The proposed design has a U-slot slot etched on the beveled radiating patch to achieve the initial notch band operation. Further, a pair of split-ring resonators (SRRs) is loaded on the backside of the radiating patch for achieving the first rectangular notch by inductive coupling. Additionally, two EBG structures are embedded on the backside to achieve the second rectangular notch. The antenna is having an overall size of 25×25×1.6 mm^3 and is designed and fabricated on an FR4 substrate (ε_r = 4.3) with a loss tangent of 0.025.

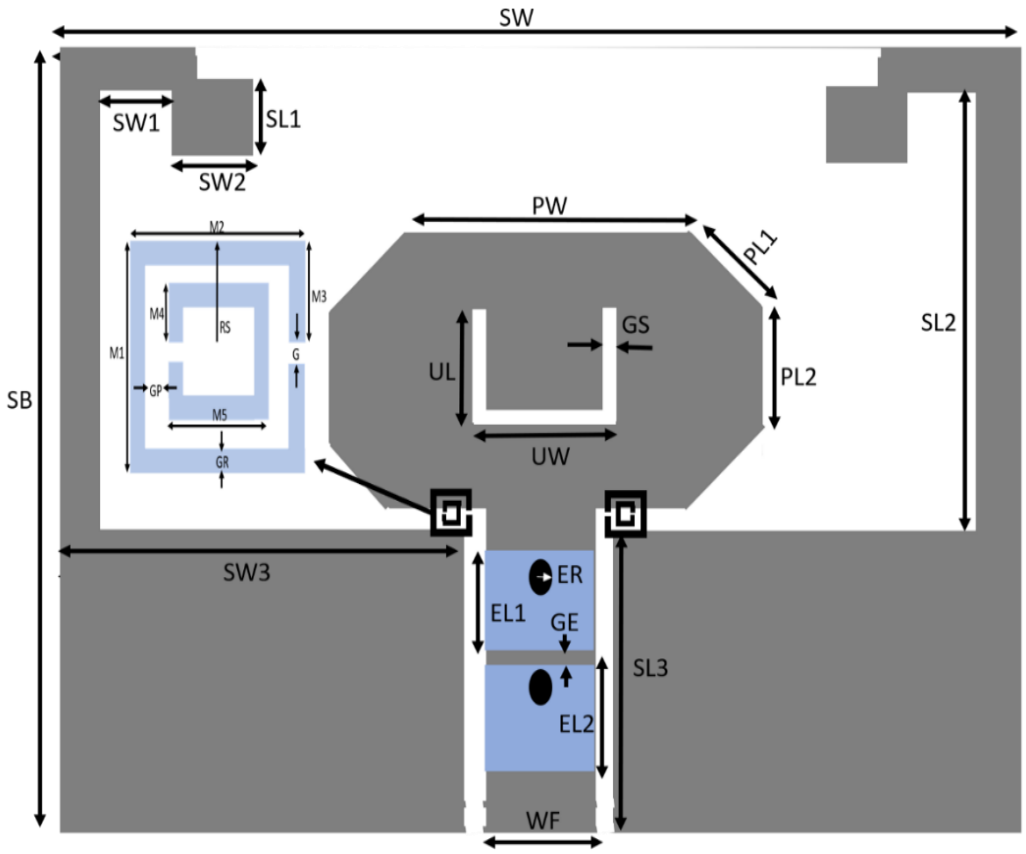

Fig..5.1 Design configuration of the proposed antenna

Firstly, the modified ground plane, CPW feeding, and beveling techniques have been utilized to achieve the desired UWB operation in the proposed design. The positioning of the U-slot, SRRs, and EBG structures has been done carefully and also the dimensions of these structures have been carefully chosen after multiple iterations on the CST Microwave Studio. The different parameters such as current distribution,

radiation pattern, gain, and group delay have been studied extensively for UWB operation in all iterations and the dimensions which provide the optimal results have been selected in the final design. Table 5.2 has been utilized to represent the final dimensions of the proposed design

Table 5.2. Dimensions of the proposed antenna in mm

SB	25	SL1	3	SL2	16	G	0.28
SL3	8	SW	25	SW1	2.6	WF	3
SW2	3	SW3	10.6	PW	10	GR	0.14
PL1	3.54	PL2	3	UL	4	GP	0.24
UW	6	GS	0.5	EL1	3.5	M4	0.48
EL2	3.9	ER	0.6	GE	0.5	M5	1.24
M1	2	M2	2	M3	0.86	RS	1

5.3. Design Process

The overall design process of the proposed antenna is divided into three steps i.e., the design of the UWB antenna, the realization of the first rectangular notch in the UWB antenna, and realization of second rectangular notch UWB antenna.

5.3.1 Step 1: Design of the UWB Antenna

Initially, for achieving the UWB operation, CPW feeding and beveling technique has been utilized in the proposed design. As given in the literature, these techniques have been frequently employed in various designs for achieving wider bandwidth and omnidirectional radiation pattern, which is essential for UWB antennas [115], [146], [173],[176]. A 50 Ω transmission line having a width of 3 mm has been used to feed the radiating patch to transfer maximum power to the antenna. Furthermore, the excitation signal is also chosen based on the given FCC indoor mask of UWB systems.

As shown in Fig. 5.2, the S_{11} of the initially designed antenna is below -10 dB for the entire UWB range (3.1 GHz – 10.6 GHz) and bandwidth of the antenna is 9.24 GHz from 2.63 GHz to 11.87 GHz. The simulated radiation pattern of the antenna is omnidirectional in the UWB range except at some higher frequencies. Hence, to improve the radiation characteristics of the antenna, the dimensions of the ground plane

are optimized. It was observed that the two square-shaped arms of the ground plane have a drastic effect on the gain and radiation characteristics of the antenna. Moreover, the equivalent impedance model of the UWB antenna and its response has been also presented in Fig. 5.2

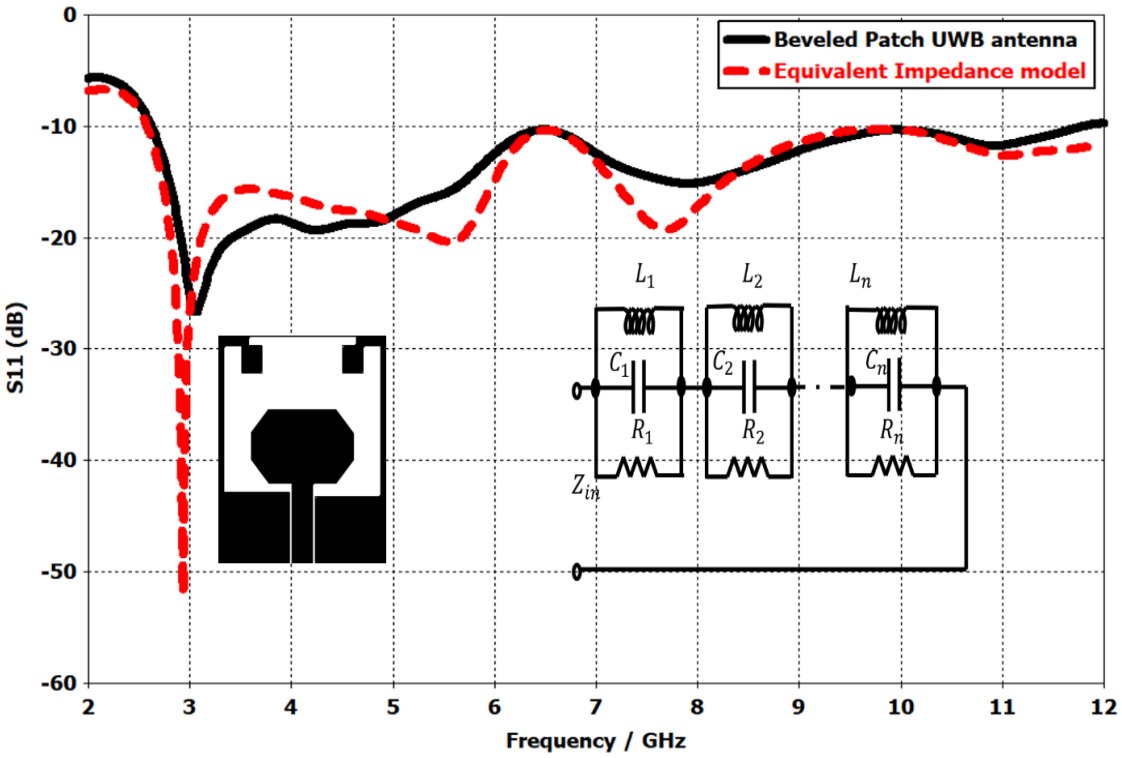

Fig. 5.2. S_{11} of the initial UWB antenna

5.3.2 Step 2: First Rectangular Notch Band Realization

One of the major challenges in notch band realization for UWB antennas is to find the suitable notch band structures and their placement in UWB antennas. Since these structures also affect the other desired UWB antenna parameters such as gain, radiation pattern, bandwidth, group delay, etc. In the proposed design, for achieving the first rectangular notch a pair of SRRs and a U-Slot have been utilized. Initially, the U-slot dimensions have been chosen to achieve the spiculate notch with a center frequency of 6.5 GHz. The basic design equation of U-slot for achieving notch band characteristics is given by

$$F_n = \frac{C}{2(L_s + W_s)\sqrt{\varepsilon_{eff}}} \qquad (5.1)$$

where C presents the speed of light, ε_r is the dielectric constant of the substrate and F_n denotes the notch frequency. Further, L_s and W_s represent the length and width of the U-slot.

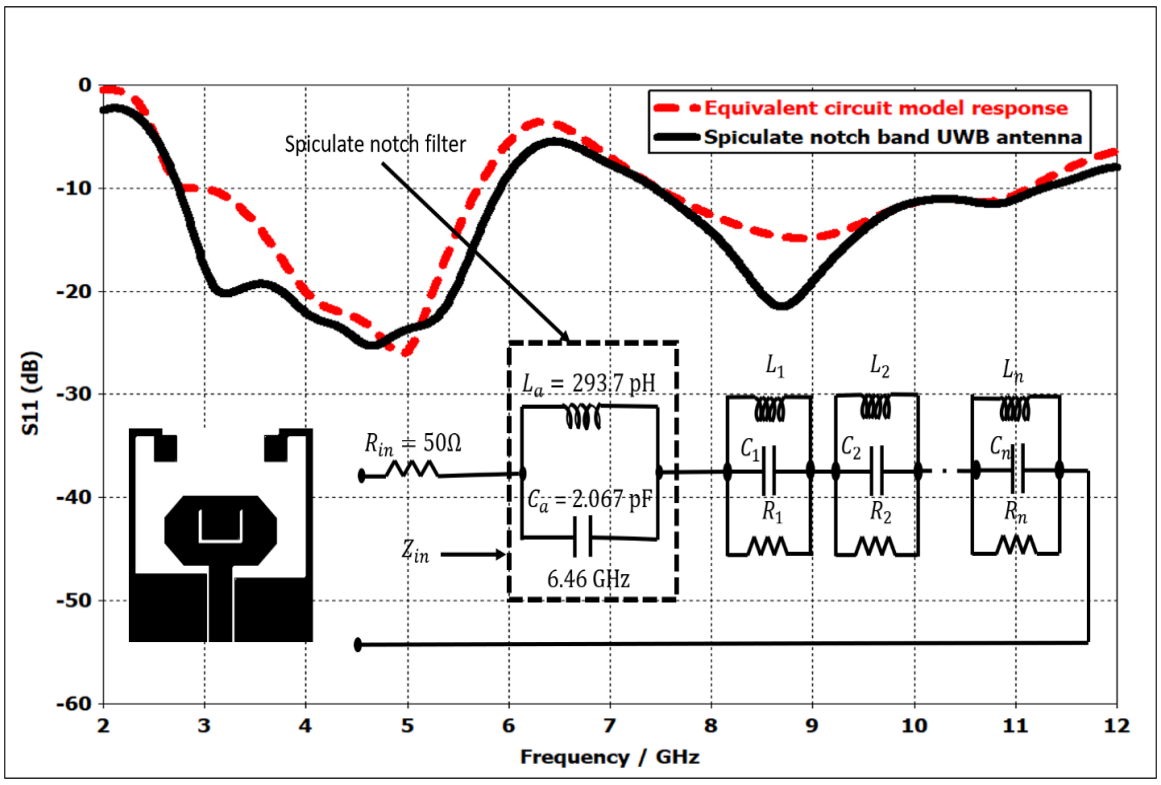

Fig. 5.3. S_{11} with U-slot

Initially, based on the Eq.1 the calculated value of "$2L_s + W_s$" was 14.2 mm approximately. However, in simulated results, the center frequency was observed at 6.31 GHz. So, the positioning of the slot and the final value of "$2L_s + W_s$" is optimized to 10 mm for optimal results. The variation in F_n was more predominant when the dimensions of L_s are changed as compared to W_s.Therefore the value of W_s is kept same while optimizing the notch frequency. After optimization of the U-slot, the center notch frequency is achieved at 6.46 GHz i.e., from 5.91 GHz to 7.45 GHz as shown in Fig.5.3. Moreover, the equivalent circuit model of the design is also represented in Fig. 5.3. The circuit diagram and values of the lumped components for the spiculate notch

filter are calculated based on the filter synthesis tool available in CST Microwave Studio.

To achieve the first rectangular notch for the proposed design the resonances of U-slot and a pair of SRRs have been merged. The initial dimensions of SRR for the resonating frequency (f_c) i.e., given by

$$f_c = \frac{1}{2\pi}\sqrt{\frac{1}{L_S C_s}} \tag{5.2}$$

Where, C_s presents the total equivalent capacitance of the SRR and it can be estimated by calculating the distributive capacitance amongst the two SRR rings and the capacitance due to the gap as

$$C_s = \left(2\, r_a - \frac{G}{2}\right) C_p + \frac{\varepsilon_0\, W1\, T1}{2G} \tag{5.3}$$

Where $T1$ and $W1$ are the thickness and width of the rings respectively and ε_0 presents the free space permittivity. The split opening are having same dimensions i.e., G. Further the average dimension of the ring is given by

$$r_a = RS - T1 - \frac{GP}{2} \tag{5.4}$$

The parameter C_p gives the capacitance per unit length and can be calculated as

$$C_p = \frac{\sqrt{\varepsilon_e}}{cZ_c} \tag{5.5}$$

wherein Equ. (5.5), c is the speed of light, Z_c is the characteristic impedance and ε_e effective permittivity of the medium. The total equivalent inductance for a wire with fixed length S_L and thickness of M_t is given as

$$L_s = 0.0002\, S_L \left(2.303 log_{10}\, \frac{4S_L}{M_t} - \Omega\right) \mu H \tag{5.6}$$

where Ω is constant with a value of 2.853 for a loop wire having square geometry. Also, for the calculation of S_L the following equation is used

$$S_L = 8RS - G \tag{5.7}$$

As shown in Fig. 5.1, the SRRs are positioned symmetrically on the backside of the CPW feed and their axis overlaps with the slot between radiating patch and ground plane. Thus input EM signal excites the SRRs pair and prevents radiations around the SRRs which yields the notch frequency. The resonance frequency of the SRR is determined using Eq (5.2)-(5.7). The parameters such as RS, $W1$, $T1$, D, and G play a vital role in calculating the desired resonance. The initial values of the L_s and C_p are calculated as 9.84 nH and 19.45 pF for a notch frequency at 6.8 GHz. For these values, the SRRs pair is having $r_a = 2.45\,mm$, $W1 = 0.36\,mm$, $T1 = 33\,\mu m$, $G_p = 0.58\,mm, G = 0.67\,mm$. However, in simulated results, the notch frequency was observed at 6.15 GHz. Therefore the SRRs pair dimensions were optimized to final values of proposed antenna after many iterations. The major observation during these iterations is the effect of RS and GR on the notch frequency.

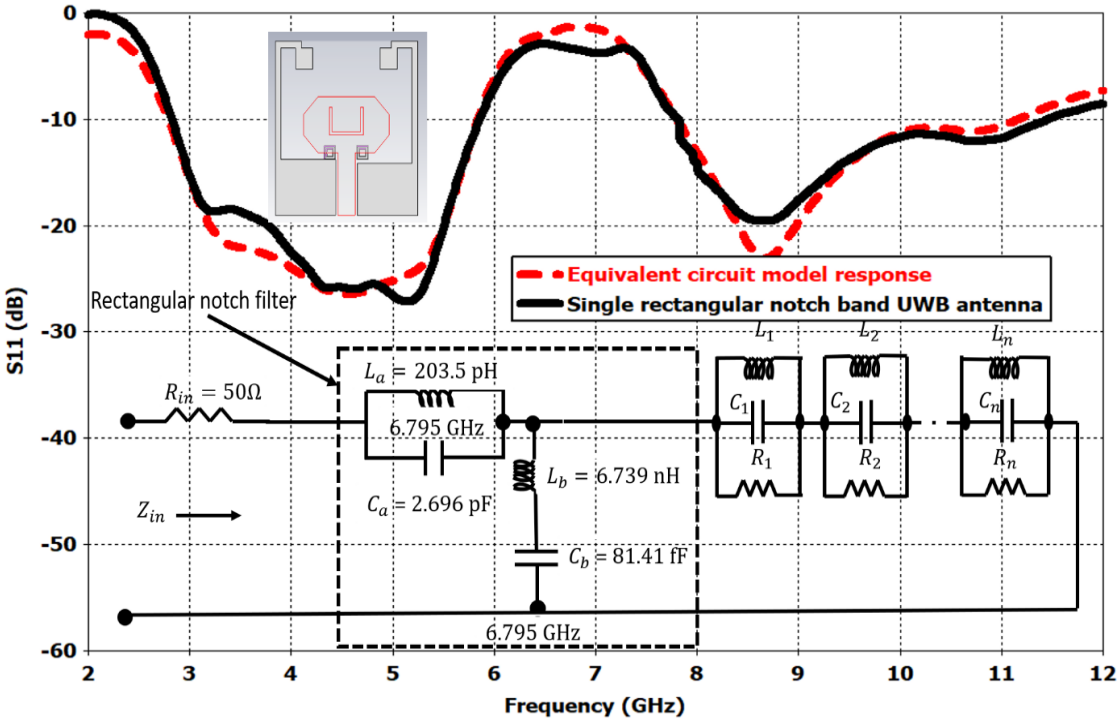

'**Fig.** 5.4 S_{11} with U-slot and SRRs pair

The variation in the dimensions of these two parameters has a maximum impact on the notch frequency. Fig.5.4 presents the first rectangular notch band characteristics in the proposed antenna. The SRRs pair is coupled with the beveled radiating patch and U-

slot to achieve the first rectangular notch. The response of the higher-order notched filter and the rectangular notch is also compared and suitable values of the circuit elements have been chosen. In the S_{11} response for the rectangular notch, the bandwidth of 1.67 GHz is achieved from 5.96 - 7.63 GHz with a center frequency of 6.795 GHz.

5.3.3 Step 3: Second Rectangular Notch Band Realization

The weakness of spiculate band notch is that it is not able to seamlessly reject the frequencies from lower to a higher value (f_L and f_H) in the notched band. Hence, to overcome this drawback rectangular notches have been designed in the proposed antenna. There are many types of EBG structures that have been used in UWB antennas for achieving band notch characteristics. As mentioned in Section 5.3.2, the concept of merging resonances of two EBG structures have been employed. However, the mushroom type EBG structure is most popular and is used in the proposed design for achieving the second rectangular notch. The operation of the mushroom type EBG structure can be described as an array of LC filters. Their values can be calculated from the movement of current through their vias and also the gap between the adjacent patches. The values of L and C can be calculated as [148]

$$L = \mu_0 h \tag{5.8}$$

and

$$C = \frac{W\varepsilon_0(1+\varepsilon_r)}{\pi}\cosh^{-1}\left(\frac{2W+g}{g}\right) \tag{5.9}$$

In Eq. 5.8 and Eq. 5.9 h and W represent the height and width of the patch and g represents the gap width. Further, $\varepsilon_o, \varepsilon_r$ and μ_o represents the permittivity of free space, dielectric constant, and free space permeability respectively. The bandgap is calculated as [148]

$$w = \frac{1}{\sqrt{LC}} \tag{5.10}$$

$$BW = \frac{\Delta w}{w} = \frac{1}{\eta}\sqrt{\frac{L}{C}} \tag{5.11}$$

where η is the free space impedance with a value of 120 π.

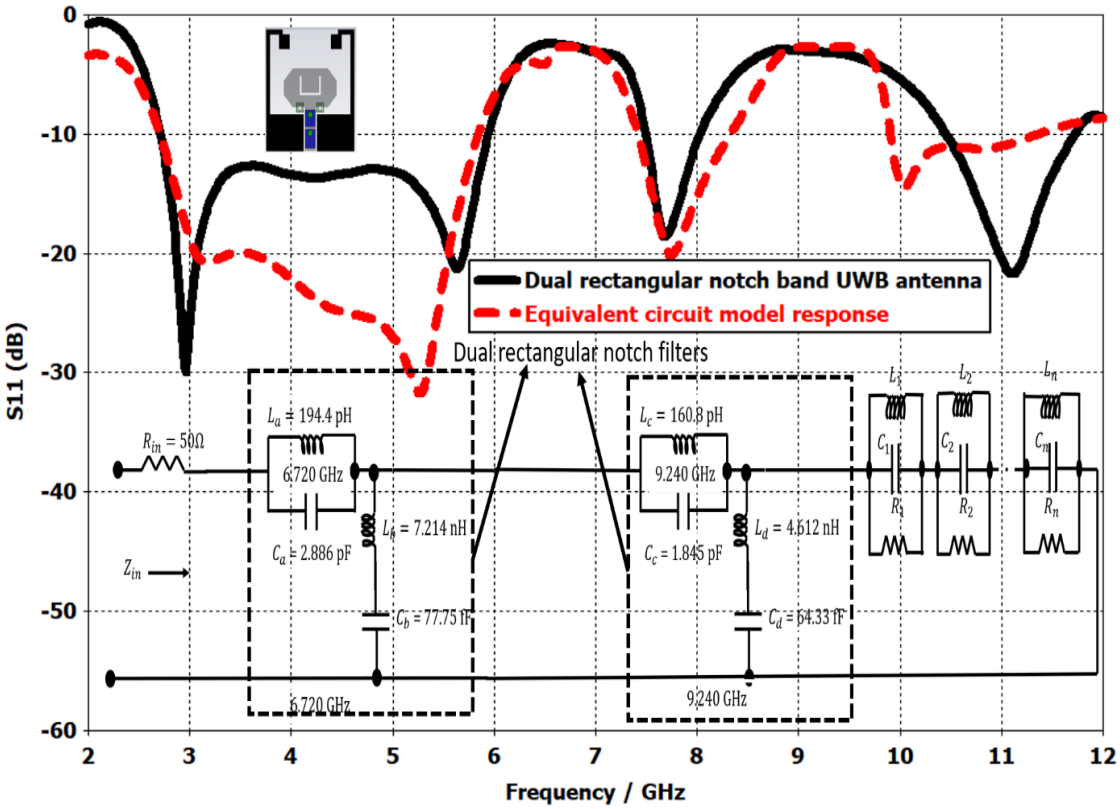

Fig. 5.5 S_{11} with U-slot, SRRs pair, and EBG structures

Fig. 5.5, represents the S_{11} plot for the proposed antenna with a dual rectangular notch and the equivalent circuit model with the calculated values of the lumped components has been presented. In this plot, it can be observed from Fig. 5.5 that the first rectangular notch is not affected while achieving the second rectangular notch. Furthermore, the UWB operation is also not affected and the plot ranges from 2.72 GHz to 11.72 GHz. Also, the two notched bands range from 5.94 GHz to7.5 GHz and 8.02 GHz to 10.46 GHz respectively.

5.4 Parametric Study

A thorough parametric study of the proposed antenna has been carried out to evaluate the performance of the antenna and to identify the control parameters for both the notch bands. While determining the control parameters for notch bands their impact on the other essential parameters for UWB operation has been analyzed.

5.4.1 Controlling the First Rectangular Notch

Fig. 5.6 represents the notch band controllability of the first rectangular notch by changing the values of GS and GR. The coupling between the U-slot and pair of SRR is responsible for the first rectangular notch and by changing the thickness of both structures the variation in the notch band has been analyzed. The values of GS and GR have been varied from 0.1 mm to 1 mm and 0.07 mm to 0.28 mm respectively. By doing this, the values of f_H and f_L varies from 5.89 GHz to 7.91 GHz and the values i.e., GS = 0.5 mm and GR = 0.14 mm are selected. The chosen values provided a bandwidth of 1.67 GHz with a center frequency of 6.795 GHz.

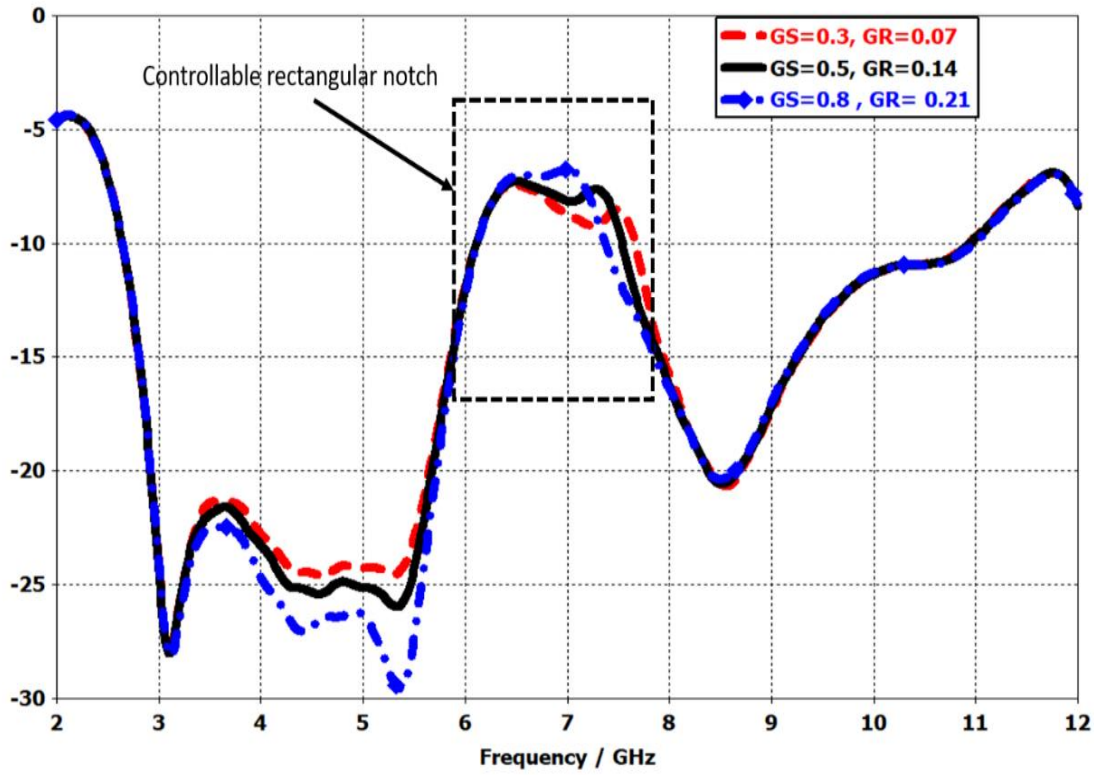

Fig. 5.6 Controllable rectangular notch by varying GS (mm) and GR (mm)

5.4.2 Controlling the Second Rectangular Notch

Similar to the control parameters for the first rectangular notch, EL1 and EL2 are the control parameters for the second rectangular notch. For both parameters, the values have been varied as shown in Fig. 5.7 and Fig. 5.8. For controlling the notch, EL1

values are changed in the range from 3.1 mm to 3.9 mm and correspondingly, the values of f_H and f_L varies from 7.92 GHz to 10.91 GHz.

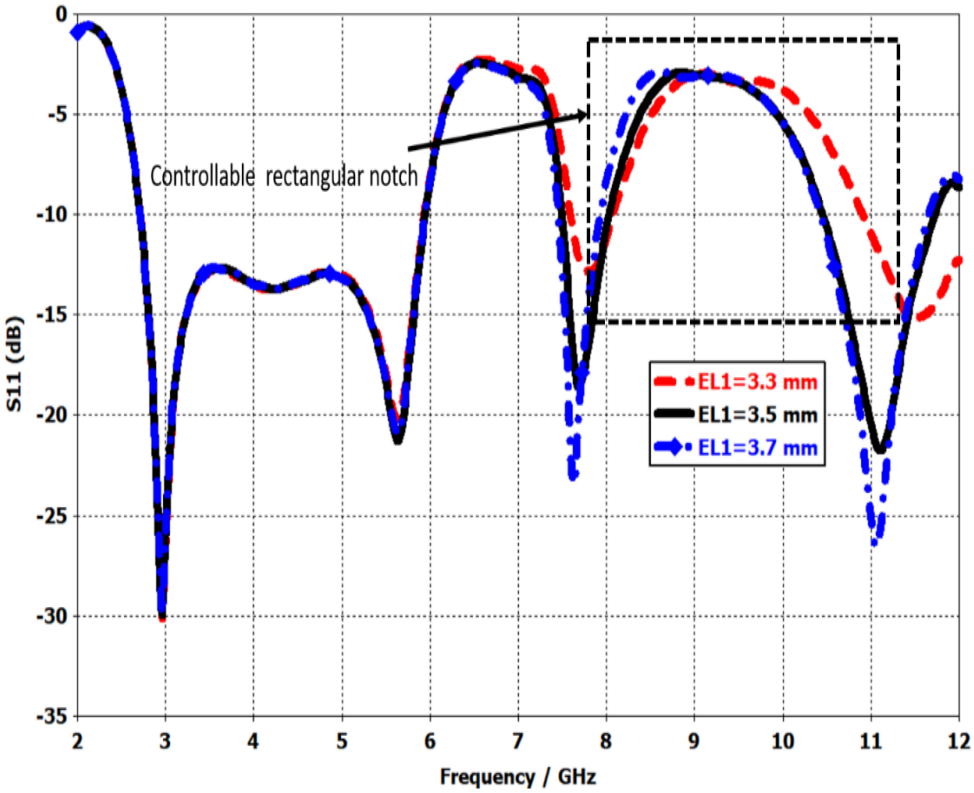

Fig. 5.7 Controllable rectangular notch by varying EL1

The optimal value of EL1 is chosen as 3.5 mm as it provided results that are consistent with the other UWB system requirements. Similarly, EL2 values are changed from 3.5 mm to 4.1 mm and f_H and f_L from 7.87 GHz to 11.51 GHz. The final selected value os EL2 is 3.9 mm which provides a bandwidth of 2.44 GHz i.e., from 8.02 to 10.46 GHz. While varying the values of EL1 and EL2 there was no significant effect on the first rectangular notch.

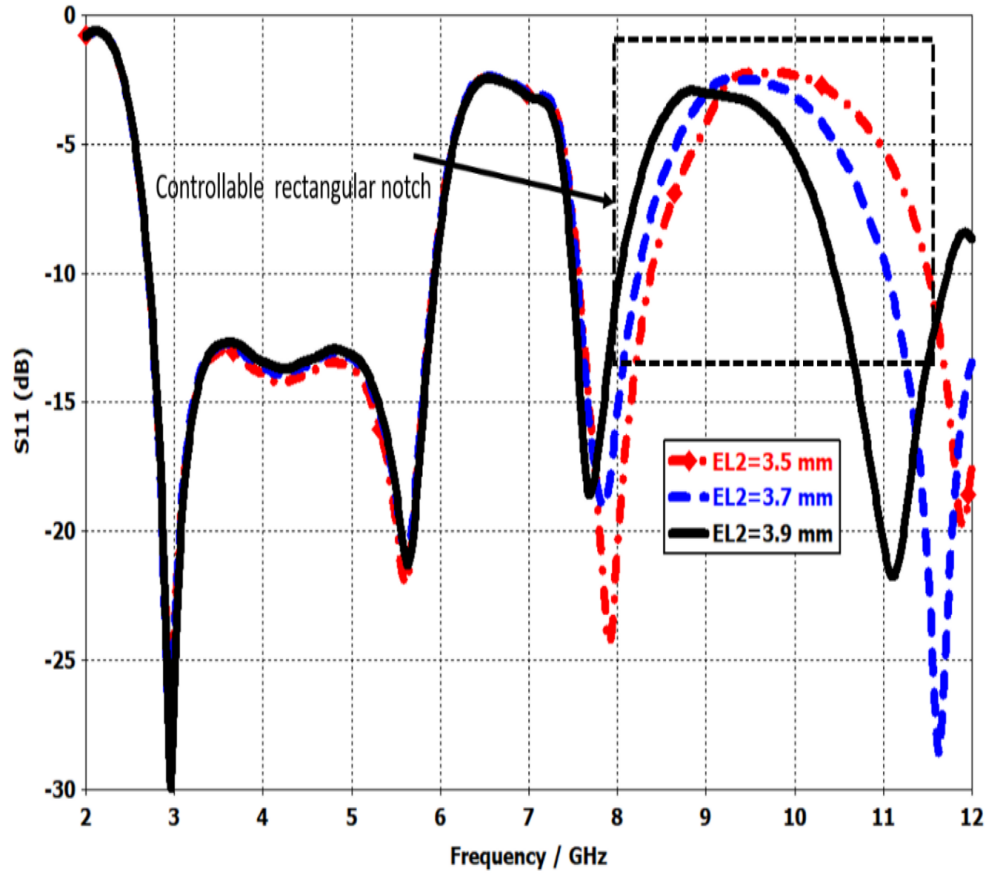

Fig. 5.8 Controllable rectangular notch by varying EL2

5.4.3 Surface Current Distribution

Notch frequency bands are created in the proposed design by embedding three notch structures i.e., U-slot, SRRs pair, and two mushroom type EBG structures. It has been also observed that by using these notch structures there is no major re-tuning of the overall dimensions of the antenna is required. The basic design concept of the notch function is to fine-tune the total length of the notch structure to approximately half-wavelength of the required notched frequency. However, for other frequencies, the addition of notch structure has only a few effects. Based on this idea, the surface current distribution of the design at different frequencies has been presented by Fig. 5.9 and Fig. 5.9 (a) presents the surface current concentration of the antenna at 4 GHz (i.e., passband of the antenna).

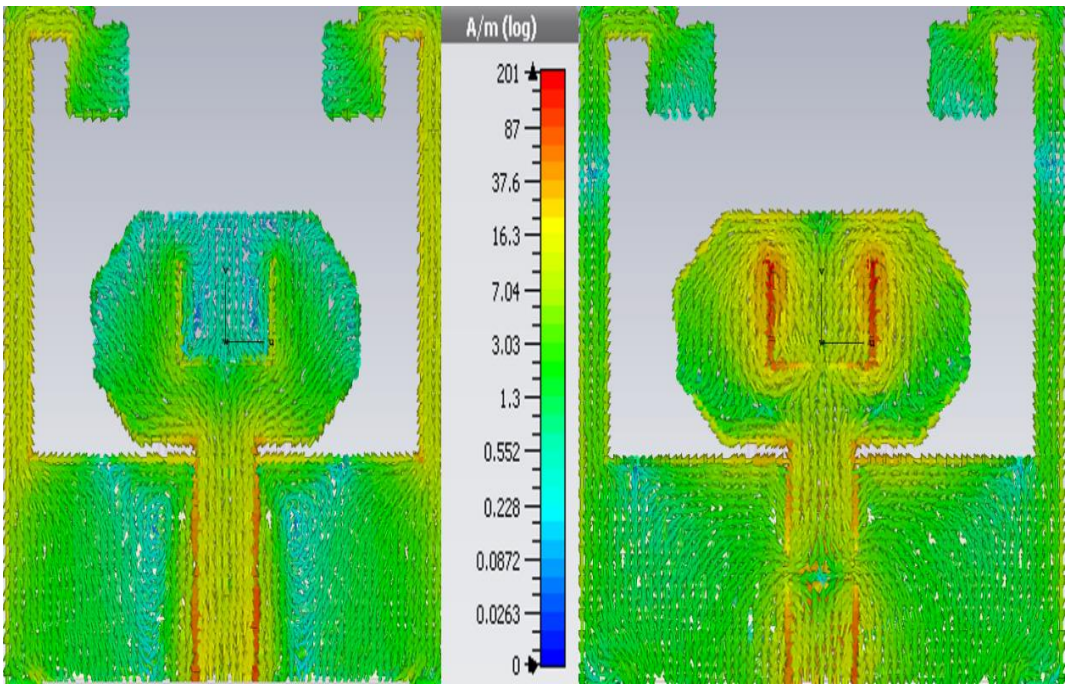

(a) (b)

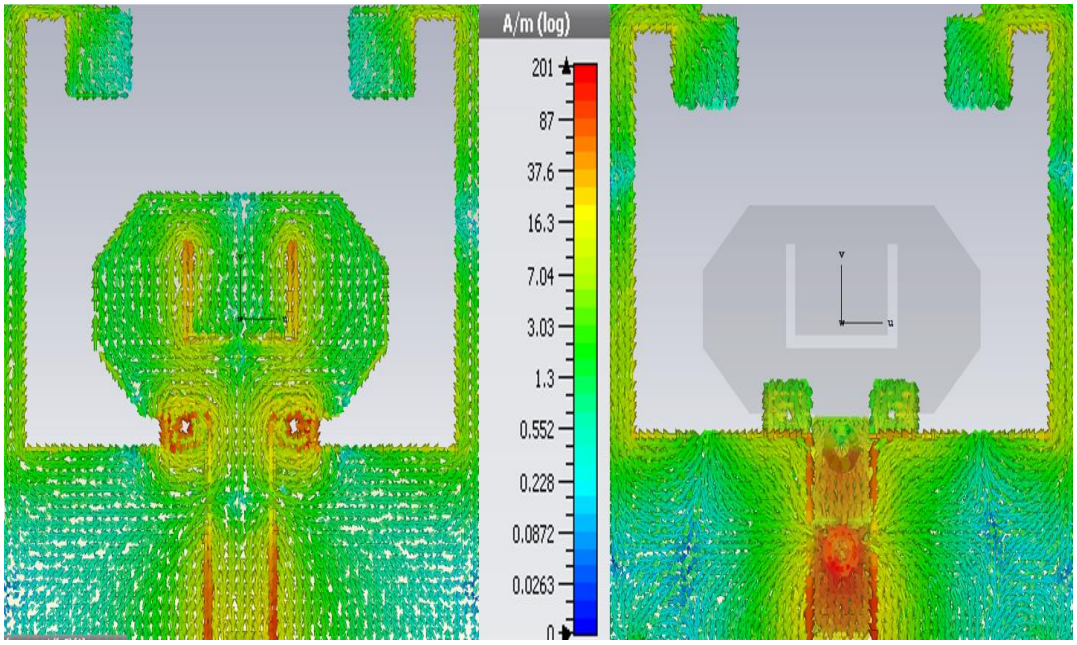

(c) (d)

Fig. 5.9 Surface current distribution at (a) 4 GHz (b) 6.46 GHz (c) 6.795 GHz (d) 9.24 GHz

It can be noticed that the surface current is mainly flowing along the feedline as well as the side arms of the ground plane and the current concentration is negligible around the notch structures. However, in Fig. 5.9 (b), the maximum current concentration simulated at 6.46 GHz is around the U-slot (i.e., the initial spiculate notch center frequency). Hence, for the excited surface currents, destructive interference occurs in the antenna, which causes the antenna to be non-responsive at this notch frequency. Similarly in Fig. 5.9 (c), the maximum surface current at 6.795 GHz is concentrated around the U-slot and the pair of SRRs (i.e., the center frequency of the first rectangular notch). Thus, these two-notch structures are responsible for making the antenna non-responsive at the first rectangular notch. Lastly, the second rectangular notch i.e., 8.02 GHz to 10.46 GHz is achieved by the combination of two EBG structures. Because, as depicted in Fig. 5.9 (d) most of the surface current concentration is around the two EBG structures which are simulated at a frequency of 9.24 GHz (i.e., the center frequency for the second rectangular notch).

5.5 Time-Domain Analysis

In UWB systems the signal transmission is done through narrow pulses. Hence, it is essential to evaluate the performance of the antenna in the time domain. Three important factors to evaluate this are dispersion analysis, SFF, and group delay. To calculate the dispersion analysis and SFF, two identical antennas are placed in face to face and side by side configuration at a distance greater than far-field distance i.e., 200 mm for this design. Similarly, for group delay measurement the antennas were placed at a distance greater than far-field distance. Fig. 5.9 presents the dispersion analysis of the proposed antenna for both configurations i.e., face to face and side by side. The normalized amplitude of the input signal and radiated at distance is identical. However, some ringing phenomenon is detected in both configurations due to the notch band structures embedded in the design. This phenomenon is negligible in the initial design i.e., without any notch band structure. The PSD of the input as well as the radiated signal can be visualized in Fig. 5.11. It depicts that the PSD of the input signal used to excite the proposed antenna is following the FCC indoor mark limit. Moreover, the spectrum of the radiated signal is also maintaining the limit provided by the FCC for UWB signal transmission.

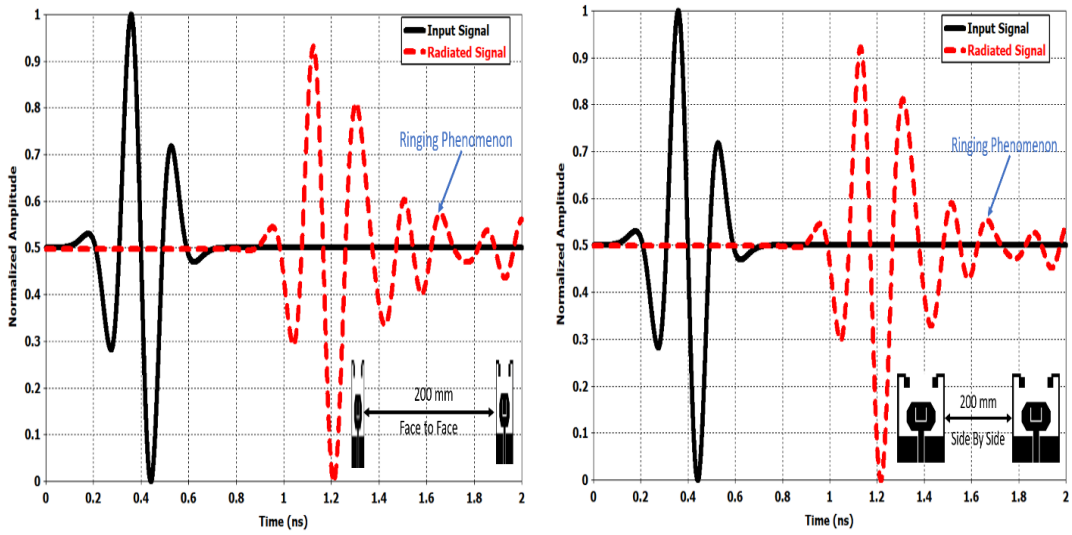

(a) (b)

Fig. 5.10 Normalized input and radiated signal for the proposed antenna (a) Face to face (b) Side by side

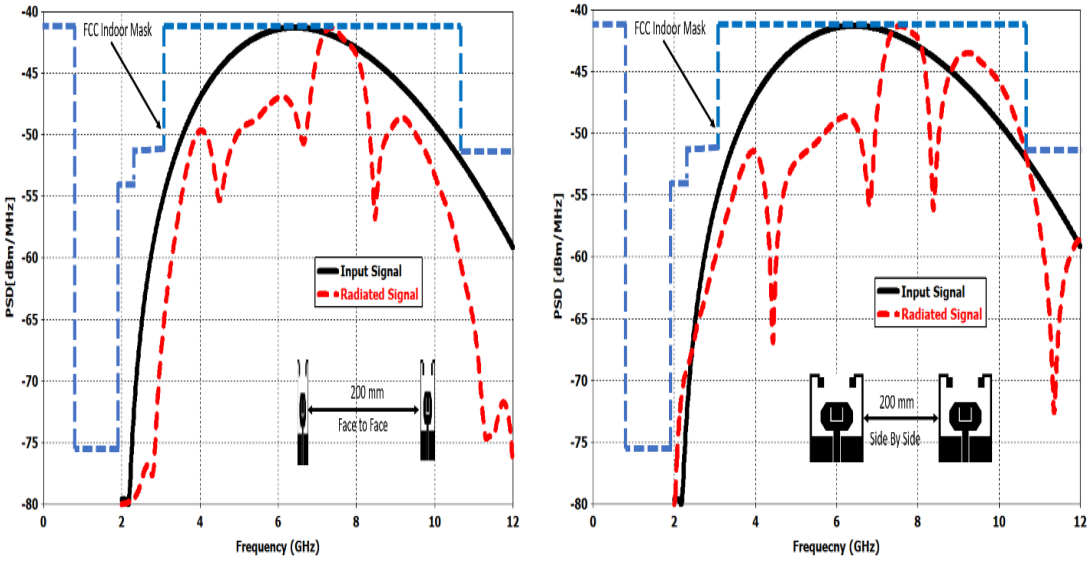

Fig. 5.11 PSD of the input and radiated signal of the proposed antenna (a) Face to Face (b) Side by side

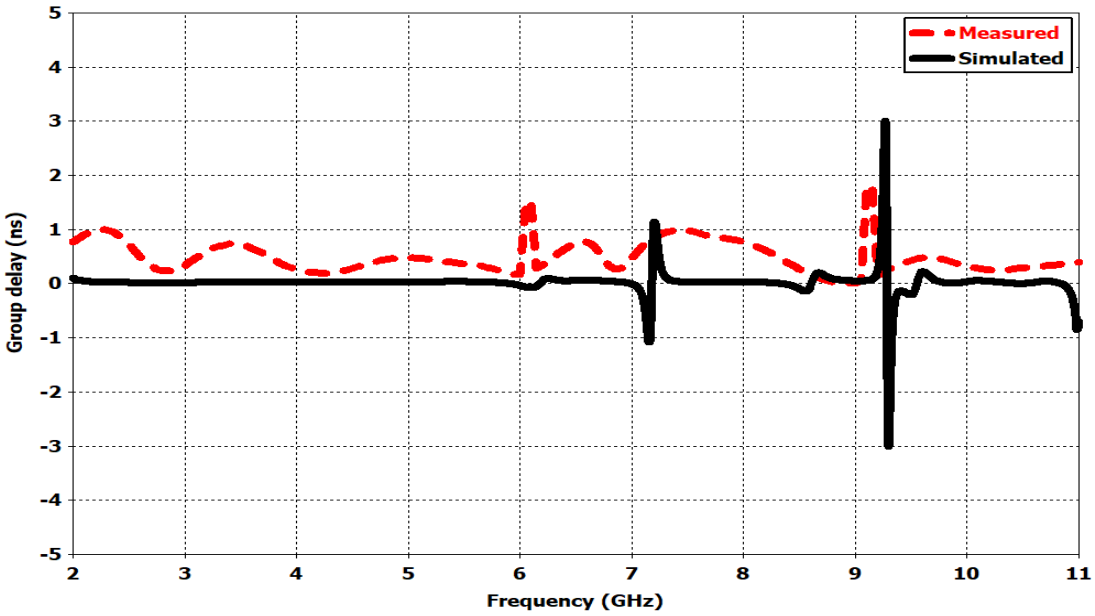

Fig. 5.12 Simulated and measured group delay of the proposed antenna

As discussed in Chapter 4, Another important parameter to assess the time-domain performance of the UWB antenna is SFF. The values of fidelity factor in both configurations i.e., face to face and side by side are 0.938 and 0.941 respectively which is well above the acceptable value of 0.80 in UWB systems.

Finally, group delay parameter which measures the amount of distortion produced in the signal radiated from the antenna at a distance is presented in Fig. 5.12. It can be observed from Fig. 5.12 that the group delay is flat throughout the UWB range except at frequencies in the two notched band. Hence, it can be concluded that very low distortion is produced between the transmitting and receiving antenna for the passband.

5.6. Measured Results

The fabricated prototype and its measurement setup are shown in Fig. 5.13. The measurement of the S_{11} was performed on the Microwave network analyzer (N5247A PNA-X) with a range of 10 MHz to 67 GHz. Similarly, to measure the gain and radiation pattern the antenna was placed in an anechoic chamber. As illustrated in Fig 5.14 and Fig. 5.15 the overall simulated and measured results for S_{11} and gain show

very good agreement with each other. The variations in the notch bands, as well as the lower and higher frequency, could be due to the fabrication, connector, and cable losses.

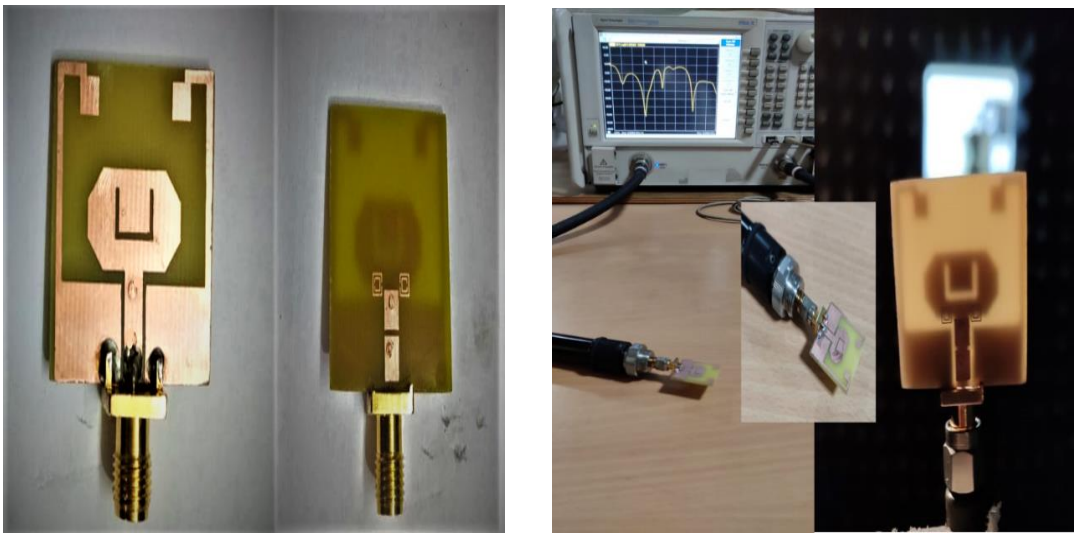

(a) (b)

Fig. 5.13 Antenna fabrication and measurement (a) Fabricated prototype of the antenna (b) Measurement setup of the proposed antenna

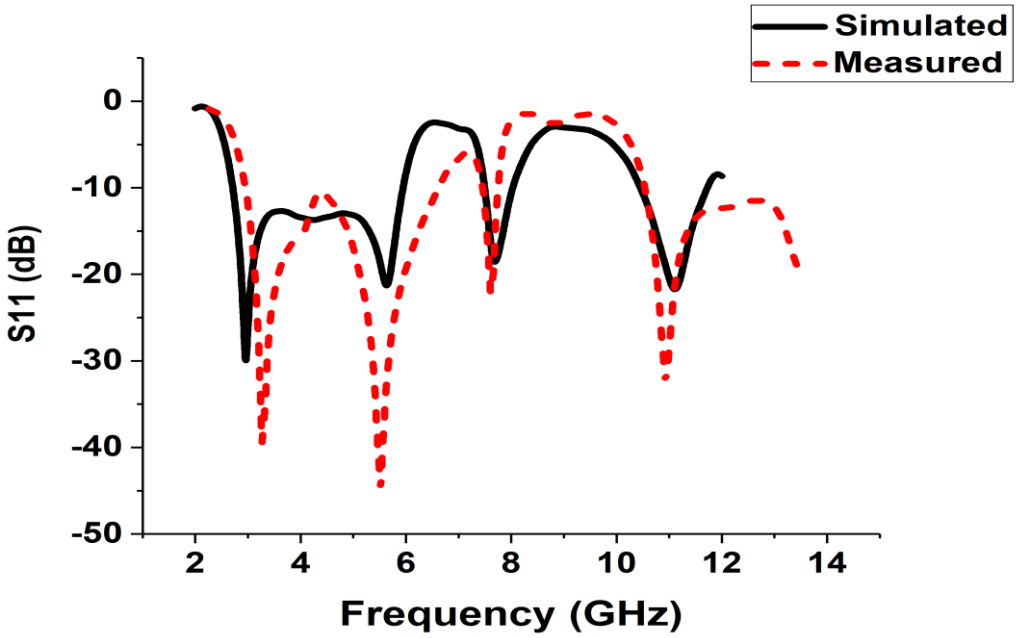

Fig. 5.14 Simulated and measured S_{11} of the antenna

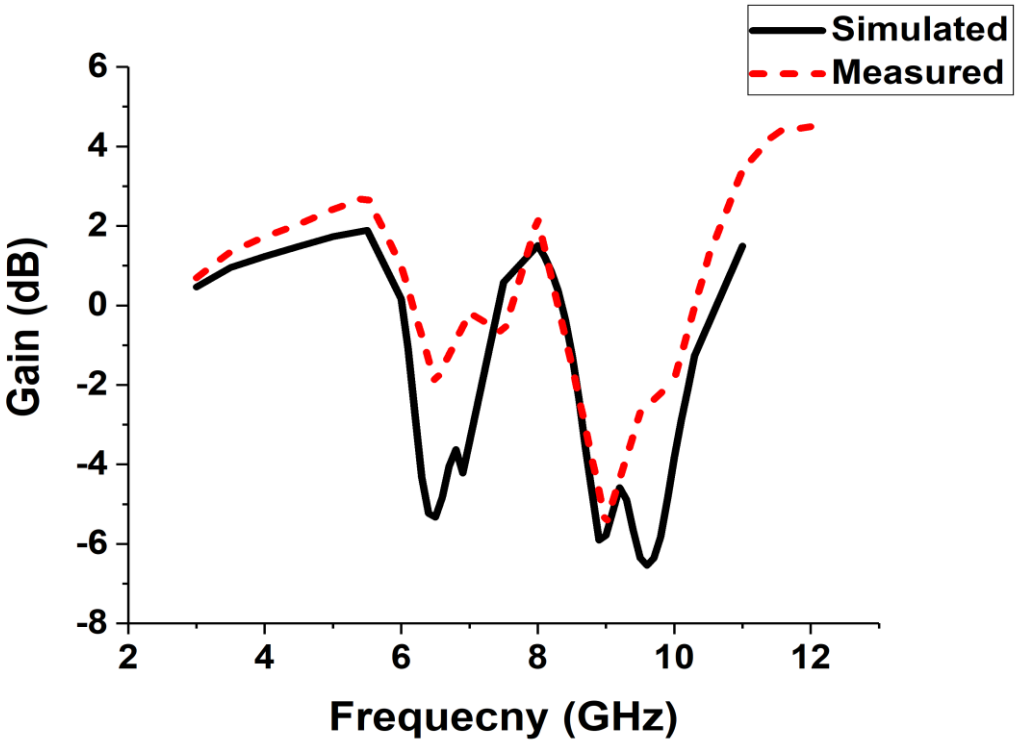

Fig. 5.15 Simulated and measured gain of the antenna

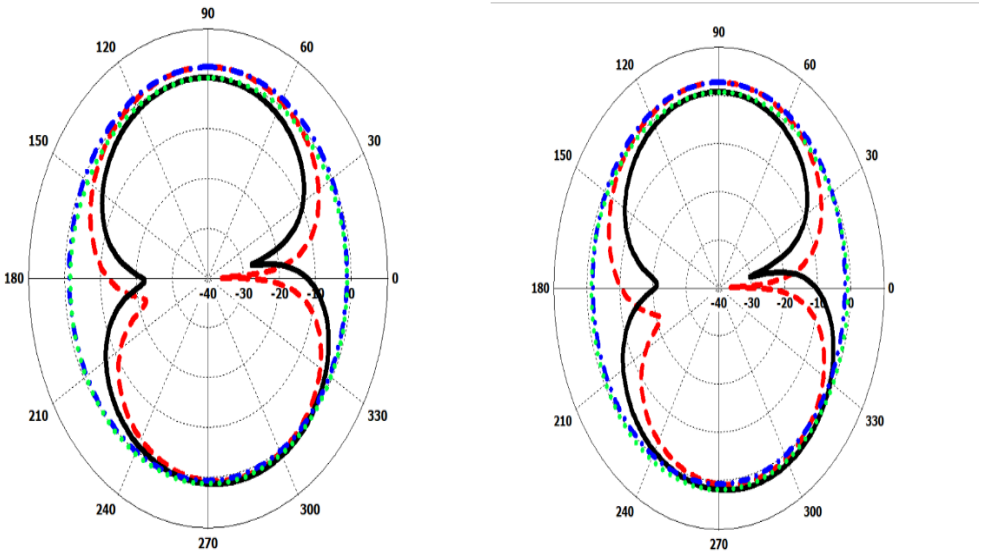

(a) (b)

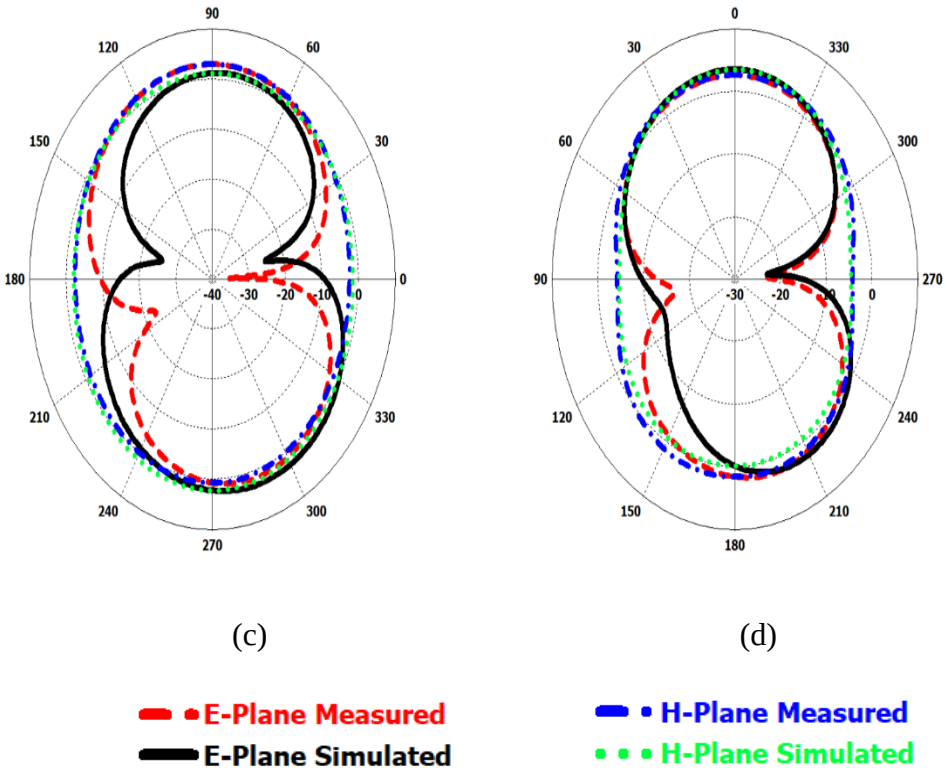

Fig. 5.16 Radiation pattern of the proposed antenna at (a) 3.48 GHz (b) 5.62 GHz (c) 7.68 GHz (d) 10.5 GHz

Finally, the simulated and measured radiation pattern is presented in Fig. 5.16. it can be observed that the radiation pattern is omnidirectional in H-plane and bi-directional in E-plane. This solves the purpose of the UWB operation of the antenna.

5.7 Summary

A planar CPW fed beveled patch antenna with dual rectangular notch band characteristics is presented in this chapter. Also, the importance of achieving higher-order notch has been discussed. The proposed antenna provides good radiation characteristics as well as stable gain throughout the UWB range except for the two rectangular notches where it decreases to negative values. The time-domain performance is as per the requirements of UWB systems and other simulated as well as measured results also show good agreement with each other. All this makes the proposed antenna a good candidate for UWB systems.

Chapter 6
Conclusions and Future Scope

In this chapter, the conclusions of the thesis work based on the study carried out in the field of planar UWB antenna design with band notch characteristics have been presented. The prime objective of the study was to evaluate the performance of these antennas and identify the existing research gaps. On the basis of these gaps, new UWB antennas designs with band notch characteristics have been presented in this work.

6.1 Conclusions

In Chapter 1, a brief introduction to UWB systems and the various guidelines imposed by FCC on these systems have been presented. The applications and advantages of these systems have been also discussed. Further, this chapter also gives the importance of UWB antennas is the aforementioned systems. The need for band notch characteristics in these antennas. Based on this, an exhaustive literature survey of the various techniques employed by the researchers to achieve band notch characteristics in planar UWB antennas has been presented in Chapter 2.

In Chapter 3, the techniques studied in literature have been analyzed and simulated on planar antennas to achieve UWB and band notch operation. Also, the fabrication and testing of these simulated designs have been carried out to validate the simulated results.

A new planar UWB antenna with band notch characteristics based on the complete UWB system requirements have been presented in Chapter 4. This design has been thoroughly analyzed in the time domain to fulfill the time domain requirements of UWB systems. Further, the excitation signal of the designed antenna has been chosen based on FCC indoor mask for UWB systems. The notch band in this antenna has been highly optimized without affecting the other essential characteristics of UWB antennas. Lastly, Chapter 5 gives a novel planar UWB antenna with dual rectangular notch band characteristics. In this design, two higher-order notches have been realized. The filter

synthesis of these notches has been carried out to compare the rectangular and spiculate notch band. Moreover, other simulated as well as measured results have been presented to validate the design for UWB systems.

The main contributions of this thesis work are summarized as:

- Comparative analysis of UWB antennas with band notch characteristics
- Design and fabrication of a planar UWB antenna with band notch characteristics based on complete UWB system requirements
- Design and fabrication of planar UWB antenna with rectangular notch band characteristics
- Performance validation of the proposed work with the existing state of the art

6.2 Future Works

The proposed work is focused on the design and fabrication of planar UWB antennas with band notch characteristics. The work has been carried out extensively based on the research gaps identified in the literature. However, there are a few dimensions of this work that need to be touched in the future. Hence, here are a few issues that can be addressed in future work:

- Design and development of UWB MIMO antennas with optimized band notch characteristics
- Design and performance evaluation of UWB MIMO antennas with rectangular notch band characteristics
- Performance Evaluation UWB antennas in Future Wireless Applications

List of Publications

Journal

[1] G. Kumar and R. Kumar, "A Survey on Planar Ultra-Wideband Antennas with Band notch Characteristics : Principle , Design , and Applications," *AEU - Int. J. Electron. Commun.*, vol. 109, pp. 76–98, 2019.

[2] G. Kumar, R. Kumar, D. Singh, and M. Singh, "A Miniaturized and Circularly Polarized L-Shaped Slot Antenna for Ultra-wideband Applications," *Int. J. Recent Technol. Eng.*, vol. 8, no. 4, 2019.

[3] G. Kumar, D. Singh, and R. Kumar, "Design and synthesis of planar UWB antenna with an accurate WLAN notch band optimization,"*Journal of Communications Technology and Electronics* ***(Communicated)***

[4] G. Kumar, D. Singh, and R. Kumar, "A planar CPW fed UWB antenna with dual rectangular notch band characteristics incorporating U- slot, SRRs, and EBGs," *AEU - International Journal of Electronics and Communications* ***(Communicated)***

International Conference

[1] G. Kumar and R. Kumar, "Design and analysis of CPW fed planar antenna for ultra-wideband applications," in *Proceedings - 2nd International Conference on Intelligent Circuits and Systems, ICICS 2018*, 2018.

[2] G. Kumar, D. Singh, and R Kumar, "A circular monopole Ultra-wideband antenna with a notch band at 5.8 GHz," in *Proceedings – 3rd International Conference on Intelligent Circuits and Systems, ICICS 2020*, 2020. ***(Accepted)***

Bibliography

[1] J. Zhang, P. V. Orlik, Z. Sahinoglu, A. F. Molisch, and P. Kinney, "UWB Systems for Wireless Sensor Networks," *Proc. IEEE*, vol. 97, no. 2, pp. 313–331, 2009.

[2] M. Bettayeb and S. F. A. Shah, "State of the art ultra-wideband technology for communication systems: a review," in *10th IEEE International Conference on Electronics, Circuits, and Systems, ICECS*, 2003, pp. 1276–1279.

[3] T. K. K. Tsang and M. N. El-gamal, "Ultra-wideband (UWB) communication systems: An overview," in *the 3rd International IEEE-NEWCAS Conference*, 2005, pp. 381–386.

[4] J. R. Fernandes and D. Wentzloff, "Recent Advances in IR-UWB Transceivers: An Overview," in *Proceedings of IEEE International Symposium on Circuits and Systems*, 2010, pp. 3284–3287.

[5] P. Taylor, S. Jiang, M. J. Skibniewski, Y. Yuan, and C. Sun, "Ultra-Wide Band Applications in Industry: A Critical Review," *J. Civ. Eng. Manag.*, vol. 17, no. 3, pp. 37–41, 2011.

[6] Y. Rahayu, T. A. Rahman, R. Ngah, and P. S. Hall, "Ultra-Wideband Technology and its Applications," in *5th IFIP International Conference on Wireless and Optical Communications Networks (WOCN)*, 2008, pp. 1–5.

[7] B. Levitas, "UWB time-domain measurements," in *The Second European Conference on Antennas and Propagation, EuCAP*, 2007, pp. 1–8.

[8] B. Allen *et al.*, "Ultra-Wideband: Applications, Technology and Future perspectives," in *International workshop on convergent technologies (IWCT)*, 2005, pp. 1–6.

[9] H. Sheng, P. Orlik, A. M. Haimovich, L. J. Cimini, and J. Zhang, "On the Spectral and Power Requirements for Ultra-Wideband Transmission," in *IEEE International Conference on Communications*, 2003, pp. 738–742.

[10] M. Di Benedetto and B. R. Vojcic, "Ultra-Wide Band Wireless Communications: A Tutorial," *J. Commun. networks*, vol. 5, no. 4, pp. 290–302, 2003.

[11] M. Kotzev, M. Kreitlow, and F. Gronwald, “Design and analysis of ultra-wideband antennas for transient field excitations,” *Adv. Radio Sci.*, vol. 14, pp. 25–29, 2016.

[12] M. Mighani and M. Akbari, “New UWB Monopole Planer Antenna with Dual Band Notched,” *Prog. Electromagn. Res. C*, vol. 52, pp. 153–162, July 2014.

[13] H. Oraizi and N. V. Shahmirzadi, “Frequency- and time-domain analysis of a novel UWB reconfigurable microstrip slot antenna with switchable notched bands,” *IET Microwaves, Antennas Propag.*, vol. 11, no. 8, pp. 1127–1132, 2017.

[14] G. R. Aiello and G. D. Rogerson, “Ultra-Wideband Wireless Systems,” *IEEE Microw. Mag.*, vol. 4, no. 2, pp. 36–47, 2003.

[15] T. S. P. See and Z. N. Chen, “A Small UWB Antenna for Wireless USB,” in *IEEE International Conference on Ultra-Wideband*, 2007, pp. 198–203.

[16] T. S. P. See and Z. N. Chen, “Experimental Characterization of UWB Antennas for On-Body Communications,” *IEEE Trans. Antennas Propag.*, vol. 57, no. 4, pp. 866–874, 2009.

[17] P. Cao, Y. Huang, and J. Zhang, “A UWB monopole antenna for GPR application,” in *Proceedings of 6th European Conference on Antennas and Propagation*, 2012, pp. 2837–2840.

[18] A. Afyf and L. Bellarbi, “A novel miniaturized UWB antenna for microwave imaging,” in *International Conference on Multimedia Computing and Systems*, 2014, pp. 1475–1478.

[19] Vivek Kumar and B. Gupta, “On-body measurements of SS-UWB patch antenna for WBAN applications,” *Int. J. Electron. Commun.*, vol. 70, no. 5, pp. 668–675, 2016.

[20] N. Behdad and K. Sarabandi, “A compact antenna for ultrawide-band applications,” *IEEE Trans. Antennas Propag.*, vol. 53, no. 7, pp. 2185–2192, 2005.

[21] N. Fortino, J. Y. Dauvignac, G. Kossiavas, and R. Staraj, “Design optimization of UWB printed antenna for omnidirectional pulse radiation,” *IEEE Trans. Antennas Propag.*, vol. 56, no. 7, pp. 1875–1881, 2008.

[22] W. K. Toh, Z. N. Chen, and X. Qing, “A Planar UWB Antenna with a Broadband Feeding Structure,” IEEE Trans. Antennas Propag., vol. 57, no. 7, pp. 2172–2175, 2009.

[23] T. Dissanayake, M. R. Yuce, and C. Ho, “Design and Evaluation of a Compact Antenna for Implant-to-Air UWB Communication,” *IEEE Antennas Wirel. Propag. Lett.*, vol. 8, pp. 153–156, 2009.

[24] W. K. Toh, Z. N. Chen, X. Qing, and T. S. P. See, “A planar UWB diversity antenna,” *IEEE Trans. Antennas Propag.*, vol. 57, no. 11, pp. 3467–3473, 2009.

[25] P. S. Bakariya, S. Dwari, and M. Sarkar, “Triple band notch UWB printed monopole antenna with enhanced bandwidth,” *AEU - Int. J. Electron. Commun.*, vol. 69, no. 1, pp. 26–30, 2014.

[26] M. D. Ardakani, J. Pourahmadazar, and S. O. Tatu, “A monopole antenna with notch-frequency function for UWB application,” in *32nd General Assembly and Scientific Symposium of the International Union of Radio Science, URSI GASS*, Aug. 2017, pp. 1–4

[27] S. B. T. Wang, A. M. Niknejad, and R. W. Brodersen, “Circuit Modeling Methodology for UWB Omnidirectional Small Antennas,” *IEEE J. Sel. areas Commun.*, vol. 24, no. 4, pp. 871–877, 2006.

[28] Q. Chu and Y. Yang, “A Compact Ultrawideband Antenna With 3.4/5.5 GHz Dual Band-Notched Characteristics,” *IEEE Trans. Antennas Propag.*, vol. 56, no. 12, pp. 3637–3644, 2008.

[29] Y. Wang and J. Z. Li, “An equivalent circuit modelling method for ultra-wideband antennas,” Prog. Electromagn. Res., vol. 82, pp. 433–445, 2008.

[30] T. G. Ma and S. J. Wu, “Ultrawideband band-notched folded strip monopole antenna,” *IEEE Trans. Antennas Propag.*, vol. 55, no. 9, pp. 2473–2479, 2007.

[31] F. Zhu *et al.*, “Multiple band-notched UWB antenna with band-rejected elements integrated in the feed line,” *IEEE Trans. Antennas Propag.*, vol. 61, no. 8, pp. 3952–3960, 2013.

[32] E. S. Jang, C. Y. Kim, D. G. Yang, and S. S. Hong, “Suppressed band characteristics of an UWB conical monopole antenna with split loops based on the equivalent circuit,” *Int. J. Antennas Propag.*, vol. 2017, 2017.

[33] A. Yadav, D. Sethi, and R. K. Khanna, “Slot loaded UWB antenna: Dual band notched characteristics,” *AEU - Int. J. Electron. Commun.*, vol. 70, no. 3, pp. 331–335, 2016.

[34] X. Qu, S.-S. Zhong, and W. Wang, “Study of the band-notch function for UWB circular disc monopole antenna,” *Microw. Opt. Technol. Lett.*, vol. 48, no. 1, pp. 1667–1670, 2006.

[35] Y. Li, W. Li, and Q. Ye, “A CPW-Fed Circular Wide-Sot UWB Antenna with Dual-Notch Bands by Combining Slot and Parasitic Element Techniques,” *Microw. Opt. Technol. Lett.*, vol. 56, no. 5, pp. 4130–4136, 2013.

[36] A. Vasylchenko, W. De Raedt, and G. A. E. Vandenbosch, “Design and Parametric Analysis of a Very Compact UWB Antenna with Band Rejection Feature,” in *Proceedings of IWAT, Chiba, Japan*, 2008, pp. 8–11.

[37] J. R. Panda and R. S. Kshetrimayum, “A Compact CPW-Fed Hexagonal 5 GHz/6 GHz Band-Notched Antenna with a U-Shaped Slot for Ultrawideband Communication Systems,” in *International Conference on Signal Processing and Communications*, 2010.

[38] J. Xu, D. Y. Shen, G. T. Wang, X. H. Zhang, X. P. Zhang, and K. Wu, “A small UWB antenna with dual band-notched characteristics,” *Int. J. Antennas Propag.*, vol. 2012, pp. 1–8, 2012.

[39] Shivnarayan and B. R.Vishvakarma, “Analysis of slot loaded microstrip patch antenna,” in *IEEE Antennas and Propagation Society Symposium*, 2004, pp. 2420–2423.

[40] T.-G. Ma and C.-H. Tseng, “An Ultrawideband Coplanar Waveguide-Fed Tapered Ring Slot Antenna,” IEEE Trans. Antennas Propag., vol. 54, no. 4, pp. 1105–1110, 2006.

[41] T. Li, C. Zhu, X. Cao, and J. Gao, “Bandwidth enhancement of compact monopole antenna with triple band rejections,” *Electron. Lett.*, vol. 52, no. 1, pp. 8–10, 2016.

[42] F. E. Mahmood, H. M. AlSabbagh, and R. Edwards, “CPW-Fed UWB Antenna with Band-Notch by Hexagonal Shape Slot,” in *International Conference on Future Communication Networks*, 2012, pp. 69–71.

[43] S. Das, D. Mitra, and S. R. B. Chaudhuri, “Design of UWB Planar Monopole Antennas with Etched Spiral Slot on the Patch for Multiple Band-Notched Characteristics,” *Int. J. Microw. Sci. Technol.*, vol. 2015, 2015.

[44] H. T. Chattha, M. K. Ishfaq, Y. Saleem, Y. Huang, and S. J. Boyes, “Band-notched ultrawide band planar inverted-F antenna,” *Int. J. Antennas Propag.*, vol. 2012, 2012.

[45] S. Rong-hua, X. Xu, J. Dong, and Q. Luo, “Design and Analysis of a novel Dual Band-notched UWB Antenna,” *Int. J. Antennas Propag.*, vol. 2014, 2014.

[46] C. Sim, W. Chung, and C. Lee, “An octagonal UWB monopole antenna with 5GHz band-notch function,” *Microw. Opt. Technol. Lett.*, vol. 51, no. 1, pp. 74–78, 2009.

[47] G. Srivastava, S. Dwar, and B. K. Kanaujia, “A compact triple band notch circular ring antenna for UWB applications,” *Microw. Opt. Technol. Lett.*, vol. 57, no. 1, pp. 668–672, 2015.

[48] J.-F. Li, D.-L. Wu, and Y.-J. Wu, “Dual Band-notched UWB MIMO Antenna with Uniform Rejection Performance,” *Prog. Electromagn. Res.*, vol. 54, pp. 103–111, 2017.

[49] X. Chen, F. Xu, and X. Tan, “Design of a Compact UWB Antenna with Triple Notched Bands Using Nonuniform Width Slots,” *J. Sensors*, vol. 2017, pp. 1–10, 2017.

[50] M. Hayouni, F. Choubani, T. H. Vuong, and J. David, “Main Effects Ensured by Symmetric Circular Slots Etched on the Radiating Patch of a Compact Monopole Antenna on the Impedance Bandwidth and Radiation Patterns,” *Wirel. Pers. Commun.*, vol. 95, no. 4, pp. 4243–4256, 2017.

[51] G. Liu, Y. Liu, and S. Gong, “Compact uniplanar UWB MIMO antenna with band-notched characteristic,” *Microw. Opt. Technol. Lett.*, vol. 59, no. 9, pp. 2207–2212, 2017.

[52] A. Syed and R. W. Aldhaheri, “A Very Compact and Low Profile UWB Planar Antenna with WLAN Band Rejection,” *Sci. World J.*, vol. 2016, 2016.

[53] R. Azim, M. Tariqul Islam, N. Misran, B. Yatim, and H. Arshad, “Design and realization of a planar ultrawideband antenna with notch band at 3.5 GHz,” *Sci. World Journal Scientific World J.*, vol. 2014, 2014.

[54] T. Li, C. Zhu, X. Cao, and J. Gao, “Bandwidth enhancement of compact monopole antenna with triple band rejections,” *Electron. Lett.*, vol. 52, no. 1, pp. 8–10, 2016.

[55] X. Li, L. Yan, W. Pan, and B. Luo, “A compact printed quadruple band-notched UWB antenna,” *Int. J. Antennas Propag.*, vol. 2013, 2013.

[56] Y. S. Li, X. D. Yang, C. Y. Liu, and T. Jiang, “Compact CPW-fed ultra-wideband antenna with dual band-notched characteristics,” *Microw. Opt. Technol. Lett.*, vol. 46, no. 14, pp. 967–968, 2010.

[57] Y. S. Li, X. D. Yang, Q. Yang, and C. Y. Liu, “Compact coplanar waveguide fed ultra-wideband antenna with a notch band characteristic,” *AEU - Int. J. Electron. Commun.*, vol. 65, no. 11, pp. 961–966, 2011.

[58] D. H. Werner and S. Gangul, “An Overview of Fractal Antenna Engineering Research,” *IEEE Antennas Propag. Mag.*, vol. 45, no. I, pp. 38–57, 2003.

[59] W. J. Lui, C. H. Cheng, and H. B. Zhu, “Compact frequency notched ultra-wideband fractal printed slot antenna,” *IEEE Microw. Wirel. Components Lett.*, vol. 16, no. 4, pp. 224–226, 2006.

[60] S. Tripathi, A. Mohan, and S. Yadav, “A Compact Koch Fractal UWB MIMO Antenna with WLAN Band-Rejection,” *IEEE Antennas Wirel. Propag. Lett.*, vol. 14, pp. 1565–1568, 2015.

[61] F. B. Zarrabi, Z. Mansouri, N. P. Gandji, and H. Kuhestani, “Triple-notch UWB monopole antenna with fractal Koch and T-shaped stub,” *AEU - Int. J. Electron. Commun.*, vol. 70, no. 1, pp. 64–69, 2016.

[62] R. Ghatak, A. Karmakar, and D. R. Poddar, “A circular shaped sierpinski carpet fractal UWB monopole antenna with band rejection capability,” *Prog. Electromagn. Res. C*, vol. 24, pp. 221–234, Aug. 2011.

[63] R. Ghatak, A. Karmakar, and D. R. Poddar, “Hexagonal boundary Sierpinski carpet fractal shaped compact ultrawideband antenna with band rejection functionality,” *AEU - Int. J. Electron. Commun.*, vol. 67, no. 3, pp. 250–255, 2013.

[64] Y. K. Choukiker and S. K. Behera, “Modified Sierpinski square fractal antenna covering ultra-wide band application with band notch characteristics,” *IET Microwaves, Antennas Propag.*, vol. 8, no. 7, pp. 506–512, 2013.

[65] M. Sahoo and S. Sahu, “Design and development of UWB notch antenna with fractal geometry,” in *International Conference on Circuit, Power and Computing Technologies,* 2015.

[66] S. Rajkumar, K. T. Selvan, and P. H. Rao, “Compact 4 element Sierpinski Knopp fractal UWB MIMO antenna with dual band notch,” *Microw. Opt. Technol. Lett.,* vol. 60, no. 4, pp. 1023–1030, 2018

[67] A. Karmakar, S. Verma, M. Pal, and R. Ghatak, “An ultra-wideband monopole antenna with multiple fractal slots with dual band rejection characteristics,” *Prog. Electromagn. Res. C,* vol. 31, pp. 185–197, May 2012.

[68] J. Banerjee, A. Karmakar, and R.Ghatak, “An Ultra-Wideband Monopole Antenna using Fractal Shaped Parasitic Resonator for Band Notching Characteristics,” in *International Conference on Microwave and Photonics,* 2015, pp. 2–3.

[69] M. Naghshvarian Jahromi, A. Falahati, and R. M. Edwards, “Application of fractal binary tree slot to design and construct a dual band-notch CPW-ground-fed ultra-wide band antenna,” *IET Microwaves, Antennas Propag.,* vol. 5, no. 12, pp. 1424–1430, 2011.

[70] M. Smierzchalski, P. Kurgan, and M. Kitlinski, “Improved selectivity compact band-stop filter with Gosper Fractal-Shaped Defected Ground Structures,” *Microw. Opt. Technol. Lett.,* vol. 52, no. 1, 2010.

[71] Y. S. Li, X. D. Yang, C. Y. Liu, and T. Jiang, “Analysis and investigation of a cantor set fractal UWB antenna with notch-band characteristic,”*Prog. Electromagn. Res. B,* vol. 33, pp. 99–114, Mar. 2011.

[72] Y. Li, X. Yang, C. Liu, and T. Jiang, “Miniaturization cantor fractal ultrawideband antenna with a notch band characteristic,” *Microw. Opt. Technol. Lett.,* vol. 54, no. 5, 2012.

[73] R. Ghatak, B. Biswas, A. Karmakar, and D. R. Poddar, “A Circular Fractal UWB Antenna Based on descartes circle theorem with band rejection capability,” *Prog. Electromagn. Res. C,* vol. 37, pp. 235–248, Jan. 2013.

[74] M. Naser-Moghadasi, R. A. Sadeghzadeh, T. Sedghi, T. Aribi, and B. S. Virdee, “UWB CPW-Fed Fractal Patch Antenna with Band-Notched Function

Employing Folded T-Shaped Element," *IEEE Antennas Wirel. Propag. Lett.,* vol. 12, pp. 504–507, 2013.

[75] B. Biswas, R. Ghatak, A. Karmakar, and D. R. Poddar, "Dual Band Notched UWB Monopole Antenna Using Embedded Omega Slot and Fractal Shaped Ground Plane," *Prog. Electromagn. Res. C*, vol. 53, pp. 177–186, Sept. 2014.

[76] A. Gorai, C. Goswami, M. Pal, and R. Ghatak, "A Planar Elliptical Shaped UWB Antenna with Triple Band Notch Characteristics using Hybrid Fractal Slots," in *IEEE Applied Electromagnetics Conference (AEMC),* 2013.

[77] Y. Song, Y. C. Jiao, T. L. Zhang, J. B. Jiang, X. Zhang, and F. S. Zhang, "Frequency notched UWB slot antenna with a fractal-shaped slot," *J. Electromagn. Waves Appl.,* vol. 23, no. 2–3, pp. 321–327, 2009.

[78] R. W. Ziolkowski, P. Jin, and C. C. Lin, "Metamaterial-inspired engineering of antennas," *Proc. IEEE,* vol. 99, no. 10, pp. 1720–1731, 2011.

[79] J. D. Baena et al., "Equivalent-circuit models for split-ring resonators and complementary split-ring resonators coupled to planar transmission lines," *IEEE Trans. Microw. Theory Tech.,* vol. 53, no. 4, pp. 1451–1460, 2005.

[80] Y. Zhang, W. Hong, C. Yu, Z. Q. Kuai, Y. D. Don, and J. Y. Zhou, "Planar ultrawideband antennas with multiple notched bands based on etched slots on the patch and/or split ring resonators on the feed line," *IEEE Trans. Antennas Propag.,* vol. 56, no. 9, pp. 3063–3068, 2008.

[81] N. M. Awad and M. K. Abdelazeez, "Bluetooth/UWB circular patch antenna with dual band notches," in *IEEE Jordan Conference on Applied Electrical Engineering and Computing Technologies (AEECT),* 2013, pp. 8–11.

[82] M. G. Wahab, W. Swelam, and M. Abdeazeem, "Novel Miniaturized UWB Antenna with Triple Band-notched Characteristics Utilizing SRR and Folded U-shaped Slot," in *Progress in Electromagnetics Research Symposium — Spring (PIERS), St Petersburg, Russia,* 2017.

[83] S. Kundu and S. K. Jana, "Leaf-shaped CPW-fed UWB antenna with triple notch bands for ground penetrating radar applications," *Microw. Opt. Technol. Lett.,* vol. 60, no. 4, pp. 930–936, 2018.

[84] G. Mishra and S. Sahu, "Nature Inspired tree shaped antenna with dual band notch for UWB applications," *Microw. Opt. Technol. Lett.,* vol. 58, no. 7, 2016.

[85] G. Mishra and S. Sahu, “Modified Octahedron Shaped Antenna with Parasitic Loading Plane Having Dual Band Notch Characteristics for UWB Applications,” *Int. J. RF Microw. Comput. Eng.*, vol. 26, no. 5, pp. 210–224, 2016.

[86] B. Yan, D. Jiang, R. Xu, and Y. Xu, “A UWB band-pass antenna with triple-notched band using common direction rectangular complementary split-ring resonators,” *Int. J. Antennas Propag.*, vol. 2013, 2013.

[87] M. M. Islam, M. R. I. Faruque, and M. T. Islam, “A compact 5.5 GHz band-rejected UWB antenna using complementary split ring resonators,” *Sci. J.*, vol. 2014, 2014.

[88] W. Liu and T. Jiang, “Design and Analysis of a Tri-band Notch UWB Monopole Antenna,” *Progress in Electromagnetics Research Symposium*, Shanghai, China, 2016, pp. 2039–2041.

[89] M. E. J. M. K. A. Rahim and N. A. S. R. Dewan, “Flexible ultra-wideband antenna incorporated with metamaterial structures: multiple notches for chipless RFID application,” *Appl. Phys. A*, pp. 3–7, 2017.

[90] K. Kumar and N. Gunasekaran, “A compact multiband notch UWB antenna,” *Int. J. Antennas Propag.*, vol. 2012, 2012.

[91] Y. Li, W. Li, and Q. Ye2, “A compact UWB antenna with dual band-notch characteristics using nested split ring resonator and stepped impedance resonator,” *Microw. Opt. Technol. Lett.*, vol. 55, no. 12, pp. 4130–4136, 2013.

[92] Y. Li, W. L, and W. Yu, “A CPW-Fed circular slot UWB antenna with WLAN Band and X-Band Filtering Characteristics using Hybrid Resonators,” *Microw. Opt. Technol. Lett.*, vol. 56, no. 4, 2014.

[93] J. Zhang, P. Cao, Y. Huang, R. Alrawashdeh, and X. Zhu, “Compact planar ultra-wideband antenna with quintuple band-notched characteristics,” *IET Microwaves, Antennas Propag.*, vol. 9, no. 3, pp. 206–216, 2015.

[94] Q. Li, J. Fang, J. Wang, and Z. Li, “Compact Printed Ultra-Wide Band Antenna with Notched Band Employing GSRR,” in *IEEE International Conference on Microwave and Millimeter Wave Technology*, 2016.

[95] R. Cicchetti, E. Miozzi, and O. Testa, “Wideband and UWB antennas for wireless applications: A comprehensive review,” *Int. J. Antennas Propag.,* vol. 2017, 2017.

[96] T. Arshed and F. A. Tahir, “A miniaturized triple band-notched UWB antenna,” *Microw. Opt. Technol. Lett.,* vol. 59, no. 10, pp. 2581–2586, 2017.

[97] D. Yadav, M. P. Abegaonkar, S. K. Koul, V. Tiwari, and D. Bhatnagar, “A compact dual band-notched UWB circular monopole antenna with parasitic resonators,” *AEU - Int. J. Electron. Commun.,* vol. 84, pp. 313–320, 2018.

[98] M. Alibakhshi Kenari, “Design and modeling of new UWB metamaterial planar cavity antennas with shrinking of the physical size for modern transceivers,” *Int. J. Antennas Propag.,* vol. 2013, 2013.

[99] M. Alibakhshi-Kenari and M. Naser-Moghadasi, “Novel UWB miniaturized integrated antenna based on CRLH metamaterial transmission lines,” *AEU - Int. J. Electron. Commun.,* vol. 69, no. 8, pp. 1143–1149, 2015.

[100] M. Alibakhshi-Kenari, M. Naser-Moghadasi, R. Ali Sadeghzadeh, B. Singh Virdee, and E. Limiti, “New Compact antenna based on simplified CRLH-TL for UWB wireless communication systems,” *Int. J. RF Microw. Comput. Eng.,* vol. 26, no. 3, pp. 217–225, 2016.

[101] Y. Li, W. Li, and W. Yu, “A Multi-Band / UWB MIMO / Diversity Antenna with an Enhanced Isolation Using Radial Stub Loaded Resonator,” *ACES J.,* vol. 28, no. 1, pp. 8–20, 2013.

[102] F. Wang, Z. Duan, S. Li, Z. Wang, and Y. Gong, “Compact UWB MIMO antenna with metamaterial-inspired isolator,” *Prog. Electromagn. Res. C,* vol. 84, pp. 61–74, Apr. 2018.

[103] H. X. Xu et al., “Analysis and design of two-dimensional resonant-type composite right/left-handed transmission lines with compact gain-enhanced resonant antennas,” *IEEE Trans. Antennas Propag.,* vol. 61, no. 2, pp. 735–747, 2013.

[104] H. X. Xu, G. M. Wang, J. G. Liang, M. Q. Qi, and X. Gao, “Compact circularly polarized antennas combining meta-surfaces and strong space-filling meta-resonators,” *IEEE Trans. Antennas Propag.,* vol. 61, no. 7, pp. 3442–3450, 2013.

[105] H. X. Xu, G. M. Wang, M. Q. Qi, and T. Cai, “Compact fractal left-handed structures for improved cross-polarization radiation pattern,” *IEEE Trans. Antennas Propag.*, vol. 62, no. 2, pp. 546–554, 2014.

[106] H. X. Xu, G. M. Wang, Z. Tao, and T. Cai, “An octave-bandwidth half Maxwell fish-eye lens antenna using three-dimensional gradient-index fractal metamaterials,” *IEEE Trans. Antennas Propag.*, vol. 62, no. 9, pp. 4823–4828, 2014.

[107] H. X. Xu et al., “Multifunctional microstrip array combining a linear polarizer and focusing metasurface,” *IEEE Trans. Antennas Propag.*, vol. 64, no. 8, pp. 3676–3682, 2016.

[108] S. Zhu, H. Liu, and P. Wen, “A new method for achieving miniaturization and gain enhancement of vivaldi antenna array based on anisotropic metasurface,” *IEEE Trans. Antennas Propag.*, vol. 67, no. 3, pp. 1952–1956, 2019.

[109] F. Yang and Y. Rahmat-Samii, “Microstrip Antennas Integrated with Electromagnetic Band-Gap (EBG) Structures: A Low Mutual Coupling Design for Array Applications,” *IEEE Trans. Antennas Propag.*, vol. 51, no. 10, pp. 2936–2946, 2003.

[110] M. Rahman and M. a. Stuchly, “Transmission line-periodic circuit representation of planar microwave photonic bandgap structures,” *Microw. Opt. Technol. Lett.*, vol. 30, no. 1, pp. 15–19, 2001.

[111] L. Peng and C. L. Ruan, “UWB band-notched monopole antenna design using electromagnetic-bandgap structures,” *IEEE Trans. Microw. Theory Tech.*, vol. 59, no. 4, pp. 1074–1081, 2011.

[112] M. Yazdi and N. Komjani, “Design of a band-notched UWB monopole antenna by means of an EBG structure,” *IEEE Antennas Wirel. Propag. Lett.*, vol. 10, pp. 170–173, 2011.

[113] N. K. Kiem, H. N. B. Phuong, and D. N. Chien, “Design of compact 4 × 4 UWB-MIMO antenna with WLAN band rejection,” *Int. J. Antennas Propag.*, vol. 2014, 2014.

[114] K. A. Alshamaileh, M. J. Almalkawi, and V. K. Devabhaktuni, “Dual Band-Notched Microstrip-Fed Vivaldi Antenna Utilizing Compact EBG Structures,” *Int. J. Antennas Propag.*, vol. 2015, 2015.

[115] L. I. N. Peng, B. Wen, X. Li, X. Jiang, and S. Li, “CPW Fed UWB Antenna by EBGs With Wide Rectangular Notched-Band,” *IEEE Access*, vol. 4, pp. 9545–9552, 2017.

[116] N. Jaglan, S. D. Gupta, B. K. Kanaujia, and S. Srivastava, “Band notched UWB circular monopole antenna with inductance enhanced modified mushroom EBG structures,” *Wirel. Networks*, vol. 24, no. 2, pp. 383–393, 2018.

[117] H. Liu and Z. Xu, “Design of UWB monopole antenna with dual notched bands using one modified electromagnetic-bandgap structure,” *Sci. World J.*, vol. 2013, 2013.

[118] F. Xu, Z. X. Wang, X. Chen, and X.-A. Wang, “Dual band-notched UWB antenna based on spiral electromagnetic-bandgap structure,” *Prog. Electromagn. Res. B*, vol. 39, pp. 393–409, 2012.

[119] W. Wu, B. Yuan, and A. Wu, “A Quad-Element UWB-MIMO Antenna with Band-Notch and Reduced Mutual Coupling Based on EBG Structures,” *Int. J. Antennas Propag.*, vol. 2018, 2018.

[120] T. Li, H.-Q. Zhai, G.-H. Li, and C.-H. Liang, “Design of compact UWB band-notched antenna by means of electromagnetic-bandgap structures,” *Electron. Lett.*, vol. 48, no. 11, pp. 608–609, 2012.

[121] R. L. Haupt and M. Lanagan, “Reconfigurable Antennas,” *IEEE Antennas Propag. Mag.*, vol. 55, no. 1, pp. 49–61, 2013.

[122] C. L. Goldsmith, Z. Yao, S. Eshelman, and D. Denniston, “Performance of Low-Loss RF MEMS Capacitive Switches,” *IEEE Microw. Guid. Wave Lett.*, vol. 8, no. 8, pp. 269–271, 1998.

[123] Y. Li, W. Li, and W. Yu, “A Switchable UWB Slot Antenna using SIS-HSIR and SIS-SIR for Multi-Mode Wireless Communications Applications” *ACES J.*, vol. 27, no. 4, pp. 1–4, 2012.

[124] Y. Li, W. Li, and Q. Ye2, “A Reconfigurable wide slot antenna integrated with SIRS for UWB/Multiband communication applications,” *Microw. Opt. Technol. Lett.*, vol. 55, no. 1, 2012.

[125] Y. Li, W. Li, and Q. Ye, “A CPW-fed circular wide-slot UWB antenna with wide tunable and flexible reconfigurable dual notch bands,” *Sci. World J.*, vol. 2013, 2013.

[126] Y. Li, W. Li, and Q. Ye, “A reconfigurable triple-notch-band antenna integrated with defected microstrip structure band-stop filter for ultra-wideband cognitive radio applications,” *Int. J. Antennas Propag.*, vol. 2013, 2013.

[127] A. Danideh and R. A. Sadeghzadeh, “Cpw-fed slot antenna for mimo system applications,” *Microw. Opt. Technol. Lett.*, vol. 6, no. 1, pp. 3872–3875, 2013.

[128] D. Thiripurasundari and D. S. Emmanuel, “CPW Fed Slot Antenna with Reconfigurable Rejection Bands for UWB Application,” *Radio electron. Commun. Syst.*, vol. 56, no. 6, pp. 278–284, 2013.

[129] S. Jacob, S. Nimisha, P. V Anila, and P. Mohanan, “UWB Antenna with Reconfigurable Band - Notched Characteristics using Ideal Switches,” in *IEEE International Microwave and RF Conference (IMARC)*, 2014, vol. 1, pp. 136–139.

[130] Y. Li, W. Li, and Q. Ye, “A compact circular slot UWB antenna with multimode reconfigurable band-notched characteristics using resonator and switch techniques,” *Microw. Opt. Technol. Lett.*, vol. 56, no. 3, pp. 570–574, 2014.

[131] B. Badamchi, A. Valizade Shahmirzadi, C. Ghobadi, and J. Nourinia, “Design of compact reconfigurable ultra-wideband slot antenna with switchable single/dual band notch functions,” *IET Microwaves, Antennas Propag.*, vol. 8, no. 8, pp. 541–548, 2014.

[132] S. Y. Shrivishal Tripathi, Akhilesh Mohan, “A compact fractal UWB antenna with reconfigurable band notch functions,” *Microw. Opt. Technol. Lett.*, vol. 58, no. 3, pp. 509–514, 2015.

[133] A. Toktas, “A compact reconfigurable printed antenna with band-notched characteristic,” *Microw. Opt. Technol. Lett.*, vol. 61, no. 1, pp. 245–250, 2018.

[134] Antonino-Daviu, E.Cabedo-Fabre´s, M.Ferrando-Bataller, and A.Vila-Jimenez, *“Active UWB antenna with tunable band-notched behaviour,”* Electron. Lett., vol. 43, no. 18, pp. 982–984, 2007.

[135] T. Li, \ Cheng Zhu, X. Cao, and J. Gao, “Compact UWB antenna with sharp tunable band notched chracteristics,” *Microw. Opt. Technol. Lett.*, vol. 58, no. 3, pp. 529–532, 2016.

[136] W. Wu, Y. B. Li, R. Y. Wu, C. B. Shi, and T. J. Cui, “Band-Notched UWB Antenna with Switchable and Tunable Performance,” *Int. J. Antennas Propag.*, vol. 2016, 2016.

[137] D. Draskovic, J. R. O. Fernandez, and C. Briso Rodríguez, “Planar ultrawideband antenna with photonically controlled notched bands,” *Int. J. Antennas Propag.*, vol. 2013, 2013.

[138] E. Varouti et al., “Properties of Aluminum-Substituted YIG with Applications in Tunable Notched UWB Antennas,” in *Loughborough Antennas and Propagation Conference (LAPC)*, Nov. 2014.

[139] M. Nejatijahromi, M. Naghshvarianjahromi, and M. Rahman, “Compact CPW Fed Switchable UWB Antenna as an Antenna Filter at Narrow-Frequency Bands,” *Prog. Electromagn. Res. C*, vol. 81, pp. 199–209, Feb. 2018.

[140] M. Nejatijahromi, M. U. Rahman, and M. Naghshvarianjahromi, “Continuously Tunable WiMAX Band-Notched UWB Antenna with Fixed WLAN Notched Band,” *Prog. Electromagn. Res. Lett.*, vol. 75, pp. 97–103, Jan. 2018.

[141] H. X. Xu et al., “Tunable microwave metasurfaces for high-performance operations: Dispersion compensation and dynamical switch,” *Sci. Rep.*, vol. 6, no. November, pp. 1–10, 2016.

[142] H. X. Xu et al., “Aberration-free and functionality-switchable meta-lenses based on tunable metasurfaces,” *Appl. Phys. Lett.*, vol. 109, no. 19, 2016.

[143] H.-X. Xu, G.-M. Wang, T. Cai, J. Xiao, and Y.-Q. Zhuang, “Tunable Pancharatnam–Berry metasurface for dynamical and high-efficiency anomalous reflection,” Opt. Express, vol. 24, no. 24, p. 27836, 2016.

[144] H. X. Xu et al., “Dynamical control on helicity of electromagnetic waves by tunable metasurfaces,” *Sci. Rep.*, vol. 6, pp. 1–10, Mar. 2016.

[145] A. Gupta, A. Kansal, and P. Chawla, “Design of a patch antenna with square ring- shaped-coupled ground for on- / off body communication,” *Int. J. Electron.*, vol. 106, no. 12, pp. 1814–1828, 2019.

[146] Q. X. Chu and Y. Y. Yang, “A compact ultrawideband antenna with 3.4/5.5 GHz dual band-notched characteristics,” *IEEE Trans. Antennas Propag.*, vol. 56, no. 12, pp. 3637–3644, 2008.

[147] V. N. K. R. Devana and A. M. Rao, “Compact UWB monopole antenna with quadruple band notched characteristics notched characteristics,” *Int. J. Electron.,* vol. 107, no. 2, pp. 175–196, 2020.

[148] G. Kumar and R. Kumar, “A Survey on Planar Ultra-Wideband Antennas with Band notch Characteristics: Principle, Design, and Applications,” *AEUE - Int. J. Electron. Commun.,* vol. 109, pp. 76–98, 2019.

[149] D. Ustun and A. Akdagli, “Design of Band-Notched UWB using a Hybrid optimization based on ABC and DE Algorithms,” AEUE - *Int. J. Electron. Commun.,* vol. 87, pp. 10–21, 2018.

[150] Y. Du, X. Wu, and J. Sidé, “Design of Sharp Roll-Off Band Notch with Fragment-Type Pattern Etched on UWB Antenna,” *IEEE Antennas Wirel. Propag. Lett.,* vol. 17, no. 12, pp. 2404–2408, 2018.

[151] S. Koziel, S. Member, and A. Bekasiewicz, “Fast Simulation-Driven Design Optimization of UWB Band-Notch Antennas,” *IEEE Antennas Wirel. Propag. Lett.,* vol. 15, pp. 926–929, 2016.

[152] H. Xu, W. Nie, and Y. Liu, “A Coplanar Waveguide Fed UWB Antenna using Embedded E-shaped Structure with WLAN,” *J. RF-Engineering Telecommun.,* vol. 72, no. 7–8, pp. 2–9, 2018.

[153] J.-B. Jiang, Z.-H. Yan, and C. Wang, “A novel compact UWB notch-filter antenna with a dual-Y-shaped slot,” *Prog. Electromagn. Res. Lett.,* vol. 14, pp. 165–170, 2010.

[154] J. Dong, Q. Li, and L. Deng, “Design of Fragment-Type Antenna Structure Using an Improved BPSO,” *IEEE Trans. Antennas Propag.,* vol. 66, no. 2, pp. 564–571, 2017.

[155] P. Taylor, J. Jiang, X. Zhang, Z. Yan, Y. Song, and W. Wu, “Band-Notched UWB Printed Antenna with an Inverted C-Slotted Ground,” *J. Electromagn. Waves Appl.,* vol. 22, no. 14–5, pp. 37–41, 2015.

[156] J. R. Kelly, P. S. Hall, P. Gardner, K. L. Wong, and P. Antennas, “Band-Notched UWB Antenna Incorporating a Microstrip Open-Loop Resonator,” *IEEE Trans. Antennas Propag.,* vol. 59, no. 8, pp. 3045–3048, 2011.

[157] W. Lui, C. Cheng, and H. Zhu, “Improved Frequency Notched Ultrawideband Slot Antenna Using Square Ring Resonator,” *IEEE Trans. Antennas Propag.,* vol. 55, no. 9, pp. 2445–2450, 2007.

[158] R. Hua and C. Chou, “Design of a Multi resonator Loaded Band-Rejected Ultrawideband Planar Monopole Antenna with Controllable Notched Bandwidth,” *IEEE Trans. Antennas Propag.,* vol. 56, pp. 2875–2883, 2008.

[159] E. Pancera, D. Modotto, A. Locatelli, F. M. Pigozzo, and C. De Angelis, “Novel Design of UWB Antenna with Band – Notch Capability,” in *10th European Conference on Wireless Technology,* Oct. 2007, pp. 48–50.

[160] Y. Li, W. Shao, L. You, and B. Wang, “An Improved PSO Algorithm and Its Application to UWB Antenna Design,” *IEEE Antennas Wirel. Propag. Lett.,* vol. 12, no. 3, pp. 1236–1239, 2013.

[161] S. Wu, C. Kang, K. Chen, and J. Tarng, “Study of an Ultrawideband Monopole Antenna with a Band-Notched Open-Looped Resonator,” *IEEE Trans. Antennas Propag.,* vol. 58, no. 6, pp. 1890–1897, 2010.

[162] Q. Chu, S. Member, C. Mao, and H. Zhu, “A Compact Notched Band UWB Slot Antenna with Sharp Selectivity and Controllable Bandwidth,” *IEEE Trans. Antennas Propag.,* vol. 61, no. 8, pp. 3961–3966, 2013.

[163] C. Hong, C. Ling, I. Tarn, and S. Chung, “Design of a Planar Ultrawideband Antenna with a New Band-Notch Structure,” *IEEE Trans. Antennas Propag.,* vol. 55, no. 12, pp. 3391–3397, 2007.

[164] F. Consoli and S. Barbarino, “UWB circular slot antenna with an inverted-L notch filter for the 5 GHz WLAN band,” *Prog. Electromagn. Res.,* vol. 104, no. March 2014, pp. 1–13, 2010.

[165] Y. D. Dong, W. Hong, Z. Q. Kuai, and J. X. Chen, “Analysis of Planar Ultrawideband Antennas with On-Ground Slot Band-Notched Structures,” *IEEE Trans. Antennas Propag.,* vol. 57, no. 7, pp. 1886–1893, 2009.

[166] Z. Tu, W. Li, and Q. Chu, “Single-Layer Differential CPW-Fed Notch-Band Tapered-Slot UWB Antenna,” *IEEE Antennas Wirel. Propag. Lett.,* vol. 13, pp. 1296–1299, 2014.

[167] A. Kaabal, M. El, S. Ahyoud, and A. Asselman, “Spectral and Time Domains Analysis of Pentagon UWB Antenna with WLAN Band-notched using

Electromagnetic Band-Gap Structures," in *International Conference on Wireless Networks and Mobile Communications (WINCOM)*, 2015.

[168] J. R. Panda and R. S. Kshetrimayum, "A Compact CPW-Fed Hexagonal 5 GHz / 6 GHz Band-Notched Antenna with a U-Shaped Slot for Ultrawideband Communication Systems," in *International Conference on Signal Processing and Communications (SPCOM)*, 2010, pp. 2–6.

[169] S. T. Abraha, S. Member, and C. Okonkwo, "Performance Evaluation of IR-UWB in Short-Range Fiber Communication Using Linear Combination of Monocycles," *J. Light. Technol.*, vol. 29, pp. 1143–1151, 2011.

[170] S. Henrique, I. Barboza, J. Alejandro, A. Palacio, E. Pontes, and S. T. Kofuji, "Fifth Derivative Gaussian Pulse Generator for UWB Breast Cancer Detection System," in *IEEE International Conference on Ultra-Wide Band (ICUWB)*, Sept. 2014

[171] M. Serhir, "Transient UWB Antenna Near-Field and Far-Field Assessment from Time Domain Planar Near-Field Characterization: Simulation and Measurement Investigations," *IEEE Trans. Antennas Propag.*, vol. 4868–487, no. 11, 2015.

[172] A. J. Kerkhoff and H. Ling, "Design of a Band-Notched Planar Monopole Antenna Using Genetic Algorithm Optimization," *IEEE Trans. Antennas Propag.*, vol. 55, no. 3, pp. 604–610, 2007.

[173] J. Y. Siddiqui, S. Member, C. Saha, Y. M. M. Antar, and L. Fellow, "Compact SRR Loaded UWB Circular Monopole Antenna with Frequency Notch Characteristics," *IEEE Trans. Antennas Propag.*, vol. 62, no. 8, pp. 4015–4020, 2014.

[174] P. P. Shome and T. Khan, "A state-of-art review on band-notch characteristics in UWB antennas," *RF Microw. Comput. Eng.*, vol. 29, no. 2, pp. 1–16, 2018.

[175] A. Sohail, K. S. Alimgeer, A. Iftikhar, B. Ijaz, K. W. Kim, and W. Mohyuddin, "Dual notch band UWB antenna with improved notch characteristics," *Microw. Opt. Technol. Lett.*, vol. 60, no. 4, pp. 925–930, 2018.

[176] H. S. Singh and S. Kalraiya, "Design and analysis of a compact WiMAX and WLAN band notched planar monopole antenna for UWB and bluetooth applications," *RF Microw. Comput. Eng.*, pp. 1–10, Jan. 2018.

[177] A. Iqbal, A. Smida, N. K. Mallat, and M. T. Islam, “A Compact UWB Antenna with Independently Controllable Notch Bands,” *Sensors (Switzerland)*, vol. 19, no. 6, pp. 1–12, 2019.

[178] A. S. A. El-hameed, M. G. Wahab, A. Elboushi, and M. S. Elpeltagy, “Miniaturized triple band-notched quasi-self-complementary fractal antenna with improved characteristics for UWB applications,” *AEUE - Int. J. Electron. Commun.*, vol. 108, pp. 163–171, 2019.

[179] A. H. Nazeri, A. Falahati, and R. M. Edwards, “A novel compact fractal UWB antenna with triple reconfigurable notch reject bands applications,” *AEUE - Int. J. Electron. Commun.*, vol. 101, pp. 1–8, 2019.

[180] R. Sanyal, P. Pratim, and S. Sarkar, “Octagonal nut shaped monopole UWB antenna with sextuple band notched characteristics,” *AEUE - Int. J. Electron. Commun.*, vol. 110, 2019.

[181] L. Han, “Reconfigurable ultra-wideband monopole antenna with single, dual, and triple-band notched functions,” *RF Microw. Comput. Eng.*, vol. 29, no. 9, pp. 2–11, 2019.

[182] N. Yang, Z. N. Chen, Y. Y. Wang, and M. Y. W. Chia, “A two-layer compact electromagnetic bandgap (EBG) Structure and its applications in microstrip filter design,” *Microw. Opt. Technol. Lett.*, vol. 37, no. 1, pp. 62–64, 2003.

[183] A. A. Gheethan and D. E. Anagnostou, “Dual Band-Reject UWB Antenna with Sharp Rejection of Narrow and Closely-Spaced Bands Ahmad,” *IEEE Trans. Antennas Propag.*, vol. 60, no. 4, pp. 2071–2076, 2012.

[184] T. Ma and J. Tsai, “Band-Rejected Ultrawideband Planar Monopole Antenna with High Frequency Selectivity and Controllable Bandwidth Using Inductively Coupled Resonator Pairs,” *IEEE Trans. Antennas Propag.*, vol. 58, no. 8, pp. 2747–2752, 2010.

[185] J. Y. Siddiqui, S. Member, C. Saha, Y. M. M. Antar, and L. Fellow, “Compact Dual SRR Loaded UWB Monopole Antenna with Dual Frequency and Wideband Notch Characteristics,” *IEEE Antennas Wirel. Propag. Lett.*, vol. 14, pp. 100–103, Sept. 2014.

[186] W. Li, Z. Tu, Q. Chu, S. Member, and X. Wu, “Differential Stepped Slot UWB Antenna with Common-Mode Suppression and Dual Sharp-Selectivity Notched Bands,” *IEEE Antennas Wirel. Propag. Lett.*, vol. 15, pp. 1120–1123, 2015.